European Funds
Knowledge Education Development

European Union
European Social Fund

„BioTechNan - the programme of interdisciplinary cross-institutional post gradual studies KNOW in the field of Biotechnology and Nanotechnology"

DOCTORAL DISSERTATION

Charge transfer compounds as sources of laser light

Martyna Durko-Maciąg, MSc. Eng.

Supervisors:

Prof. Jarosław Myśliwiec, Wroclaw University of Science and Technology

Dr. Julien Massue, French National Centre for Scientific Research & University of Strasbourg

Wrocław, 2022

Wrocław University of Science and Technology

Uniwersytet Wrocławski

Wrocław University of Environmental and Life Sciences

The project is co-financed by the European Union from the European Social Fund

Dla Męża
oraz Rodziców

ACKNOWLEDGMENTS

This dissertation would not be possible if it weren't for a few precious people. I would like to sincerely thank them for all the freely given aid and a good word. Without this support, the presented work would not have seen the light of day.

First of all, my supervisors – Professor Jarosław Myśliwiec and Doctor Julien Massue. To Prof. Myśliwiec - thank you very much for the help you have given me for over five years of working together. All the discussions, both the longer and shorter ones, your kindness and the understanding shown to me are priceless. To Dr. Massue - even though I spent only a few months in Strasbourg, the patience you have shown a novice like me was invaluable. Thank you very much for the time devoted to me, spent not only together in the laboratory, but also for all the discussions. Dear Sirs, thank you again.

I would also like to thank everyone with whom I worked to a greater or lesser extent during my PhD. To the COMBO group - thank you for taking me in, a complete outsider, and helping me whenever I had a problem. Thibault and Timothée, thank you for always being there for me. If it wasn't for you, I certainly would not be able to survive in the chemistry lab. Both of you always took the time to explain things to me – thank you so much.

To our 'light amplifiers' - thank you for all the time we have spent together, whether at weekly meetings or during our memorable relocations. In particular, I would like to thank Dr. Konrad Cyprych - each of our conversations was stimulating. Your experience, open-mindedness, and simply your curiosity always made me come up with new ideas, with which you have guided me many times. Thank you for always supporting me and never refusing to help. I will always be grateful.

My partners from the office, my comrades-in-arms, my dear friends – Dr. Anna Popczyk and Martyna Janeczko (names given in the alphabetical order, so that there will be no misunderstandings later!). We have certainly been through a lot together - you know very well what I wish to thank you for. If it weren't for you, I would never have made it to the end. Our conversations (both the stupider and smarter ones), joint trips (maybe the next one a little bit further than Lower Silesia?), or simply just the glances exchanged during awkward meetings always brought a lot of joy to my life. Nobody understood me like you. The words *Thank you* will never be enough.

Na sam koniec chciałabym również podziękować paru osobom z mojej najbliższej rodziny, które również przyczyniły się do powstania tej pracy. Do Macieja, Agaty i Gabrieli Durko – choć nie zawsze rozumieliście, co dokładnie robię, to zawsze czułam wasze wsparcie. Dziękuję wam za nie – w końcu możecie powiedzieć, że skończyłam studia!

Moi kochani Rodzice – wasza niezachwiana wiara we mnie zawsze dodawała mi skrzydeł. Bardzo wam dziękuję, że umożliwiliście mi życie, jakie obecnie wiodę. To dzięki wam jestem, kim jestem, mogłam się rozwinąć jako osoba. Wasze wsparcie jest bezcenne – nigdy nie zdołam się wam odpłacić za całą dobroć, jaką mi daliście.

Mojemu drogiemu Mężowi – Konrad, dziękuję Ci za Twój spokój. Gdyby nie Twoje opanowanie, to nigdy bym nie skończyła doktoratu. Zawsze byłeś przy mnie, przy każdym wzlocie i upadku. Wielokrotnie słuchałeś moich długich wywodów – Twoja cierpliwość do mnie jest nieoceniona. Dziękuję.

Martyna Durko-Maciąg

TABLE OF CONTENTS

EXPERIMENTAL INVESTIGATIONS

ABSTRACT IN POLISH

Streszczenie w języku polskim

Niniejsza rozprawa została zrealizowana w ramach projektu BioTechNan – Program Interdyscyplinarnych Środowiskowych Studiów Doktoranckich KNOW z obszaru Biotechnologii i Nanotechnologii, między:

1) Politechniką Wrocławską - Wydział Chemiczny, Katedra Inżynierii i Modelowania Materiałów Zaawansowanych;

2) Francuskim Narodowym Centrum Badań Naukowych oraz Uniwersytetem w Strasburgu, Francja - instytut ICPEES.

Badania eksperymentalne przedstawione w rozprawie dotyczą związków z przeniesieniem ładunku, tj. niedostępnych komercyjnie organicznych chromoforów typu ESIPT (*Excited-State Intramolecular Proton Transfer*), które mogą zostać wykorzystane w zjawiskach wzmocnienia światła. W pracy skupiono się na scharakteryzowaniu związków chemicznych w kontekście interakcji światło-materia. Znakomita większość badanych chromoforów oparta była na 2-(2'-hydroksyfenylo)benzazolu, który był odpowiednio modyfikowany na drodze syntezy chemicznej w celu przestrajania właściwości emisyjnych badanej pochodnej. Ta część badań była wykonywana w trakcie staży w instytucie ICPEES we Francji, pod opieką doktora Juliena Massue. Oprócz przeprowadzonej syntezy, w tamtejszym laboratorium przeprowadzono pomiary właściwości spektroskopowych badanych pochodnych, m. in. pomiary absolutnej wydajności kwantowej pastylek bromku potasu domieszkowanych danym barwnikiem. Zarówno zsyntezowane chromofory, jak i te dostarczone przez dr Massue, były następnie analizowane w laboratoriach Politechniki Wrocławskiej, pod opieką profesora Jarosława Myśliwca. Zakres badań eksperymentalnych obejmował zarówno podstawową charakteryzację materiałów pod kątem pomiarów absorpcji i emisji w formie rozcieńczonych roztworów oraz domieszkowanych filmów polimerowych, jak i bardziej skomplikowanych zjawisk, tj. randomicznej akcji laserowej czy wzmocnionej emisji spontanicznej. Wyznaczono podstawowe parametry opisujące te zjawiska, takie jak wartości progów laserowania czy współczynnik wzmocnienia. Równolegle przeprowadzano badania nad znalezieniem praktycznych zastosowań dla barwników typu ESIPT, np. możliwość skonstruowania laserów typu DFB przestrajalnych w czasie rzeczywistym, polichromatycznych laserów czy też ich aplikacji jako fotoinicjatory w mikrofabrykacji.

ABSTRACT IN ENGLISH

Streszczenie w języku angielskim

This dissertation was carried out as part of the BioTechNan project - the program of interdisciplinary cross-institutional post-graduate studies KNOW in the field of Biotechnology and Nanotechnology, between:

1) Wroclaw University of Science and Technology - Faculty of Chemistry, Advanced Materials Engineering and Modeling Group;

2) French National Center for Scientific Research and University of Strasbourg, France - at The Institute of Chemistry and Processes for Energy, the Environment and Health (ICPEES).

The experimental studies presented in the dissertation are concerned with charge transfer compounds, i.e. commercially unavailable organic Excited-State Intramolecular Proton Transfer (ESIPT) chromophores that can be applied in the phenomena of light amplification. The work focuses on the characterization of these materials in the context of light-matter interactions. The vast majority of the investigated chromophores were based on a 2-(2'-hydroxyphenyl)benzazoles scaffold, which was appropriately modified by chemical synthesis in order to tune the emission properties of the tested derivative. This part of the research was carried out during internships at the ICPEES institute in France, under the supervision of Dr. Julien Massue. In addition to the synthesis, measurements of the spectroscopic properties of the tested derivatives were carried out in this laboratory, including measurements of the absolute quantum yield of potassium bromide pellets doped with the chromophore. All compounds, both the synthesized and those provided by Dr. Massue, were then analyzed in the laboratories of the Wroclaw University of Science and Technology, under the supervision of Prof. Jarosław Myśliwiec. The scope of the conducted experimental research included both the basic characterization of materials in terms of absorption and emission measurements in the form of dilute solutions and doped polymer films, as well as more complicated effects, such as random lasing action or amplified spontaneous emission. The basic parameters describing these phenomena, such as the lasing threshold values or the optical gain, were determined. Simultaneously, research was carried out on finding practical applications for the ESIPT dyes, e.g. the possibility of constructing real-time tunable DFB lasers, polychromatic lasers, or as photoinitiators in microfabrication.

ABBREVIATIONS

3HF	3-Hydroxyflavone
A	Acceptor
ACQ	Aggreagation-Caused Quenching
AIE	Aggregation-Induced Emission
AIEE	Aggregation-Induced Emission Enhancement
ASE	Amplified Spontaneous Emission
D	Donor
DFB	Distributed Feedback
DTWM	Degenerated Two-Wave Mixing
ES	Excited State
ESICT	Excited-State Intramolecular Charge Transfer
ESIPT	Excited-State Intramolecular Proton Transfer
FWHM	Full Width at Half Maximum
GS	Ground State
GSIPT	Ground-State Intramolecular Proton Transfer
HBI	2-(2'-Hydroxyphenyl)benzimidazole
HBO	2-(2'-Hydroxyphenyl)benzoxazole
HBT	2-(2'-Hydroxyphenyl)benzothiazole
HBX	2-(2'-Hydroxyphenyl)benzazole
HOMO	Highest Occupied Molecular Orbital
HPS	Hexaphenylsilole
IC	Internal Conversion
ICT	Intramolecular Charge Transfer
ISC	Intersystem crossing
JAF	J-Aggregates Formation
LUMO	Lowest Unoccupied Molecular Orbital
NEt2	N,N-diethylaniline
NMe2	N,N-dimethylaniline
OFET	Organic Field Effect Transistor
OLED	Organic Light Emitting Diode
OSSL	Organic Solid State Lasers
PMMA	Poly(methyl methacrylate)
PS	Polystyrene
PVK	Poli(vinyl carbazol)
QY	Quantum Yield
RIM	Restriction of Intramolecular Motion
RIR	Restriction of Intramolecular Rotation
RIV	Restriction of Intramolecular Vibration
RL	Random Lasing
S	Singlet State
SA	Salicylic Acid
SSDL	Solid-State Dye Lasers
T	Triplet State

TES	Triethylsilyl
THF	Tetrahydrofuran
TICT	Twisted Intramolecular Charge Transfer
TIPS	Triisopropylsilyl
TMS	Trimethylsilyl
TPP	Two-Photon Polimeryzation
VCSEL	Vertical-Cavity Surface-Emitting Laser
VR	Vibrational Relaxation
VSL	Variable Stripe Length

FOREWORD

Since the dawn of time, all interaction of light and matter has aroused interest. There is nothing surprising in this - without sunlight, there would be no life on Earth. A prime example is photosynthesis, which releases oxygen, an element essential for the life of many species, including humans. Additionally, solar energy is one of the renewable sources - it practically cannot be exhausted. Therefore, no one is surprised by the enormous progress in lighting technologies, which are not only practical (such as home lighting, car lights, solar panels), but also aesthetic. It is more and more popular, and more acceptable by the public, to replace fireworks with displays of illumination, for which lasers are very often used.

Although the first laser, i.e. a source of intense and coherent light with a specific color, was invented more than 60 years ago by Theodor Maiman on a ruby crystal, research in this direction is not stopping. On the contrary, one could say that along with technological progress the development of lasers raises, which in turn promotes the former. Lasers nowadays, sometimes called the miracle of the twentieth century, do not necessarily have to be of large dimensions, which makes their implementation in various applications easier. After all, in many lecture halls one can find laser pointers that fit in the palm of the hand. Another example, perhaps less common now but still worth mentioning, are the CD/DVD or Blu-ray discs, for which a laser is needed to read the stored data. In addition to commercial applications, this intense source of radiation is more and more often used in medicine, ranging from tissue imaging, through phototherapy, wound decontamination, or even during surgery. Laser vision correction is becoming more popular and available. As a result of this increasing range of applications, the search for stable, efficient, and inexpensive lasers is underway.

One of the possibilities to meet these requirements is the organic laser, which is technologically easier to obtain than its inorganic counterparts. The first such devices appeared shortly after Maiman's invention, in 1966. Initially, they were used in the form of dye solutions, then as mixtures in polymers, creating guest-host systems. Such structures are more convenient and cheaper to manufacture. Unfortunately, organic compounds are inherently more susceptible to light, which results in their much lower stability compared to inorganic lasers. Therefore, the emphasis is on reducing the energy required for laser action to reduce material degradation. There is a group of compounds that seem to be tailored for such applications – the ESIPTs. This acronym stands for Excited-State Intramolecular Proton Transfer and is related to many

compounds found in nature, with salicylic acid as the primary example. These specific chromophores are the core of the presented dissertation, with the following **hypothesis**:

*Organic chromophores exhibiting **E**xcited-**S**tate **I**ntramolecular **P**roton **T**ransfer phenomena are able to amplify light through stimulated emission in a four-level system. Their properties can be tuned to match desired application through chemical substitution and/or change of the surrounding matrix.*

This manuscript is dedicated to the investigation of noncommercial Excited-State Intramolecular Proton Transfer (ESIPT) compounds, the majority of which are based on 2-(2'-hydroxyphenyl)benzazole. Change of the heteroatom in this scaffold, as well variations in the π-conjugated substituents, influence the photophysical properties of the compound. Two Schiff bases are also investigated, which are characterized by electron-donor and -acceptor moieties, hence intramolecular charge transfer is also possible. The tautomerization in the excited state of these compounds is promoted by an intramolecular hydrogen bond present between hydrogen donor and acceptor moieties. As the main goal of the thesis is to develop light amplifying systems, at the beginning fundamental characterization of the compounds was performed to determine absorption and emission spectra. The information obtained from these investigations made it possible to determine the pumping conditions for the stimulated emission to occur. Secondly, as nowadays the majority of the organic lasers are designed in the solid-state, the influence of aggregation and crystallization on the emissive properties was inspected, followed by the fabrication of dye-doped polymeric thin films. These structures served as planar waveguides, which enabled the determination of the basic light amplification properties, such as threshold, net gain, or sample photostability. Similar experiments were conducted for concentrated solutions and amorphous powders. The possibility to obtain random or distributed feedback lasing was investigated. The use of different geometries made it possible to estimate possible applications of the ESIPT compounds.

The presented dissertation can be divided into two parts: theoretical and experimental, with seven chapters in total. In the first three, background regarding light-matter interaction is presented, beginning with fundamental aspects (absorption, relaxation, scattering) through the processes of spontaneous and stimulated emission, with the description of the laser at the end.

As organic chromophores are investigated in this thesis, the related theoretical background was discussed as well. Chapter 4 opens the experimental section with a detailed description of investigated chromophores and applied methods. Since part of the research was conducted in France under the guidance of Dr. Julien Massue, relevant synthetic details are also given. Chapter 5 contains the experimental results provided with an explanation and discussion. Based on the obtained data some practical applications were achieved, which are presented in Chapter 6. In the last chapter general conclusions are enclosed. The two appendixes provide synthetic details on non-published investigated chromophores, as well as the Author's research achievements.

THEORETICAL INTRODUCTION

1. Light-matter interaction: fundamental aspects

In this introductory chapter, a few fundamental processes related to matter-light interaction are presented. The important optical effects described in this section provide the basics for the understanding of more complex phenomena, such as light amplification.

1.1. Absorption

The first process that needs to be taken into consideration when light-matter interactions are discussed is absorption. To present this phenomenon in the simplest way, two energy levels of an atom or molecule of material can be considered: the ground (E_1) and excited (E_2) states. Unless an external stimulus is applied, for example a lightwave, the atom/molecule will remain stable at the lower energy level. If the electromagnetic wave passes through the material, then there is a finite probability that the energy equal to the difference between E_1 and E_2 will be taken by the material, resulting in its elevation to a higher energy level. This is the absorption process, with a graphical illustration given in Figure 1.1.1.

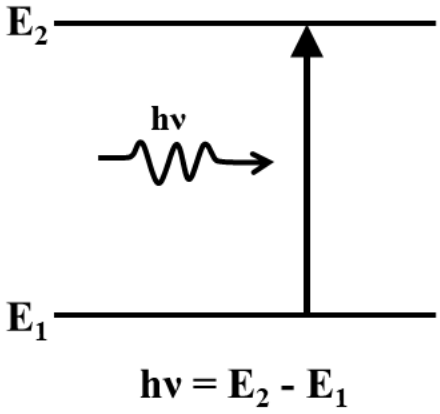

Figure 1.1.1. *Scheme of absorption.*

Various mathematical descriptions of absorption were given through the years, out of which a few should be highlighted. The first was given in the 18th century by Pierre Bouguer,[1] and then by Johann H. Lambert (who cited the former's essay in his paper).[2] These scientists independently investigated changes in the intensity of a beam that was passing through a medium along with its length. Their findings are now known as Bouguer-Lambert law. August Beer has continued this path of research,[3] which led to the formation of an equation known today as Lamber-Beer law (1.1.). Almost a century after the findings of Bouguer and Lamber were published, the german scientist stated that the concentration of the solution (c, expressed in $mol \cdot L^{-1}$) also influences the intensity of light passing through (I_T). Hence, absorbance (A) is dependent on the material's molar attenuation coefficient (ε, $L \cdot mol^{-1} \cdot cm^{-1}$), its concentration, and the length of the path that the light has to travel through (l, cm).

$$log\frac{I_0}{I_T} = \varepsilon cl \equiv A \tag{1.1.}$$

If the ratio of transmitted (I_T) and incident (I_0) light is investigated, then another characteristic parameter of the absorbing medium is obtained, namely the transmittance (T):

$$\frac{I_T}{I_0} = T \tag{1.2.}$$

It should be noted, that according to the Lamber-Beer law, the molar attenuation coefficient is a value independent of the concentration, while a linear relationship between the absorbance and the latter exists. However, any deviation from these relationships does not contradict the general validity of equation 1.1. This law applies strictly to the absorption of monochromatic radiation and the situation in which the molecular state of the tested substance does not change as a result of changes in concentration, i.e. the formation of associations, aggregates, or molecular dissociation. Aggregation, and its influence on the photophysical properties, will be described in detail in further chapters.

Nonetheless, when it comes to linear optics, the intensity of the incident beam does not affect the absorption value, simply because the light has close to no effect on the material. This fact enables easy and repeatable measurements with spectrophotometers, without the need to perform calibration. As such, the absorption measurement is one of the most commonly performed characterizations of organic materials, both in solution and in the solid state. For the latter, however, one should also take into consideration light scattering, which is described more in detail in the next subsections.

1.2. Relaxation

Absorption of the energy, as postulated previously, raises the molecule to unstable higher energy levels. Hence, an excess of energy needs to be released. Following the *excitation*, different relaxation pathways can be followed: either radiative or nonradiative. The first process occurs when the molecule loses its excitation energy in the form of an emitted photon. The nonradiative decay, more common in nature, occurs by energy transfer to surrounding molecules, followed by conversion of it through oscillations or rotations into heat. The excited molecule can also dissociate or react chemically.

A diagram can be constructed to schematically present energy flow in the molecule, as proposed by a polish scientist and violinist, Aleksander Jablonski, in 1933.[4] This graphical construction can depict both singlet and triplet electronic states, at the ground or excited energy levels, as presented in an exemplary diagram in Figure 1.2.1.

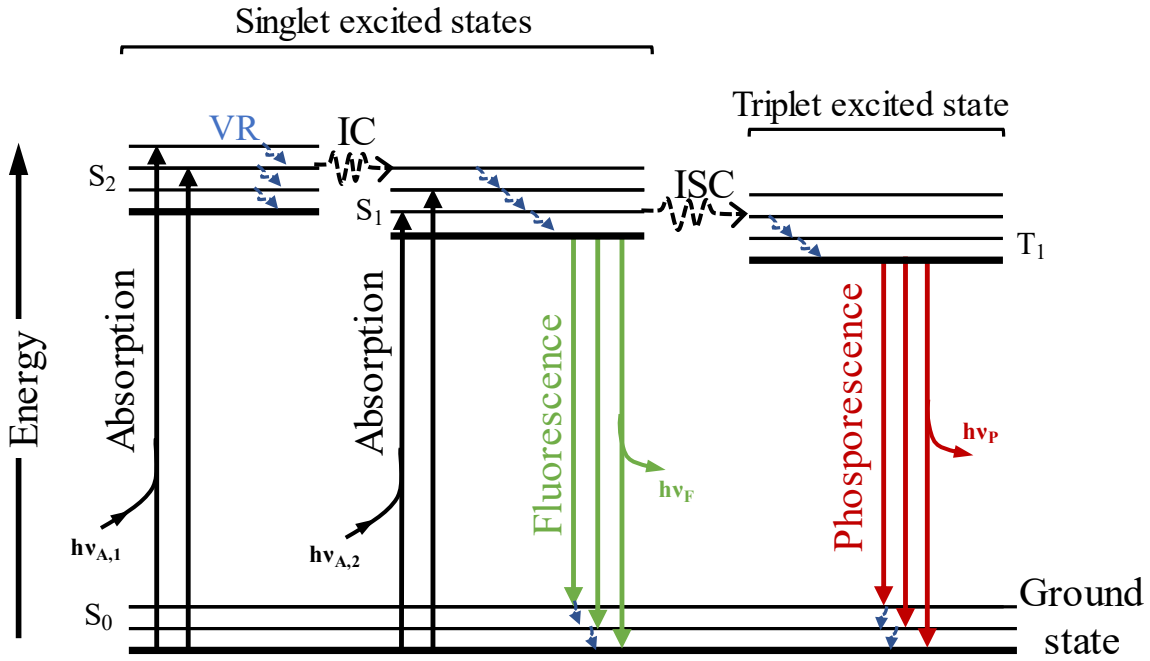

Figure 1.2.1. *The Jablonski diagram. Solid lines correspond to radiative processes, the dashed to the nonradiative ones. IC – Internal Conversion, VR – Vibrational Relaxation, ISC – Intersystem Crossing, S – singlet state, T – triplet state, F – Fluorescence, P – Phosphorescence.*

The analysis of the behavior of the molecule following excitation yields a lot of important information about the chemical structure or photophysical properties. Hence, emission measurements are treated as an integral part of the compound's characterization, complementary to the absorption. As presented in the Jablonski diagram, there are several ways for the molecule to release excess energy:

Vibrational Relaxation (VR) - $S_n^* \rightarrow S_n$ or $T_n^* \rightarrow T_n$; 10^{-12} to 10^{-10} s - This process occurs when an excited particle collides with surrounding molecules and, with the inelastic return of energy, very fast descends down to the lowest oscillatory level of the electronic state. If the vibrational relaxation takes place in excited states, the surrounding molecules may be unable to

absorb all of the excess energy, and therefore a spontaneous emission process may occur. The following transition happens vertically according to the Franck-Condon rule, and thus the observed fluorescence spectrum has an oscillating structure that characterizes a lower electronic state.

Internal Conversion (IC) - $S_1 \rightarrow S_0$, $T_2 \rightarrow T_1$; 10^{-14} to 10^{-11} s - A non-radiative transition between states of the same multiplicity. The probability of this process increases when the vibrational levels of two energy states overlap. The molecule then de-excites without photon emission to a lower state of the same multiplicity, followed by kinetic relaxation through VR to the lowest oscillatory level. If the transition took place from S_1 to S_0, then it is equivalent to the conversion of the excitation energy into non-excited oscillation energies, as a result of which no photon emission is observed. It is often the last result of light absorption by non-fluorescent species.

Intersystem Crossing (ISC) - $S_1 \rightarrow T_1$, $T_1 \rightarrow S_0$; 10^{-11} to 10^{-6} s – another non-radiative transition, but between states of different multiplicity, which is in principle forbidden due to the spin multiplicity of the starting and ending states. Nonetheless, spin-orbital coupling makes it feasible through inversion of the excited electron's spin due to its interaction with the orbital angular momentum of non-circular orbits. When the vibrational levels of the two excited states overlap, the chance of this process occurring increases since little or no energy must be acquired or lost in the transition. It is common for heavy-atom molecules, for example those containing bromine or sulfur.

Fluorescence - $S_1 \rightarrow S_0$; 10^{-9} to 10^{-6} s - As the first of the radiative and spontaneous processes, fluorescence occurs due to the transitions between electronic states of the same multiplicity at the time of the excitation of the sample. If the deactivation of the excited molecule (M^*) occurs only through fluorescence, its initial intensity (I_0, at the termination of excitation) decreases exponentially with time t (1.3.).[5] The τ_0 denotes the natural mean lifetime of the molecules in the excited state, which depends only on the probability of a spontaneous radiant transition $M^* \rightarrow M$, while k_f is fluorescence time constant ($\tau_0 = 1/k_f$).

$$I_T = I_0 \exp(-k_f t) = I_0 \exp(-t/\tau_0) \qquad (1.3.)$$

However, the observed emission is almost always of lower energy than the absorbed photons, thus observed at longer wavelengths (see Figure 1.2.2.). Described non-radiative de-excitation pathways also need to be considered, also for the fluorescence lifetime determination. If one looks only at the monomolecular processes, then the deactivation of molecules in the first excited singlet state (M^*) can be described by the following first-order kinetic equation (1.4.):[5]

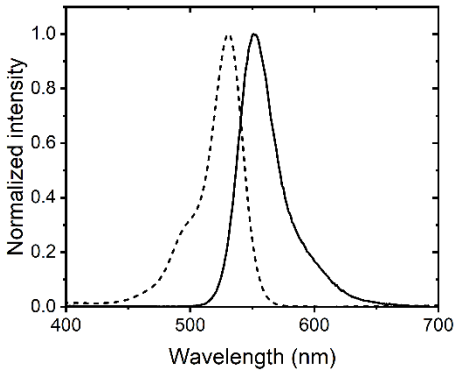

Figure 1.2.2. *Absorption (dashed) and emission (solid) spectra of diluted solution of Rhodamine 6G in ethanol.*

$$-\frac{d[M^*]}{dt} = (k_f + k_{VR} + k_{IC})[M^*] \tag{1.4.}$$

Which leads to fluorescence lifetime (1.5.):

$$\tau = \frac{1}{k_f + k_{VR} + k_{IC}} \tag{1.5.}$$

The τ is slightly shorter than the natural mean lifetime (τ_0) and can be directly measured during the fluorescence decay time experiment. This value is proportional to one of the most important parameters of the fluorescent compounds – the quantum yield (1.6.). It can be defined as the ratio of the number of photons emitted from the molecule to the number of photons that were emitted by the excitation source and absorbed by the sample, at the same time and in equal volume. This value is almost always lower than 1.

$$\Phi_{PL} = \frac{\tau}{\tau_0} \tag{1.6.}$$

This relation is correct for all cases, with the exception of diluted gases, in the case of which the equilibrium of the excited oscillatory levels settles slowly. The fluorescence quenching may also occur in two-molecular systems (donor-acceptor) or due to concentration, however, this will be described more in detail in further subchapters.

Phosphorescence - $T_1 \rightarrow S_0$; 10^{-3} to 10^2 s - The second radiative process that can be undergone by the molecule, hypothesized by A. N. Tierenin (1943)[5] and G. N. Lewis with M. Kasha (in

1944).[6] The first successful experimental confirmation of this process was by an EPR experiment conducted by C. Hutchison and B. Mangum in 1958.[7]

If the molecule can, as a result of intersystem crossing, move from the singlet state to the excited state ($S_1 \rightarrow T_1$), then there is a finite possibility of photon emission through phosphorescence. While this radiative relaxation should be forbidden similarly to the ISC, the spin-orbital coupling makes it possible. Through vibrational relaxation and after descending to the lowest oscillatory level T_1, emission of photons takes place. The observed signal is weak but may persist for a relatively long time, even for many hours. This implies that the much shorter fluorescence process instantaneously converts the absorbed radiation into emitted energy, whereas phosphorescence accumulates energy before releasing it.

1.3. Scattering of light

As previously stated, observation of either radiant or non-radiative transitions is only feasible when the resonance requirement is met ($\Delta E = E_2 - E_1$). This is accomplished by either matching the energy of the electromagnetic wave to the difference in energy levels of the molecule (radiative decay) or by isoenergetic energy dissipation (non-radiative). However, when energy is not absorbed by the material or transferred to other states, radiation scattering occurs. At the molecular level, it is manifested as the combination of refraction, reflection, and transmission.

In a matter similar to absorption, light scattering leads to a decrease of a transmitted intensity. The scattering cross-section σ_{scatt} [cm^2] can be calculated when the interaction length (z, cm) and the density of scattering particles (N, cm^{-3}) are taken into account:[8]

$$I_T = I_0 \exp\left(-\sigma_{scatt} N z\right) \tag{1.7.}$$

The scattering can be deemed as *elastic* or *inelastic*: the former occurs when the interaction does not influence the incident photon's energy, merely its propagation direction. When the energy is not preserved, then the latter type takes place. The scattering can be further specified by the relation of the scattering particles and the wavelength of incident light. If dispersion occurs on structures of a lower size than the wavelength, such as molecules or local fluctuations of optical density, then it's a Rayleigh type.[9,10] As these sites are randomly oriented, the photons are scattered in all directions. When it occurs, the longer wavelengths are less scattered than the shorter ones, with intensity in proportion to $1/\lambda^4$.

Mie scattering appears when the situation is reversed in comparison to the first-mentioned type.[11] It occurs as a result of light interaction with particles with dimensions close to or bigger in dimensions than the wavelength, such as colloids, aerosols or other systems containing fine structures. As a result interference of light coming from different parts of the scatterer can be observed and the energy of photons is preserved. The intensity is very weakly dependent on the λ, becoming completely independent for particles of sizes greater than the wavelength. Their shape and structure directly influence the intensity and angular distribution of light. This type of scattering is an important part of this dissertation, as it influences light propagation of the incident wavelength more than the Rayleigh type, with greater scattering losses, thus directly impacting possible light amplification applications. It will be discussed more in detail in the following chapters.

On the other hand, variations of both photon energy and frequency are observed for inelastic scattering at sound waves (Brillouin)[12] or vibrations (Raman).[13] These processes can disturb potential photonic applications, but also can be used constructively for example in optical phase conjugation or frequency conversion (with stimulated Raman scattering).[8]

Scattering changes along with the density of the media. Generally speaking, if the medium is denser, then the intensity of the sideways scattering is smaller. If the particles are positioned close to one another, then equally numerous photons are scattered, overlapping one another and resulting in their interference, as already mentioned for the Mie dispersion, either constructive or destructive. Hence, energy transfer from the latter areas to the former is promoted. The more monolithic and dense media are prone to stronger destructive interference in the transverse direction, and less destructive to the sides and back, resulting in photon transmission mostly forwards.[14] As a result, the incident beam suffers relatively minor attenuation. For example, glass and plastics are usually transparent and amorphous solids. Sideways scattering on these structures is usually very low, however, any imperfections such as scratches and settling dust will enhance this effect. This fact will be brought up again in the chapter on random lasing.

2. *Organic chromophores*

In this chapter more complex processes involving organic matter are presented. As charge transfer compounds are a topic of this dissertation, a careful examination of their properties is enclosed.

2.1. Solvatochromism and ICT

If one looks back on various processes involved in the deactivation of an excited molecule, it becomes clear that the surrounding medium has a significant effect on the emission properties of the materials. Nonetheless, the observed fluorescence is usually shifted towards longer wavelengths than the incident radiation (the difference named as Stokes shift, after the irish physicist), simply because a part of its energy is transferred to the environment. Such behavior suggests that the emission intensity should be dependent on the solvent's ability to absorb the electronic and oscillation energy. Indeed, it was observed that fluorescence quenching occurs in solvents that are characterized by the widely separated oscillating levels, enabling absorption of large quanta of energy. Water is one of the leading examples. However, it should be noted that other effects also need to be considered. Hydrogen bonds between solvent and the chromophore, or internal charge transfer also influence the overall emissive properties.

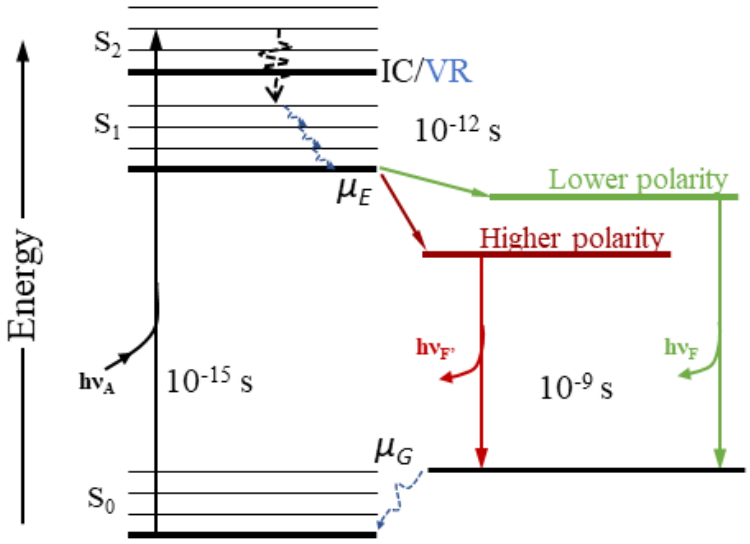

Figure 2.1.1. *A Jablonski diagram showing fluorescence of molecule in solvents of different polarity.*[16]

The influence of the solvent on the spectral properties of materials was defined as *solvatochromism* in 1922 by Hantzsch.[15] Usually, solvent polarity is the first topic of investigation, however, other effects need to be considered. A Jablonski diagram showing the possible behavior of the molecule in solvents of two different polarities is given in Figure 2.1.1.

In most basic cases, absorption leads to the excitation of the molecule to either the first or second singlet state, followed by rapid decay to the lowest oscillation level of S_1, with the excess vibrational energy consumed by the solvent. Usually, organic fluorophores are characterized by a higher dipole moment in the excited state (μ_E) than in the ground state (μ_D). In polar media, the excited states are further stabilized by the solvent molecules, by their reorientation or relaxation around μ_E.[16] It is observed as a red-shift of the emission, as this stabilization lowers the energy of the fluorophore's excited state. Generally, the higher polarity, the bigger the shift towards the longer wavelengths (towards the infrared), i.e. a bathochromic shift. A shift towards shorter wavelengths (ultraviolet), called a hypsochromic shift, occurs when the excited state is less polar than the ground state. Typically the molecular sensitivity to the solvent polarity is significantly more pronounced when the fluorophore is polar itself. Nonetheless, these effects are less striking on absorption spectra. Such fact can be easily explained when one looks at the timescales of absorption and non-radiative decays. The former is much faster, and as such can be treated as an instantaneous action. Hence, the molecule is exposed to the same environment before and after absorption because the solvent does not have enough time to reorient itself around the dipole moment of excited states.

The influence of solvent relaxation on the observed emission spectrum can be described mathematically through the Lippert-Mataga method (2.1.).[17,18] It takes into account the factor of the orientation polarizability (Δf) and the Stokes shift between corresponding absorption and emission maxima ($\Delta\nu$, cm^{-1}):

$$\Delta\nu = \frac{2}{hc}\frac{(\mu_E-\mu_G)^2}{a^3}\Delta f \qquad (2.1.)$$

Where h – Planck's constant, c – the speed of light, a – radius of the cavity where molecule resides, and dipole moments in excited (μ_E) and ground (μ_G) states. It is a linear correlation, but only when the luminescence is a result of the dipolar interaction of the solvent and the fluorophore. The orientation polarizability can be calculated from equation (2.2.) by taking into account the relative dielectric permittivity (ε) of the solvent and its refractive index (n):

$$\Delta f = \frac{\varepsilon-1}{2\varepsilon+1} - \frac{n^2-1}{2n^2+1} \qquad (2.2.)$$

As can be seen from this equation, both polarity and the refractive index of the solvent have an effect on the observed Stokes shift. The first is a static constant depending on molecular

and electronic motions, with an increase of which a larger difference between absorption and emission maxima can be observed. On the other hand, a higher refractive index makes the shift smaller due to its dependence on the electron motions within the solvent molecules. To understand the different effects of both ε and *n* on the Stokes shift, the stabilization of ground and excited states should be analyzed (defined as the difference in their corresponding energy, ΔE). It is decreased in more polar solvents due to the local of the electrons in the solvent molecules. However, it only occurs after the reorientation of the dipoles, which in turn requires movement of the whole molecule. On the contrary, while the refractive index also promotes the decrease in the excited state energy, the electron redistribution is not time-dependent. Hence, its influence on the Stokes shift is minor.

Besides spectral shifts observed due to polarity, emission changes can be induced by the hydrogen bonds forming between molecules of the fluorophore and the protic solvent. The latter refers to the structures with hydroxyl or other groups capable of hydrogen bonding. As can be deduced from the Lippert-Mataga equation, the Stokes shift is generally larger in these cases, for example in water or ethanol solutions. Surprisingly, the opposite can be observed for a specific group of dyes – Excited State Intramolecular Proton Transfer (ESIPT) compounds, which will be discussed in detail in a separate subchapter, as they are a part of this dissertation.

There's a class of fascinating compounds, which are prone to Intramolecular Charge Transfer (ICT), which heavily influences their photophysical properties. These materials have a specific structure formed of two crucial moieties: donor (D) and acceptor (A). The latter withdraws the electrons, while the former donates them. To facilitate the charge transfer, an π-conjugated group of molecules needs to connect the donor and acceptor, almost like a bridge. The most basic structure of such a D-π-A molecule is given in Figure 2.1.2. These compounds are also often referred to as *push-pull* due to the ongoing charge transfer.

In the ICT compounds, after excitation, there is an increase in charge separation in the molecule due to the transfer of electrons from donor to acceptor moieties. Then, depending on the solvent polarity, different species are of the lowest energy. In polar media, the ICT state is favorable due to enhancement of the dipole moment, while in non-polar solvents non-separated species of locally excited (LE) state are of the lowest energy. As a result, a bathochromic shift of emission is seen with the increase of a solvent's polarity.

The described charge transfer can also occur between two different molecules, as is the case in photosynthetic reactions or metabolism,[19] but as with ICT, one needs to be an electron-donating, while the other electron-accepting one. The structure of the moiety significantly influences its overall ability to either donate or withdraw electrons. As such, one can tailor the optical properties of the material according to its application through molecular engineering of its structure. Some of the strongest donating groups are those with lone electron pairs, like alcohol or amine moieties, or ethers. The tendency to withdraw electrons is apparent in systems with π-bonds to electronegative atoms, e.g. aldehydes, ketones, esters, cyano or nitro groups.

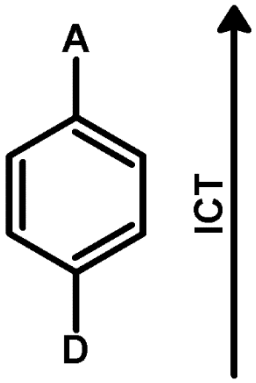

Figure 2.1.2.
Structure of D-π-A system.

2.2. Aggregation

Interpretation of photophysical properties of fluorophores is not a trivial matter. Previously described methods, like Lippert-Mataga, cannot be applied when concentration effects take place. While the increase in absorption is logical due to the Lambert-Beer law, for most fluorophores a decrease in emission intensity is observed for highly concentrated solutions. The first reports on this quenching were presented by Forster and Kasper for the pyrene molecule more than half a century ago (1954).[20] It was later found that the collision of aromatic molecules in the ground and excited-state facilitates the formation of exciplexes and sandwich-like excimers, which is correlated to the aggregation of these moieties. These processes are common to most aromatic structures. Photophysical properties determined for the diluted solutions cannot be extended to the more concentrated ones, which is a fundamental problem when it comes to the application of fluorophores, as they are most commonly used in the solid state. Additionally, even when the materials are first applied as dilute solutions, they can also suffer from the locally increased concentration due to their accumulation, for example as a result of sectionally induced thermal effects promoting the creation of concentration gradient. As such, aggregation is generally associated with these processes, which are referred to as Aggregation-Caused Quenching (ACQ).

To properly explain the origin of the fluorescence quenching, oscillations of molecules need to be analyzed. In diluted solutions, the fluorophore can be treated as an isolated single

moiety, as its molecules are separated from one another by the solvent molecules. At this point, they can be regarded as single dipoles or oscillators. However, when the concentration is increased, the corresponding distance decreases. This in turn facilitates the electrostatic interactions between each oscillator. In the aggregates, which can be treated as neutral particles, electron and hole pairs are localized in the same molecular site. Hence, they are referred to as strongly bound excitons. In 1964 Alexander Davydov has proposed that the formation of the molecular excitons is responsible for the changes in photophysical properties.[21] According to this paper, aggregates can be viewed as highly ordered structures of constituting molecules, which couple with one another in a purely electrostatic manner, with no prominent overlapping of their electronic density. Michael Kasha proposed that the excitons can be represented as a dimer of two aromatic molecules (monomers).[22–24]

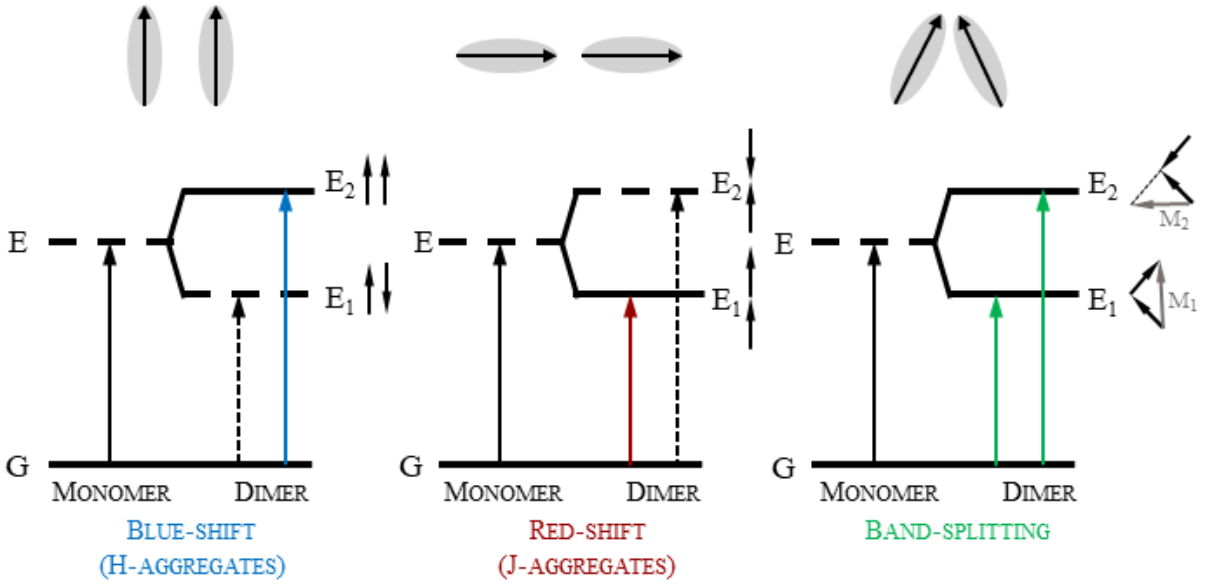

Figure 2.2.1. *The Kasha model: exciton band structure in dimers of various geometries.*[22,23]

In the Kasha model, presented in Figure 2.2.1., resonances between excited electron states are shown, with the assumption that the transition dipoles of monomers are oriented along their long axes. Their interaction promotes the splitting of non-degenerated states into two separate levels. The angle between the transition dipoles is a deciding factor in whether the higher or lower energy levels are involved, as it determines attractive/repulsive interactions. The transition to upper levels (E_2) can occur for the dipoles with opposing orientations (head-to-head: H-aggregates), enabling absorption of higher energy by the dimer in comparison to the monomer, resulting in a blue-shift of the emission (if observed). Theoretically, the fluorescence from this state to the ground state is forbidden as the emissive level is of lower energy, resulting

in an emission quenching. Additionally, when the vector sum of dipole moments is zero, the lower level (E_1) is forbidden and thus cannot be excited. The H-aggregation is common for planar molecules, which are prone to π-π-stacking. However, highly emissive H-aggregates were observed,[25,26] in discrepancy to the theoretically forbidden transitions. One of the possible explanations is based on vibrational modes contributions, which broaden the absorption and emission bands.[27]

When the molecules aggregate in head-to-tail geometry (J-aggregates) then the situation is reversed, as this arrangement of dipole moments promotes their attraction. The lower energy level (E_1) can be accessed by electronic excitation, enabling fluorescence. Therefore, a red-shifted and much narrower emission is detected. Cyanines or other polymethine dyes aggregate in this manner.[28] Besides the seemingly perfect geometries of J- and H-aggregates, an oblique dimer can also be formed. In this case, dipoles can arrange in-phase in both energy levels (E_1 and E_2) enabling their electronic excitation. Hence, in dimers splitting into two levels is observed, seen in absorption/emission spectra as double-bands: red- and blue-shifted, for each of the energy levels.

The aggregation itself is dependent on many factors, besides the structure of the fluorophore. Polarity or viscosity of the solvent, the temperature, or even air humidity influence this process. In addition, the aggregation itself is time-dependent, which influences experimental procedures. Of course, aggregates of higher order can form, as in the example of polymers.[29,30] The interpretation of the mechanisms in such cases is even more difficult. As presented for the J-dimers, aggregation does not always lead to emission quenching. Actually, in 2001 Ben Zhong Tang and his group discovered a phenomenon: *Aggregation-Induced Emission* (AIE).[31,32] They observed during the preparation of the thin-layer chromatography plate that the silole molecules are strongly emissive when aggregated, but non-luminescent in the diluted solutions (see Figure 2.2.2.). This discovery changed the direction of the research at the time: instead of engineering the molecules in such a way so that they cannot aggregate (for example by functionalization with polar hydrophilic groups or bulky cyclic units), a new concept in the fluorophore structures was introduced. Additionally, it highly broadened the range of possible applications: where aggregation was previously detrimental, it turned out that it could also be

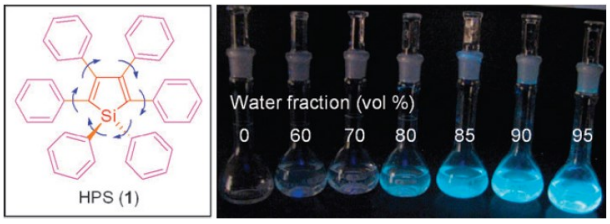

Figure 2.2.2. *The chemical structure of the hexaphenylsilole (HPS) and its acetonitrile/water mixtures.*[31]

useful, for example in the creation of turn-on/off sensors. As such, the fluorophores which undergo this beneficial process can be referred to as AIEgens.

The possible mechanisms of AIE surpass the obvious J-aggregate formation. In order to find the origin of the appearance of the highly-emissive species, Tang's group investigated other silole derivatives. They noted that these molecules gradually aggregate when measured in good-solvent/bad-solvent mixtures, as the appearance of the latter promotes precipitation. As most organic fluorophores are hydrophobic, water is often used as the medium with poor solubility. When its content is increased, the emission intensity raises alongside the bathochromic shift. A slight broadening of the absorption spectra was noted, which was contributed to the Mie scattering effect on the aggregated siloles.[33,34] J-aggregates formation (JAF), *cis-trans* isomerization, ESIPT, or twisted intramolecular charge transfer (TICT) were investigated as possible origins of the emission enhancement, however, they were not fully consistent with the experimental results. Finally, it was decided that molecular motions, or rather lack thereof, are responsible for the AIE phenomena.

It turns out, that the HPS molecule is non-emissive in dilute solutions due to phenyl groups connected to the silole core, which makes it very conformationally flexible. The separation of the fluorophore species by the solvent molecule enables the rotation of each phenyl moiety around the single bond. These motions consume excitation energy, preventing the fluorescence from occurring. However, when aggregated, HPS molecules cannot arrange through π-π stacking, restricting the rotations simply by the close physical position in relation to one another. Thus, the non-radiative decay is blocked, which facilitates the radiative processes. This effect was named *Restriction of Intramolecular Rotation* (RIR).

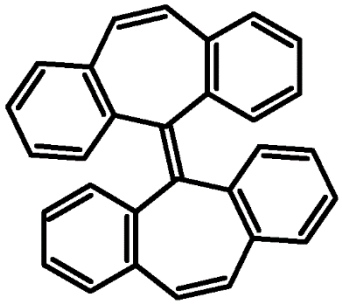

Figure 2.2.3. *Structure of THBA.*

Of course, not all AIEgens have HPS-structure. A tetrabenzoheptafulvalene (THBA) can be presented as a prime example: this molecule has no rotatable units (see Figure 2.2.3.), thus RIR cannot be responsible for the AIE effect which was observed.[35] It was proved that vibrational motions of the phenyl rings are sufficiently blocked upon aggregation, giving rise to a new mechanism: *Restriction of Intramolecular Vibration* (RIV). Further experiments[36,37] proved that it is possible to design a molecule, where both RIV and RIR take place. In such cases, the induced emission is a result of *Restriction of Intramolecular Motions* (RIM). For Schiff bases (a subgroup of imines), AIE experiments were

also conducted successfully,[38–40] nonetheless in some cases the emission enhancement was due to hydrolysis with water, rather than the restriction of the motion itself.[41]

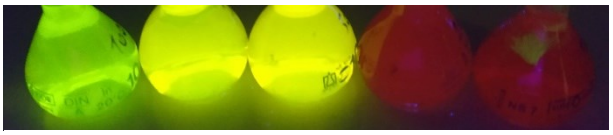

Figure 2.2.4. *An AIEE molecule in THF/water mixtures under the UV light. The increase in water concentration goes from left to right (0, 25, 50, 75 and 99%).*

The described AIE mechanisms also play a significant role in molecules, which are emissive in solutions in the first place. When the aggregation results in an increase of the fluorescence intensity, in this case, the use of *Aggregation-Induced Emission Enhancement* (AIEE) is a proper term. Additionally, in some cases the increase in emission intensity is only up to a certain good-solvent/bad-solvent ratio: ACQ and AIE/AIEE constantly compete with one another. An example of this behavior is depicted in Figure 2.2.4. Nevertheless, the aggregation of organic molecules enormously influences their properties, enabling the use of AIEgens in various applications, both industrial and academic. Application in medicine as biosensors[42–44] or bioimaging stains[45–47] were realized, as well as theranostic probes.[48,49] Chemical sensing of specific ions,[50,51] harmful species,[52–54] gases,[55,56] or even exposives[57,58] was achieved. Specific conditions needed to observe emission can be designed for morphology visualization,[59,60] or for fingerprint imaging,[61] crucial in forensic science. More commercial and useful in everyday life OLED devices can be manufactured,[62,63] OFETs,[64] waveguides,[65] or liquid crystal displays.[66,67]

2.3. Excited-State Intramolecular Proton Transfer

Excited-State Intramolecular Proton Transfer (ESIPT) compounds constitute one of the most fascinating groups of organic fluorophores, the origins of which can be dated to the 1950s and pioneer works by Albert Weller on salicylic acid and its methyl derivative.[68,69] He observed that both molecules undergo tautomerization from the normal form as a result of the excitation (see Figure 2.3.1.), upon which a red-shifted emission is seen. The origin of such conformational changes lies in the specific structure of these fluorophores, which amounts to a presence of an intramolecular hydrogen bond between the donor (-OH) and the acceptor groups, in this case a carbonyl one (- C = O). In the ground state, this form is marked as Normal. The photoexcitation leads to a redistribution of electric charges, increasing the proton-donor acidity and the acceptor basicity, and as such can be deemed as a charge-transfer process. Hence, very fast proton transfer between two donor-acceptor moieties (ESIPT) takes place,

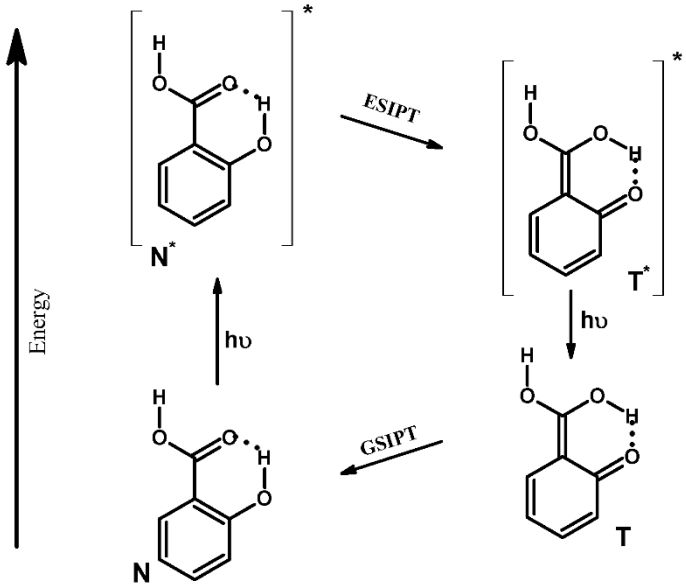

Figure 2.3.1. *ESIPT photocycle of salicylic acid. Normal and Tautomeric forms are denoted by N and T, respectively. The dotted lines mark hydrogen bonds.*

resulting in the formation of a species with a different electronic structure (excited Tautomer), followed by radiative decay to the ground-state. The observed emission is of lower energy, thus shifted to longer wavelengths. Additionally, different absorbing (N) and emitting (T) species exclude detrimental self-reabsorption. The T form is of higher energy than N, which promotes a reverse tautomerization (Ground-State Intramolecular Proton Transfer, GSIPT) and non-radiative relaxation. All these processes form a closed four-level photocycle: N → N^* → T^* → T → N. Due to ESIPT, these specific molecules are characterized by large Stokes' shifts, even exceeding 200 nm. Besides the relaxation by fluorescence, the excited tautomer isomerization to *trans*-moiety, which is nonfluorescent. This transformation is rarely encountered, as an energy barrier needs to be crossed, nonetheless it's possible.[70–72] Second non-radiative deactivation channel exists: an intersystem crossing to the excited singlet state of the tautomer, which can be discriminated from *cis-trans* isomerization by time-resolved spectroscopy.[73–76]

The photophysical properties of the ESIPTs, due to inherent hydrogen bond, are dependent on the environmental conditions, such as solvent, polarity, pH, humidity, etc. For example, in polar media a rotamerization of the Normal form can take place, as observed for 2-(2'-hydroxyphenyl)benzazole (HBX) derivatives (Figure 2.3.2.). The ground state Normal form is the enol (E) specie, which is stable in non-polar or hydrocarbon solvents due to relatively high H-bonding energy. Upon excitation, a single emission band is observed (from Tautomer: excited keto form). However, rotamerization can take place in solvents with increased polarity, depleting the

HBO: X = O
HBI: X = NH
HBT X = S

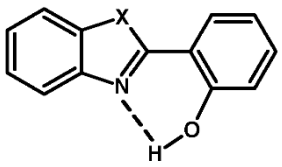

Enol form (E)

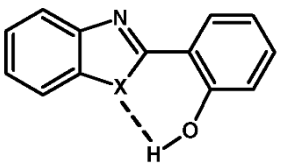

Rotamer (E')

*Figure **2.3.2.** Enol and rotamer forms of HBX.*

E population in exchange for E' molecules, in which a hydroxyl group hydrogen is bonded to the heteroatom instead of the nitrogen. Thus, the former species are more stable in a polar environment due to the higher dipole moment. This phenomenon can be easily distinguished in the emission spectra: through a band located at shorter wavelengths forms. When the equilibrium between E and E' forms exists, then a dual-emission is realized. Modification of the HBX structure allows to engineer molecules prone to rotamerization even in non-polar solvents,[77] due to a decrease in the relative energy difference of two rotamers. In addition, the proton-acceptor and donor groups can interact with the solvent molecules and form an intermolecular hydrogen bond, instead of with one another. Such occurrence is observed in polar or protic solvents, promoting E^* emission at the cost of depleted excited keto species, for example in 3-hydroxyflavone (3-HF).[78] Dual-emission can be realized simply by a change of the solvent, giving rise to ratiometric polarity probes. On the other hand, the hampering of ESIPT in the solid-state does not occur, as the solvent molecules are absent. Therefore the observed emission comes from excited keto species.[78]

As the ESIPT mechanism and its dependence on environmental conditions have been studied exclusively, another process was discovered. The intramolecular hydrogen bond, depending on its strength, can be disrupted due to changes in the pH. Group of Rodriguez-Prieto have thoroughly investigated this matter in 1996, on the example of 2-(2'-hydroxyphenyl)benzimidazole (HBI).[79] As it turns out, HBI can reach four different conformations, which are depicted in Figure 2.3.3. In neutral pH, the ESIPT photocycle is realized in a straightforward 4-level manner: with one absorption maximum (enol form, 320 nm) and dual emission (E^* - 350 nm, K^* - 447 nm), which is due to an investigation in aqueous solution and partial frustration of the ESIPT. The absorption spectra were shifted towards longer wavelengths in more acidic solutions as a result of the protonation of the acceptor group. Hence, no proton transfer could occur in the excited state. Interestingly, besides the blue-shifted band (370 nm), a second band was observed: of almost identical shape and position as that of excited keto species. As water molecules were present in the solution, this phenomenon was ascribed to excited-state deprotonation of the protonated form due to temporarily increased acidity of the phenolic group in the excited state. On to contrary, an increase in pH gave rise to a new red-shifted absorption band at 350 nm, which upon excitation allowed to observe a blue-shifted (418 nm) emission due to consecutive deprotonation of the enol species. Hence, one can design a triple-emissive system based on a single ESIPT molecule through control of the prototropic solvents.

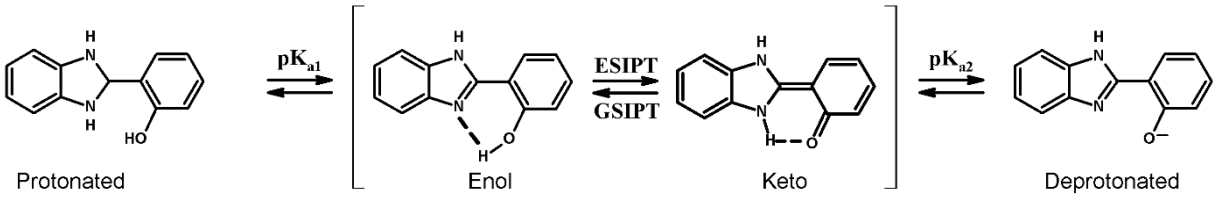

Figure 2.3.3. *Possible forms of 2-(2'-hydroxyphenyl)benzimidazole (HBI).*[79]

Intramolecular Charge Transfer is a phenomenon that was described previously. However, it can be applied to ESIPT molecules, functionalized with electron-withdrawing and accepting groups. As such the transient alternations can be enhanced, leading to Excited-State Intramolecular Charge Transfer (ESICT). In such a case, both proton and charge transfer take place upon photoexcitation. Depending on the rate of each reaction, either can occur prior to the other. For instance, an introduction of *p*-N,N-dimethylamine to 3-hydroxyflavone made it possible to achieve a dual-state emitter with i) polarity-dependent emission band related to excited charge-transfer state, and ii) red-shifted independent K^*.[80,81]

The many intricacies of ESIPT photocycle bring about the possibility to finely tune the absorption and emission properties. Various studies on substitution effects were conducted, proving that even minimalistic change in the structure significantly impacts the photophysical parameters of the molecule, such as methyl or methoxy substitution of salicylic acid which influences whether dimers can form in solutions.[82,83] The 2-(2'-hydroxyphenyl)benzoxazoles were modified with electron-donating and withdrawing moieties of various strengths by Park Soo Young's group.[84] They have found that stronger acceptors shift the fluorescence towards longer wavelengths, while the donors have the opposite effect, which was further confirmed by semi-empirical molecular orbitals calculations. Flor Rodriguez-Prieto's group investigated σ-hydroxyarylbenzazoles through time-resolved and steady-state spectroscopy.[85] They confirmed that the introduction of electron-donors and acceptors enables tailoring of non- and radiative decays. Moreover, these conformational changes determine the ESIPTs sensitivity toward temperature and viscosity. More recently, Koji Araki has proven that solid-state emission can also be finely tuned by a change of the surrounding matrix.[86] 2-(2'-hydroxyphenyl)imidazopyridine was used as a dopant in guest-host thin films. The ESIPT phenomena could be turned on/off due to interactions of the dye with various investigated polymeric matrices, leading to single or dual-emission profiles. On the other hand, fluorescence quenching of ESIPTs solutions was quite often encountered due to Twisted Intramolecular Charge Transfer (TICT),[87,88] and it was later found that the insertion of the dyes in the rigid matrix limits the rotation and enhances overall fluorescence. A similar effect can be achieved

with substitution with rigid π-conjugated moieties, which at the same time allows for fine-tuning of the emission and lowers the probability of crossing the conical intersection in the excited state.[89–91]

While the correct interpretation of the photophysical properties of ESIPTs remains challenging to this day, it was made easier by the evolution of time-resolved measurements (for example transient absorption) or theoretical calculations. Due to their complex and environment-dependent photophysical properties, ESIPT dyes have found various applications. Besides the examples that were quoted earlier, various sensors were realized, from ions,[92–94] small molecules,[95–97] explosives,[98] or bioprobes.[99–101] Electrochromic modulators,[102] or biomembranes,[103] or drug release probes[104,105] were constructed. ESIPTs have found their use in industrial and commercial applications too, for example in optoelectronic devices such as OLEDs,[106–108] and lasers. The latter, however, will be thoroughly described in the next subchapters, as it is very relevant to the topic of this dissertation.

3. *Light amplification*

This last introductory chapter contains the description of light amplification and related phenomena, such as stimulated emission. Conditions that need to be filled for the lasing action to occur will be presented, as well as the conventional laser construction. Different types of light amplification that can be realized in organic materials will be described, such as Amplified Spontaneous Emission, and Random or Distributed Feedback Lasing. This section ends with an overview of organic compounds which have found their application in light amplification.

3.1. Spontaneous and stimulated emission

While the photoluminescence was described in detail in *Chapter 1*, at this point it should be noted that the radiative processes can be generated in two possible ways. First, *spontaneous* (fluorescence) occurs through a decay from a higher energy state to a ground state ($E_2 \rightarrow E_1$, see Figure 3.1.1.). As a result, the emitted photon propagates in a random direction. Its frequency can be easily calculated (eq. 3.1.), with *h* – the Planck's constant.

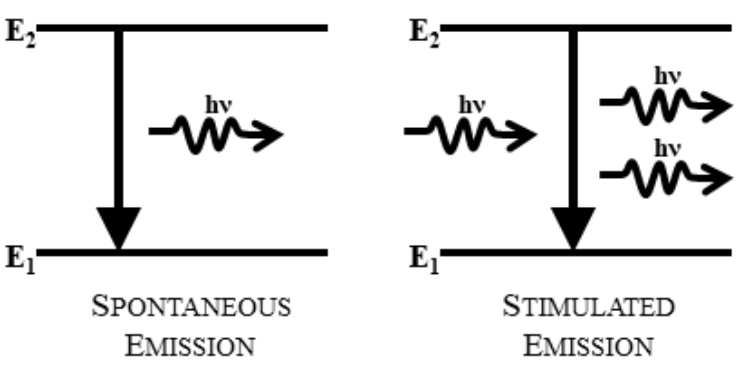

Figure 3.1.1. *Schematic diagram of spontaneous and stimulated emission.*

$$\nu_0 = \frac{E_2 - E_1}{h} \tag{3.1.}$$

As absorption is the opposite process to emission ($E_1 \rightarrow E_2$), its probability B_{12} is finite and can be expressed by:

$$\frac{dN_1}{dt} = -B_{12} N_1 U(\nu) \tag{3.2.}$$

Where: N_1 is the number of atoms/molecules per unit volume (population) at the E_1 level and time *t* (s), and U(ν) – density of incident energy. Hence, B_{12} ($m^3J^{-1}s^{-2}$) is an Einstein coefficient,[109] which states the probability of absorption and excitation from level 1 to 2 per second and per frequency. The probability of the opposite process (A_{21}, s^{-1}), the spontaneous

emission $E_2 \rightarrow E_1$, is defined by the proportional relation of the population at a higher energy level (N_2) and its decay rate:

$$\frac{dN_2}{dt} = -A_{21}N_2 \tag{3.3.}$$

The minus sign was applied to balance the negative time derivative, as the probability is positive. The inversion of A_{21} gives the spontaneous emission lifetime, which for organic materials corresponds to values of 10^{-9} – 10^{-7} s:

$$\tau_{SpE} = \frac{1}{A_{21}} \tag{3.4.}$$

Stimulated emission, however, occurs when a system is in an excited state (E_2). If interaction with a photon of frequency ν equal to the frequency of spontaneous emission occurs, then the transition $E_2 \rightarrow E_1$ is forced (Figure 3.1.1.), observed by emission of the photon with the same parameters as the incident one: it propagates in the same direction, with the same frequency and polarization. This behavior shows a fundamental difference between spontaneous and stimulated emission, as for the former there is no phase relation between photons emitted from neighboring molecules. This phenomenon, like absorption, occurs as a result of applied stimuli, thus it's dependent on the intensity of incident light U(ν):

$$\frac{dN_2}{dt} = -B_{21}N_2U(\nu) \tag{3.5.}$$

As stated by Einstein, from the thermodynamical point of view, stimulated emission can be seen as negative absorption if two involved levels (E_1 and E_2) are non-degenerate:

$$B_{12} = B_{21} = B \tag{3.6.}$$

Degeneration of those two levels, however, does not make this equation invalid. If the number of states *g* (corresponding to the level's degeneracy) are taken into account, then:

$$g_1B_{12} = g_2B_{21} \tag{3.7.}$$

If we consider thermodynamic equilibrium (eq. 3.8.), then take into account Boltzmann statistics and Planck's law of black-body thermal radiation, then the ratio of Einstein coefficients at room temperature for spontaneous and stimulated emission can be found (eq. 3.9).[110,111]

$$U(\nu)N_1B_{12} = N_2A_{21} + U(\nu)N_2B_{21} \tag{3.8.}$$

$$\frac{A_{21}}{B_{21}} = \frac{8\pi h\nu^3}{c^3} \tag{3.9.}$$

While no external stimulus is present, then the population at a higher level is smaller than at the ground state: $N_2 < N_1$.

3.2. Laser

The previous considerations are continued in this subsection to explain what a Laser is. The name is an acronym for *Light Amplification by Stimulated Emission of Radiation*. The first construction, which can be deemed as a laser, was built by Theodore Maiman in 1960 on a ruby crystal.[112] In principle, if certain conditions are met, the stimulated emission of light can be amplified resulting in laser emission.

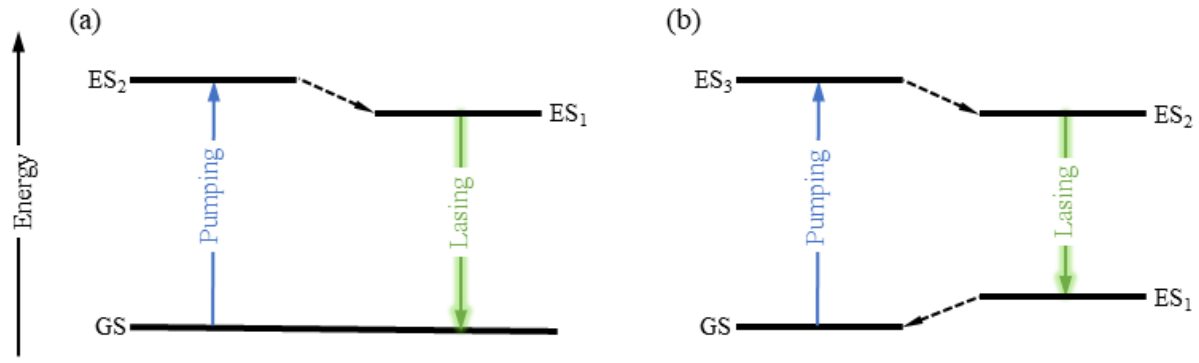

Figure 3.2.1. *Graphical representation of (a) three- and (b) four-level lasers. The dashed arrows mark non-radiative decay.*

Three major components are required for the laser to function properly, that is, as an oscillator: i) an efficient pump, which is used to excite ii) active material, emission of which is then amplified in the designed iii) resonator. The first component can be electrical (e.g. electric current, electrical discharge), optical (flash or arc lamps, diodes, other laser), or even by chemical reaction. Its role is to provide the necessary energy to obtain population inversion ($N_2 > N_1$) in the active medium, which is crucial in terms of light amplification. In such a case, stimulated emission is favored over absorption, even though both processes have the same probability. Essentially, the material cannot amplify and simply acts as an absorber when $N_2 < N_1$, as described by Boltzmann's law at the thermodynamic equilibrium:

$$\frac{N_2}{N_1} = exp\frac{-(E_2-E_1)}{kT} \tag{3.10.}$$

where k – Boltzmann's constant and T – the temperature. If the excited-state lifetimes are long enough and the pumping source is efficient (the upper level is pumped more rapidly than the lower one), then the population at the ground state is lower than at the higher energy levels and a non-equilibrium condition for amplification is met. It's impossible to create and maintain population inversion in a two-level system, as the stimulated emission and absorption would compensate one another. Hence, other solutions were found. The most common ones consist of either three or four energy states, as depicted in Figure 3.2.1a. In the first setup, the active material atoms/molecules are elevated from the ground state to a higher excited level (ES_2), after fast non-radiative decay takes place to another metastable level (ES_1, with energy higher than GS, but lower than ES_2). Laser action can occur when population inversion $N_{ES1} > N_{GS}$ is reached. Stimulated emission taking place between those two levels is very rapid: a single emitted photon forces emission from another excited molecule, *etc*.

Table 3.2.1. *Essential parameters of organic active materials.*

Parameter	**Explanation**
Quantum yields of emission	The higher, the better; especially in solid-state as it overcomes concentration-related quenching
Photostability	Should be good against both pump photons (which can facilitate undesirable photoreactions) and oxygen; the latter facilitates photobleaching
Stokes shift	Large enough to prevent self-reabsorption of the emission, but not too high to promote conversion into heat
Absorption and stimulated emission cross-section	High absorption and stimulated emission cross-sections promote efficient lasing due to the conversion of the pump into emitted light

The population inversion is more easily met in a four-level system (Figure 3.2.1b.), in which pumping leads to an even higher energy state (ES_3). Similarly as in the previous system, non-radiative processes lead to the partial release of energy. As the pumping does not affect ES_1, an instant population inversion is formed and an avalanche photon emission can take place between ES_2 and ES_1 states. The cycle is closed by non-radiative relaxation to the ground state, enabling continuous operation. However, if population inversion is obtained between ES_1 and

GS, then secondary lasing action can occur. It should be noted that population inversion itself does not guarantee light amplification. Hence, a good organic laser material should fulfill various parameters, which are listed in Table 3.2.1. along with the reasoning.

The last essential element for the lasing action to occur is the resonator. It provides a positive feedback loop and determines the resonant frequencies of the oscillating laser field, which is seen in the emission spectrum as characteristic narrow peaks of longitudinal modes. The cavity is responsible for filtering the output beam and its spatial profile, as the only modes that can be amplified are those which are self-replicating in the structure in a closed loop. Hence, it defines the transverse pattern of the output laser beam. The simplest cavity is composed of two mirrors, at a given distance L, where the spontaneously emitted photons can travel back and forth, forming a standing wave. The resonance of oscillations occurs when the resonator length is an integer of half-wavelengths:

$$L = \frac{m\lambda}{2} \tag{3.11.}$$

The resonant frequencies are equal to:

$$\nu = \frac{mc}{2L} \tag{3.12.}$$

Where m – a positive integer, c – speed of light. Photons of different frequencies are not amplified. The (3.12.) equation also provides the frequency difference of two consecutive modes that can be obtained in a resonator of a given length:

$$\Delta\nu = \frac{c}{2L} \tag{3.13.}$$

Both (3.11.) and (3.12.) equations show, that there exists a finite number of modes, which can be obtained from the resonator. They are further limited by the spontaneous emission – it's not possible to amplify nonexistent light.

While many geometries of resonators can be realized, the most common way of verifying whether the material has light amplifying properties is to fabricate planar waveguides, for example thin films. Such structures confine light due to total internal reflection phenomena, promoted by a higher refractive index of the material than that of the surroundings, substrate included. Thus, light can be guided within. Such structure, while not a resonator itself, can be sandwiched in between two mirrors, which provide feedback for the lasing action. Obtained systems are named as Vertical Cavity Surface Emitting Lasers (VCSELs). A different type of

cavity can be realized by spatial modification of the surface of the waveguide, for example in Distributed Feedback, to which a separate subchapter is given.

All three laser components influence the final properties of emitted light. However, a few general characteristics can be distinguished. The laser beam is:

1) Monochromatic – the emitted line presents itself as a very sharp peak in the spectrum, much more narrow than spontaneous emission;
2) Directional;
3) Coherent – as light amplification is a result of stimulated emission, then emitted photons maintain polarization, phase and frequency. Thus, they are indistinguishable;
4) Bright.

The lasers can be characterized not only by the wavelengths of obtained emission but also by the parameters of their operation. The first is a gain factor G, which describes the amplification of light in the active medium as a simple ratio of the intensities of the output and incident light. This parameter is related to the gain coefficient (g), the length of active material (L), and the laser intensity (I_{las}):

$$G = e^{gLI_{las}} \tag{3.14.}$$

Another important parameter is the laser threshold, defined as the value of pumping energy upon which the gain balances the losses (for example absorption or scattering). When this value is exceeded, a laser action occurs. The intensity of the emitted light is linearly dependent on the pumping energy. Generally speaking, the higher gain and lower the threshold, the better.

3.3. Amplified Spontaneous Emission

Amplified spontaneous emission (ASE) phenomena can occur in materials, in which a waveguiding effect can take place. As such, upon excitation, spontaneous emission is observed. When it propagates in the active material and the gain overcomes losses, the population inversion is achieved and the fluorescence is amplified, resulting in a significant narrowing of the spectrum. Since no external resonators are used, the ASE is often referred to as “mirrorless lasing”. The emission narrowing is a result of preferential amplification of the photons from the maximum of broadband fluorescence spectra. While ASE emission is usually of higher full width at half maximum values than lasing, it is often used to determine whether

a given material is capable of light amplification. It should be clearly stated, however, that the ASE itself is not lasing. While some properties are maintained, e.g. polarization or directionality of the output beam, no resonator is present, and as such cannot significantly influence the observed emission.

The measurement of ASE in thin films enables the determination of the net gain coefficient with the use of the universal Variable Stripe Length technique.[113,114] When a pumping beam is in an almost one-dimensional stripe shape (height << length, l) and the longer dimension can be precisely controlled, the VSL enables the extraction of the net gain parameter (γ, cm^{-1}) by processing both emitted light (I) and the applied stripe length (l, cm), as the light amplification occurs along the axis of the stripe:

$$I = \frac{I_0}{\gamma}(e^{\gamma l} - 1) \tag{3.15.}$$

The obtained parameter is a modal value, as it includes both optical gain (g) and the losses of the waveguide (α, including self-reabsorption and waveguide losses):

$$\gamma = g - \alpha \tag{3.16.}$$

As emission extraction is dependent on the refractive index of both thin film and the substrate, also the layer thickness influences the determined value. Additionally, when high optical gains are involved, the gain saturation occurs at much shorter stripe lengths. Hence, all these factors need to be taken into consideration during the measurements.

3.4. Random Laser

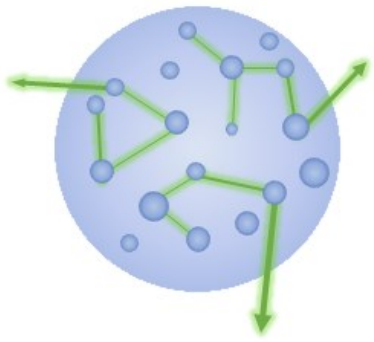

***Figure 3.4.1**. Multiple light scattering in random laser.*

Organic materials have a major advantage in comparison to inorganic semiconductors: their processing is relatively simple. As such, various resonator geometries can be realized, both in bulk (like linear Fabry-Perot cavity) or on a macroscopic scale. The former can be composed of a dye-doped polymer block placed in between two mirrors, while the latter as electrospun polymeric nanofibers or microfabricated ring resonators. Of particular interest for this dissertation are spontaneously formed cavities, realized as organic nano- and

microcrystals dispersed in a polymer matrix. These structures can form during the fabrication of the sample for light amplification measurements. As described in previous subchapters, these sites can act as scattering centers, which brings additional losses to the lasing action and is generally considered detrimental as the threshold increases.

However, there exists a very specific type of lasing, in which elastic scattering plays a constructive role. It is deemed as Random Lasing (theoretically introduced by Wiersma and Lagendijk in 1995),[115] where the scattering centers elongate the path length for the photons, which in turn reinforces the light amplification, and provide the feedback for the lasing action. These factors are true when i) the light is confined in the structure long enough to be amplified, ii) the pumping energy is high enough for the gain to overcome total losses, corresponding to the laser threshold. The scattered light thus propagates through the active medium (see Figure 3.4.1.), is scattered on another irregularity, and travels further until it meets another disruption. Hence, light travels in multiple random closed-loop paths, observed as various sharp peaks in the emission spectrum. The distance which the photon travels in the sample can be parametrized. The length between two consecutive scattering centers is the *scattering* mean free path l_s (eq. 3.17.), and the distance before propagation is randomized is a *transport* mean free path l_t.

$$l_s = \frac{1}{n_s \sigma_s} \tag{3.17}$$

Where n_s – the number of scatterers per volume, σ – scattering cross-section. When the average of scattering angle Θ is taken into account, a relation between the two is found:[116]

$$l_t = \frac{l_s}{1 - \langle cos\Theta \rangle} \tag{3.18}$$

The dimensions of scattering centers determine the relationship presented in eq. (3.18.). For the bigger particles the scattering is of Mie type, with cosΘ ≈ 0.5, and for Rayleigh cosΘ = 0. When the centers are of different dimensions, those two types can be present at the same time. Hence, the correct interpretation is very difficult, as one should also take into account the transport regimes: ballistic, diffusive, and localization. Moreover, as the scattering centers are placed randomly in the medium, pumping may lead to the observation of different spectra with different modes depending on the area of illumination. Even with constant excitation energy fluctuations of output intensity occur, as random lasing is a chaotic phenomenon. Based on the feedback mechanism, random lasers can be classified into two

categories: incoherent (intensity/energy feedback), or coherent (field/amplitude feedback). The first type is characterized by an intense and quite broad signal, where no significant modes can be distinguished, as no localization processes take place. On the other hand, when scattered photons interfere with one another and form a standing wave, the modes are clearly identified as very sharp and narrow peaks, positioned at equal distances to one another, as for coherent RL. To find the dimensions of resonators responsible for these modes a Power Fourier Transform (PFT) of the spectra can be performed. Additionally, if PFTs are calculated for many different spectrums and then averaged, the corresponding harmonics are enhanced. However, if the spectra are first averaged, and then the PFT is performed, then no resonator length can be found.

While the first Random Laser was composed of Rhodamine 640 solution, to which titanium dioxide nanoparticles were added,[117] it can also be realized in solid-state films without added scatterers. In this case, the feedback can be provided through any unevenness in the sample, e.g. thickness differences, scratches, dye aggregates, etc. This specific type of lasing can be also realized in clusters of nanoparticles, dye-doped liquid crystals, or even doped opals.

3.5. Distributed Feedback

As already mentioned, slab waveguides are very convenient structures for light amplification. Resonators can be realized as diffraction gratings in the film. Such structure, of a given period Λ, provides feedback for the lasing action through Bragg scattering, giving rise to mirrorless Distributed Feedback (DFB) lasers. The cavity itself can be realized in one-, two- or three dimensions. The first type will be described in detail in this section.

The most common 1D resonator consists of a planar waveguide (active material) deposited on a substrate with a diffraction grating (see Figure 3.5.1.). The first element provides gain and light guiding. Upon pumping, emission induced in the waveguide is scattered on the present periodic modulation. The period of the grating (Λ) dictates the wavelengths of light which can

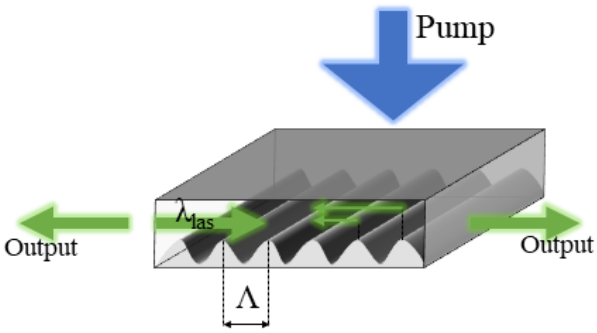

Figure 3.5.1. *Schematic structure of DFB laser at m = 2.*

interfere constructively, thus creating a counterpropagating wave, with the conditions for resonance determined by the well-known Bragg condition (eq. 3.19):

$$2n_{eff}\Lambda = m\lambda_{las} \tag{3.19.}$$

where m – order of grating, λ_{las} – wavelength of the guided mode, n_{eff} – the effective refractive index, which takes into account the refractive indices of the waveguide, the substrate, and the closest surroundings (e.g. air). The given equation is a very close approximation since the wavelength that fully fits the condition cannot be propagated in the film, which in turn makes the recombination impossible. This wavelength is a "stopband", around which constructive interference can take place with a pair of wavelengths.[118] Nevertheless, the emitted laser line is very sharp, as only one mode can be amplified in such structure. Even though each groove in the periodic modulation can be referred to as a single resonator, light can propagate throughout the whole length of the waveguide, "hopping" from one cavity to another. Hence, the total resonator length is much bigger, which in turn significantly decreases the lasing threshold.

The coupling mechanism was first presented by K. Kogelnik and C. V. Shank in 1971 on the basis of Rhodamine 6G-doped gelatin film.[119] The periodic modulation present in this type of resonator promotes variations of the gain (α) and/or refractive index of the waveguide (n) in a z-direction:

$$\alpha(z) = \alpha + \alpha_1 cos\frac{2\pi}{\Lambda}z \tag{3.20.}$$

$$n(z) = n + n_1 cos\frac{2\pi}{\Lambda}z \tag{3.21.}$$

Where α_1 and n_1 are the amplitudes of gain and refractive index, respectively. Both parameters influence the optical feedback and, depending on the active material, one can be dominant, determining the laser emission. In a follow-up work in the same year, Kogelnik and Shank proposed a construction of a tunable DFB laser – the periodic modulation providing feedback was obtained with the use of two pumping beams, which were interfered in a Rhodamine 6G/ethanol dye cell.[120] The period of the interference pattern, and thus the wavelength of emitted light, was controlled by the angle Θ at which the beams interfered:

$$\lambda_{las} = \frac{n_{eff}\lambda_{pump}}{msin\Theta} \tag{3.22.}$$

This specific setup, now known as degenerated-two wave mixing (DTWM), enabled real-time continuous tuning of the emission, not only by a change in the angle but also through

a solvent – thus by the effective refractive index changes. Depending on the period, different wavelengths can be reflected from the waveguide. This, in turn, is strongly dependent on the order of diffraction:

For m = 1: $$2n_{eff}\Lambda = \lambda_{las} \quad (3.23.)$$

For m = 2: $$n_{eff}\Lambda = \lambda_{las} \quad (3.24.)$$

At the first order, the extraction of light is difficult due to the high confinement of the propagating waves. However, the constructive coupling is more efficient, which leads to significantly decreased threshold values. The second-order structures are of particular interest, as the light is diffracted in two directions: along the waveguide and perpendicularly to it. Hence, extraction of the laser light is easier. On the other hand, lasing thresholds are usually higher than for m = 1. Additionally, no matter the order of diffraction, any variations in the thickness of the film or other irregularities (for example microscopic-sized crystals) disrupt the local periodicity. If the number of these factors is large, then in addition other additional modes may emerge, while the DFB laser line can be broadened. Hence, particular care is given to the preparation of these structures. Nonetheless, DFB lasers are a widely investigated topic since they can be compact, which in turn enables their application in integrated optical devices, for example in lab-on-chip structures.

3.6. Organic chromophores

Organic lasers date almost as far back, as the laser itself. The first successful implementations were realized at roughly the same time in 1966 by two separate groups: i) J. R. Lankard and P. P. Sorokin,[121] who reported stimulated emission from chloro-aluminum phthalocyanine molecules in ethanol, and ii) F.P. Schafer, W. Schmidt, and J. Volze.[122] The latter investigated five other cyanine derivatives in various solvents. Solid-state organic lasing was realized just a year later, in 1967, by B. H. Soffer and B. B. McFarland,[123] who introduced the term *Solid-State Dye Lasers* (SSDL). Poly(methyl methacrylate) was used as a matrix for rhodamine 6G. The term *dye* at the time was used to label highly-luminescent π-conjugated compounds.[124] These molecules are interesting in terms of their optical and electrical properties, as the present non-saturated double and triple bonds in a planar segment make them behave like semiconductors, with the overlap of the π orbitals promoting the delocalization of the electrons. Hence, since the 1960s organic lasers have been thoroughly investigated, operating in solutions

or as guest-host solid-state systems, as their easily processed tunability and large stimulated emission cross-section (the typical values of $\sigma_{abs} \sim 10^{-15}$ cm^2)[124] are very beneficial. Moreover, the organic material can be precisely shaped in order to serve both as an active medium and resonator. As described in section 3.2, the general conditions to obtain lasing action from organic molecules include strong absorption at the pump wavelength with minimized losses due to reabsorption promotes effective lasing action. High quantum yields of emission are beneficial, along with low non-radiative decay rates. Unfortunately, as organic compounds can undergo photoinduced reactions, their chemical stability is crucial in the pumping conditions. Moreover, in recent years solid-state predominates the application of solutions, making it crucial to prevent self-quenching due to decreased distances between the dye molecules. As such AIE/AIEE affinity and good solid-state emissive properties are valuable. This in turn constructively influences the photostability of organic lasers: generally higher dye loadings lower the photobleaching.

The range of organic compounds, which can be used for light amplification, is truly broad. Hence, only a few most important ones can be briefly presented in this section. The first group is the xanthene family, with the flagship dyes: the rhodamines. Their core consists of two benzenes fused by a pyran ring. Their emission, depending on the substitution, ranges from green to red region. These compounds are often water-soluble, which enables their bioapplication. Moreover, they are characterized by rather high lasing efficiency and photostability. The second important laser dye family consists of coumarins, which emit in the rather high energy region of the visible spectra: from violet to green. Generally, they are formed as a benzene connected to the pyrone ring and further substituted, which determines the photophysical properties of the coumarins. Their efficiency is relatively high, however they suffer from poor stability in comparison to xanthenes. The pyrromethene derivatives, on the other hand, form the group emissive in the orange-red-near-infrared region. These molecules are very rigid due to their planar structure: methylene and difluoroboron groups connect two pyrroles. In a similar way to the xanthenes, their efficiency is rather high, while maintaining good stability. However, both coumarins and pyrromethenes are usually soluble only in organic solvents. Besides these three families, also cyanines, rylenes, or thiophene based dyes can be highlighted as a laser medium. Nevertheless, all mentioned molecules can be used for the realization of the lasing action. The flexibility and ease of processing enabled their fabrication in various geometries, from solutions, through large single crystals, or polymeric thin films. On the other hand, their chemical structure somewhat dictates the range of emissions that can be

obtained, as described previously. Besides the structure-property relationship, there are other effects that need to be taken into consideration when the application of the dye as a laser medium in a certain wavelength range. Ultraviolet and infrared organic lasers are the most difficult to realize, with the former due to the need to apply high-energy pumping sources, which in turn promotes increased photodegradation as the risk of direct bond breaking and the creation of radicals is higher. However, these obstacles were overcome for example in spiro-derivatives[125] and silafluorenes.[126] Shifting of the emission to longer wavelengths, on the other hand, is difficult due to an increased probability of non-radiative decays which correspond to a decrease in the energy difference of HOMO-LUMO levels. Nonetheless, organic compounds have also found their application as lasers emitting in the infrared region, even up to 1.3 μm.[127]

The previously described ESIPT group is of particular interest when it comes to light amplification, as these molecules are characterized by beneficial large Stokes shifts. Additionally, these compounds are considered as nature-born laser dyes due to their photocycle which can be easily correlated with a four-level laser system. Population inversion is then easy to achieve. These materials, crucial for the research presented in this dissertation, have also been investigated in terms of light amplification in solutions and solid-state. The sensitive nature of these compounds can be exploited in order to realize lasers with desired emission range. A few results need to be highlighted, beginning with the tunable DFB lasing action in the ultraviolet region (λ_{las} = 355 nm) observed in sodium salicylate in 1970.[128] However, at that time, the lasing species were not identified, and the ESIPTs did not receive a lot of attention. The situation did not change until the amplified spontaneous emission at 530 nm observed in 1984 by Michael Kasha in 3-hydroxyflavone dissolved in methylcyclohexane, who correlated the distinctive photocycle and four-level lasing system (as depicted in Figure 3.6.1.).[129,130] The gain coefficient and lasing efficiency were reported to be comparable with that of Rhodamine 6G, a flagship laser dye. Soon after numerous papers on lasing in ESIPT solutions were published, highlighting the excitation-dependent emissive properties, which enabled observation of light

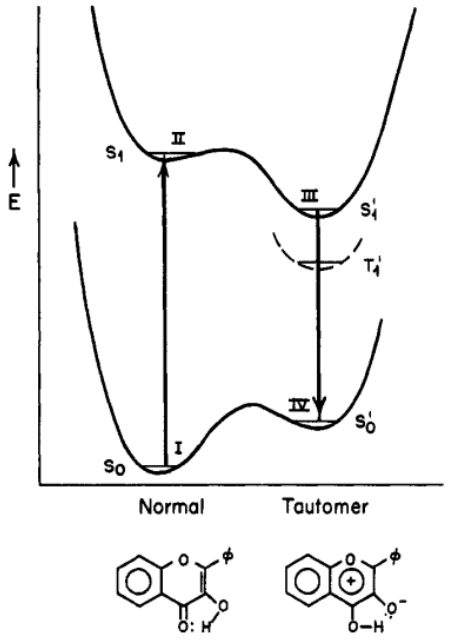

Figure 3.6.1. *Schematical representation of potential Energy curves involved in lasing action of 3-HF.*[129]

amplification from both Normal and Tautomer forms.[131–134] First observation of lasing in solid-state was performed for 2-(2'-hydroxy-5'-fluorophenyl)benzimidazole as doping in two separate polymeric films: PMMA and poly(hydroxyethyl methacrylate).[135] The incorporation of the dye in the latter has shown that ESIPT can be disrupted when in contact with hydroxy groups of the polymer chain. PMMA, however, has shown no interaction with the dye molecules, enabling its use as an inert matrix.

Great solid-state emissive properties of (hydroxyphenyl)benzothiazole derivative were presented in 2018,[136] showing that while the ASE is possible in solution and the neat film of the dye, the lasing threshold dramatically decreases for the latter, with the respective values of 21.6 $mJcm^2$ in toluene, and 8.8 μJcm^2 in neat film. Amplified spontaneous emission in the near-infrared region (λ_{las} ~ 700 nm) was also realized with highly-emissive crystallized 2'-hydroxychalocone[137] or 1,5-dihydroxyanthraquinone[138] derivatives. Nano- and microlasers were also constructed with the use of ESIPTs in the forms of wires[139–143] and spheres.[140,144,145] Even studies of polymorphism of the crystal forms of ESIPTs were conducted, as shown by Wang in 2016 on hydroxyphenyl-based analogs.[146] Based on the crystallographic structure, three distinct emissive bands were obtained, with ASE emission ranging from 612 to 714 nm. In general, while Excited-State Intramolecular Proton Transfer compounds were thoroughly studied in terms of light amplification properties,[147] the vast majority were concerned with amplified spontaneous emission. Different geometries, such as distributed feedback or random lasers, are the core of this dissertation.

Literature

1. Bouguer, P. *Essai d'optique sur la gradation de la lumière*. (Jombert, 1729).
2. Lambert, J. H. *J. H. Lambert,... Photometria, sive de Mensura et gradibus luminis, colorum et umbrae*. (sumptibus viduae E. Klett, 1760).
3. Beer. Bestimmung der Absorption des rothen Lichts in farbigen Flüssigkeiten. *Ann. Phys.* **162**, 78–88 (1852).
4. Jablonski, A. Efficiency of Anti-Stokes Fluorescence in Dyes. *Nature* **131**, 839–840 (1933).
5. Pigoń, K. & Ruziewicz, Z. *Chemia fizyczna. Tom 2*. (Wydawnictwo Naukowe PWN, 2007).
6. Lewis, G. N. & Kasha, M. Phosphorescence and the Triplet State. *J. Am. Chem. Soc.* **66**, 2100–2116 (1944).
7. Hutchison, C. A. & Mangum, B. W. Paramagnetic Resonance Absorption in Naphthalene in Its Phosphorescent State. *J. Chem. Phys.* **29**, 952–953 (1958).
8. Menzel, R. *Photonics: Linear and Nonlinear Interactions of Laser Light and Matter*. (Springer, 2007).
9. Strutt, J. W. LVIII. On the scattering of light by small particles. *London, Edinburgh, Dublin Philos. Mag. J. Sci.* **41**, 447–454 (1871).
10. Strutt, J. W. XXXVI. On the light from the sky, its polarization and colour. *London, Edinburgh, Dublin Philos. Mag. J. Sci.* **41**, 274–279 (1871).

11. Mie, G. Beiträge zur Optik trüber Medien, speziell kolloidaler Metallösungen. *Ann. Phys.* **330**, 377–445 (1908).
12. Brillouin, L. Diffusion de la lumière et des rayons X par un corps transparent homogène. *Ann. Phys.* **9**, 88–122 (1922).
13. Raman, C. V. A new radiation [Reproduced from Indian J. Phys., 1928, 2, 387–398]. *Curr. Sci.* **74**, 382–386 (1998).
14. Eugene Hecht. *Optyka*. (Wydawnictwo Naukowe PWN, 2012).
15. Hantzsch, A. Über die Halochromie und »Solvatochromie« des Dibenzal-acetons und einfacherer Ketone, sowie ihrer Ketochloride. *Berichte der Dtsch. Chem. Gesellschaft (A B Ser.* **55**, 953–979 (1922).
16. Lakowicz, J. R. *Principles of Fluorescence Spectroscopy*. *Third Edition* (Springer, 2006).
17. Lippert, E. Spektroskopische Bestimmung des Dipolmomentes aromatischer Verbindungen im ersten angeregten Singulettzustand. *Zeitschrift für Elektrochemie, Berichte der Bunsengesellschaft für Phys. Chemie* **61**, 962–975 (1957).
18. Mataga, N., Kaifu, Y. & Koizumi, M. Solvent Effects upon Fluorescence Spectra and the Dipolemoments of Excited Molecules. *Bull. Chem. Soc. Jpn.* **29**, 465–470 (1956).
19. Misra, R. & Bhattacharyya, S. P. Intramolecular Charge Transfer: Theory and Applications. *Intramolecular Charge Transfer* (2018) doi:https://doi.org/10.1002/9783527801916.ch2.
20. Forster, T. & Kasper, K. Ein konzentrationsumschlag der fluoreszenz des pyrens. *Zeitschrift Fur Elektrochemie* **59**, 976–980 (1955).
21. Davydov, A. S. The Theory of Molecular Excitons. *Sov. Phys. Uspekhi* **7**, 145–178 (1964).
22. Kasha, M., Rawls, H. R. & Ashraf El-Bayoumi, M. The exciton model in molecular spectroscopy. *Pure Appl. Chem.* **11**, 371–392 (1965).
23. Kasha, M. Energy Transfer Mechanisms and the Molecular Exciton Model for Molecular Aggregates. *Radiat. Res.* **20**, 55–70 (1963).
24. McRae, E. G. & Kasha, M. Enhancement of phosphorescence ability upon aggregation of dye molecules. *J. Chem. Phys.* **28**, 721–722 (1958).
25. Yao, H. & Ashiba, K. Highly fluorescent organic nanoparticles of thiacyanine dye: A synergetic effect of intermolecular H-aggregation and restricted intramolecular rotation. *RSC Adv.* **1**, 834–838 (2011).
26. Rösch, U., Yao, S., Wortmann, R. & Würthner, F. Fluorescent H-Aggregates of Merocyanine Dyes. *Angew. Chemie Int. Ed.* **45**, 7026–7030 (2006).
27. Spano, F. C. The Spectral Signatures of Frenkel Polarons in H- and J-Aggregates. *Acc. Chem. Res.* **43**, 429–439 (2010).
28. Würthner, F., Kaiser, T. E. & Saha-Möller, C. R. J-aggregates: From serendipitous discovery to supramolecular engineering of functional dye materials. *Angew. Chemie - Int. Ed.* **50**, 3376–3410 (2011).
29. Middleton, L. R. & Winey, K. I. Nanoscale Aggregation in Acid- and Ion-Containing Polymers. in *Annual Review of Chemical and Biomolecular Engineering* (ed. Prausnitz, J. M.) vol. 8 499–523 (2017).
30. Qin, A., Lam, J. W. Y. & Tang, B. Z. Luminogenic polymers with aggregation-induced emission characteristics. *Prog. Polym. Sci.* **37**, 182–209 (2012).
31. Luo, J. *et al.* Aggregation-induced emission of 1-methyl-1,2,3,4,5-pentaphenylsilole. *Chem. Commun.* 1740–1741 (2001) doi:10.1039/B105159H.
32. Tang, B. Z. *et al.* Efficient blue emission from siloles. *J. Mater. Chem.* **11**, 2974–2978 (2001).
33. Hong, Y., Lam, J. W. Y. & Tang, B. Z. Aggregation-induced emission: Phenomenon, mechanism and applications. *Chem. Commun.* 4332–4353 (2009) doi:10.1039/b904665h.
34. Chen, J. *et al.* Synthesis, Light Emission, Nanoaggregation, and Restricted Intramolecular Rotation of 1,1-Substituted 2,3,4,5-Tetraphenylsiloles. *Chem. Mater.* **15**, 1535–1546 (2003).
35. Leung, N. L. C. *et al.* Restriction of Intramolecular Motions: The General Mechanism behind Aggregation-Induced Emission. *Chem. – A Eur. J.* **20**, 15349–15353 (2014).
36. Banal, J. L., White, J. M., Ghiggino, K. P. & Wong, W. W. H. Concentrating Aggregation-Induced Fluorescence in Planar Waveguides: A Proof-of-Principle. *Sci. Rep.* **4**, 4635 (2014).
37. Sharma nee Kamaldeep, K., Kaur, S., Bhalla, V., Kumar, M. & Gupta, A. Pentacenequinone derivatives for preparation of gold nanoparticles: facile synthesis and catalytic application. *J.*

Mater. Chem. A **2**, 8369–8375 (2014).
38. Han, T. *et al.* Defect-sensitive crystals based on diaminomaleonitrile-functionalized Schiff base with aggregation-enhanced emission. *J. Mater. Chem. C* **1**, 7314–7320 (2013).
39. Yu, Z. *et al.* Aggregation induced emission in the rotatable molecules: the essential role of molecular interaction. *J. Mater. Chem.* **22**, 16927–16932 (2012).
40. Liu, G. *et al.* Schiff base derivatives containing heterocycles with aggregation-induced emission and recognition ability. *J. Mater. Chem. C* **2**, 2684–2691 (2014).
41. Pramanik, B. & Das, D. Aggregation-Induced Emission or Hydrolysis by Water? the Case of Schiff Bases in Aqueous Organic Solvents. *J. Phys. Chem. C* **122**, 3655–3661 (2018).
42. Liu, Y. *et al.* Specific Detection of d-Glucose by a Tetraphenylethene-Based Fluorescent Sensor. *J. Am. Chem. Soc.* **133**, 660–663 (2011).
43. Wang, X., Hu, J., Zhang, G. & Liu, S. Highly Selective Fluorogenic Multianalyte Biosensors Constructed via Enzyme-Catalyzed Coupling and Aggregation-Induced Emission. *J. Am. Chem. Soc.* **136**, 9890–9893 (2014).
44. Yu, Y. *et al.* Thiol-Reactive Molecule with Dual-Emission-Enhancement Property for Specific Prestaining of Cysteine Containing Proteins in SDS-PAGE. *ACS Appl. Mater. Interfaces* **5**, 4613–4616 (2013).
45. Yu, Y. *et al.* Cytophilic Fluorescent Bioprobes for Long-Term Cell Tracking. *Adv. Mater.* **23**, 3298–3302 (2011).
46. Zhang, C. *et al.* Cell Membrane Tracker Based on Restriction of Intramolecular Rotation. *ACS Appl. Mater. Interfaces* **6**, 8971–8975 (2014).
47. Hong, Y., Chen, S., Leung, C. W. T., Lam, J. W. Y. & Tang, B. Z. Water-soluble tetraphenylethene derivatives as fluorescent 'light-up' probes for nucleic acid detection and their applications in cell imaging. *Chem. Asian J.* **8**, 1806–1812 (2013).
48. Yuan, Y., Feng, G., Qin, W., Tang, B. Z. & Liu, B. Targeted and image-guided photodynamic cancer therapy based on organic nanoparticles with aggregation-induced emission characteristics. *Chem. Commun.* **50**, 8757–8760 (2014).
49. Ding, D., Li, K., Liu, B. & Tang, B. Z. Bioprobes Based on AIE Fluorogens. *Acc. Chem. Res.* **46**, 2441–2453 (2013).
50. Khandare, D. G., Kumar, V., Chattopadhyay, A., Banerjee, M. & Chatterjee, A. An aggregation-induced emission based "turn-on" fluorescent chemodosimeter for the selective detection of ascorbate ions. *RSC Adv.* **3**, 16981–16985 (2013).
51. Hong, Y. *et al.* Fluorogenic Zn(II) and Chromogenic Fe(II) Sensors Based on Terpyridine-Substituted Tetraphenylethenes with Aggregation-Induced Emission Characteristics. *ACS Appl. Mater. Interfaces* **3**, 3411–3418 (2011).
52. Huang, X., Gu, X., Zhang, G. & Zhang, D. A highly selective fluorescence turn-on detection of cyanide based on the aggregation of tetraphenylethylene molecules induced by chemical reaction. *Chem. Commun.* **48**, 12195–12197 (2012).
53. Zhang, Y., Li, D., Li, Y. & Yu, J. Solvatochromic AIE luminogens as supersensitive water detectors in organic solvents and highly efficient cyanide chemosensors in water. *Chem. Sci.* **5**, 2710–2716 (2014).
54. Sanji, T. *et al.* Fluorescence "Turn-On" Detection of Melamine with Aggregation-Induced-Emission-Active Tetraphenylethene. *Chem. – A Eur. J.* **18**, 15254–15257 (2012).
55. Liu, Y. *et al.* Fluorescent Chemosensor for Detection and Quantitation of Carbon Dioxide Gas. *J. Am. Chem. Soc.* **132**, 13951–13953 (2010).
56. Cai, Y. *et al.* A sensitivity tuneable tetraphenylethene-based fluorescent probe for directly indicating the concentration of hydrogen sulfide. *Chem. Commun.* **50**, 8892–8895 (2014).
57. Wang, J.-H., Feng, H.-T. & Zheng, Y.-S. Synthesis of tetraphenylethylene pillar[6]arenes and the selective fast quenching of their AIE fluorescence by TNT. *Chem. Commun.* **50**, 11407–11410 (2014).
58. Gao, M., Lam, J. W. Y., Liu, Y., Li, J. & Tang, B. Z. A new route to functional polymers: atom-economical synthesis of poly(pyrazolylnaphthalene)s by rhodium-catalyzed oxidative polycoupling of phenylpyrazole and internal diynes. *Polym. Chem.* **4**, 2841–2849 (2013).
59. Iasilli, G. *et al.* Aggregation-Induced Emission of Tetraphenylethylene in Styrene-Based Polymers. *Macromol. Chem. Phys.* **215**, 499–506 (2014).

60. Wu, Y. *et al.* Memory chromic polyurethane with tetraphenylethylene. *J. Polym. Sci. Part B Polym. Phys.* **52**, 104–110 (2014).
61. Li, Y., Xu, L. & Su, B. Aggregation induced emission for the recognition of latent fingerprints. *Chem. Commun.* **48**, 4109–4111 (2012).
62. Chen, S., Zhao, Z., Tang, B. Z. & Kwok, H. S. Non-doped white organic light-emitting diodes based on aggregation-induced emission. *J. Phys. D. Appl. Phys.* **43**, 95101 (2010).
63. Qin, W. *et al.* Crafting NPB with tetraphenylethene: a win–win strategy to create stable and efficient solid-state emitters with aggregation-induced emission feature, high hole-transporting property and efficient electroluminescence. *J. Mater. Chem. C* **2**, 3756–3761 (2014).
64. Luo, H. *et al.* A Cruciform Electron Donor–Acceptor Semiconductor with Solid-State Red Emission: 1D/2D Optical Waveguides and Highly Sensitive/Selective Detection of H2S Gas. *Adv. Funct. Mater.* **24**, 4250–4258 (2014).
65. Gu, X. *et al.* Polymorphism-Dependent Emission for Di(p-methoxylphenyl)dibenzofulvene and Analogues: Optical Waveguide/Amplified Spontaneous Emission Behaviors. *Adv. Funct. Mater.* **22**, 4862–4872 (2012).
66. Park, J. W. *et al.* High Contrast Fluorescence Patterning in Cyanostilbene-Based Crystalline Thin Films: Crystallization-Induced Mass Flow Via a Photo-Triggered Phase Transition. *Adv. Mater.* **26**, 1354–1359 (2014).
67. Zhao, D. *et al.* Light-Emitting Liquid Crystal Displays Based on an Aggregation-Induced Emission Luminogen. *Adv. Opt. Mater.* **3**, 199–202 (2015).
68. Weller, A. Über die Fluoreszenz der Salizylsäure und verwandter Verbindungen. *Naturwissenschaften* **42**, 175–176 (1955).
69. Weller, A. Innermolekularer Protonenübergang im angeregten Zustand. *Zeitschrift für Elektrochemie, Berichte der Bunsengesellschaft für Phys. Chemie* **60**, 1144–1147 (1956).
70. Sliwa, M. *et al.* Investigation of ultrafast photoinduced processes for salicylidene aniline in solution and gas phase: toward a general photo-dynamical scheme. *Photochem. Photobiol. Sci.* **9**, 661–669 (2010).
71. Yuan, H. J. *et al.* A quantum-chemical insight into the tunable fluorescence color and distinct photoisomerization mechanisms between a novel ESIPT fluorophore and its protonated form. *Spectrochim. Acta Part A – Molecular Biomol. Spectrosc.* **183**, 123–130 (2017).
72. Sliwa, M. *et al.* Comparative Investigation of Ultrafast Photoinduced Processes in Salicylidene-Aminopyridine in Solution and Solid State. *J. Phys. Chem. C* **113**, 11959–11968 (2009).
73. Das, K., Sarkar, N., Majumdar, D. & Bhattacharyya, K. Excited-State Intramolecular Proton-Transfer and Rotamerism of 2-(2'-hydroxyphenyl)benzimidazole. *Chem. Phys. Lett.* **198**, 443–448 (1992).
74. Das, K. *et al.* Excited-Sate Intramolecular Proton-Transfer in 2-(2'-hydroxyphenyl)benzimidazole and 2-(2'-hydroxyphenyl)benzoxazole – Effect of Rotamerism and Hydrogen-Bonding. *J. Phys. Chem.* **98**, 9126–9132 (1994).
75. Klicova, L. *et al.* Adiabatic Triplet State Tautomerization of p-Hydroxyacetophenone in Aqueous Solution. *J. Phys. Chem. A* **116**, 2935–2944 (2012).
76. Stephan, J. S. & Grellmann, K. H. Photoisomerization of 2-(2'-hydroxyphenyl)benzoxazole – Formation and Decay of the trans-Keto Tautomer in Dry and in Water-containing 3-methylpentane. *J. Phys. Chem.* **99**, 10066–10068 (1995).
77. Iijima, T. *et al.* Excited-State Intramolecular Proton Transfer of Naphthalene-Fused 2-(2 '-Hydroxyaryl)benzazole Family. *J. Phys. Chem. A* **114**, 1603–1609 (2010).
78. Sengupta, P. K. & Kasha, M. Excited-State Proton-Transfer Spectroscopy of 3-hydroxyflavone and quercetin. *Chem. Phys. Lett.* **68**, 382–385 (1979).
79. Mosquera, M., Penedo, J. C., Rodriguez, M. C. R. & Rodriguez-Prieto, F. Photoinduced inter- and intramolecular proton transfer in aqueous and ethanolic solutions of 2-(2'-hydroxyphenyl)benzimidazole: Evidence for tautomeric and conformational equilibria in the ground state. *J. Phys. Chem.* **100**, 5398–5407 (1996).
80. Chou, P. T. *et al.* Femtosecond dynamics on excited-state proton charge-transfer reaction in 4'-N,N-Diethylamino-3-hydroxyflavone. The role of dipolar vectors in constructing a rational mechanism. *J. Phys. Chem. A* **109**, 3777–3787 (2005).
81. Klymchenko, A. S., Pivovarenko, V. G. & Demchenko, A. P. Elimination of the hydrogen

bonding effect on the solvatochromism of 3-hydroxyflavones. *J. Phys. Chem. A* **107**, 4211–4216 (2003).
82. Lahmani, F. & Zehnacker-Rentien, A. Effect of Substitution on the Photoinduced Intramolecular Proton Transfer in Salicylic Acid. *J. Phys. Chem. A* **101**, 6141–6147 (1997).
83. Smoluch, M., Joshi, H., Gerssen, A., Gooijer, C. & van der Zwan, G. Fast Excited-State Intramolecular Proton Transfer and Subnanosecond Dynamic Stokes Shift of Time-Resolved Fluorescence Spectra of the 5-Methoxysalicylic Acid/Diethyl ether Complex. *J. Phys. Chem. A* **109**, 535–541 (2005).
84. Seo, J., Kim, S., Park, S. & Soo, Y. P. Tailoring the excited-state intramolecular proton transfer(ESIPT) fluorescence of 2-(2′-hydroxyphenyl)benzoxazole derivatives. *Bull. Korean Chem. Soc.* **26**, 1706–1710 (2005).
85. Ríos Vázquez, S., Ríos Rodríguez, M. C., Mosquera, M. & Rodríguez-Prieto, F. Excited-State Intramolecular Proton Transfer in 2-(3‘-Hydroxy-2‘-pyridyl)benzoxazole. Evidence of Coupled Proton and Charge Transfer in the Excited State of Some o-Hydroxyarylbenzazoles. *J. Phys. Chem. A* **111**, 1814–1826 (2007).
86. Furukawa, S., Shono, H., Mutai, T. & Araki, K. Colorless, Transparent, Dye-Doped Polymer Films Exhibiting Tunable Luminescence Color: Controlling the Dual-Color Luminescence of 2-(2′-Hydroxyphenyl)imidazo[1,2-a]pyridine Derivatives with the Surrounding Matrix. *ACS Appl. Mater. Interfaces* **6**, 16065–16070 (2014).
87. Knyazhansky, M. I., Metelitsa, A. V, Bushkov, A. J. & Aldoshin, S. M. Role of structural flexibility in fluorescence and photochromism of the salicylideneaniline: The ‘“aldehyde”’ ring rotation. *J. Photochem. Photobiol. A-Chemistry* **97**, 121–126 (1996).
88. Kim, S., Seo, J. & Park, S. Y. Torsion-induced fluorescence quenching in excited-state intramolecular proton transfer (ESIPT) dyes. *J. Photochem. Photobiol. A-Chemistry* **191**, 19–24 (2007).
89. Massue, J. *et al.* Solution and solid-state Excited-State Intramolecular Proton Transfer (ESIPT) emitters incorporating Bis-triethyl-or triphenylsilylethynyl units. *Dye. Pigment.* **160**, 915–922 (2019).
90. Massue, J., Ulrich, G. & Ziessel, R. Effect of 3,5-disubstitution on the optical properties of luminescent 2-(2′-Hydroxyphenyl)benzoxazoles and their borate complexes. *European J. Org. Chem.* 5701–5709 (2013) doi:10.1002/ejoc.201300616.
91. Skonieczny, K. *et al.* How To Reach Intense Luminescence for Compounds Capable of Excited-State Intramolecular Proton Transfer? *Chem. Eur. J.* **22**, 7485–7496 (2016).
92. Wang, Q. *et al.* An efficient ratiometric fluorescent probe for tracking dynamic changes in lysosomal pH. *Analyst* **140**, 5563–5569 (2015).
93. Liu, M. *et al.* Fluorescent probes for the detection of magnesium ions (Mg2+): from design to application. *RSC Adv.* **8**, 12573–12587 (2018).
94. Maity, D., Kumar, V. & Govindaraju, T. Reactive Probes for Ratiometric Detection of Co2+ and Cu+ Based on Excited-State Intramolecular Proton Transfer Mechanism. *Org. Lett.* **14**, 6008–6011 (2012).
95. Xu, Z. *et al.* A highly selective fluorescent probe for fast detection of hydrogen sulfide in aqueous solution and living cells. *Chem. Commun.* **48**, 10871–10873 (2012).
96. Chen, L., Wu, D. & Yoon, J. An ESIPT based fluorescence probe for ratiometric monitoring of nitric oxide. *Sensors Actuators B Chem.* **259**, 347–353 (2018).
97. Miller, E. W., Albers, A. E., Pralle, A., Isacoff, E. Y. & Chang, C. J. Boronate-Based Fluorescent Probes for Imaging Cellular Hydrogen Peroxide. *J. Am. Chem. Soc.* **127**, 16652–16659 (2005).
98. Li, D. *et al.* Supersensitive detection of explosives by recyclable AIE luminogen-functionalized mesoporous materials. *Chem. Commun.* **48**, 7167–7169 (2012).
99. Shvadchak, V. V, Klymchenko, A. S., de Rocquigny, H. & Mély, Y. Sensing peptide–oligonucleotide interactions by a two-color fluorescence label: application to the HIV-1 nucleocapsid protein. *Nucleic Acids Res.* **37**, e25–e25 (2009).
100. Wang, Y., Hu, Y., Wu, T., Zhou, X. & Shao, Y. Triggered Excited-State Intramolecular Proton Transfer Fluorescence for Selective Triplex DNA Recognition. *Anal. Chem.* **87**, 11620–11624 (2015).
101. Bertman, K. A. *et al.* A fluorescent flavonoid for lysosome detection in live cells under “wash

free" conditions. *J. Mater. Chem. B* **6**, 5050–5058 (2018).
102. Klymchenko, A. S. & Demchenko, A. P. Electrochromic modulation of excited-state intramolecular proton transfer: The new principle in design of fluorescence sensors. *J. Am. Chem. Soc.* **124**, 12372–12379 (2002).
103. Klymchenko, A. S. *et al.* Novel Two-Band Ratiometric Fluorescence Probes with Different Location and Orientation in Phospholipid Membranes. *Chem. Biol.* **9**, 1199–1208 (2002).
104. Biswas, S. *et al.* 'AIE + ESIPT' assisted photorelease: fluorescent organic nanoparticles for dual anticancer drug delivery with real-time monitoring ability. *Chem. Commun.* **54**, 168–171 (2018).
105. Barman, S. *et al.* Coumarin–benzothiazole–chlorambucil (Cou–Benz–Cbl) conjugate: an ESIPT based pH sensitive photoresponsive drug delivery system. *J. Mater. Chem. B* **3**, 3490–3497 (2015).
106. Tarkka, R. M., Zhang, X. J. & Jenekhe, S. A. Electrically generated intramolecular proton transfer: Electroluminescence and stimulated emission from polymers. *J. Am. Chem. Soc.* **118**, 9438–9439 (1996).
107. Park, S., Kwon, O. H., Lee, Y. S., Jang, D. J. & Park, S. Y. Imidazole-based excited-state intramolecular proton-transfer(ESIPT) materials: Observation of thermally activated delayed fluorescence(TDF). *J. Phys. Chem. A* **111**, 9649–9653 (2007).
108. Kim, S., Seo, J., Jung, H. K., Kim, J.-J. & Park, S. Y. White Luminescence from Polymer Thin Films Containing Excited-State Intramolecular Proton-Transfer Dyes. *Adv. Mater.* **17**, 2077–2082 (2005).
109. Albert Einstein. The Quantum Theory of Radiation. *Phys. Zeitschrift* **18**, (1917).
110. Boudrioua, A., Chakaroun, M. & Fischer, A. *An Introduction to Organic Lasers*. (Elsevier, 2017). doi:https://doi.org/10.1016/B978-1-78548-158-1.50009-2.
111. Hooker, S. & Webb, C. *Laser Physics*. (OUP Oxford, 2010).
112. Maiman, T. H. Stimulated Optical Radiation in Ruby. *Nature* **187**, 493–494 (1960).
113. Negro, L. D., Bettotti, P., Cazzanelli, M., Pacifici, D. & Pavesi, L. Applicability conditions and experimental analysis of the variable stripe length method for gain measurements. *Opt. Commun.* **229**, 337–348 (2004).
114. Cerdán, L., Costela, A. & García-Moreno, I. On the characteristic lengths in the variable stripe length method for optical gain measurements. *J. Opt. Soc. Am. B* **27**, 1874–1877 (2010).
115. Wiersma, D. S., van Albada, M. P. & Lagendijk, A. Random laser? *Nature* **373**, 203–204 (1995).
116. Cao, H. Lasing in random media. *Waves Random Media* **13**, (2003).
117. Lawandy, N. M., Balachandran, R. M., Gomes, A. S. L. & Sauvain, E. Laser action in strongly scattering media. *Nature* **368**, 436–438 (1994).
118. Kogelnik, H. & Shank, C. V. Coupled-wave theory of distributed feedback lasers. *J. Appl. Phys.* **43**, 2327–2335 (1972).
119. Kogelnik, H. & Shank, C. V. Stimulated emission in a periodic structure. *Appl. Phys. Lett.* **18**, 152–154 (1971).
120. Shank, C. V., Bjorkholm, J. E. & Kogelnik, H. Tunable distributed-feedback dye laser. *Appl. Phys. Lett.* **18**, 395 (1971).
121. Sorokin, P. P. & Lankard, J. R. Stimulated Emission Observed from an Organic Dye, Chloro-aluminum Phthalocyanine. *IBM J. Res. Dev.* **10**, 162–163 (1966).
122. Schäfer, F. P., Schmidt, W. & Volze, J. Organic Dye Solution Laser. *Appl. Phys. Lett.* **9**, 306–309 (1966).
123. Soffer, B. H. & McFarland, B. B. Continuoulsy Tunable, Narrow-Band Organic Dye Lasers. *Appl. Phys. Lett.* **10**, 266–267 (1967).
124. Forget, S. & Chenais, S. *Organic Solid- State Lasers*. (Springer, 2013).
125. Johansson, N. *et al.* Solid-State Amplified Spontaneous Emission in Some Spiro-Type Molecules: A New Concept for the Design of Solid-State Lasing Molecules. *Adv. Mater.* **10**, 1136–1141 (1998).
126. Mo, Y., Tian, R., Shi, W. & Cao, Y. Ultraviolet-emitting conjugated polymer poly(9,9′-alkyl-3,6-silafluorene) with a wide band gap of 4.0 eV. *Chem. Commun.* 4925–4926 (2005) doi:10.1039/B507518A.
127. Casalboni, M. *et al.* 1.3 μm light amplification in dye-doped hybrid sol-gel channel waveguides. *Appl. Phys. Lett.* **83**, 416–418 (2003).

128. Myer, J. A., Itzkan, I. & Kierstead, E. Dye Lasers in the Ultraviolet. *Nature* **225**, 544–545 (1970).
129. Chou, P., McMorrow, D., Aartsma, T. J. & Kasha, M. The proton-transfer laser. Gain spectrum and amplification of spontaneous emission of 3-hydroxyflavone. *J. Phys. Chem.* **88**, 4596–4599 (1984).
130. Khan, A. U. & Kasha, M. Mechanism of four-level laser action in solution excimer and excited-state proton-transfer cases. Proc. Natl. Acad. Sci. 80, 1767 LP – 1770 (1983).
131. Uzhinov, B. M. & Druzhinin, S. I. Excited state proton transfer dye lasers. *Russ. Chem. Rev.* **67**, 123–136 (1998).
132. Douhal, A., Amat-Guerri, F., Lillo, M. P. & Acuña, A. U. Proton transfer spectroscopy of 2-(2'-hydroxyphenyl)imidazole and 2-(2'-hydroxyphenyl)benzimidazole dyes. *J. Photochem. Photobiol. A Chem.* **78**, 127–138 (1994).
133. Costela, A. Proton-Transfer Laser. 2807–2808 (1986).
134. Costela, A., Muñoz, J. M., Douhal, A., Figuera, J. M. & Acuña, A. U. Experimental test of a four-level kinetic model for excited-state intramolecular proton transfer dye lasers. *Appl. Phys. B* **49**, 545–552 (1989).
135. Acuña, A. U. *et al.* Proton-transfer lasing from solid organic matrices. *Chem. Phys. Lett.* **187**, 98–102 (1991).
136. Mai, V. T. N. *et al.* Low Amplified Spontaneous Emission Threshold and Efficient Electroluminescence from a Carbazole Derivatized Excited-State Intramolecular Proton Transfer Dye. *ACS Photonics* **5**, 4447–4455 (2018).
137. Zhang, H. *et al.* Organic Crystals with Near-Infrared Amplified Spontaneous Emissions Based on 2′-Hydroxychalcone Derivatives: Subtle Structure Modification but Great Property Change. *Angew. Chemie - Int. Ed.* **54**, 8369–8373 (2015).
138. Geng, Y. *et al.* Multifunctional Organic Single-Crystalline Microwire Arrays toward Optical Applications. *Adv. Funct. Mater.* 2113025 (2022).
139. Wang, X. *et al.* Near-Infrared Organic Single-Crystal Lasers with Polymorphism-Dependent Excited State Intramolecular Proton Transfer. *Adv. Opt. Mater.* **5**, 1700027 (2017).
140. Wang, X. *et al.* Shape-Engineering of Self-Assembled Organic Single Microcrystal as Optical Microresonator for laser Applications. *Sci. Rep.* **4**, 7011 (2014).
141. Wang, X. *et al.* Tunable Near-Infrared Organic Nanowire Nanolasers. *Adv. Funct. Mater.* **27**, 1703470 (2017).
142. Wu, J.-J. *et al.* Near-Infrared Organic Single-Crystal Nanolaser Arrays Activated by Excited-State Intramolecular Proton Transfer. *Matter* **2**, 1233–1243 (2020).
143. Zhang, W., Yan, Y., Gu, J., Yao, J. & Zhao, Y. S. Low-threshold wavelength-switchable organic nanowire lasers based on excited-state intramolecular proton transfer. *Angew. Chemie - Int. Ed.* **54**, 7125–7129 (2015).
144. Tao, Y. C., Wang, X. D. & Liao, L. S. Active whispering-gallery-mode optical microcavity based on self-assembled organic microspheres. *J. Mater. Chem. C* **7**, 3443–3446 (2019).
145. Wang, X. *et al.* Near-Infrared Lasing from Small-Molecule Organic Hemispheres. *J. Am. Chem. Soc.* **137**, 9289–9295 (2015).
146. Cheng, X. *et al.* Multicolor Amplified Spontaneous Emissions Based on Organic Polymorphs That Undergo Excited-State Intramolecular Proton Transfer. *Chem. - Eur. J.* **22**, 4899-4903 (2016).
147. Yan, C.-C.; Wang, X.-D.; Liao, L.-S. Organic Lasers Harnessing Excited State Intramolecular Proton Transfer Process. *ACS Photonics* **7**, 1355-1366 (2020).

EXPERIMENTAL INVESTIGATIONS

4. Materials and Methods

This chapter presents a detailed overview of all experimental methods and procedures, as well as investigated compounds presented in this dissertation.

4.1. Compounds

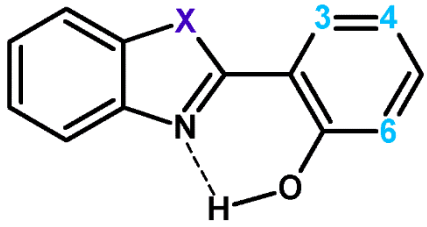

Figure 4.1.1. *HBX structure.*

Excited-State Intramolecular Proton Transfer (ESIPT) compounds are the core of this thesis, consisting of sixteen 2-(2'-hydroxyphenyl)benzazole (HBX, Figure 4.1.1.) and two 2-((phenylimino)methyl)phenole (A) derivatives (Figure 4.1.4.).

The former are based on the well-known scaffold, substituted with either nitrogen (HBI), oxygen (HBO), or sulfur (HBT). Further functionalization of HBX at either 3-, 4-, or 6- position of the phenol ring with ethynyl extended trialkylsilyl groups or dialkylaniline directly influences rigidity and intramolecular charge transfer of the molecule, in turn modifying fluorescent properties of the compound in terms of both spontaneous and stimulated emission. Partial or full frustration of ESIPT phenomena is possible via π-conjugation substitution, such as presented functionalization with *m*-N,N-dimethyl- or *p*-N,N-diethylaniline of HBO scaffold. The influence of molecular structure on emissive properties of investigated compounds will be thoroughly discussed in the next chapters. The chemical structures of investigated HBX molecules are presented in Figure 4.1.2. Analysis of functionalized 2-((phenylimino)methyl)phenole substituted with different electron-withdrawing groups (fluoro or cyano) is presented in further subchapters.

Presented molecules due to their inherent intramolecular hydrogen bond and confirmed ESIPT behavior are good candidates for light amplification studies. As shown in the theoretical introduction, reversible and fast tautomerization following excitation is a four-level cycle, which can easily be compared to the favorable four-level laser system. Hence, presented molecules were investigated as candidates for the light amplification systems.

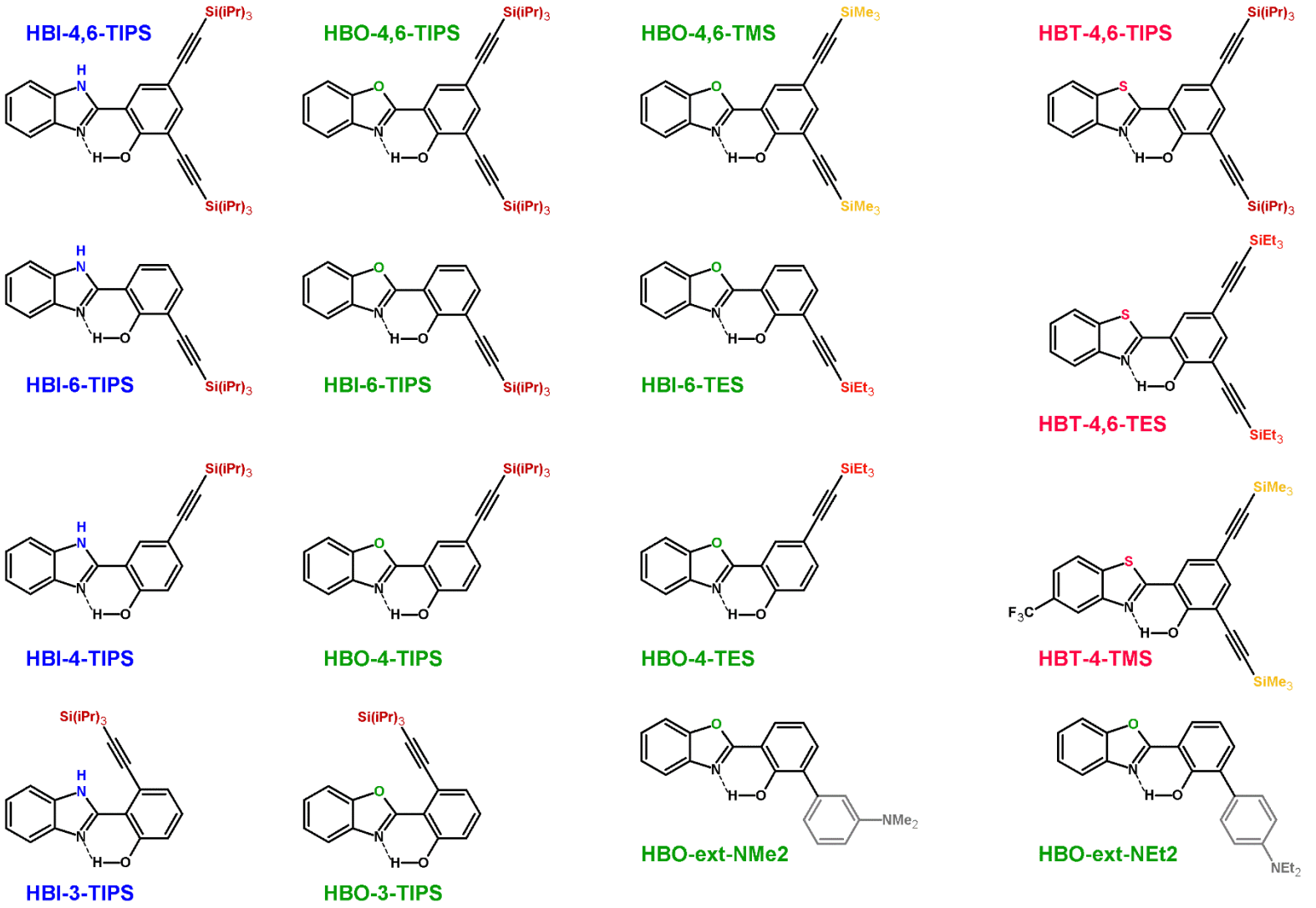

Figure 4.1.2. *Chemical structures of investigated HBX compounds with designated acronyms.*

2-(2'-hydroxyphenyl)benzoxazoles (HBO)

Table 4.1.1. *Full IUPAC name and acronym of HBO molecules.*

Acronym	Full name
HBO-4,6-TMS	2-(benzo[d]oxazol-2-yl)-4,6-bis((trimethylsilyl)ethynyl)phenol
HBO-6-TES	2-(benzo[d]oxazol-2-yl)-6-((triethylsilyl)ethynyl)phenol
HBO-4-TES	2-(benzo[d]oxazol-2-yl)-4-((triethylsilyl)ethynyl)phenol
HBO-6-TIPS	2-(benzo[d]oxazol-2-yl)-6-((triisopropylsilyl)ethynyl)phenol
HBO-4-TIPS	2-(benzo[d]oxazol-2-yl)-4-((triisopropylsilyl)ethynyl)phenol
HBO-3-TIPS	2-(benzo[d]oxazol-2-yl)-3-((triisopropylsilyl)ethynyl)phenol
HBO-4,6-TIPS	2-(benzo[d]oxazol-2-yl)-4,6-bis((triisopropylsilyl)ethynyl)phenol
HBO-ext-NMe2	3-(benzo[d]oxazol-2-yl)-3'-(dimethylamino)-[1,1'-biphenyl]-2-ol
HBO-ext-NEt2	3-(benzo[d]oxazol-2-yl)-4'-(diethylamino)-[1,1'-biphenyl]-2-ol

The first group that can be separated from all investigated compounds can be formed from hydroxyphenylbenzoxazoles, and can be further divided by the mono- or bis- substitution of the ethynyl-extended alkyl moiety: trimethylsilyl (**TMS**), triethylsilyl (**TES**) or triisopropylsilyl (**TIPS**), at the 3-, 4- or 6- positions of the phenol ring. While it's well-known that the length of the alkyl chain directly influences the solubility of the compounds, its impact on the emission properties will be described in detail in later chapters, especially in terms of light amplification. Two groups of a higher electrodonating character than trialkylsilyl were also used for the substitution of the HBO: *m*-N,N-dimethylaniline (**HBO-ext-NMe2**) and *p*-N,N-diethyloaniline (**HBO-ext-NEt2**).

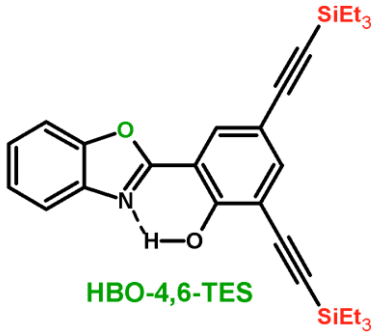

Figure 4.1.3. *Chemical structure of 2-(benzo[d]oxazol-2-yl)-4,6-bis((triethylsilyl)ethynyl)phenol.*

HBO-4,6-TES molecule (Figure 4.1.3.) is a compound that was investigated by the Author during the Master of Science's studies and is not a part of this dissertation. However, due to inherent structural similarity to other HBOs, in further chapters results obtained for this molecule will be used as a reference for other investigated dyes, in order to fully understand the influence of the compound structure on emissive properties of presented ESIPTs.

2-(2'-hydroxyphenyl)benzimidazoles (HBI)

The next group of investigated compounds consists of four mono- or bis-ethynyl-extended triisopropylsilyl (**TIPS**) substituted hydroxyphenylbenzimidazole, which serve as a reference for described HBO-TIPS compounds.

Table 4.1.2. *Full IUPAC name and acronym of HBI molecules.*

Acronym	Full name
HBI-6-TIPS	2-(1H-benzo[d]imidazol-2-yl)-6-((triisopropylsilyl)ethynyl)phenol
HBI-4-TIPS	2-(1H-benzo[d]imidazol-2-yl)-4-((triisopropylsilyl)ethynyl)phenol
HBI-3-TIPS	2-(1H-benzo[d]imidazol-2-yl)-3-((triisopropylsilyl)ethynyl)phenol
HBI-4,6-TIPS	2-(1H-benzo[d]imidazol-2-yl)-4,6-bis((triisopropylsilyl)ethynyl)phenol

2-(2'-hydroxyphenyl)benzothiazoles (HBT)

Hydroxyphenylbenzothiazoles are the last group of investigated HBXs. For these particular ESIPTs, the functionalization consisted of changing the length of the alkyl chain connected to the molecule in both 4- and 6-position of the phenolic ring. As for HBO dyes, ethynyl-extended triisopropylsilyl (**HBT-4,6-TIPS**), triethylsilyl (**HBT-4,6-TES**) and trimethylsilyl (**HBT-CF3-4,6-TMS**) groups were used for the substitution. For the latter compound, additional strong electron-withdrawing trifluoromethyl (**CF3**) group was introduced at the 5- position of the benzothiazole.

Table 4.1.3*. Full IUPAC name and acronym of HBT molecules.*

Acronym	Full name
HBT-CF3-4,6-TMS	2-(5-(trifluoromethyl)benzo[d]thiazol-2-yl)-4,6-bis((trimethylsilyl)ethynyl)phenol
HBT-4,6-TES	2-(benzo[d]thiazol-2-yl)-4,6-bis((triethylsilyl)ethynyl)phenol
HBT-4,6-TIPS	2-(benzo[d]thiazol-2-yl)-4,6-bis((triisopropylsilyl)ethynyl)phenol

Anils (A)

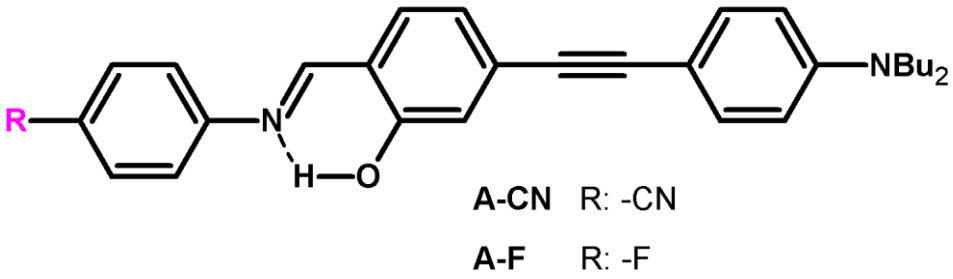

Figure 4.1.4. *Chemical structure of investigated anil derivatives.*

The last group of investigated ESIPTs consists of two 2-((phenylimino)methyl)phenole derivatives, substituted with different electron-withdrawing groups (fluoro or cyano) and ethynyl-extended *p*-N,N-dibutylaniline as electron-donating moiety.

Table 4.1.4. *Full IUPAC name and acronym of investigated anils.*

Acronym	Full name
A-CN	(E)-4-((4-((4-(dibutylamino)phenyl)ethynyl)-2-hydroxybenzylidene)amino)benzonitrile
A-F	(E)-5-((4-(dibutylamino)phenyl)ethynyl)-2-(((4-(fluoromethyl)phenyl)imino)methyl)phenol

4.2. Organic synthesis

Chemical synthesis was part of the research presented in this thesis. It was conducted during the Traineeship at the Institute of Chemistry and Processes for Energy, Environment and Health (ICPEES) – a joint research unit of the University of Strasbourg and the French National Research Council (CNRS). Compounds that were synthesized by the Author and that are part of the thesis are **HBI-4,6-TIPS. HBO-4,6-TIPS** and **HBT-4,6-TIPS**. The rest of investigated compounds were supplied by dr. Julien Massue (ICPEES). For a detailed description of the synthetic procedure of investigated dyes, the Reader is directed to Appendix A: Synthesis.

For the synthesis of HBX-4,6-TIPS dyes, commercially available reagents were used, without additional purification (unless specifically stated). In general, HBX dyes were prepared with a straightforward three-step procedure: 1) acetylation of precursor (2-hydroxy-3,5-diiodobenzaldehyde), followed by 2) Pd-catalyzed Sonogashira cross-coupling of acetate with

ethynyltriisopropylsilane, finally ending with 3) condensation with the desired aminophenol, and oxidation (with either sodium metabisulfite or 2,3-dichloro-5,6-dicyano-1,4-benzoquinone) to obtain HBX-4,6-TIPS molecule. Purification by silica gel chromatography (40-63 μm) was used to achieve pure compounds as powders. New compounds were characterized by ^{1}H NMR and ^{13}C NMR (Bruker Advance 400 MHz), as well as HR-MS (micrOTOF II, Bruker) spectroscopy.

4.3. Spectroscopic characterization

Absorption spectra of solutions were recorded with a Jasco V-730 dual-beam spectrophotometer with baseline correction. Solvents that were used to prepare diluted solutions were of spectroscopic grade and used as received, without any additional purification. Measurements were conducted at room temperature, in quartz cuvettes. The obtained signal was then recalculated as the molar attenuation coefficient at the maximum for each measured sample, however, normalized spectra are presented in the further chapters for easier comparison of the spectra profile between each compared compound.

Spontaneous emission of the same solutions, as well as polymeric thin films and KBr pellets, was recorded with a HORIBA FluoroMax-4 spectrofluorometer. Additional excitation spectra measurements were conducted for the solid-state samples in the same setup. All collected spectra were corrected. The excitation and emission slits were adjusted accordingly to each sample, to achieve a good quality signal with minimum noise. Results presented in the next chapters show (unless specified) normalized emission and excitation spectra to facilitate each band profile and position of the maximum.

Absolute photoluminescence quantum yield (Φ_{PL}) of solutions was measured with the use of an integrating sphere module of EDINBURGH Instruments FS5 spectrofluorometer. The concentration of the samples was controlled so that the absorbance at the excitation wavelength did not exceed 0.1. For the QY determination the emission spectra of pure solvent and the corresponding dye solution were collected. For the quantum yield values of the samples in the solid-state, dye-doped potassium bromide pellets were prepared by simultaneous grinding and then pressing the dye/KBr powder mixture. Absolute quantum yield values were then determined by an integrating sphere

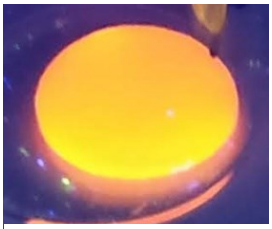

Figure 4.3.1. *KBr pellet of **A-F** under the UV light.*

fitted to the Horiba FluoroMax-4 spectrofluorometer, with a non-doped KBr pellet as a reference. Some of the presented quantum yield values of KBr pellets were supplied by dr Massue and are referenced accordingly in the supplied tables.

4.4. Aggregation-Induced Emission Enhancement (AIEE)

Good emissive properties of the molecules in the aggregated form are one of the requirements for the construction of organic solid-state lasers. Aggregation-Induced Emission (AIE) or its Enhancement (AIEE) measurements of investigated compounds can provide valuable information on the mechanisms of light amplification in studied samples, both in solutions and in solid-state. These experiments were conducted through investigation of both intensity and the profile of the emission spectra of ESIPTs in good-solvent/bad-solvent mixtures, with different volume ratios (from 100/0 to almost 0/100). Both HBXs and anils are well soluble in tetrahydrofuran (THF), but completely insoluble in water. Molecules, due to intermolecular van der Waals forces, act then as hydrophobic species. Hence, they move away from the hydrophilic water molecules, forming structures with the smallest possible surface area through aggregation. Since THF and water are fully miscible, they were chosen as the medium for the AIE/AIEE experiments. For the measurements, a series of THF/water mixtures were prepared, to which a dye/THF solution was injected to maintain the same mass concentration of the dye in each mixture. Emission spectra were recorded in the quartz cuvettes for the same parameters (excitation wavelength, slits – adjusted accordingly to the sample) with a HORIBA FluoroMax-4 Spectrofluorometer. Care was given to keep the same time interval between dye/solvents-mixture preparation and its measurement, to limit the influence of time on the formation of the aggregates, which can impact recorded emission spectra.

4.5. Solid-state samples preparation

For light amplification measurements, thin polymeric films doped with investigated compounds were prepared to serve as guest-host systems. Each ESIPT dye was acting as an active material in an inert (polymeric) matrix. As described in the literature, such a system benefits from decreased photobleaching and limited aggregation-caused quenching (ACQ), while maintaining the possibility of molecule movement among long polymer chains. Additionally, even though there is some freedom of rotation, it is still slightly limited, which

has a beneficial effect in deactivating the non-radiative relaxation of the molecule after excitation.

As such, commercially available poly(methyl methacrylate) (PMMA, Sigma Aldrich®, M_w = 350 kDa) and polystyrene (PS, Sigma Aldrich®, M_w = 280 kDa) were chosen as the inert matrix. All films were prepared by drop-casting technique, with the procedure as follows. First, the chosen polymer was dissolved in toluene at room temperature in order to get a 5.0% weight by weight solution. The 1.0% w/w dye/toluene solution was prepared simultaneously. After complete dissolution of both polymer and the chromophore, both solutions were then mixed to achieve a mixture where the dye/matrix dry weight ratio was equal to 1.0%. After solubilization, the blend was then deposited on clean glass substrates and left in the toluene saturated atmosphere at room temperature until completely dry. The layer thickness was investigated with Veeco DEKTAK 3 profilometer.

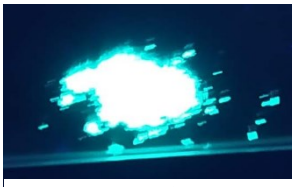

Figure 4.5.1. *HBI-3-TIPS powder under the UV light.*

Apart from polymeric thin films, light amplification properties of ESIPT compounds were also investigated in a form of a pure powder. To prepare samples for the measurement small amount of the studied compound (*ca*. 15-20 mg) was placed in between two clean glass substrates, immobilized, and then used for the experiments.

4.6. Light amplification measurements

Conducted light amplification experiments involved investigation of possibility to obtain amplified spontaneous emission (ASE), random lasing (RL) or distributed feedback lasing (DFB) in either pure powders, dye-doped polymeric thin films, or concentrated solutions. In order to do that, a setup presented in Figure 4.6.1. was constructed.

For the experiments Nd:YAG nanosecond pulse laser (Surelite II, Continuum) was utilized, with a 5 ns pulse duration and 10 Hz repetition rate. Used laser is characterized by a Gaussian distribution of the output beam, with a circular cross-section. The generated laser wavelength is 1064 nm, however, second- (532 nm) and third-harmonic (355 nm) generations are also obtained. The latter was used as a pumping source for the investigated ESIPT dyes since their maximum absorption lies in the range of 300-400 nm. The ultraviolet excitation beam was separated from other wavelengths with the use of a beam separator, consisting of

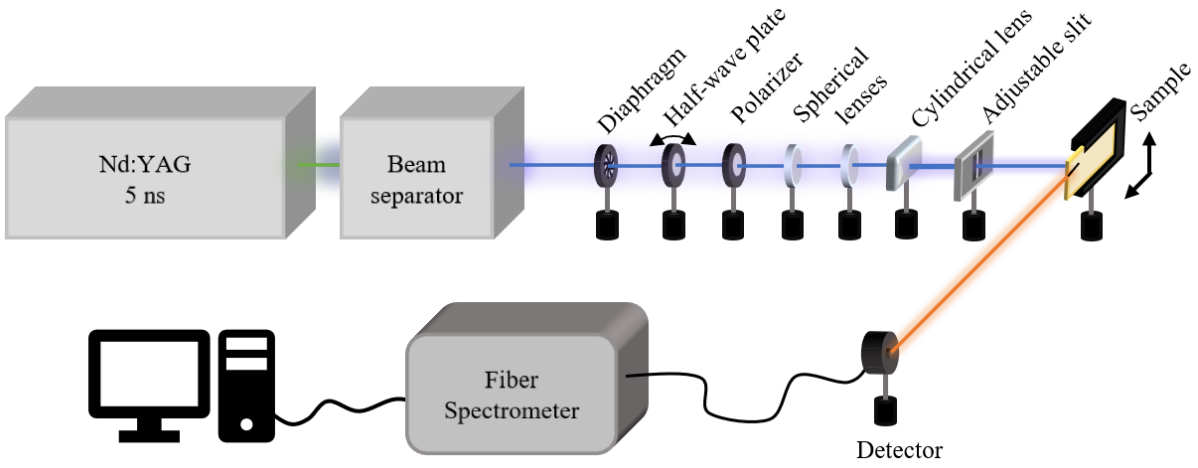

Figure 4.6.1. *Schematical representation of experimental setup used for ASE/RL measurements.*

a specific system of mirrors (Continuum, SSP-2). Redirecting of the 1064 and 532 nm does not lead to complete blocking of these beams, however, their energy is negligible. The energy of the third-harmonic was controlled by a half-wave plate rotation in regards to the polarizer and/or a laser shutter delay, and measured by the Coherent FieldMaxII-TOP power meter connected to the Coherent EnergyMax-J-10MB-HE sensor, with 100 pulses to obtain an average value. Next, a system of convex and cylindrical lenses was placed to shape the beam to the stripe-like area, focused on the sample surface. This configuration allows applying the Variable Stripe Length (VSL) method as a means to determine parameters of the compound, such as net gain. The pumping beam was incident to the sample surface, at its edge to limit waveguiding effects. The size of the exciting area was precisely controlled with the use of an adjustable slit placed in between the cylindrical lens and the sample. For determination of the lasing threshold area of 5 mm x 0.7 mm in dimension was used. For the net gain coefficient measurements length of the stripe was changed. Emitted light coming from the sample was collected perpendicularly, with the use of an Andor Shamrock SR-163 fiber spectrometer (resolution: 0.07 nm). Background noise was afterward subtracted from each recorded spectra. Studied thin films or powders were placed in a sample holder as is, however for light amplification experiments of the solutions a quartz cuvette was used, with a 1.0 mm optical path length. The signal from the powders was collected with an Andor Shamrock i500 fiber spectrometer.

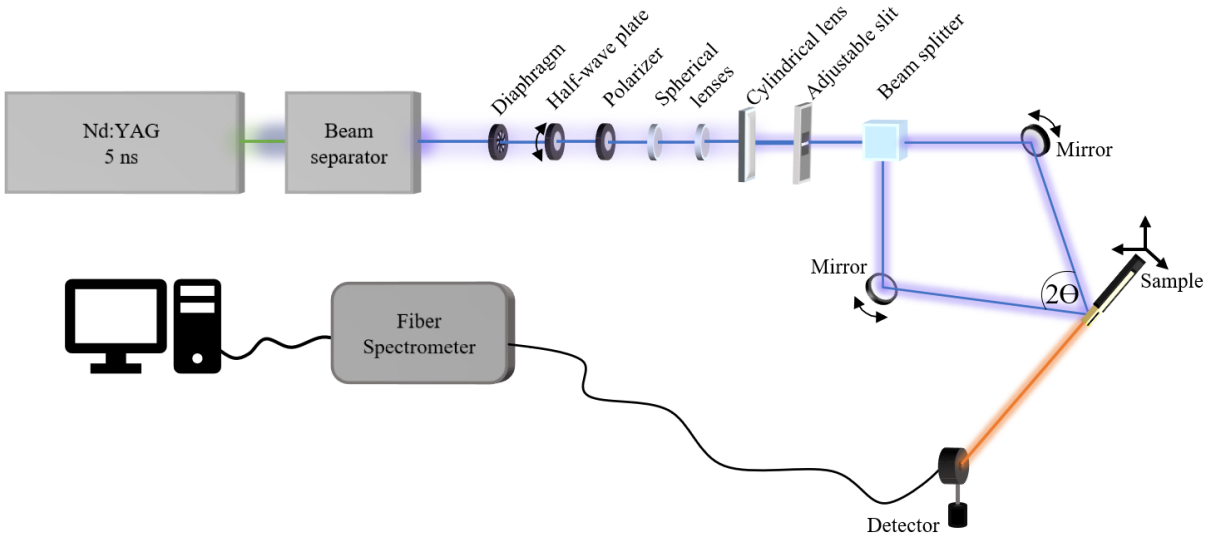

Figure 4.6.2. *Schematical representation of experimental setup used for DFB measurements.*

Distributed feedback lasing was studied by a dynamic holographic method on the same polymeric films that were investigated in the previously described setup. As such, a Degenerated Two-Wave Mixing (DTWM) system was constructed based on the ASE/RL setup and is presented in Figure 4.6.2. Due to the insertion of the beam splitter, the pumping beam splits into two separate waves, making it possible to interfere with one another on the sample surface with the use of 355 nm-dedicated mirrors. Hence, excitation and generation of the temporary periodical optical resonator happen at the same time. As described in the theoretical introduction, interference of two coherent waves leads to the formation of a diffraction pattern with a set period, that can be dynamically and precisely controlled by a simple change of the interference angle Θ through the mirror's rotation, thus enabling real-time tuning of the emission.

5. Experimental results

This chapter contains a presentation and discussion of obtained experimental results in investigated ESIPT compounds. First, fundamental photophysical properties in solution and solid-state are presented. Next, Aggregation-Induced Emission Enhancement (AIEE) is described. The last subchapter is dedicated to light amplification measurements of dye-doped polymeric thin films, amorphous powders, and concentrated solutions.

5.1. Photophysical properties

Even though the topic of this dissertation is related to light amplification, the fundamental photophysical properties of investigated ESIPTs need to be taken into account. Hence, absorption and emission spectra were measured at diluted concentrations in non-polar toluene, which can be used to verify the proton transfer in an almost inert matrix.

The majority of molecules presented in the thesis dissertation are based on 2-(2'-hydroxyphenyl)benzazoles (HBX), with either oxygen (HBO), nitrogen (HBI), or sulfur (HBT) heteroatoms. The first group, the HBOs, is the most numerous. It consists of nine compounds, substituted at either 3-, 4-, or 6- position of the phenyl ring. Subgroups can be formed, based on the used substituent, with the main group as modified by ethynyl-extended triisopropylsilyl moiety (TIPS): **HBO-3-TIPS**, **HBO-4-TIPS**, **HBO-6-TIPS**, and **HBO-4,6-TIPS**. All these molecules show significant absorption in the ultraviolet region, with relatively structured multiple bands (Figure 5.1.1a) with the maximum of lowest energy bands positioned at 322-371 nm. Excitation of the latter bands results in a red-shifted single emission in the green region of the visible spectrum (496-526 nm, Figure 5.1.1b), with the highest Stokes shift recorded for **HBO-3-TIPS** (more than 10800 cm^{-1}), and the lowest for the bis-substituted molecule (**HBO-4,6-TIPS**, <8000 cm^{-1}). Nonetheless, significant bathochromic shifts of both absorption and emission are observed for the latter in comparison to mono-substituted HBO derivatives. The observed emission can be assigned to the radiative decay of excited keto species. Determined quantum yield values are relatively high: 15-55%. **HBO-4-TIPS** exhibits the lowest value of QY, while the introduction of the second ethynyl-extended moiety at the 6- position (**HBO-4,6-TIPS**) increases this parameter drastically (to 55%).

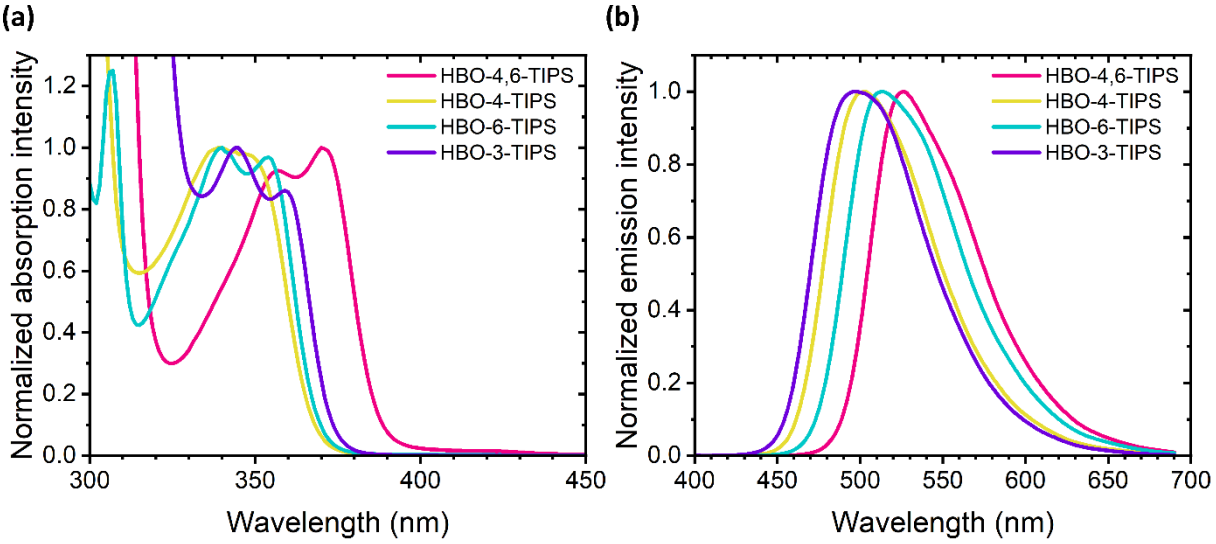

Figure 5.1.1. *Normalized (a) absorption and (b) emission spectra of* ***HBO-TIPS*** *derivatives in toluene (λ_{exc} = 355 nm).*

A change in the length of the alkyl group does not appear to significantly influence the photophysical properties of HBOs. Nevertheless, the bis-substituted π-extended trimethylsilyl derivative (**HBO-4,6-TMS**) exhibits slightly blueshifted absorption (λ_{abs} = 368 nm) and emission bands (λ_{em} = 523 nm), with a lower quantum yield (47%), in comparison to triisopropylsilyl analog (371 nm, 526 nm, 55%, respectively). The beneficial influence of the longer alkyl chains in bis-substituted HBOs can be further confirmed by the **HBO-4,6-TES** compound (QY = 55%). It should be noted that the bis-substituted triethylsilyl material is not a novel derivative as its light amplifying properties were investigated by the Author during the Master studies.[1] However, numerous comparisons will be made as this molecule also belongs to the presented HBO family. Nevertheless, the influence of the alkyl chain lengths is not as pronounced in mono-substituted derivatives. **HBO-6-TIPS** and **HBO-6-TES** analogs are almost indistinguishable, with the emission maxima at 513 and 512 nm, and quantum yield values of 43 and 45% respectively. Substitution with a shorter alkyl chain at 4-position (**HBO-4-TES**) results in a negligible hypsochromic shift of emission band (from 500 to 499 nm), while the absorption band is slightly red-shifted (338 to 345 nm). Nonetheless, all ethynyl-trialkylsilyl substituted hydroxyphenylbenzoxazoles are characterized by large Stokes shifts, ascribed to proton transfer in the excited state and following radiative decay from keto species (Figure 5.1.2.). Two electrodonating alkylaniline groups introduced at 6-position (**HBO-ext-NEt2** and **HBO-ext-NMe2**) lead to red-shifted emission with smaller quantum yield, in comparison to the trialkylsilyl counterparts. Additionally, in the first case, partial frustration of the proton transfer occurs, resulting in dual-emission (466 and 567 nm) due to the

stronger electrodonating character of the substituent, with the lowest quantum yield value of all investigated ESIPTs: 4%. N,N-methylaniline has a weaker donating character, hence the ICT process is not as pronounced in **HBO-ext-NMe2.** Thus, a single emission band is observed (525 nm), corresponding to proton transfer in the excited state, with QY = 16% (see Figure 5.1.2.). A summary of photophysical properties of described HBO derivatives is delisted in Table 5.1.1. All these compounds show increased values of quantum yield, as unsubstituted 2-(2'-hydroxyphenyl)benzoxazole was previously reported to exhibit QY <1% in non-polar solvents.[2,3]

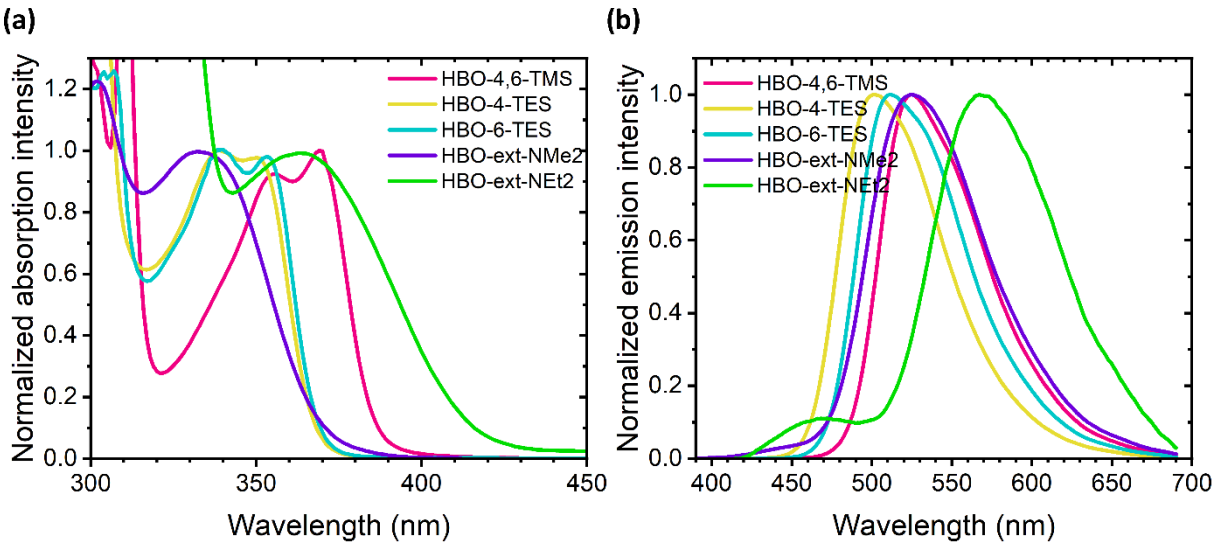

Figure 5.1.2. *Normalized (a) absorption and (b) emission spectra of* ***HBO-TES/TMS/ext-aniline*** *derivatives in toluene (λ_{exc} = 355 nm).*

Table 5.1.1. *Photophysical data for investigated HBO dyes in toluene.*

Compound	λ_{abs} [nm]	ε [$M^{-1}cm^{-1}$]	λ_{em} [nm]	Δν [cm^{-1}]	Φ_{PL}
HBO-4,6-TMS	368	13300	523	8053	0.47
HBO-4-TES	345	12050	499	8945	0.17
HBO-6-TES	340	16600	512	9881	0.45
HBO-3-TIPS	322	17500	496	10895	0.22
HBO-4-TIPS	338	16000	500	9586	0.15
HBO-6-TIPS	340	17600	513	9919	0.43
HBO-4,6-TIPS	371	15700	526	7943	0.55
HBO-ext-NMe2	332	18300	525	11037	0.16
HBO-ext-NEt2	362	7200	466/567	6165/9988	0.04

λ_{abs} – absorption maximum, ε – molar attenuation coefficient, λ_{em} – emission maximum (with λ_{exc} = 355 nm), Δν - Stokes shift, Φ_{PL} – absolute quantum yield of emission

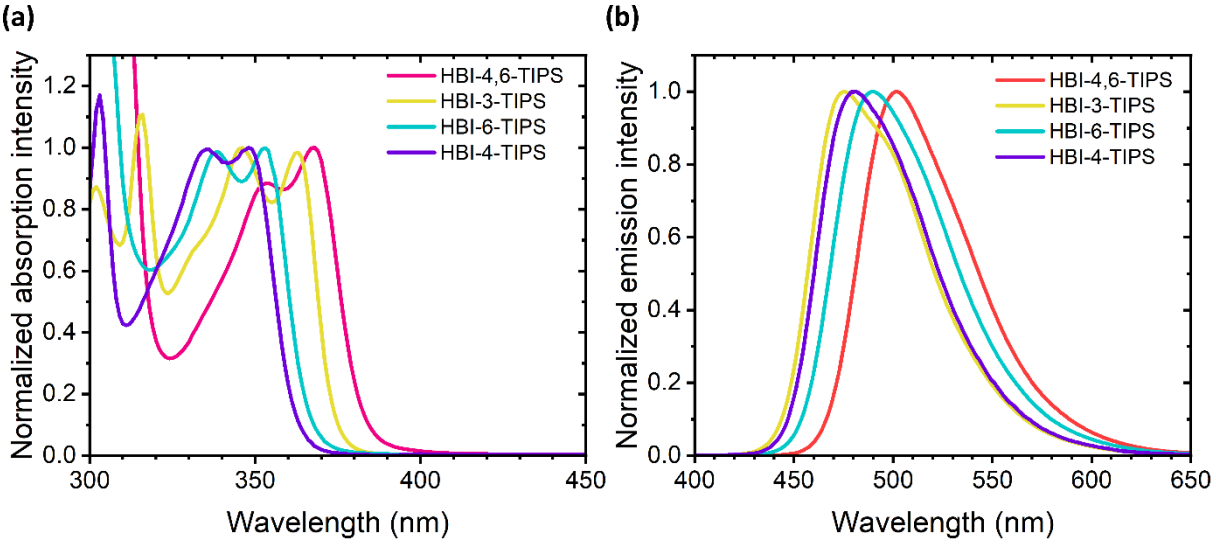

Figure 5.1.3. *Normalized (a) absorption and (b) emission spectra of* ***HBI*** *derivatives in toluene (λ_{exc} = 355 nm).*

The next family, hydroxyphenylbenzimidazoles, consists of four mono- or bis-substituted with ethynyl-extended triisopropylsilyl moieties: **HBI-3-TIPS**, **HBI-4-TIPS**, **HBI-6-TIPS**, and **HBI-4,6-TIPS**. Their absorption profiles are very similar to HBO-TIPS, with weakly structured bands positioned at 346-368 nm. However, excitation of these bands results in a significantly blue-shifted emission (475-502 nm) in comparison to oxygen-substituted analogs. Moreover, the quantum yields of emission are much higher, with outstanding values of 74-98%, which are almost three times higher than those reported for unsubstituted HBI.[2] Progressive bathochromic shifts of both absorption and emission spectra are observed along with the increased distance between the ethynyl-TIPS substituent and the nitrogen atom, which is not involved in hydrogen bonds, i.e. at corresponding 3-, 4- and 6- positions, with the biggest red-shift recorded for bis-substituted derivative (**HBI-4,6-TIPS**), as presented in Figure 5.1.3. Nonetheless, the single emission bands observed at the border of blue and green light are the result of radiative relaxation following the tautomerization of the molecule in the excited state, with the photophysical parameters included in the table below.

Table 5.1.2. *Photophysical data for investigated HBI dyes in toluene.*

Compound	λ_{abs} [nm]	ε [$M^{-1}cm^{-1}$]	λ_{em} [nm]	Δν [cm^{-1}]	Φ_{PL}
HBI-3-TIPS	346	18800	475	7849	0.96
HBI-4-TIPS	347	16100	481	8028	0.74
HBI-6-TIPS	353	15000	490	7920	0.91
HBI-4,6-TIPS	368	15800	502	7254	0.98

λ_{abs} – absorption maximum, ε – molar attenuation coefficient, λ_{em} – emission maximum (with λ_{exc} = 355 nm), Δν - Stokes shift, Φ_{PL} – absolute quantum yield of emission

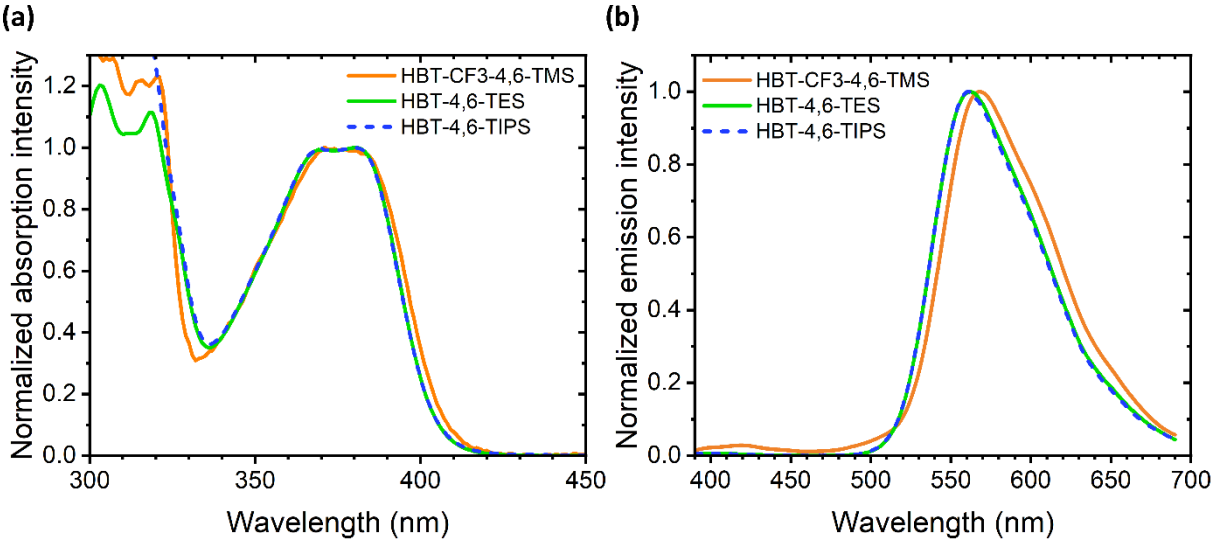

Figure 5.1.4. *Normalized (a) absorption and (b) emission spectra of* ***HBT*** *derivatives in toluene (λ_{exc} = 355 nm).*

The least numerous subgroup of HBXs consists of hydroxyphenylbenzotriazole derivatives: **HBT-CF3-4,6-TMS**, **HBT-4,6-TES**, and **HBT-4,6-TIPS**. They differ in the length of the alkyl chain in the substituent, with the exception of the former compound, which is also substituted with strong electron-withdrawing trifluoromethyl moiety. As a result of such modification, in the excited state, apart from proton transfer, a redistribution of electrons towards the CF_3 group is promoted, causing partial frustration of the first process. This is observed through dual emission (at 376 and 567 nm), like in HBO derivatives substituted with *N,N*-diethylaniline (**HBO-ext-NEt2**).

Table 5.1.3. *Photophysical data for investigated HBT dyes in toluene.*

Compound	λ_{abs} [nm]	ε [$M^{-1}cm^{-1}$]	λ_{em} [nm]	Δν [cm^{-1}]	Φ_{PL}
HBT-CF3-4,6-TMS	376	16200	376/567	8959	0.13
HBT-4,6-TES	378	10400	562	8661	0.26
HBT-4,6-TIPS	378	8400	561	8630	0.26

λ_{abs} – absorption maximum, ε – molar attenuation coefficient, λ_{em} – emission maximum (with λ_{exc} = 355 nm), Δν - Stokes shift, Φ_{PL} – absolute quantum yield of emission

In the case of the previously described groups, the increase in chain length caused the emission and absorption bands to shift towards lower energies (and thus longer wavelengths). This is confirmed in the case of the absorption bands in HBTs (376-378 nm), however, the opposite tendency is shown if the emission is taken into account (561-567 nm). With that said, the shifts are not very pronounced, as depicted in Figure 5.1.4. and Table 5.1.3. The emission

observed for these compounds is in a green-yellow region, significantly bathochromically shifted in comparison to unsubstituted HBT, which was reported to be emissive at 490 nm.[4]

When corresponding bis-substituted HBX analogs are compared, a clear tendency is seen. Emission at shortest wavelengths (and highest energies) is observed for nitrogen analog (**HBI-4,6-TIPS**, λ_{em} = 502 nm, 98 %), followed by oxygen (**HBO-4,6-TIPS,** λ_{em} = 526 nm, 55 %), with the sulfur-substituted derivative as the most red-shifted one (**HBT-4,6-TIPS,** λ_{em} = 561 nm, 26 %). Simultaneously, the fluorescence quantum yield values decrease, which is a common phenomenon, as the probability of non-radiative relaxation pathways increases along with the emission wavelength, since the energy is more easily converted into heat released to the local environment. These findings are in correlation to the theoretical calculations performed for unsubstituted hydroxyphenylbenzazoles.[5]

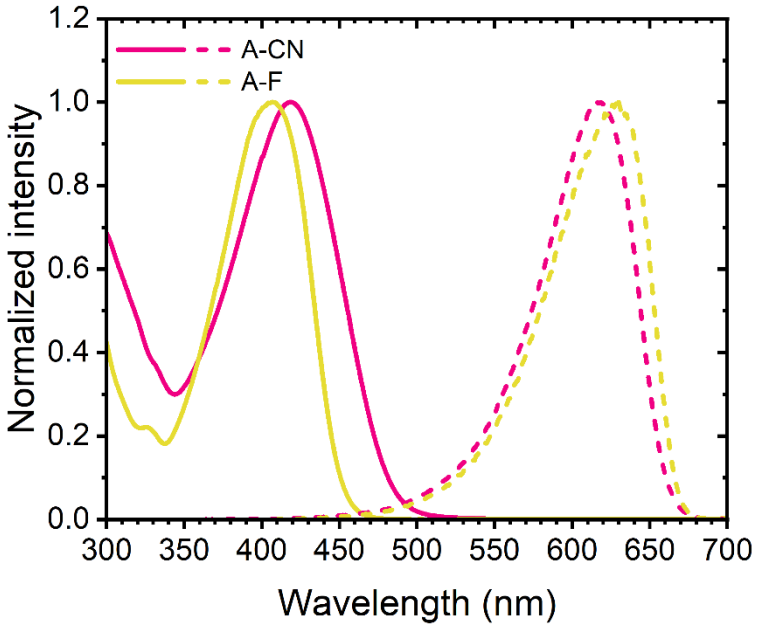

Figure 5.1.5. *Normalized absorption (solid) and emission (dashed) spectra of* ***anil*** *derivatives in toluene (λ_{exc} = 390 nm).*

The two investigated anil derivatives (**A-F** and **A-CN**) exhibit absorption bands on the border between ultraviolet and visible light, with the maximum at 407 and 419 nm, respectively, the excitation of which leads to red emission (630 and 616 nm, Figure 5.1.5). The recorded Stokes shift is smaller for the anil substituted with a cyano group, which is a strong electro-withdrawing moiety, in comparison to a weaker fluoro-derivative. The stronger ICT phenomenon beneficially influences the quantum yield of emission, as this value is higher for **A-F** than **A-CN**.

Table 5.1.4. *Photophysical data for investigated anils in toluene.*

Compound	λ_{abs} [nm]	ε [$M^{-1}cm^{-1}$]	λ_{em} [nm]	Δν [cm^{-1}]	Φ_{PL}
A-CN	419	23200	616	7633	0.12
A-F	407	26300	630	8697	0.05

λ_{abs} – absorption maximum, ε – molar attenuation coefficient, λ_{em} – emission maximum (with λ_{exc} = 355 nm), Δν - Stokes shift, Φ_{PL} – absolute quantum yield of emission

The photophysical properties of studied ESIPT compounds made it possible to determine the best pumping wavelength for light amplification measurements. Hence, the ultraviolet region was deemed as the most appropriate. Unfortunately, due to technical restrictions in the laser laboratory, only one wavelength could be obtained in this range, i.e. 355 nm. Hence, this wavelength was chosen to investigate the spontaneous emission of dye-doped PMMA films. All compounds have shown an intense emission, positioned at wavelengths similar to those observed for toluene solutions. Therefore the proton transfer in the excited state in these solid-state samples was confirmed.

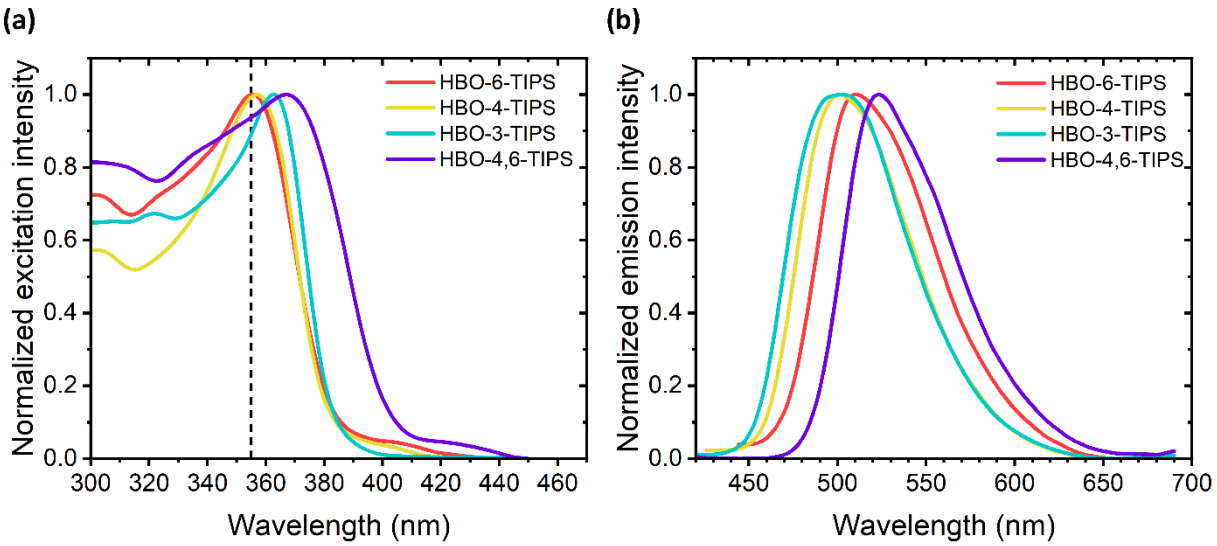

Figure 5.1.6. *Normalized (a) excitation and (b) emission spectra of 1% w/w* ***HBO-TIPS****/PMMA films. The dashed line marks the excitation wavelength (355 nm).*

The HBO-TIPS derivatives were found to be emissive in the blue-green region of visible light (see Figure 5.1.6.), with maxima positioned at 501 – 523 nm. Curiously, the most blue-shifted emission was observed for HBOs substituted at 3- and 4- positions, with their emission profiles of both compounds strongly overlapping one another. Excitation spectra measured for both dyes show single bands, with maxima at 363 and 357 nm respectively. The former (**HBO-3-TIPS**) is characterized by the highest full width at half maximum value (75 nm), slightly larger than **HBO-4-TIPS** (70 nm). Substitution at 6-position with the ethynyl-triisopropylsilyl moiety leads to a bathochromic shift of emission (by 7 nm, **HBO-6-TIPS** λ_{em} = 510 nm), even further pronounced for the bis-substituted analog (**HBO-4,6-TIPS**, 523 nm). As the dependence of the layer thickness and spontaneous aggregates/crystals sizes on the determined quantum yield of emission was found, these values are not given. However, PLQY was calculated for the dye-doped potassium bromide pellets, as their surfaces are flat with the set

dimensions of the investigated sample. Moreover, the determined absolute values were found to be independent of the concentration of the dye in the pellet. Hence, they can be used as a reliable parameter when compounds are compared with one another. These values for HBO-TIPS analogs are high: with the lowest for **HBO-3-TIPS** (49%) and a striking 82% for the **HBO-4,6-TIPS**, much higher than for mono-substituted analogs at 4- or 6- positions (58% and 51%, respectively). The significantly higher values of quantum yield in solid-state in comparison to toluene solutions can be explained by the beneficial rigidification of the hydroxyphenylbenzoxazole scaffold in the solid matrix.

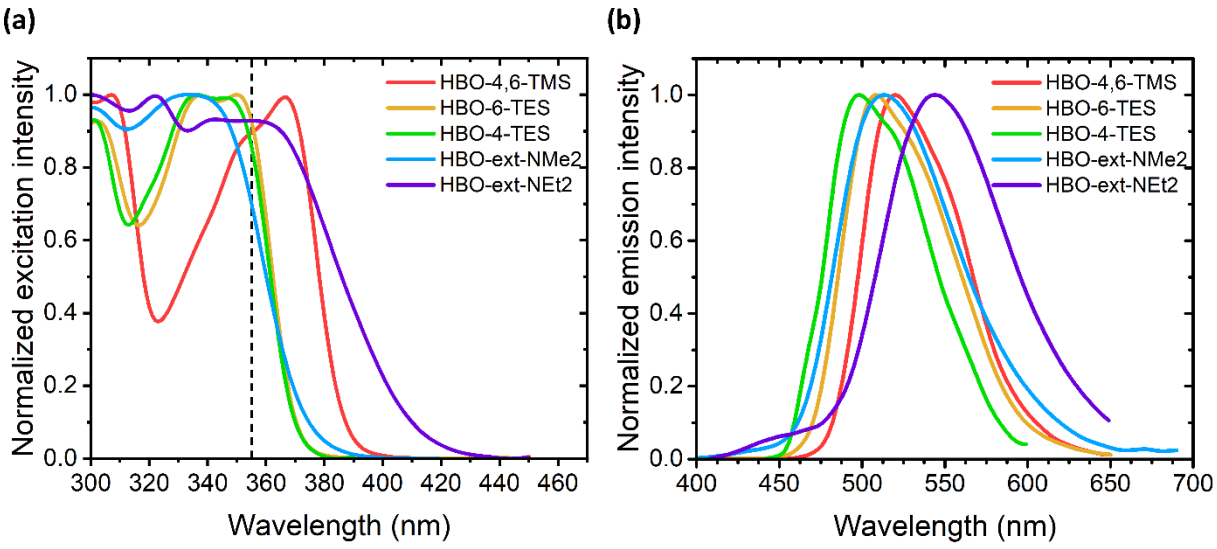

Figure 5.1.7. *Normalized (a) excitation and (b) emission spectra of other 1% w/w* ***HBO****/PMMA films. The dashed line marks the excitation wavelength (355 nm).*

When the length of the alkyl chains is shortened, a slight hypsochromic shift of emission is observed for bis-substituted HBOs (presented in Figure 5.1.7.), along with a decrease in quantum yield. These relations are in correlation with findings recorded for toluene solutions of corresponding dyes. The possible explanation lies in the restrictions of vibrations of alkyl chains in the solid-state due to a smaller distance between the molecules, which is more significant for the longer substituents (**HBO-4,6-TIPS**) than for the shorter ones (**HBO-4,6-TMS**). Hence, non-radiative decay pathways are limited and emission of higher energy photons (thus, shorter wavelengths) is observed. The same influence of the alkyl chain length on the position of emission maximum and QY was noted for substitutions at 4- and 6-positions (**HBO-4-TES** and **HBO-6-TES**), with the former emitting at shorter wavelengths. The beneficial influence of restriction of motions in the inert polymeric matrix is also notable for alkylaniline-substituted HBOs, with quantum yield values of 41 and 36% for **HBO-ext-NMe2** and **HBO-**

ext-NEt2 respectively, with the observed emission of significantly blue-shifted (513 and 557 nm) in comparison to the corresponding toluene solutions. For the latter compound, as in toluene solution, partial frustration of ESIPT phenomena occurs due to substitution with a slightly stronger electrodonating group, leading to a presence of a weak band positioned around 450 nm. Nonetheless, the quantum yield values in KBr pellets are high in all HBO derivatives, enabling the solid-state applications of these compounds. A summary of photophysical properties of described HBO derivatives is delisted in the table below (5.1.5.).

Table 5.1.5. *Photophysical data for investigated HBO dyes in the solid-state.*

Compound	λ_{exc} [nm][a]	λ_{em} [nm][a]	$\Delta\nu$ [cm^{-1}][a]	FWHM [nm][a]	λ_{em} [nm][b]	Φ_{PL} [b]
HBO-4,6-TMS	366	520	8092	68	534	0.70[6]
HBO-6-TES	350	508	8886	73	514	0.53[6]
HBO-4-TES	336	498	9682	71	504	0.66[6]
HBO-6-TIPS	355	510	8561	72	536	0.51
HBO-4-TIPS	357	501	8051	70	504	0.58[7]
HBO-3-TIPS	363	503	7667	75	496	0.49[7]
HBO-4,6-TIPS	367	523	8127	70	530	0.82[7]
HBO-ext-NMe2	333	513	10537	81	528	0.41
HBO-ext-NEt2	322	450/557	12674	92	440/560	0.36

λ_{exc} – excitation maximum, λ_{em} – emission maximum, $\Delta\nu$ – Stokes shift, FWHM – full width at half-maximum, Φ_{PL} – quantum yield of emission (determined with a spectrometer with an integrating sphere), [a] as 1% wt. doping in PMMA matrix, [b] embedded in KBr pellets.

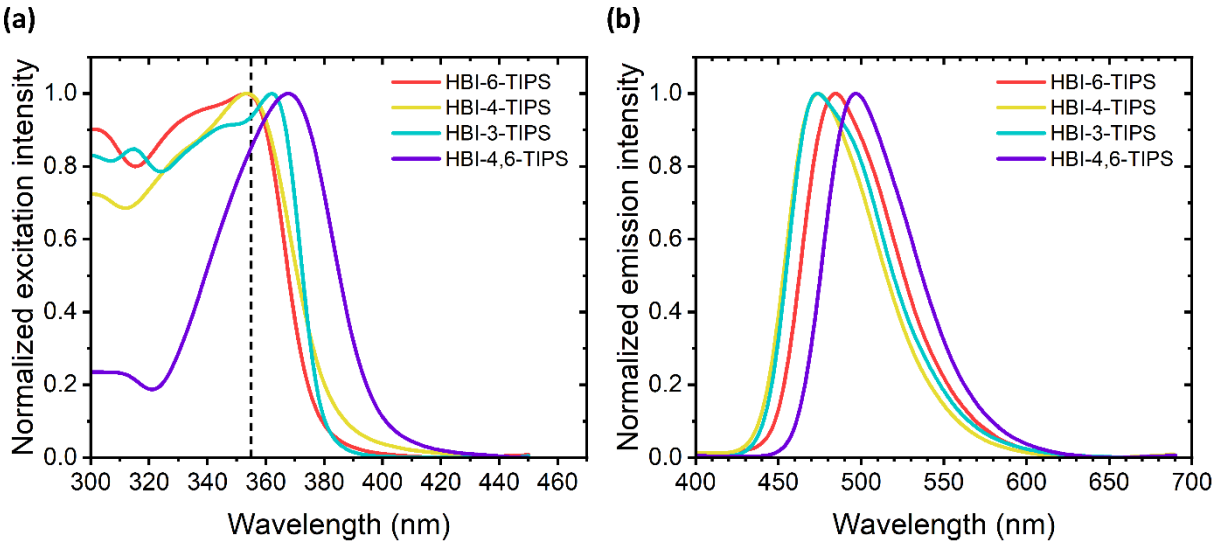

Figure 5.1.8. *Normalized (a) excitation and (b) emission spectra of 1% w/w* ***HBI****/PMMA films. The dashed line marks the excitation wavelength (355 nm).*

As for HBO-TIPS compounds, the emission of hydroxyphenylbenzimidazoles (the HBIs) can be tuned depending on the place of substitution with triisopropylsilyl moiety.

However, the introduction of nitrogen instead of oxygen promotes a more narrow and hypsochromically shifted emission in the blue region of visible spectra (see Figure 5.1.8.), with overall lower quantum yields. A reverse tendency can be observed in terms of the effect of the substitution site on the QY values in comparison to the HBO-analogs: the bis-substituted derivative is the most red-shifted and least emissive in solid-state (**HBI-4,6-TIPS,** 497 nm, 30%), while the most intense and blue-shifted emission was recorded for **HBI-3-TIPS** (474 nm, 68%). These observations can be rationalized by the influence of substitution on the planarity of HBIs and related emission quenching, as it was found that bis-substitution reinforces the planarity of the molecule and enables detrimental π-π-stacking interactions of **HBI-4,6-TIPS**. The summary of HBI's parameters is listed in the table below (5.1.6).

Table 5.1.6. *Photophysical data for investigated HBI dyes in the solid-state.*

Compound	λ_{exc} [nm][a]	λ_{em} [nm][a]	$\Delta\nu$ [cm^{-1}][a]	FWHM [nm][a]	λ_{em} [nm][b]	Φ_{PL} [b]
HBI-6-TIPS	353	484	7667	62	470	0.36
HBI-4-TIPS	354	474	7152	62	460	0.39
HBI-3-TIPS	362	474	6527	65	488	0.68
HBI-4,6-TIPS	368	497	7053	62	490	0.30

λ_{exc} – excitation maximum, λ_{em} – emission maximum, $\Delta\nu$ – Stokes shift, FWHM – full width at half-maximum, Φ_{PL} – quantum yield of emission (determined with a spectrometer with an integrating sphere), [a] as 1% wt. doping in PMMA matrix, [b] embedded in KBr pellets

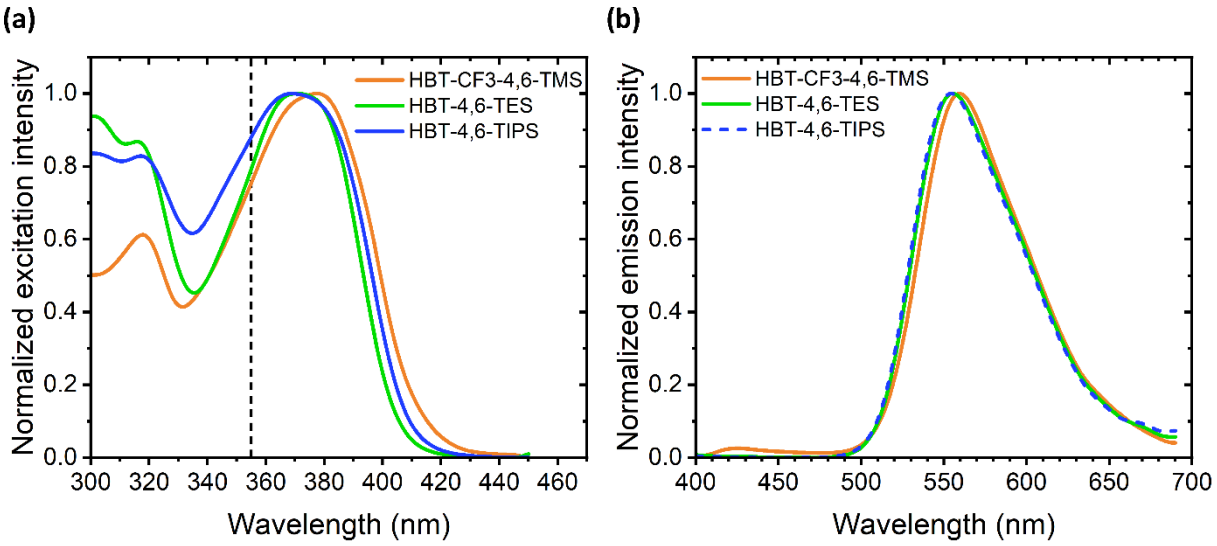

Figure 5.1.9. *Normalized (a) excitation and (b) emission spectra of 1% w/w* ***HBT****/PMMA films. The dashed line marks the excitation wavelength (355 nm).*

The sulfur substituted compounds (the HBTs) are characterized by the most broad (FWHM: 74-76 nm) and red-shifted emission (554-560 nm) from all investigated HBX derivatives, with relatively high quantum yield values (34-48%). The influence of the length of

the alkyl chain in ethynyl-extended silyl substituent is even more minor than for corresponding HBO analogs, even though a slight tendency towards emission at shorter wavelengths along with increased chain length can be noted in doped polymeric films (Figure 5.1.9). On the other hand, the introduction of a strong electron-withdrawing group (-CF_3) promotes partial frustration of the proton transfer, leading to an appearance of a weak and blue-shifted band at 425 nm (**HBT-CF3-4,6-TMS**), originating from radiative decay of excited enol form. The occurring ICT can explain the lower value of quantum yield (34%) in comparison to other HBT derivatives, as it is a competing process with the ESIPT (Table 5.1.7.).

Table 5.1.7. *Photophysical data for investigated HBT dyes in the solid-state.*

Compound	λ_{exc} [nm][a]	λ_{em} [nm][a]	$\Delta\nu$ [cm^{-1}][a]	FWHM [nm][a]	λ_{em} [nm][b]	Φ_{PL} [b]
HBT-CF3-4,6-TMS	377	425/560	8668	74	570	0.34
HBT-4,6-TES	371	555	8936	76	575	0.48
HBT-4,6-TIPS	369	554	9050	76	574	0.48[7]

λ_{exc} – excitation maximum, λ_{em} – emission maximum, $\Delta\nu$ – Stokes shift, FWHM – full width at half-maximum, Φ_{PL} – quantum yield of emission (determined with a spectrometer with an integrating sphere), [a] as 1% wt. doping in PMMA matrix, [b] embedded in KBr pellets

The last subgroup of investigated ESIPT compounds, the anil derivatives, are the least emissive. A single and broad emission band was recorded for both molecules, ascribed to radiative relaxation of excited keto tautomer. Based on low quantum yield values (see Table 5.1.8), it can be theoreticized that these anil derivatives are prone to π-π stacking and H-type aggregation, evidenced by blue-shifted emission of doped polymeric film in comparison to KBr pellet and diluted toluene solution. The low QY and relatively small Stokes shifts severely limit the solid-state applications of these compounds, at least as possible light sources. The rather unstructured excitation spectra

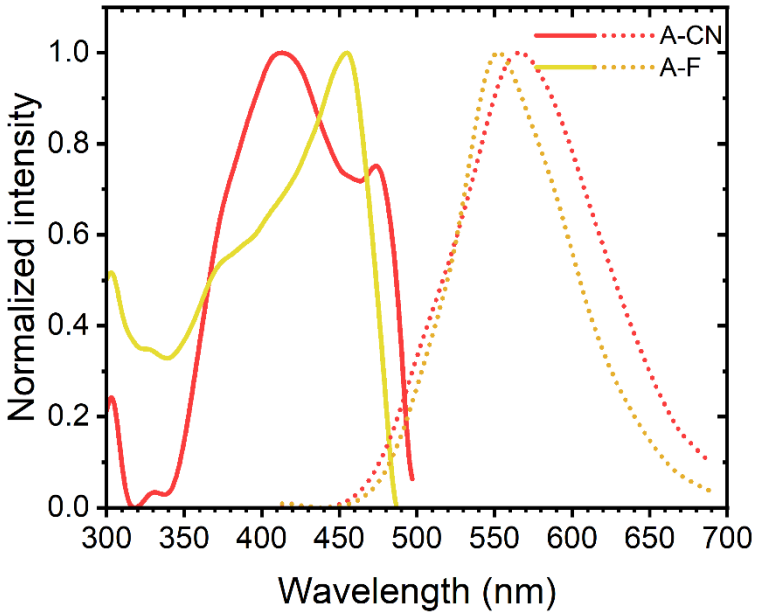

Figure 5.1.10. *Normalized excitation and emission spectra of 1% w/w* ***A-CN*** *and* ***A-F****/PMMA films (λ_{exc} 355 nm).*

(Figure 5.1.10.) show that wavelengths longer than 355 nm could be better suited as a pump in light amplification studies, even those from the visible region.

Table 5.1.8. *Photophysical data for investigated anils dyes in the solid-state.*

Compound	λ_{exc} [nm][a]	λ_{em} [nm][a]	$\Delta\nu$ [cm^{-1}][a]	FWHM [nm][a]	λ_{em} [nm][b]	Φ_{PL} [b]
A-CN	413	566	6545	114	580	0.05
A-F	455	552	3862	90	565	0.01

λ_{exc} – excitation maximum, λ_{em} – emission maximum, $\Delta\nu$ – Stokes shift, FWHM – full width at half-maximum, Φ_{PL} – quantum yield of emission (determined with a spectrometer with an integrating sphere), [a] as 1% wt. doping in PMMA matrix, [b] embedded in KBr pellets

Nevertheless, all investigated compounds can undergo proton transfer in the excited state, observed by large Stokes shifts, in both solutions and solid-state. Based on the matrix (solvent or inert polymer) different routes can be taken to finely tune the desired emission properties.

5.2. Aggregation Influence on the Emission (AIE/AIEE)

As presented in the previous subchapter, investigated compounds have different photophysical properties when the distance between corresponding molecules decreases. The promising and beneficial influence of restriction in solid matrices prompted the Author to verify whether additional effects take place, such as Aggregation-Induced Emission Enhancement. These measurements also provide additional spectroscopic data, which can be helpful in terms of the geometrical arrangements of the molecules with one another. Hence, tetrahydrofuran/water mixtures with set concentrations of the dye were prepared and investigated according to the methodology described in the previous chapter.

When the AIE phenomenon was first discovered, the ESIPT process was investigated as one of the possible mechanisms behind emission enhancement. Many compounds belonging to this family are reported to have better emissive properties in solid-state than in solutions, including many hydroxyphenylbenzazole derivatives,[8–11] as the majority of the dyes presented in this dissertation. Depending on the position of substitution with the ethynyl-extended triisopropylsilyl group, the HBOs show different properties upon water-induced aggregation. When the substituent is close to the oxygen in the benzoxazole scaffold (**HBO-3-TIPS**), the intensity of the observed emission is increased along with ongoing aggregation. Even when heavily dispersed in water (at f_{THF} = 0.01%), the recorded intensity is much higher than for pure

solution in a good solvent, as presented in Figure 5.2.1a-b. Slight shifts of the emission band towards shorter wavelengths can be seen, quite possibly originating from the restriction of intramolecular motion (RIM) of the molecule. Thus, rotation around the single band connecting benzoxazole and phenyl moieties and other non-radiative deactivation pathways are prevented. As a result, the intramolecular hydrogen bond is not disrupted, which promotes the ESIPT phenomena. Hence, **HBO-3-TIPS** has AIEE properties.

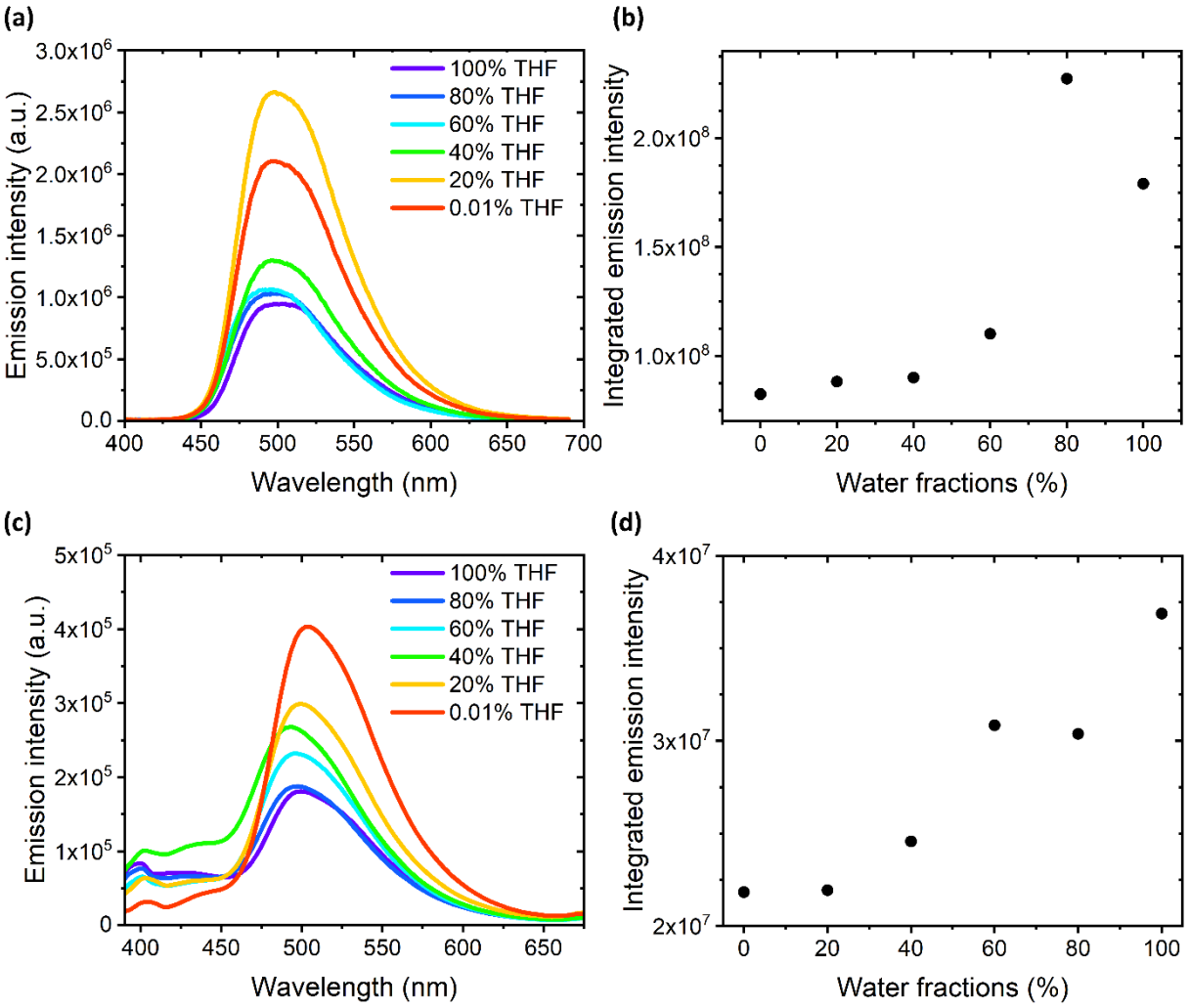

Figure 5.2.1. *Emission spectra and corresponding integrated intensity of* ***HBO-3-TIPS*** *(a,b) and* ***HBO-4-TIPS*** *(c,d) in THF/water mixtures.*

When the HBO is substituted at the 4-position, the compound behaves in a very similar way to the previously described analog. Based on the changes in the placement of the emission maxima (Figure 5.2.1c-d), a redshift of the spectra is visible along with an aggregation, giving rise to the possibility of J-aggregates formation. Moreover, no decrease in intensity is recorded for the highest fraction of water: the initial intensity is almost twice as high. **HBO-6-TIPS** is a molecule that behaves somewhat erratically when aggregated. At first, for small water

fractions (up to 20 %), an increase in emission intensity is observed (Figure 5.2.2a-b). The opposite occurs along with further aggregation, however, the recorded values are still higher than the initial one. While the primordial increase is possibly a result of beneficial RIM, the diminishing between molecules can lead to undesirable detrimental interactions such as stacking of π-conjugated planes, resulting in an emission quenching. Similar behavior was recorded for bis-substituted analog (**HBO-4,6-TIPS,** Figure 5.2.2c-d), for which a significant decrease in the fluorescence is observed for water fractions higher than 60%. The presence of ethynyl-TIPS moiety at the 4-position does not seem to be beneficial enough for the emission enhancement to take place.

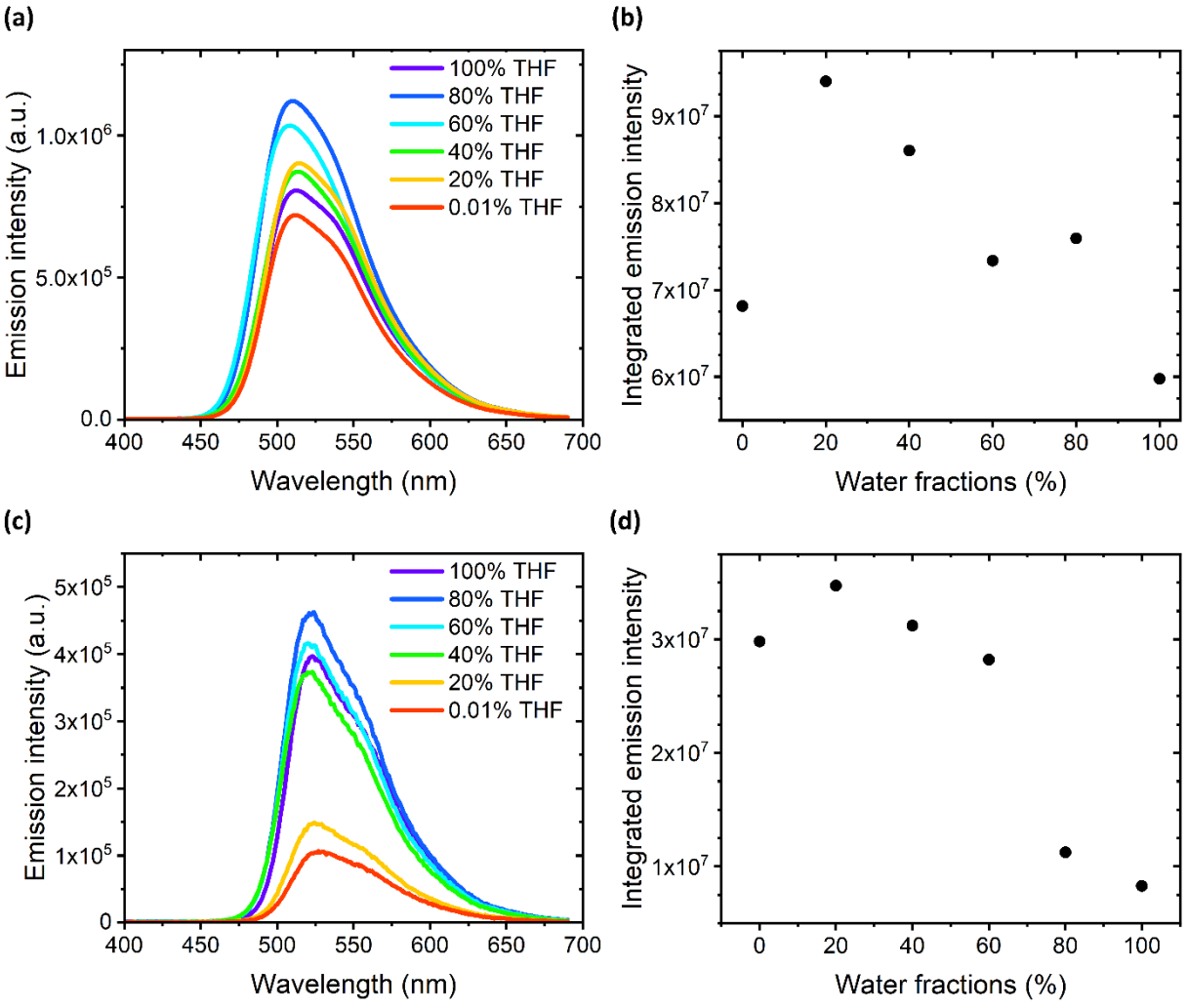

Figure 5.2.2. *Emission spectra and corresponding integrated intensity of* ***HBO-6-TIPS*** *(a,b) and* ***HBO-4,6-TIPS*** *(c,d) in THF/water mixtures.*

Curiously, the bis-substitution of the hydroxyphenylbenzoxazole with ethynyl-extended trialkylsilyl moieties of shorter chain length (**HBO-4,6-TMS**, **HBO-4,6-TES**) seems beneficial, as for both compounds a continuous increase in emission intensity is observed along with aggregation for up to 60% of water fractions. It appears that the rigidity of the molecule is increased when the alkyl chain is shorter, thus non-radiative decay pathways are limited. Further aggregation, and the corresponding decrease in distance between the molecules, leads to the behavior observed for the **HBO-6-TIPS** analog – a drastic diminishing of the emission intensity takes place (see Figure 5.2.3.). Nevertheless, presented HBO derivatives do not exhibit aggregation-caused quenching – the final intensity can be lower than the initial one, but the compounds remain highly fluorescent in such colloid mixtures.

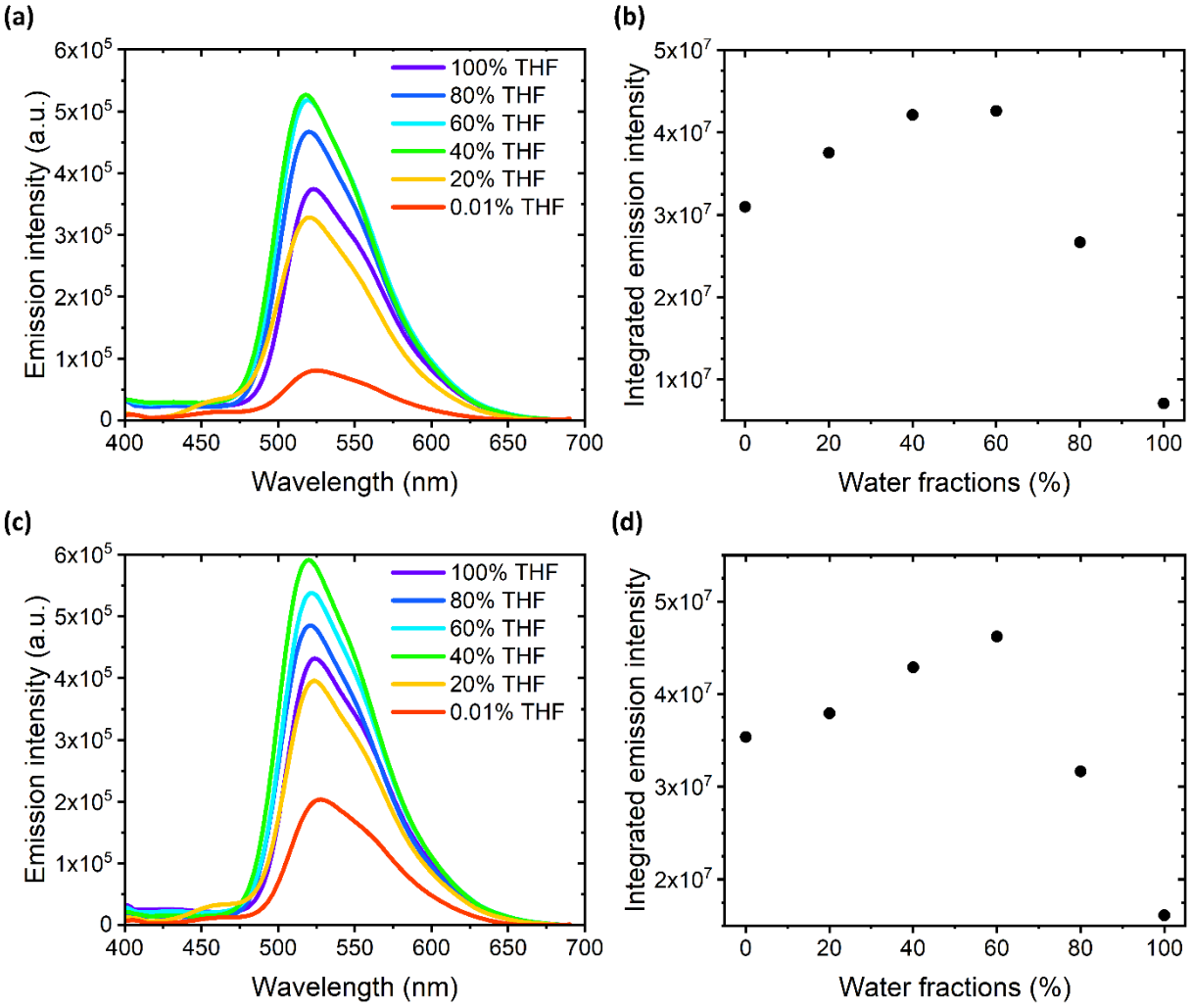

Figure 5.2.3. *Emission spectra and corresponding integrated intensity of* ***HBO-4,6-TMS****(a,b) and* ***HBO-4,6-TES*** *(c,d) in THF/water mixtures.*

The nitrogen analogs mono-substituted at 3- (**HBI-3-TIPS**) and 4- (**HBI-4-TIPS**) positions behave in the opposite way to their HBO equivalents. In these compounds, no emission enhancement can be noted for any water fraction. In addition, a hypsochromic shifting of the single emission band is progressing along with the aggregation. This observation and the gradual decrease in the fluorescence intensity can be explained by the formation of H-aggregates (see Figure 5.2.4). Additionally, hydroxyphenylbenzimidazoles are known for their affinity to form hydrogen bonds with protic solvents, like water used in the experiments. Hence, the proton transfer in the excited state is disrupted, evidenced by the diminished intensity from the excited keto tautomer. The second hypothesis seems more probable, as the quantum yield values of potassium bromide pellets remain high (68 and 39% for 3- and 4-position, respectively).

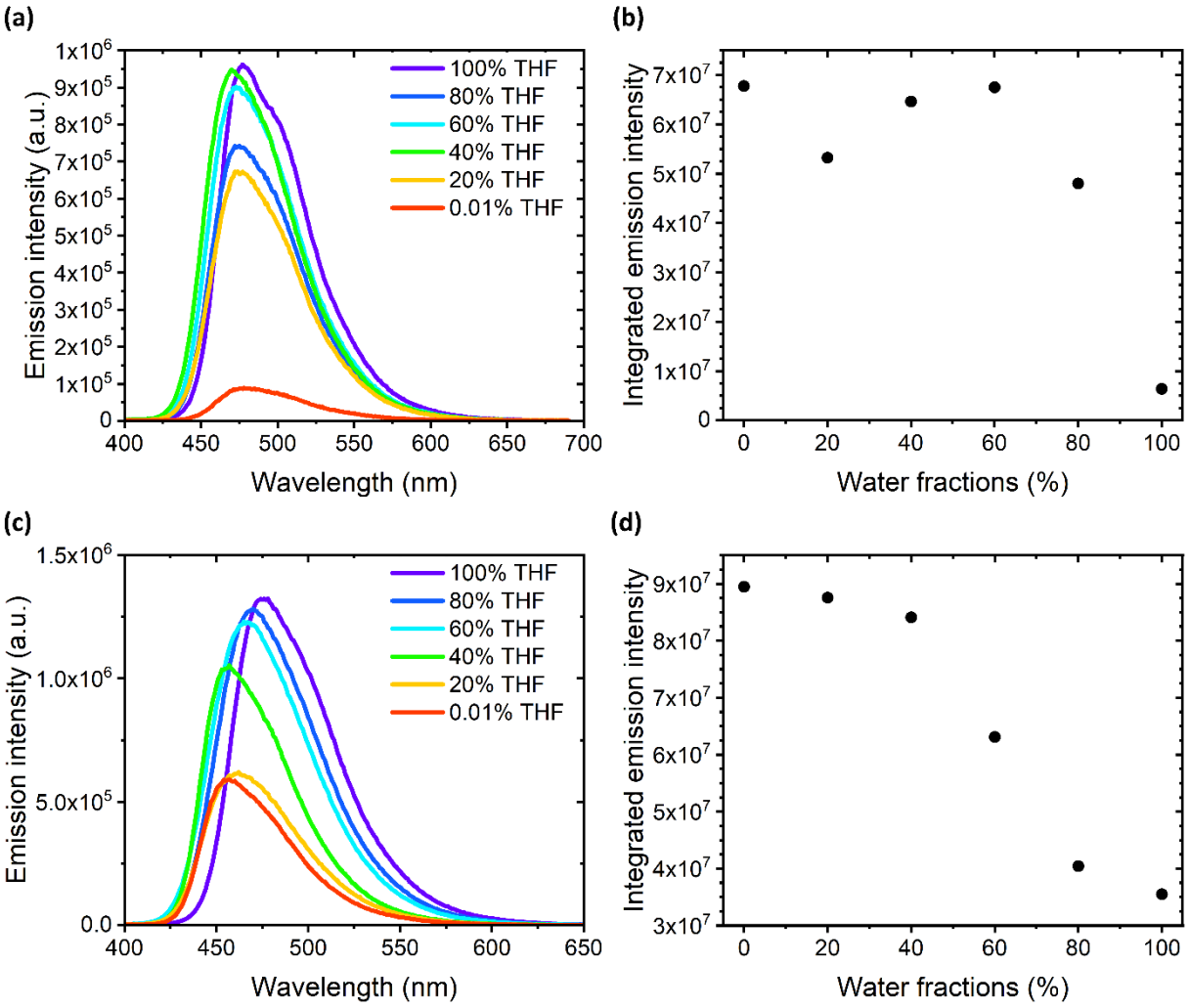

Figure 5.2.4. *Emission spectra and corresponding integrated intensity of* ***HBI-3-TIPS*** *(a,b) and* ***HBI-4-TIPS*** *(c,d) in THF/water mixtures.*

Two other nitrogen derivatives also behave contrary to their respective HBO analogs. While the mono- (at 6-) or bis-substituted (at 4,6-position) benzoxazole derivatives were less emissive along with the aggregation, the increase in water fractions in colloidal mixtures of benzimidazoles promotes the ESIPT process, thus emission is enhanced for f_{water} up to 60%. Just like in bis-substituted **HBO-4,6-TMS** and **HBO-4,6-TES**, further aggregation leads to a decreased intensity of fluorescence. In both **HBI-6-TIPS** and **HBI-4,6-TIPS,** the position and profile of the emission band do not change when the molecules are aggregated in a small extent. Hence, it can be hypothesized that the initial proximity of dye molecules with one another restricts intramolecular motions, promoting the ESIPT phenomena. However, a further decrease in the distance can result in stacking, evidenced by the blue shift of the emission maximum at low THF fractions, as depicted in Figure 5.2.5.

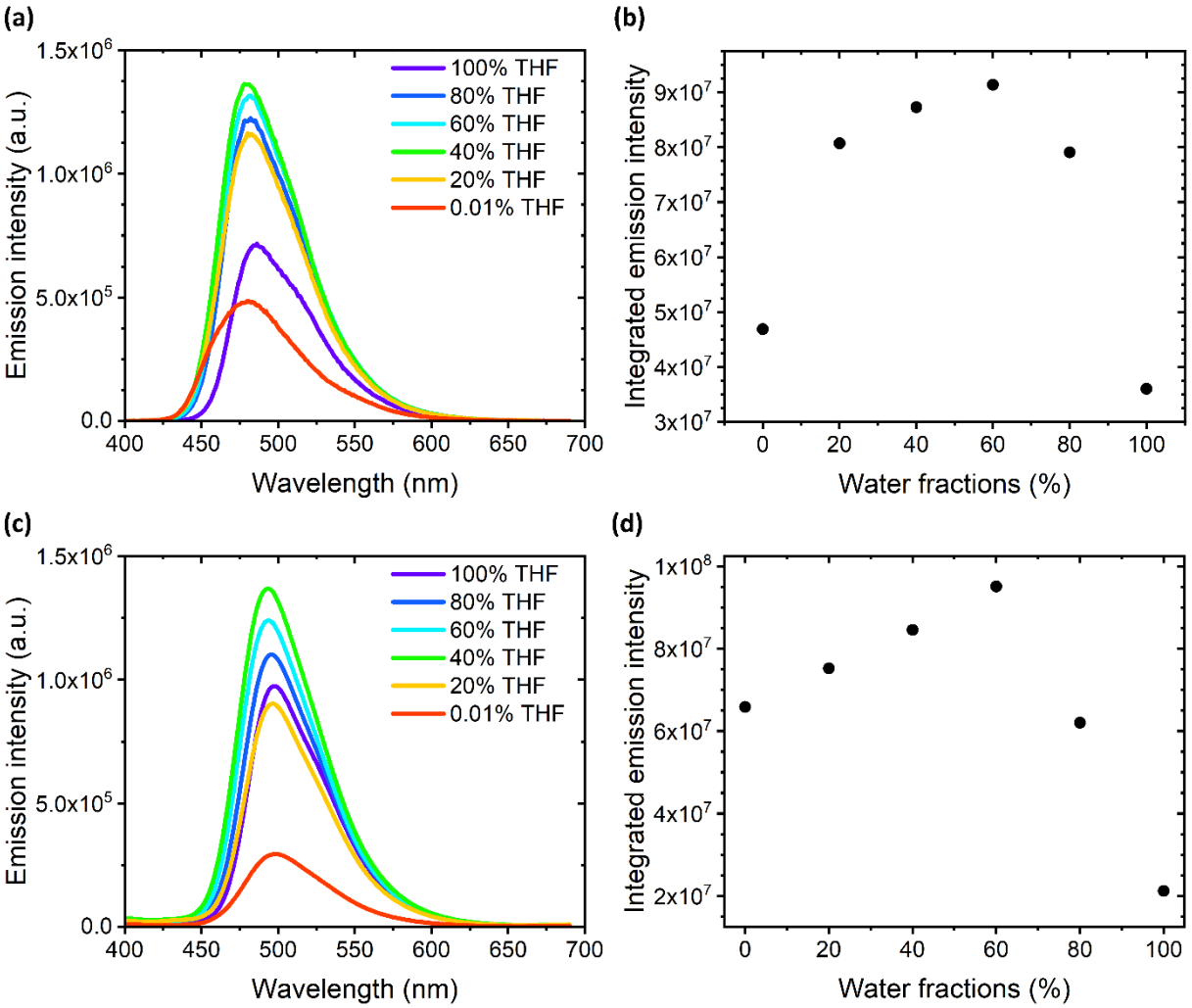

Figure 5.2.5. *Emission spectra and corresponding integrated intensity of* ***HBI-6-TIPS*** *(a,b) and* ***HBI-4,6-TIPS*** *(c,d) in THF/water mixtures.*

The HBT derivatives investigated in this dissertation have shown an affinity towards deprotonation in a protic environment. This matter is discussed more in detail in the *Applications* subchapter on the example of **HBT-CF3-4,6-TMS** is presented in *6.2. Emission tuning and sensing*. The **HBT-4,6-TIPS** derivative shows similar behavior, as depicted in Figure 5.2.6. The water fractions present in the colloidal mixtures make an environment protic enough for the deprotonation of the enol form to take place. This phenomenon results in an instant formation of the second emissive band (*ca.* 490 nm) – hypsochromically shifted in comparison to the excited keto tautomer (*ca.* 570 nm), but more red-shifted than the enol form (<400 nm). Hence, the population of molecules capable of ESIPT phenomena is diminishing, observed by a relative decrease in emission intensity. Moreover, the anionic species are highly fluorescent in diluted solutions (which explains the sudden jump for f_{water} = 20%), but are prone to π-π stacking in the solid-state, evidenced by a continuous decrease in the emission intensity. Nevertheless, the band from deprotonated form disappears from the spectra for high water fractions (f_{water} > 80 %) as it's fully quenched then.

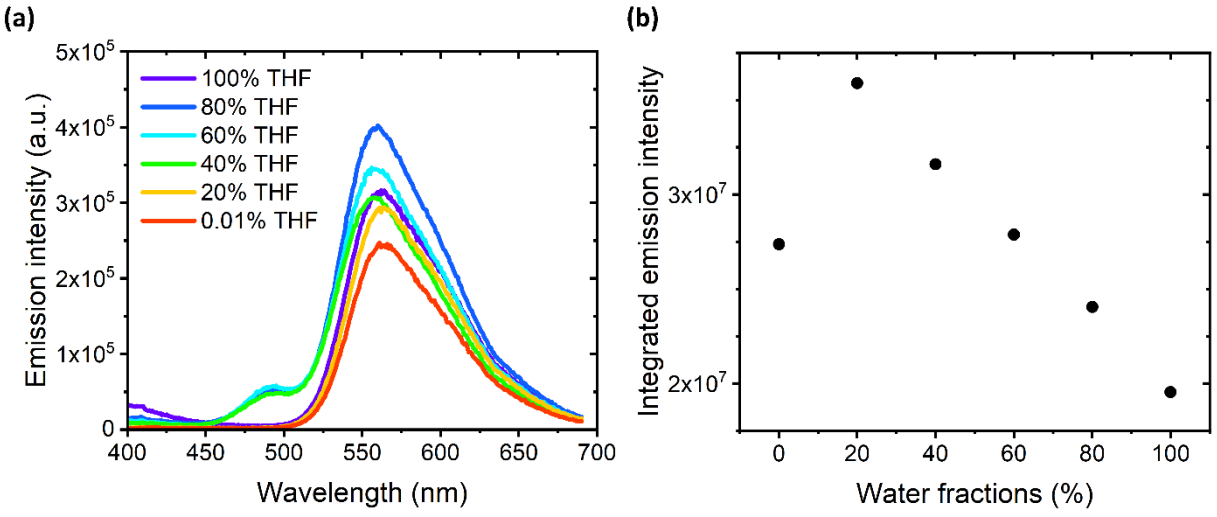

Figure 5.2.6. *(a) Emission spectra and (b) corresponding integrated intensity of* ***HBT-4,6-TIPS*** *in THF/water mixtures.*

The **A-CN** and **A-F** compounds are unfortunately prone to such stacking of the π-conjugated cores of the molecules too. In both cases, the aggregation due to an increased amount of water in the mixture leads to complete quenching of the fluorescence, as presented in Figure 5.2.7. The observed drastic decrease in the emission intensity, along with the blue shift of the band, suggests the formation of head-to-head aggregates. This possibility is further confirmed when the emission properties of the dyes dispersed in the PMMA matrix or potassium bromide are taken into account. The latter can be treated almost like a diluted solution

of the compounds in the solid-state due to the specific type of preparation of the sample. Hence, in the polymeric matrix, the dye molecules are in closer proximity, thus they can form dimers or higher-order structures. If those two facts are taken into account then a significant hypsochromic shift of the maximum of the emission band due to aggregation is clear in the investigated thin films. The emission quantum yield in KBr pellets is low for both molecules. Therefore the mechanism behind ACQ in **A-CN** and **A-F** seems quite clear.

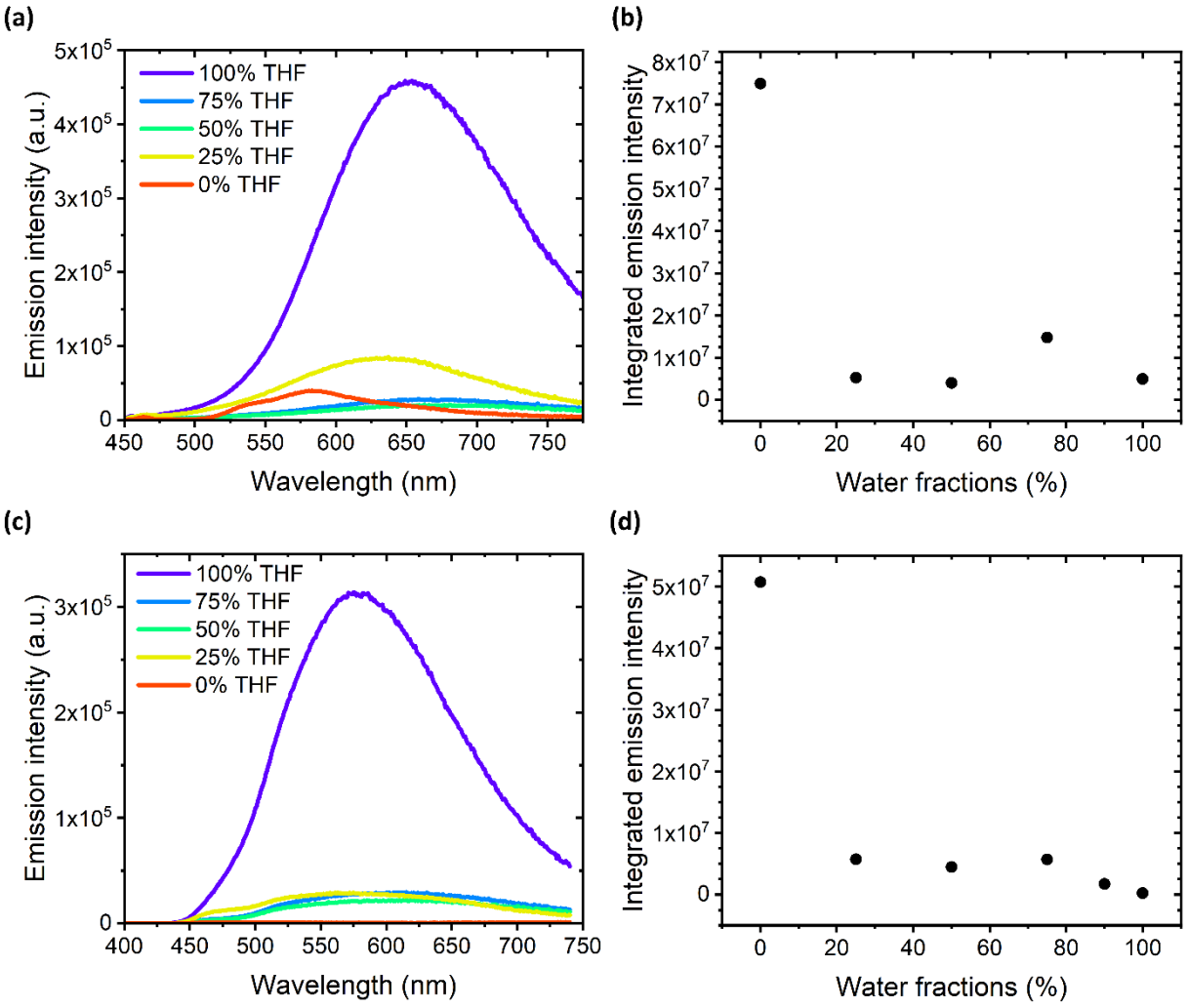

Figure 5.2.7. *Emission spectra and corresponding integrated intensity of* ***HBI-6-TIPS*** *(a,b) and* ***HBI-4,6-TIPS*** *(c,d) in THF/water mixtures.*

5.3. Light amplification

This last subchapter contains the most important results concerning light amplification properties of investigated ESIPT compounds. The experimental results and determined parameters of the dyes embedded in polymeric thin films, in concentrated solutions, and as amorphous powders are presented. Almost all of the chromophores are capable of light amplification, at least in guest-host systems, with the exception of the anil derivatives: **A-F** and **A-CN**. The letter was expected, as the spontaneous emission was poor in the solid state. Hence, lasing threshold, net gain, and other significant parameters were determined for hydroxyphenylbenzazole analogs.

POLYMERIC DYE-DOPED THIN FILMS

The ESIPT compounds presented in this thesis were used as dopants in the polymeric matrix, i.e. poly(methyl methacrylate). According to the methodology described in the previous chapter, a series of 1% w/w guest-host type samples were prepared. The hydroxyphenylbenzoxazoles are the most numerous subgroup of all investigated dyes. Hence, they are here repeatedly used as a reference for other HBX derivatives. The first compound, **HBO-3-TIPS,** when embedded in the PMMA matrix is capable of light amplification, observed as random lasing. With the position of the central emitted wavelength located at 518 nm, very clear and sharp peaks (FWHM < 0.5 nm) appear in the spectra when the sample is pumped with a 355 nm laser of high enough energy density, as presented in Figure 5.3.1a. which depicts lasing action of this mono-substituted derivative. The observed spectra and easily

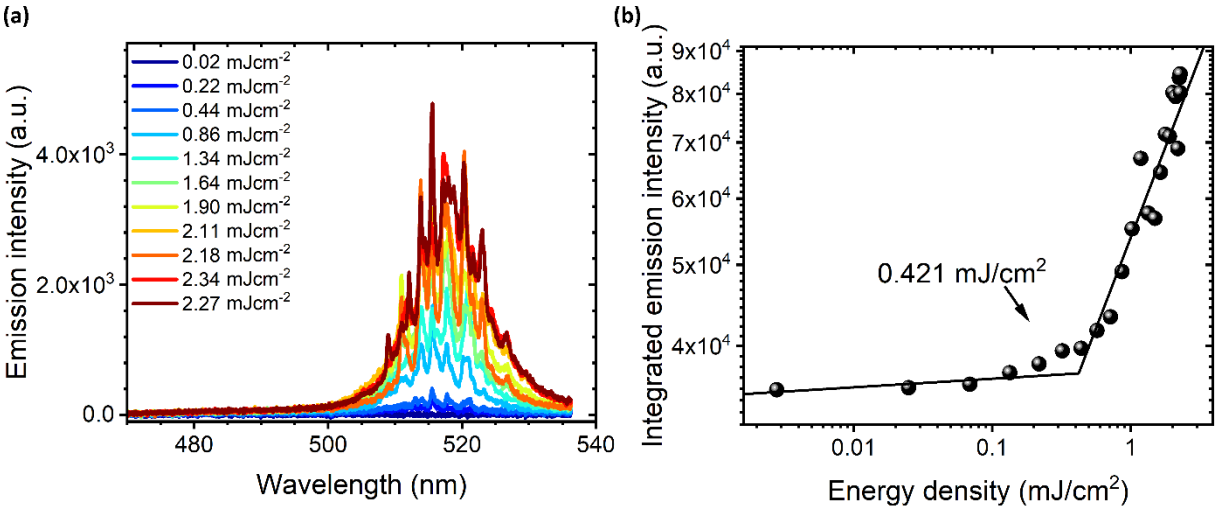

Figure 5.3.1. *(a) Random lasing spectra of 1%* ***HBO-3-TIPS****/PMMA, with corresponding (b) calculated lasing threshold (λ_{exc} = 355 nm).*

distinguishable and well-defined modes are characteristic for coherent RL. The lasing spectrum of **HBO-3-TIPS**/PMMA at energy density higher than the threshold values is much more narrow than the corresponding spontaneous emission one, with full width at half maximum of 10.7 nm, which is an almost 7 times smaller value (see Figure 5.3.2). Additionally, the lasing spectrum is moved towards longer wavelengths. Hence, it can be concluded that the pumping is efficient enough to excite aggregates and crystals that form in the PMMA matrix during the sample preparation. As the films were prepared with the use of the drop-casting method, the following evaporation of the remaining solvent at room temperature is slow, giving enough time to the dye molecules to reorient themselves in between the long polymeric chains. Thus, the formation of the dimers and aggregates of higher order is possible. These structures, along with local differences in the layer morphology, can act as scattering centers necessary for the random lasing action to occur. The lasing threshold was determined as the point of intersection of two linear functions describing the increase in emission intensity as a result of increased pumping energy density i) before and ii) after obtaining laser action (Figure 5.3.1b). The final value was estimated by the arithmetic mean of measurements performed for several different places on the sample. Hence, the lasing threshold for the **HBO-3-TIPS** was determined to be 0.32 ± 0.07 mJ·cm^{-2}, which is a comparable value with the thresholds of commercially available laser dyes. The estimated net gain value is 4.62 ± 0.84 cm^{-1}.

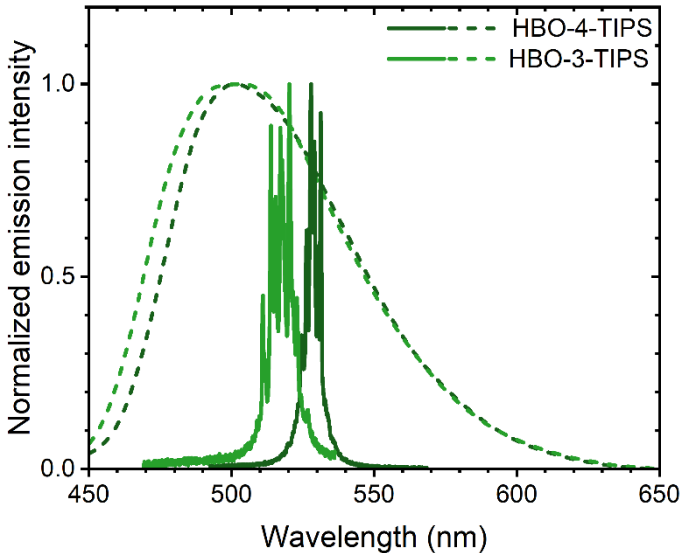

Figure 5.3.2. *Spontaneous (dashed) and stimulated (solid) emission of* ***HBO-3-TIPS*** *and* ***HBO-4-TIPS*** *in PMMA (λ_{exc} = 355 nm).*

The second mono-substituted derivative, with ethynyl-TIPS moiety at the 4-position (**HBO-4-TIPS**), shows similar behavior. The RL spectrum is, however, even further shifted towards longer wavelengths in comparison to spontaneous emission (Figure 5.3.2), with the maximum positioned at 529 nm. The full width at half maximum is the smallest of all HBX derivatives, with a value of 6.8 nm. The modes observed during the random lasing action are even more pronounced – individual peaks significantly stand out above the overall emission

band (Figure 5.3.3). The lasing parameters of **HBO-4-TIPS** are slightly lower than for **HBO-3-TIPS**, with a higher threshold (0.45 ± 0.09 mJ·cm^{-2}) and lower net gain (3.34 ± 0.36 cm^{-1}).

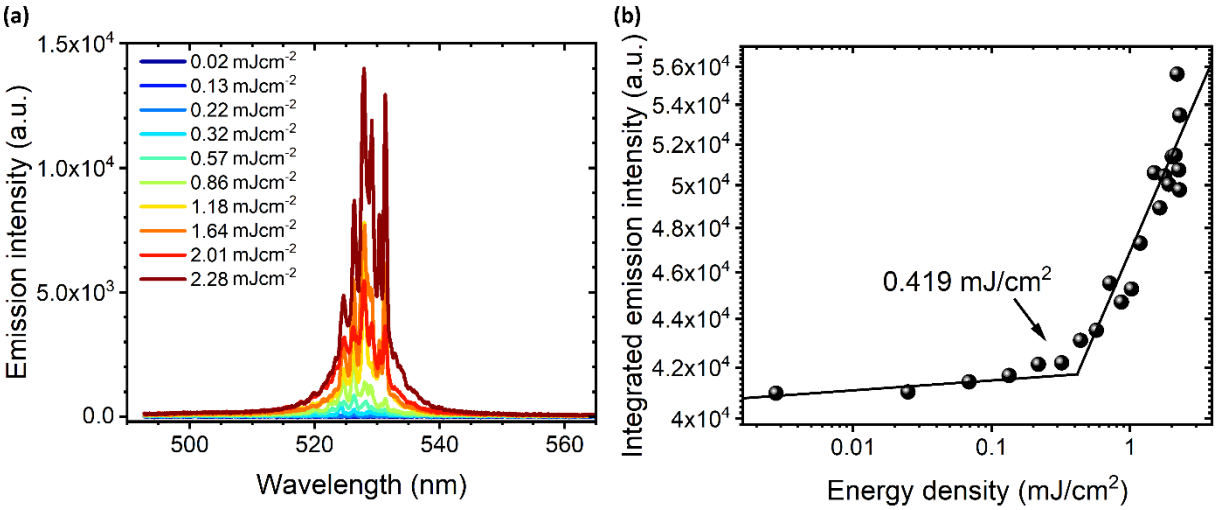

Figure 5.3.3. *(a) Random lasing spectra of 1% **HBO-4-TIPS**/PMMA, with corresponding (b) calculated lasing threshold (λ_{exc} = 355 nm).*

The highest net gain of all HBO-TIPS derivatives was determined for **HBO-6-TIPS**, with the value 8.46 ± 0.73 cm^{-1}, and the lasing threshold comparable with other mono-substituted analogs (0.45 ± 0.09 mJ·cm^{-2}). No correlation between the quantum yield of emission measured for doped potassium bromide pellet and the lasing properties can be found.

The relatively narrow spectrum of **HBO-6-TIPS** (FWHM = 9.8 nm) with the maximum at 546 nm is the most red-shifted from the corresponding spontaneous emission of polymeric thin film (by 36 nm, see Figure 5.3.4). Observed modes are relatively pronounced, with slightly broadened spikes. The density of these peaks is higher than for previously described derivatives (see Figure 5.3.5). Additionally, the positions of some of the individual spikes appear to vary with each pumping pulse.

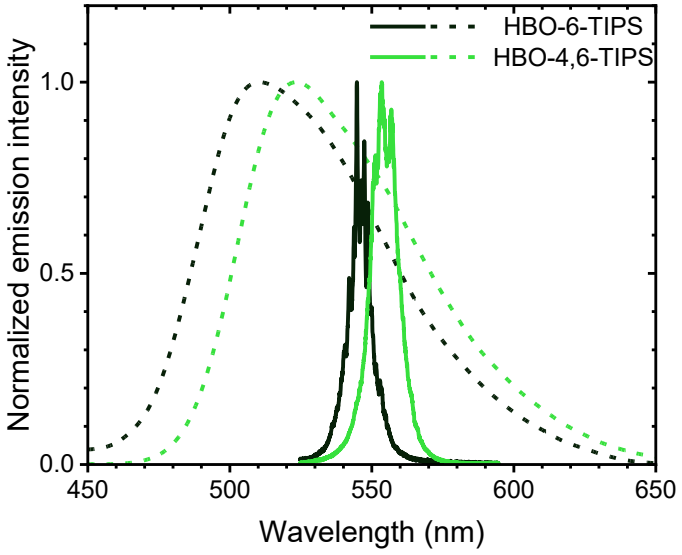

Figure 5.3.4. *Spontaneous (dashed) and stimulated (solid) emission of **HBO-6-TIPS** and **HBO-4,6-TIPS** in PMMA (λ_{exc} = 355 nm).*

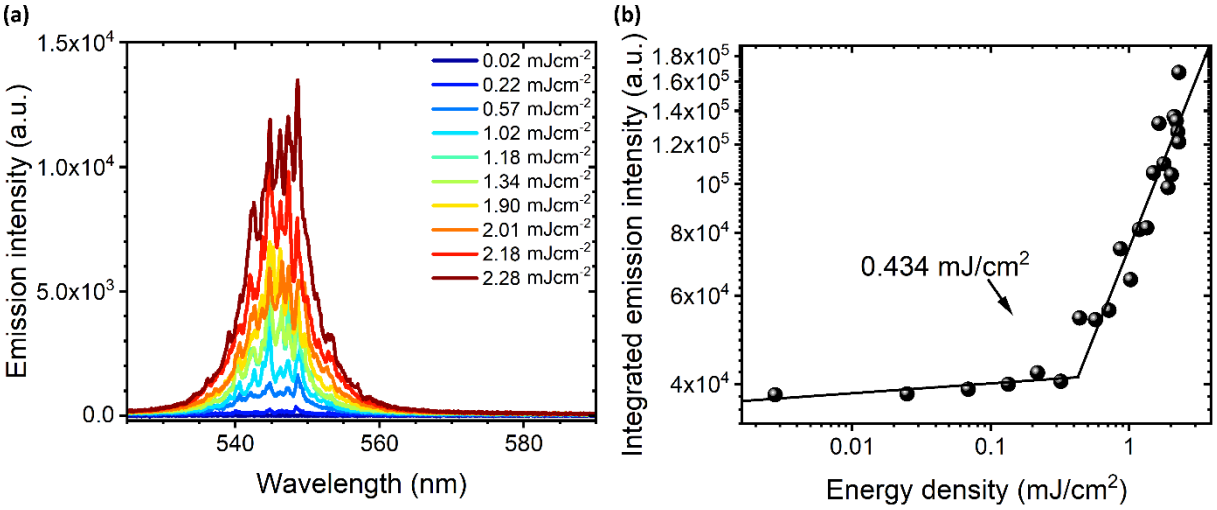

Figure 5.3.5. *(a) Random lasing spectra of 1% **HBO-6-TIPS**/PMMA, with corresponding (b) calculated lasing threshold (λ_{exc} = 355 nm).*

The last analog, bis-substituted at 4- and 6-positions with ethynyl-extended triisopropyl silyl moieties (**HBO-4,6-TIPS**), has the lowest lasing threshold of all HBO-TIPS derivatives. This value, equal to 200 μJ·cm^{-2}, corresponds with the high quantum yield value of the pure powder (82%). This property can be explained by the enlargement of π-conjugation of the whole molecule. On the other hand, the net gain is the lowest (1.73 ± 0.22 cm^{-1}). The relatively broad lasing spectrum, with full width at half maximum of almost 12 nm, is positioned at the longest wavelengths (λ_{las} = 554 nm, Figure 5.3.4). The intense output green emission is not speckle-free, as visible in the photograph taken during the light amplification experiments (Figure 5.3.6d) – besides the highly polarized and focused vertical stripe, additional bright spots can be observed. The collected lasing signal consists of many sharp spikes located closely with one another (Figure 5.3.6a), the density of which is much higher than for mono-substituted analogs. Moreover, the appearance of these modes can be recorded for pumping energy density much higher than the lasing threshold. Hence, lasing can be switched between coherent and incoherent in **HBO-4,6-TIPS** simply with the excitation energy. Additionally, during net gain measurements, stripes of quite long lengths had to be applied in order to extract lasing from within the polymeric film.

Similarly to spontaneous emission, the random lasing spectra can be tuned by the simple change of the position of substitution of the hydroxyphenylbenzoxazole. The emission of the highest energy is observed for HBO derivative with ethynyl-TIPS group substituted at 3-position, the closest to the oxygen in benzoxazole moiety. The corresponding bathochromic shifts were achieved along with the increased distance of the substituent from the heteroatom,

i.e. at 4- and 6- positions. Similarly, the introduction of an additional π-conjugated unit in **HBO-4,6-TIPS** shifted the position of the lasing spectra center even further towards longer wavelengths. These findings are compatible with observed emissions from diluted toluene solutions.

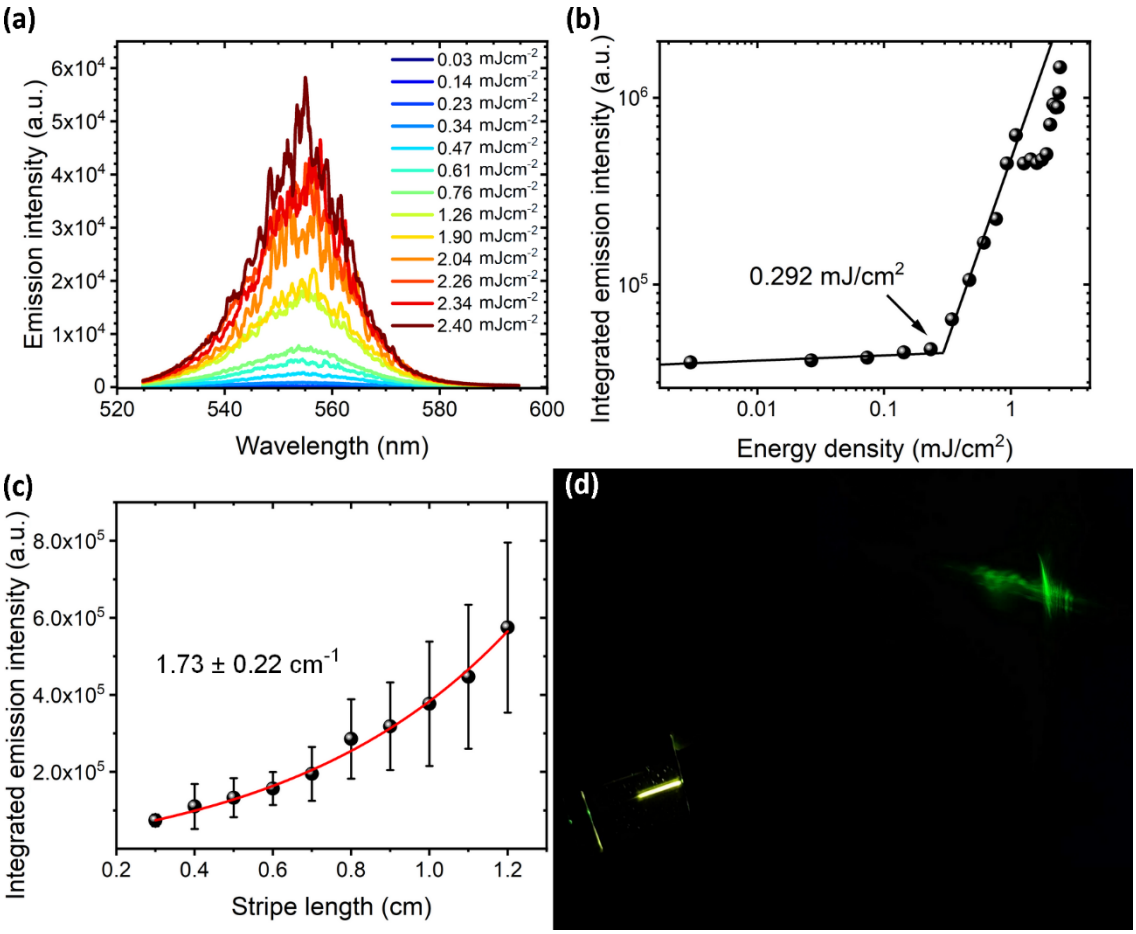

Figure 5.3.6. *(a) Random lasing spectra of 1%* ***HBO-4,6-TIPS****/PMMA, with the corresponding calculated (b) lasing threshold and (c) net gain (λ_{exc} = 355 nm). (d) Photograph taken during the measurement – with the sample in the left corner and the profile of the output beam on the right.*

Due to the inherent random nature of the investigated type of lasing, the localization of the central wavelength of the emission is not trivial. Hence, it is difficult to compare this parameter when the spectra of three consecutive bis-substituted trialkylsilyl derivatives are considered. It is evident in Figure 5.3.7. which compares spontaneous and stimulated emission of three analogs of different lengths of the alkyl chains in the substituent. These compounds emit coherent light at roughly the same wavelengths (551 – 555 nm). However, significant differences in full width at half maximum are evident, with the narrowest spectrum observed in **HBO-4,6-TIPS** (11.6 nm), and the widest in **HBO-4,6-TES** (27.9 nm)**.** As already presented for the former, switching from incoherent to coherent lasing is evident with increased pumping energy density in both **HBO-4,6-TMS** (Figure 5.3.8) and **HBO-4,6-TES**[1] samples.

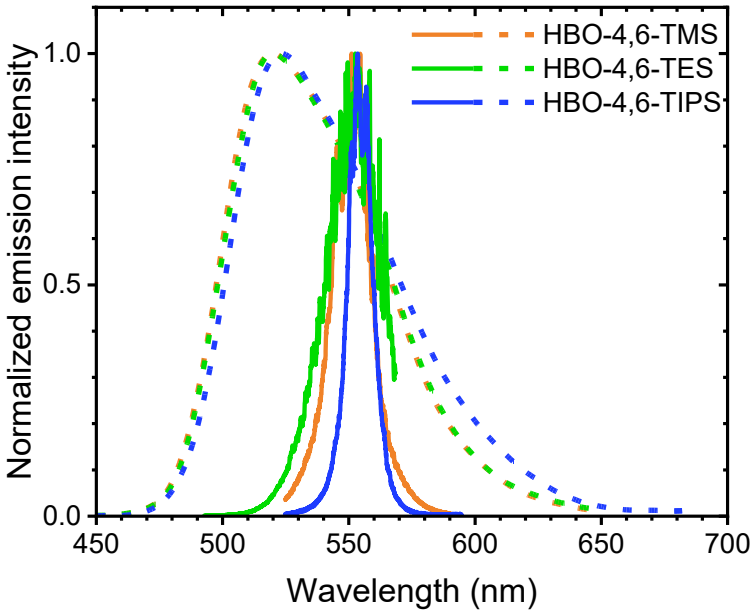

Figure 5.3.7. *Spontaneous (dashed) and stimulated (solid) emission of* ***HBO-6-TIPS*** *and* ***HBO-4,6-TIPS*** *in PMMA (λ_{exc} = 355 nm).*

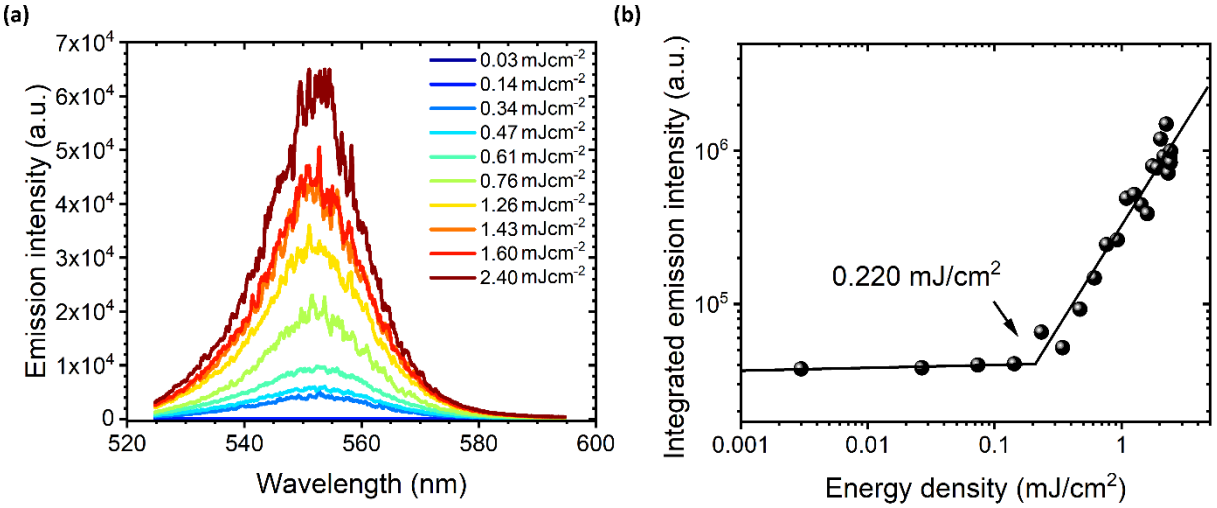

Figure 5.3.8. *(a) Random lasing spectra of 1%* ***HBO-4,6-TMS****/PMMA, with corresponding (b) calculated lasing threshold (λ_{exc} = 355 nm).*

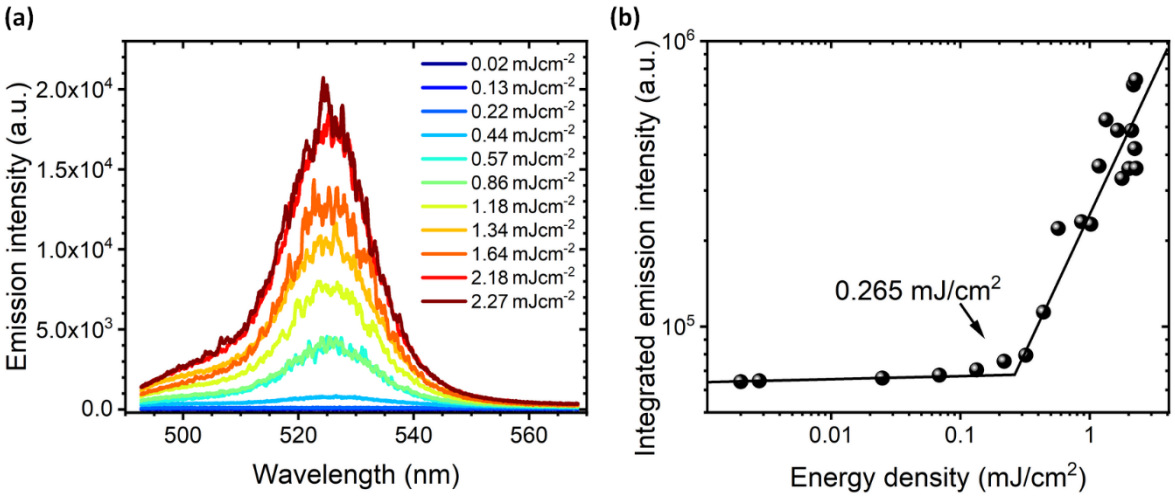

Figure 5.3.9. *(a) Random lasing spectra of 1% **HBO-4-TES**/PMMA, with the corresponding calculated (b) lasing threshold (λ_{exc} = 355 nm).*

The HBO derivatives monosubstituted with shorter alkyl chains (triethylsilyl) at 4- or 6- positions behave similarly to the corresponding HBO-TIPS ones. The random lasing action recorded for the **HBO-4-TES** analog is red-shifted in comparison to spontaneous emission (Figure 5.3.10), with the maxima at 527 and 498 nm respectively. The determined lasing threshold is lower than for the triisopropylsilyl compound, with value of 0.27 ± 0.10 mJ·cm^{-2}. This difference can be ascribed to the smaller contribution of rotation of shorter alkyl chains to the non-radiative relaxation pathways. On the other hand, the random lasing spectrum is narrower for **HBO-4-TIPS** than for the triethylsilyl derivative, which is 6.8 and 15.3 nm respectively. The net gain value determined for the latter compound is of a slightly lower value (2.80 ± 0.35 cm^{-1}). Other than the net gain and threshold parameters, those two derivatives can be distinguished by the analysis of the peaks in the spectra. Even though the compounds are emissive at almost the same wavelengths (*ca.* 528 nm), the modes are not well

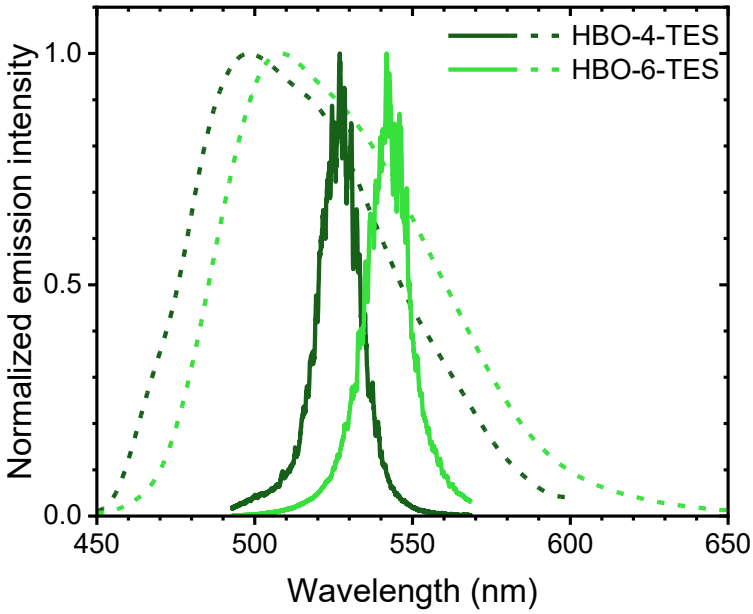

Figure 5.3.10. *Spontaneous (dashed) and stimulated (solid) emission of **HBO-6-TES** and **HBO-4-TES** in PMMA (λ_{exc} = 355 nm).*

separated and pronounced in the TES derivative. The density of the peaks is much higher, resulting in an overlapping of one another.

The same relationships can be found when **HBO-6-TES** and **HBO-6-TIPS** are compared, with central emission wavelengths located at 542 and 546 nm, respectively. In this position of substitution, an increase in alkyl chain length seems to promote a red-shift of the emission, as already observed for those dyes in toluene solutions. The full width at half maximum, as for 4-position analogs, is almost twice as large for the triethylsilyl derivative (16.4 nm). On the other hand, the pumping energy density necessary to overcome losses is doubled in **HBO-4,6-TIPS**. These values find their confirmation in fluorescence quantum yields of powders dispersed in potassium bromide pellets, as higher values are for mono-substituted triethylsilyl chromophores, both in 4- and 6-position. The beneficial influence of shorter alkyl chains can also contribute to the determined net gains, which for **HBO-6-TES** is equal to 7.38 ± 0.94 cm^{-1}. The lasing modes are more pronounced for higher energy densities (see Figure 5.3.11.) and vary with each exciting pulse. This is not the case for the TIPS compound, in which the narrow spikes are well defined even at low pumping energies (see Figure 5.3.5. for comparison).

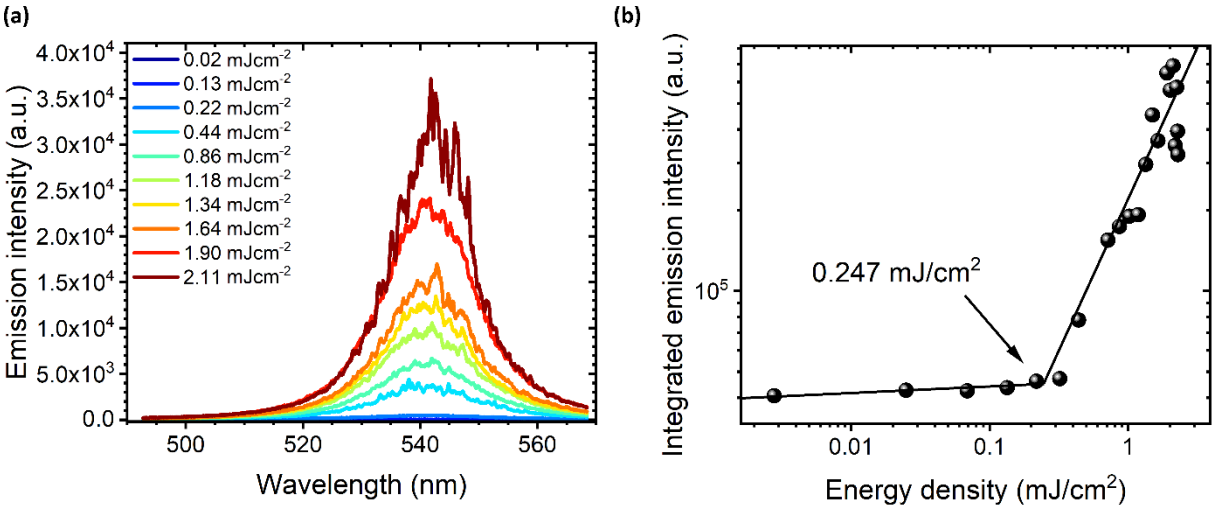

Figure 5.3.11. *(a) Random lasing spectra of 1% **HBO-6-TES**/PMMA, with corresponding (b) calculated lasing threshold (λ_{exc} = 355 nm).*

The dialkylaniline substituted hydroxyphenylbenzoxazoles are also capable of light amplification. *N,N*-dimethylaniline derivative (**HBO-ext-NMe2**) behaves in a manner similar to previously described HBO analogs, as the much narrower lasing spectrum is bathochromically shifted in comparison to spontaneous emission recorded for the same

polymeric film, as depicted in Figure 5.3.12. Even though the spectrum is broad to some extent (FWHM = 15.1 nm), singular modes can be distinguished. On the other hand, their position in relation to one another is close enough for them to be mistaken as noise, as visible in Figure 5.3.13a. Both **HBO-ext-NMe2** and **HBO-ext-NEt2** chromophores embedded in the polymeric matrix show the highest net gain values of all investigated ESIPT compounds, which for the former is equal to an outstanding 15.82 ± 2.00 cm^{-1}. At the same time, the lasing threshold is relatively low - 0.47 ± 0.10 $mJ \cdot cm^{-2}$.

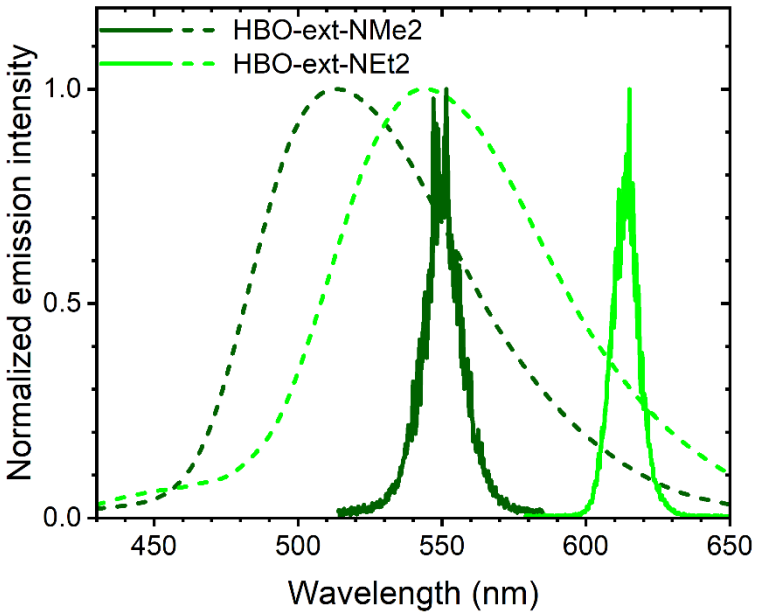

Figure 5.3.12. *Spontaneous (dashed) and stimulated (solid) emission of* ***HBO-ext-NMe2*** *and* ***HBO-ext-NEt2*** *in PMMA (λ_{exc} = 355 nm).*

The Intramolecular Charge Transfer present in the **HBO-ext-NEt2** derivative due to the stronger electron-donating character of *N,N*-diethylaniline is even more pronounced when light amplification is considered. While two emissive bands are observed when fluorescence is recorded in both toluene solution and PMMA film, excitation with a 355 nm laser results in a single stimulated emission band at *ca*. 620 nm, red-shifted from the maximum of the spontaneous emission by almost 60 nm! Hence, lasing in the red region of the visible spectrum is observed as a result of both proton transfer and electron redistribution in the excited state. Another explanation can be provided by the formation of excimers or exciplexes, which are characterized by much lower energies. The competition of ICT and ESIPT processes can provide an explanation for the higher value of lasing threshold in comparison to other HBO compounds, as it is at least three times larger (1.38 ± 0.17$mJ \cdot cm^{-2}$). Another explanation lies in the non-radiative deactivation pathways, such as the conversion of the energy excess into heat, as is common for organic compounds with large Stokes shifts. If the maximum of the excitation band of the doped PMMA film is taken into consideration (322 nm), this value is indeed high, as it's almost equal to 15000 cm^{-1}. As a result, no self-reabsorption can take place, which is crucial in purely organic solid-state lasers. Additionally, the net gain value determined for

HBO-ext-NEt2 is the highest of all investigated systems in this dissertation, with the value exceeding 20 cm^{-1}. The lasing spectrum consists of very well-defined and pronounced modes, as presented in Figure 5.3.13c, which are immediately present when the threshold is exceeded.

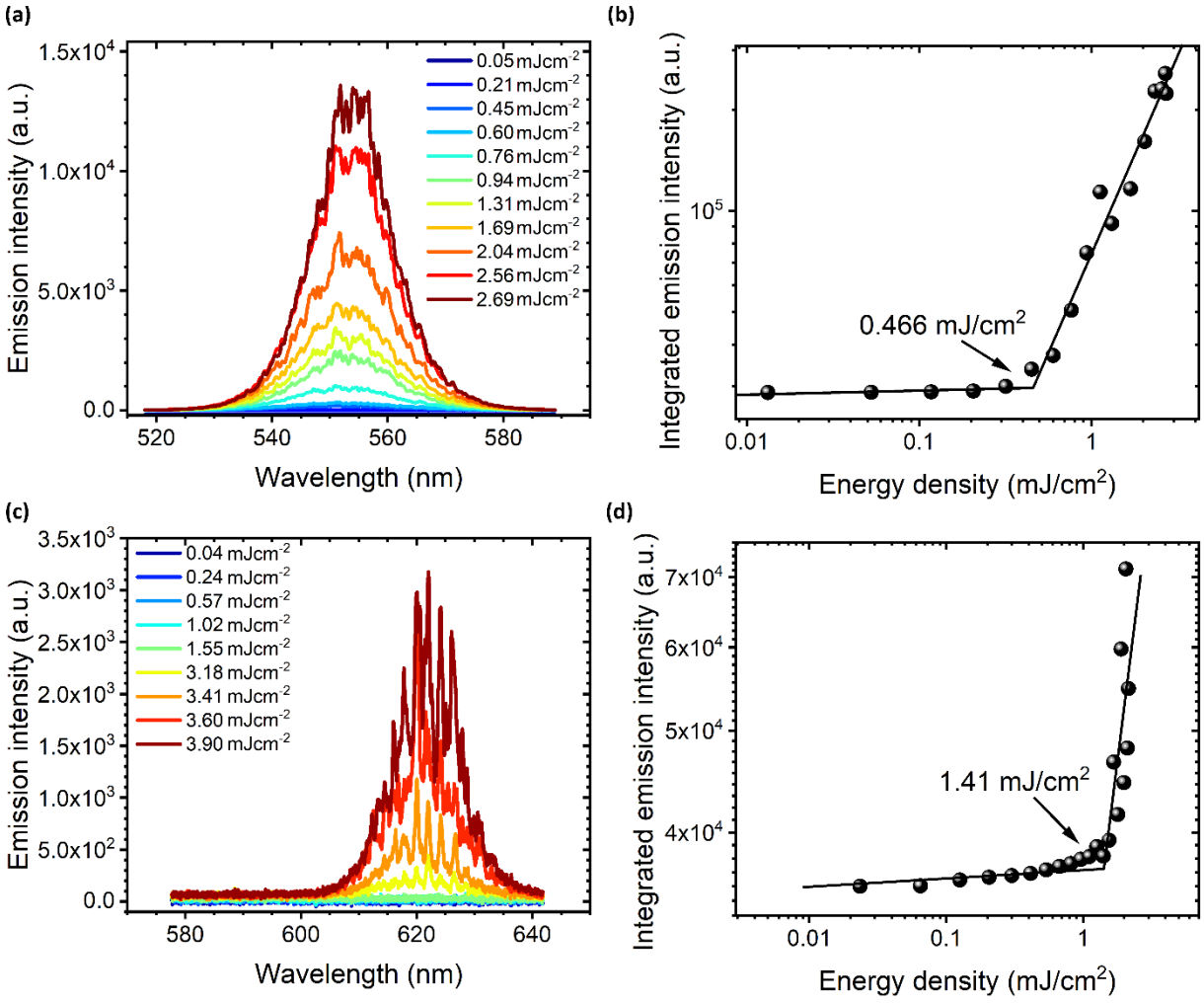

Figure 5.3.13. *Random lasing spectra of 1% (a,b)* ***HBO-ext-NMe2*** *and (c,d)* ***HBO-ext-NEt2****/PMMA, with the corresponding calculated lasing thresholds (λ_{exc} = 355 nm).*

Besides the **HBO-ext-NEt2** compound, in which ICT plays a significant role, all investigated HBO derivatives are emissive in the green region of the visible light, with an emission range spanning from 518 to 554 nm (see Figure 5.3.14, which depicts exemplary spectra at pumping energy density exceeding threshold values). The observed stimulated emission in all cases is significantly red-shifted in comparison to the fluorescence of thin films, even though the same excitation wavelength was used. The most probable reason behind the recorded bathochromic shifts is the simple difference in the energy density of the excitation source: with a laser beam it is possible to excite crystals and aggregates and to extract their emission from the thin film which behaves like a planar waveguide. In the solid state, the proton

transfer in the excited state is promoted due to the beneficial restriction of motion in the rigid polymeric matrix, hence radiative relaxation comes from the excited tautomer. Therefore, the investigated HBO derivatives are capable of light amplification through a four-level laser system, in which the lasing action occurs between excited and keto states of the keto form. The summary of the most important parameters is included in Table 5.3.1.

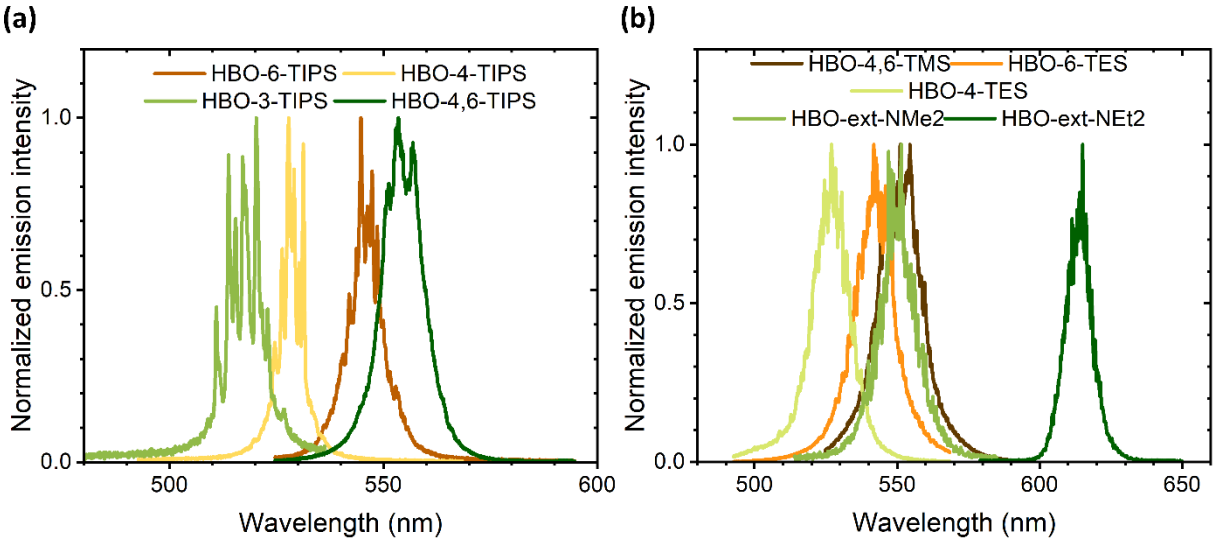

Figure 5.3.14. *Random lasing spectra of investigated 1% **HBO**/PMMA samples (λ_{exc} = 355 nm).*

Table 5.3.1. *Random lasing parameters of **HBO** group in PMMA.*

Compound	λ_{em} [nm]	FWHM [nm]	CIEx	CIEy	ρ_{th} [mJcm^{-2}]	g [cm^{-1}]
HBO-3-TIPS	518	10.7	0.069	0.766	0.41 ± 0,07	4.62 ± 0.84
HBO-4-TIPS	529	6.8	0.146	0.801	0.34 ± 0,09	3.34 ± 0.36
HBO-6-TIPS	546	9.8	0.064	0.792	0.22 ± 0,07	8.46 ± 0.73
HBO-4,6-TIPS	554	11.6	0.336	0.659	0.27 ± 0,02	1.73 ± 0.22
HBO-4,6-TMS	551	18.4	0.318	0.675	0.21 ± 0,02	4.32 ± 0.87
HBO-4-TES	527	15.3	0.137	0.798	0.27 ± 0,10	2.80 ± 0.35
HBO-6-TES	542	16.4	0.250	0.732	0.18 ± 0,07	7.38 ± 0.94
HBO-ext-NMe2	550	15.1	0.309	0.683	0.47 ± 0,10	15.82 ± 2.00
HBO-ext-NEt2	620	11.1	0.673	0.327	1.38 ± 0,17	20.38 ± 2.36

λ_{em} – central emission wavelength, FWHM – full width at half maximum, CIEx/y – CIE 1931 coordinates, ρ_{th} – threshold energy density, g – net gain.

The next group of the investigated compounds, consisting of four hydroxyphenylbenzimidazoles functionalized with ethynyl-extended triisopropylsilyl moieties, are also capable of light amplification when used as dopants in polymeric thin films. The first molecule, **HBI-3-TIPS**, emits light in the blue-green region, with the maximum of spontaneous emission located at 474 nm. Upon excitation with an ultraviolet laser beam, a bathochromically shifted stimulated emission at 498 nm (Figure 5.3.15) is observed. The band with full width at half maximum of 10.0 nm consists of randomly distributed lasing modes, which change position with each pumping pulse (Figure 5.3.16). The sharp spikes are present in a small amount. The determined lasing threshold value (0.20 ± 0.07 mJ·cm^{-2}) is lower than that of the corresponding **HBO-3-TIPS** analog, while the net gain is higher (6.14 ± 0.83 cm^{-1}).

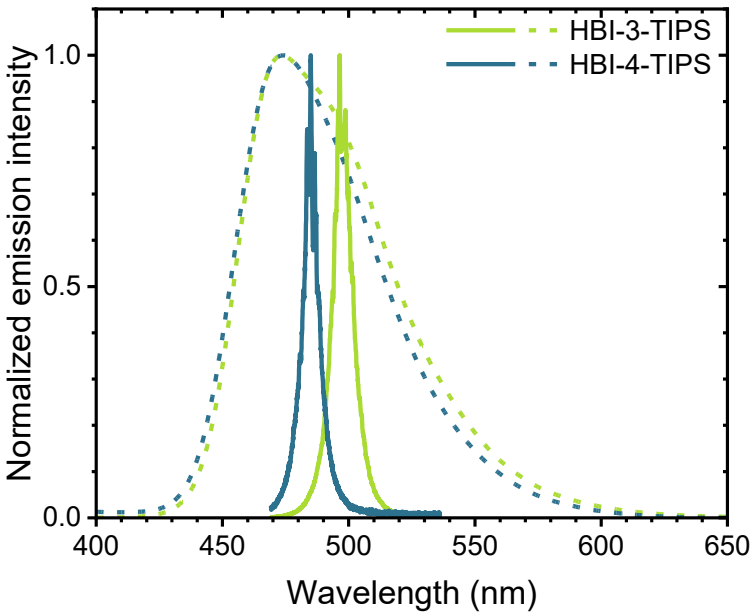

Figure 5.3.15. *Spontaneous (dashed) and stimulated (solid) emission of* ***HBI-3-TIPS*** *and* ***HBI-4-TIPS*** *in PMMA (λ_{exc} = 355 nm).*

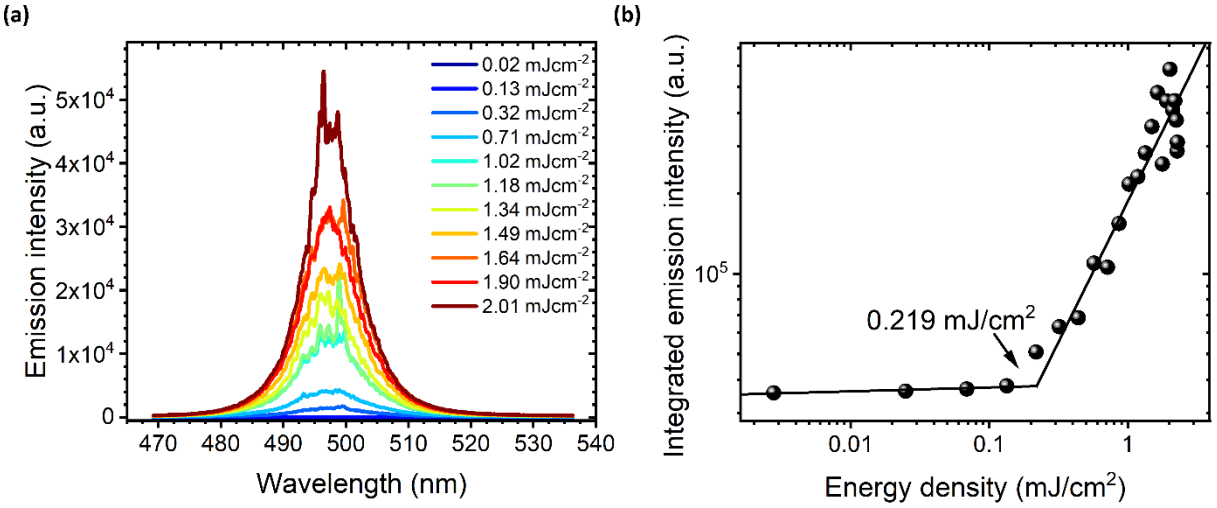

Figure 5.3.16. *(a) Random lasing spectra of 1%* ***HBI-3-TIPS****/PMMA, with corresponding (b) calculated lasing threshold (λ_{exc} = 355 nm).*

The second HBI derivative, with substituent connected to the phenyl ring at the 4-position, shows similar properties. Observed lasing modes are only visible when the energy density is high enough, even if the threshold value is exceeded (Figure 5.3.17). In this case, however, the position of the sharp spikes does not vary with each pumping pulse. Hence, the pathways are well-defined. The scattering centers, visible in the photo taken during the experiment as very bright spots on the irradiated sample, do not seem to degrade under the pumping. The observed emission is centered at 485 nm, which is the lowest emission wavelength of all investigated HBX derivatives. This value is surprising, as the observed random lasing action of **HBI-4-TIPS** does not fit the previously observed dependence between the position of substitution of the TIPS moiety in the phenyl ring, as it was recorded for HBI/toluene or HBO-TIPS/toluene/PMMA samples. If it was applicable, then the stimulated

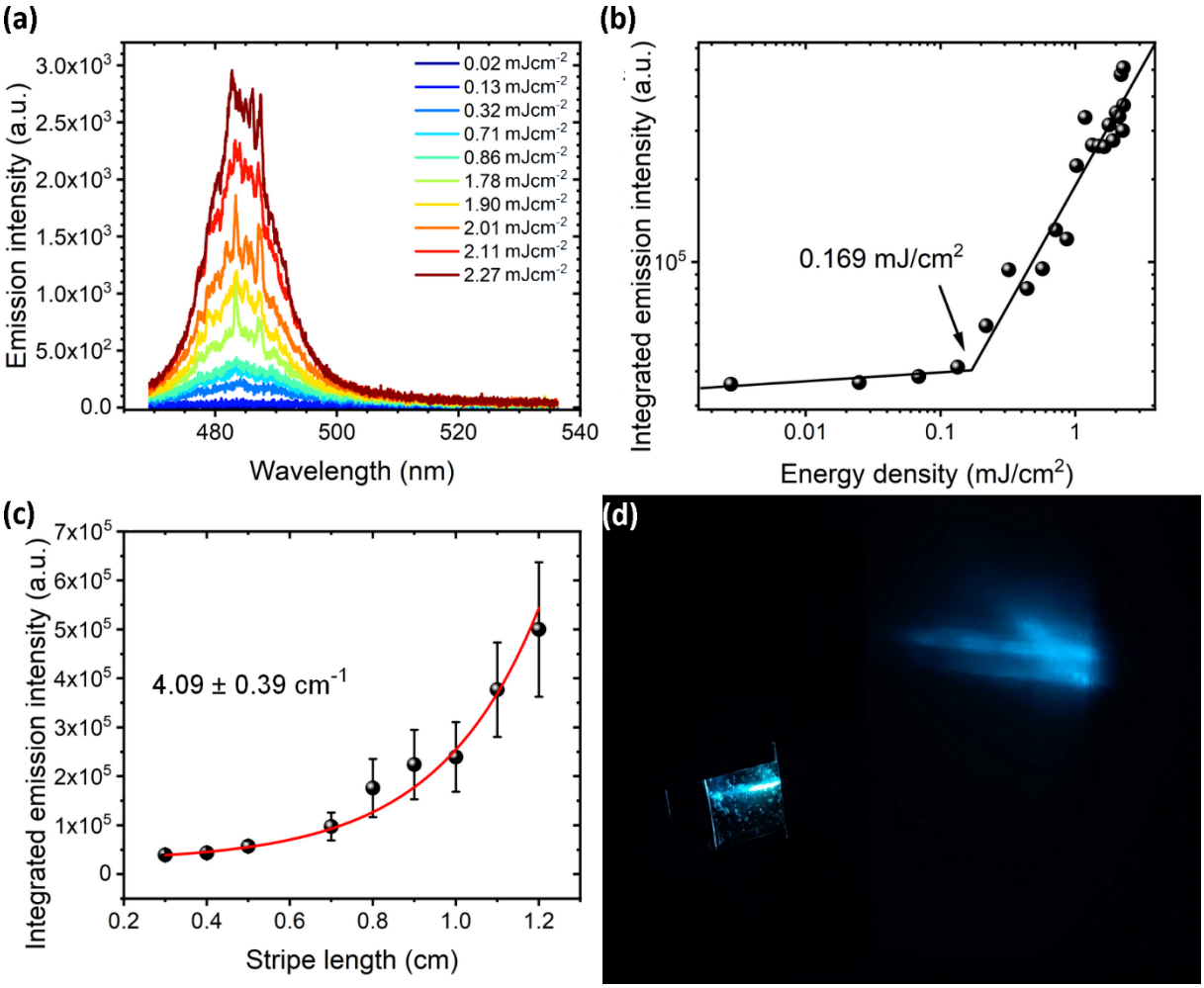

Figure 5.3.17. *(a) Random lasing spectra of 1%* ***HBI-4-TIPS****/PMMA, with the corresponding calculated (b) lasing threshold and (c) net gain (λ_{exc} = 355 nm). (d) Photograph taken during the measurement – with the sample in the left corner and the profile of output beam on the right.*

emission should have been observed at the wavelengths longer than those for **HBI-3-TIPS**. In this case, the redshift is not as pronounced, which results in blue lasing (Figure 5.3.17d). On the other hand, both lasing threshold (0.26 ± 0.17 mJ·cm^{-2}) and net gain (4.09 ± 0.39 cm^{-1}) are of competitive values in comparison to **HBO-4-TIPS**.

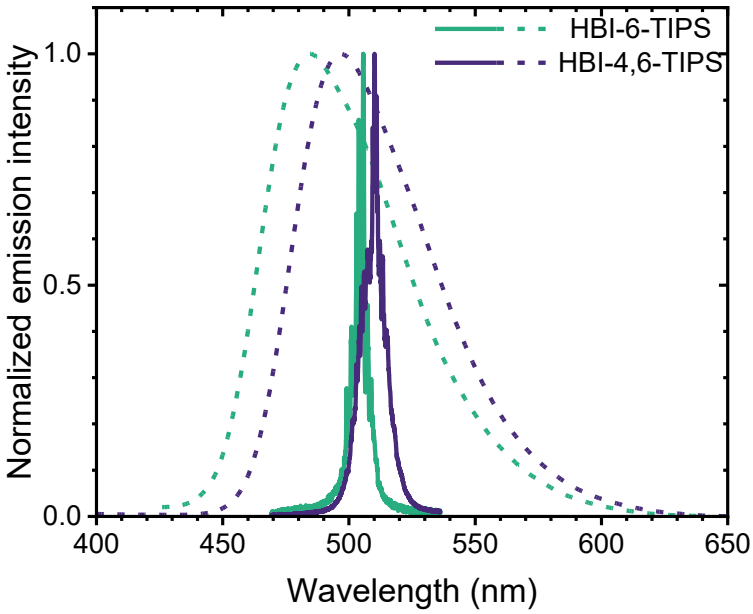

Figure 5.3.18. *Spontaneous (dashed) and stimulated (solid) emission of* ***HBI-6-TIPS*** *and* ***HBI-4,6-TIPS*** *in PMMA (λ_{exc} = 355 nm).*

The last mono-substituted derivative, **HBI-6-TIPS** does follow the previously observed tendency. The pumping with the third harmonic of an Nd:YAG laser (355 nm) leads to random lasing with a central wavelength located at 505 nm, which is of lower energy than the corresponding spontaneous emission (see Figure 5.3.18). The full width at half maximum of the stimulated emission is the lowest in all HBI derivatives (7.2 nm). The lasing modes are well-defined and easily distinguishable, even at very low pumping energies (see Figure 5.3.19). Such spectrum, in which the modes do not change positions, is characteristic of coherent random lasers, in which the optical feedback is provided by multiple scattering.

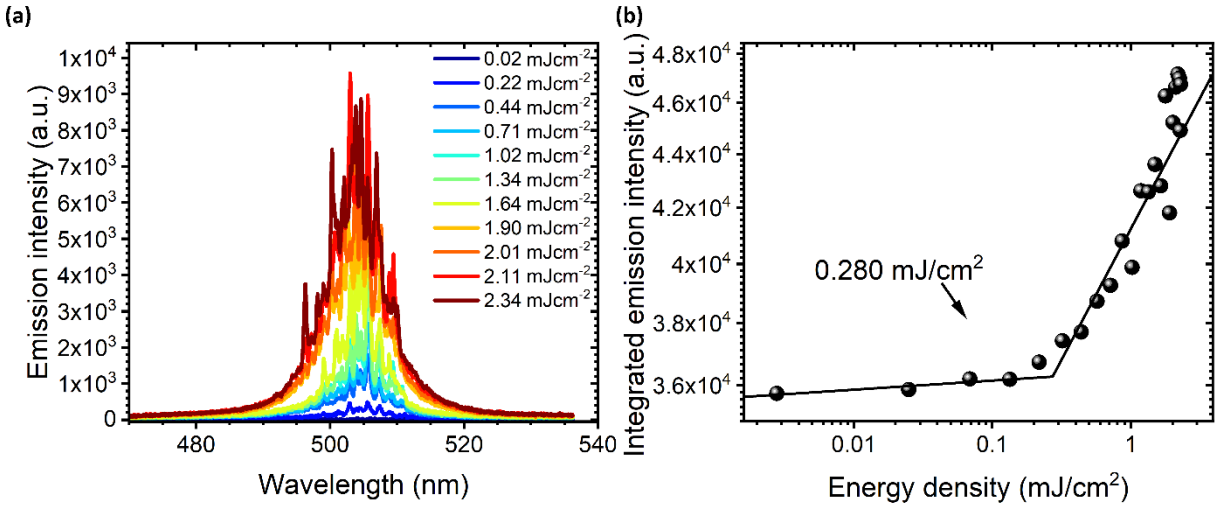

Figure 5.3.19. *(a) Random lasing spectra of 1%* ***HBI-6-TIPS****/PMMA, with corresponding (b) calculated lasing threshold (λ_{exc} = 355 nm).*

The last HBI group representative, bis-substituted **HBI-4,6-TIPS**, presents remarkable net gain – the highest of all HBX derivatives functionalized with ethynyl-extended trialkylsilyl moieties. This value, 18.17 ± 0.46 cm^{-1}, is the second only to **HBO-ext-NEt2** chromophore. Such a parameter is surprising when the quantum yield value is taken into account – 30 % - which is the lowest of all investigated compounds that are capable of light amplification. Moreover, the determined threshold is the smallest, with the energy density equal to 0.15 ± 0.07 $mJ \cdot cm^{-2}$. However, singular modes can be distinguished from the background noise for even lower energies, as depicted in Figure 5.3.20. Two separate but closely positioned bands are pronounced, located at *ca.* 500 and 520 nm. In each one, distinct modes are seen. Most probably they are a result of light localization in single crystals or aggregates, as their position does not change with each pumping pulse. At higher energy densities these two bands overlap one another, observed as random lasing spectra with the maximum at 510 nm (see Figure 5.3.21).

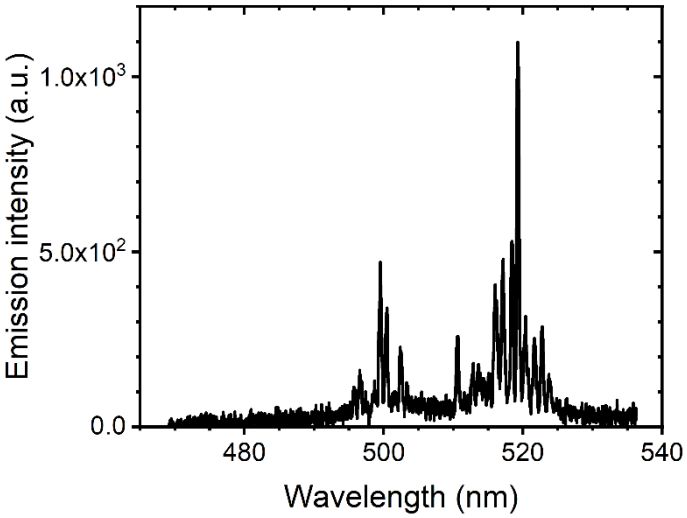

Figure 5.3.20. *Emission spectra of 1%* ***HBI-4,6-TIPS****/PMMA upon pumping with 70 μJ·cm⁻².*

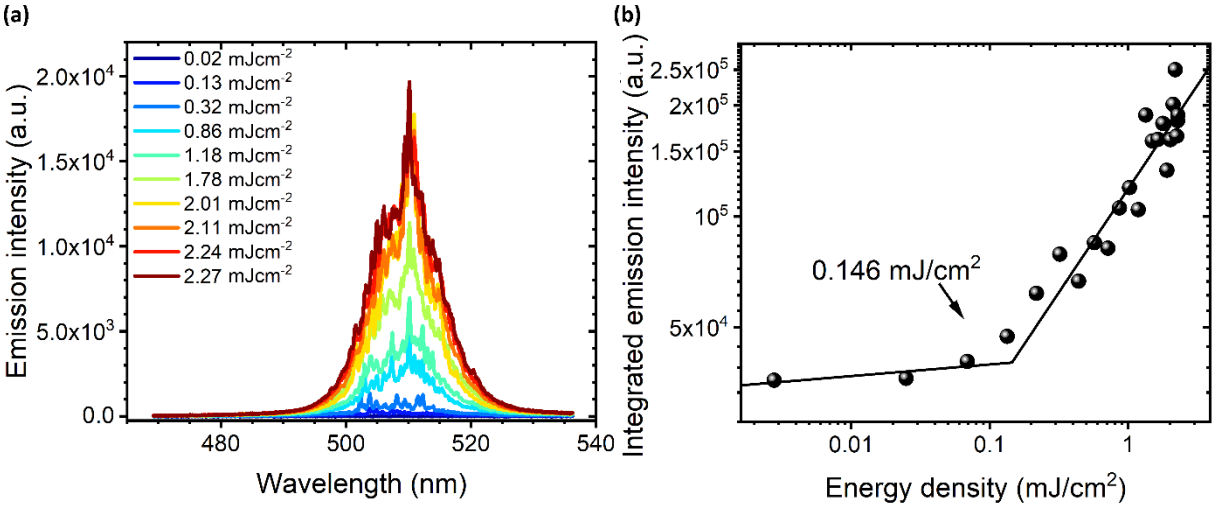

Figure 5.3.21. *(a) Random lasing spectra of 1%* ***HBI-4,6-TIPS****/PMMA, with corresponding (b) calculated lasing threshold (λ_{exc} = 355 nm).*

A joint graph representing respective positions of recorded stimulated emission of HBI derivatives embedded in the PMMA matrix is given in Figure 5.3.22., with the summary of random lasing parameters delisted in Table 5.3.2.

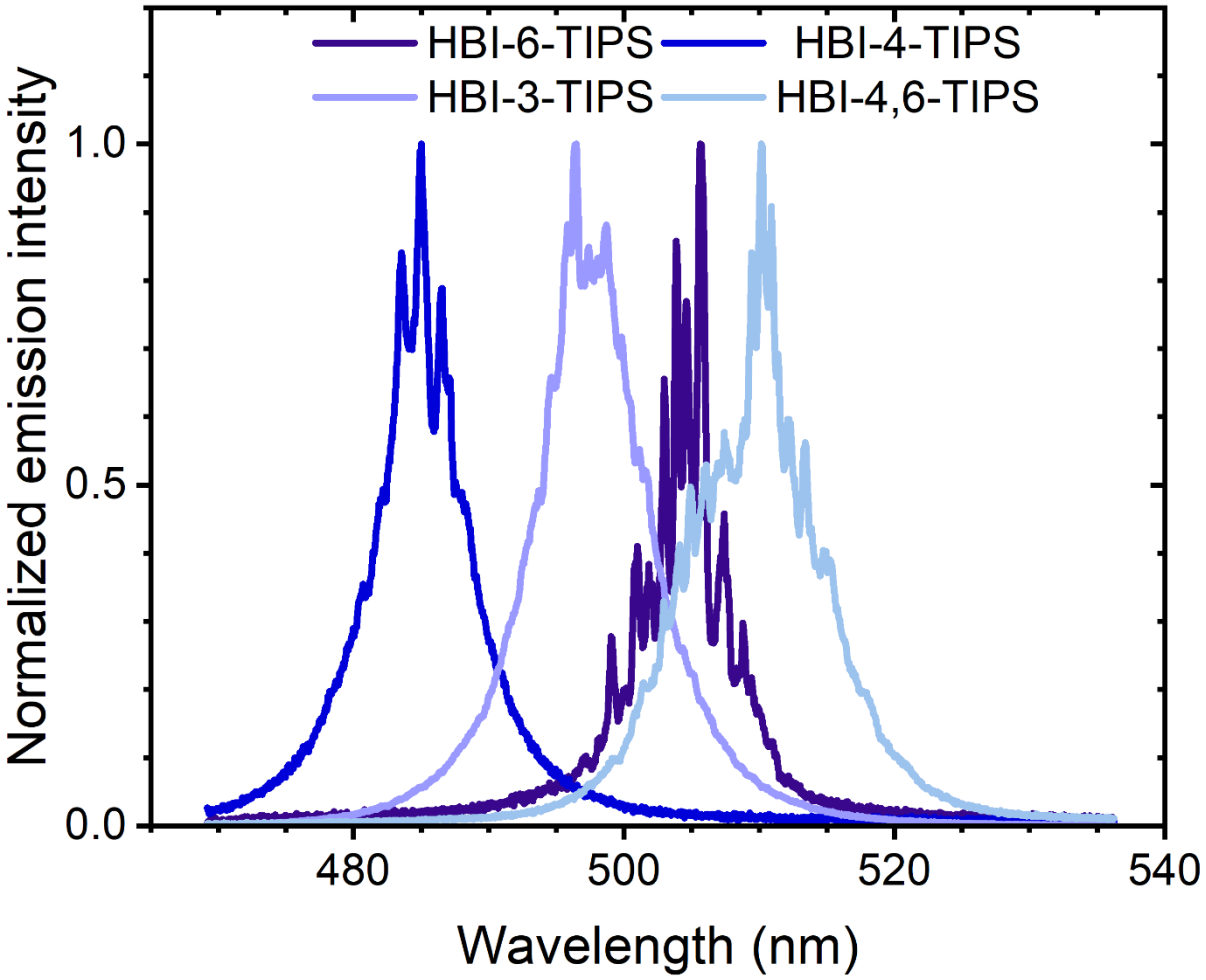

Figure 5.3.22. *Random lasing spectra of investigated 1% **HBI**/PMMA samples (λ_{exc} = 355 nm).*

Table 5.3.2. *Random lasing parameters of HBI group in PMMA.*

Compound	λ_{em} [nm]	FWHM [nm]	CIEx	CIEy	ρ_{th} [mJcm^{-2}]	g [cm^{-1}]
HBI-3-TIPS	498	10.0	0.023	0.474	0.20 ± 0.07	6.14 ± 0.83
HBI-4-TIPS	485	8.5	0.072	0.222	0.26 ± 0.17	4.09 ± 0.39
HBI-6-TIPS	505	7.2	0.023	0.606	0.22 ± 0.06	4.12 ± 0.70
HBI-4,6-TIPS	510	11.7	0.029	0.723	0.15 ± 0.07	18.17 ± 0.46

λ_{em} – central emission wavelength, FWHM – full width at half maximum, CIEx/y – CIE 1931 coordinates, ρ_{th} – threshold energy density, g – net gain.

The last subgroup, the hydroxyphenylbenzothiazoles, is emissive at the longest wavelengths, i.e. at the yellow-red region. Pumping of the doped films of these derivatives leads to light amplification manifested in the form of random lasing. Contrary to spontaneous emission of the doped film, the derivative with triisopropylsilyl chains (**HBT-4,6-TIPS**) is emissive at the lowest energies, thus the longest wavelengths, out of the three HBTs. It is also the most red-shifted in comparison to the spontaneous emission (595 and 554 nm, respectively – see Figure 5.3.23). Unfortunately, this compound is prone to rather quick photodegradation upon pumping. Several dozens of pumping pulses are enough to locally quench the stimulated emission by half. Nonetheless, the determined lasing threshold is comparable with previously described HBI and HBO systems, albeit a bit higher (0.41 ± 0.11 mJ·cm^{-2}). Similarly, the net gain value is lower – 1.45 ± 0.44 cm^{-1}.

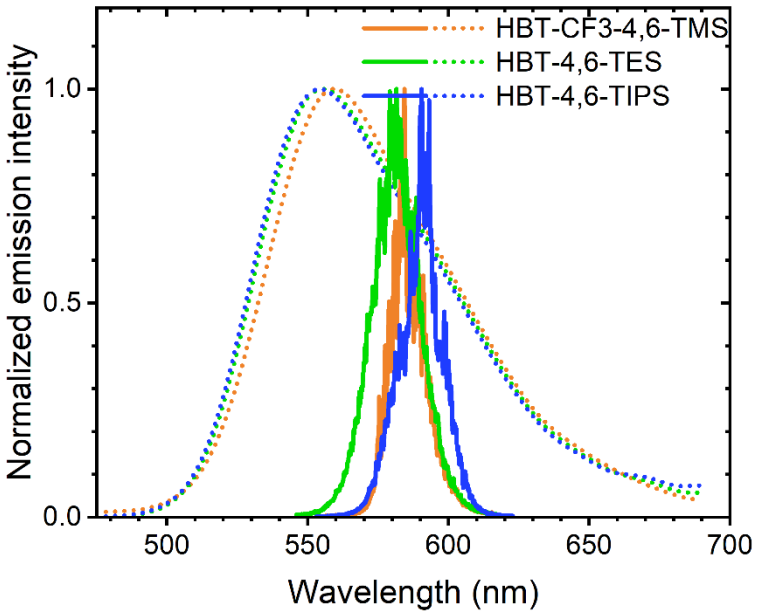

Figure 5.3.23. *Spontaneous (dashed) and stimulated (solid) emission of* ***HBT-CF3-4,6-TMS, HBT-4,6-TES*** *and* ***HBT-4,6-TIPS*** *in PMMA (λ_{exc} = 355 nm).*

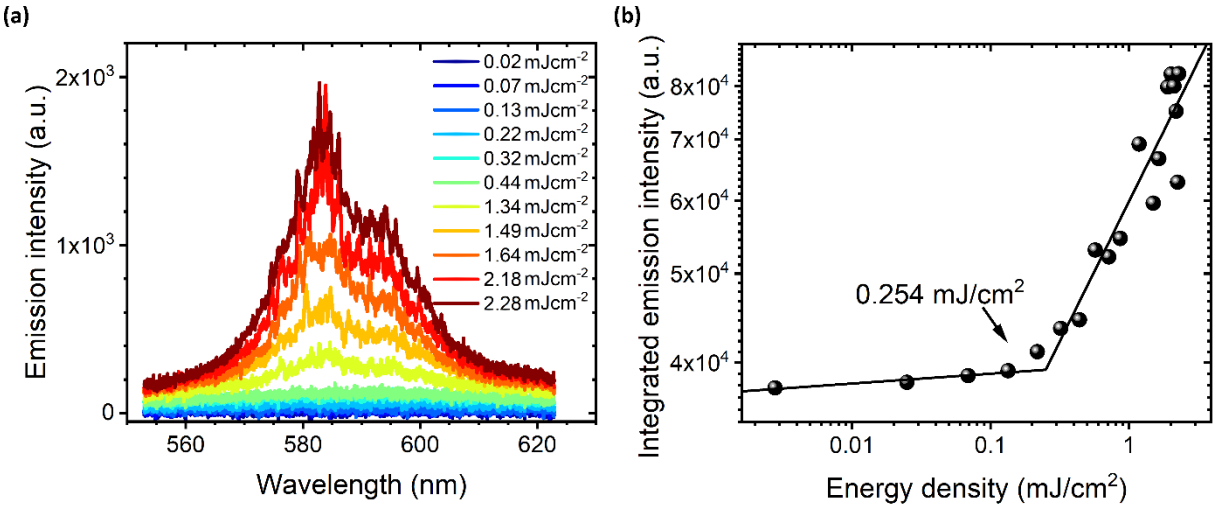

Figure 5.3.24. *(a) Random lasing spectra of 1%* ***HBT-4,6-TIPS****/PMMA, with corresponding (b) calculated lasing threshold (λ_{exc} = 355 nm).*

The second HBT derivative, with triethylsilyl moieties – **HBT-4,6-TES**, shows a similar tendency to the previous analog. The values of lasing threshold and net gain are very comparable – 0.46 ± 0.13 mJ·cm^{-2} and 1.44 ± 0.14 cm^{-1}, respectively. The full width at half maximum value, however, is the largest of all studied ESIPTs (almost 20 nm). At the same time the observed stimulated emission, seen as a series of sharp peaks positioned closely together, is of the highest energy out of the three hydroxyphenylbenzothiazoles, with the central wavelength at *ca.* 580 nm. On the other hand, when the progressive lasing action is considered, the distinct lasing modes appear at much higher energies than the determined threshold (see Figure 5.3.25). Such in-/coherent action switching was also noticed for other bis-substituted oxygen and nitrogen analogs.

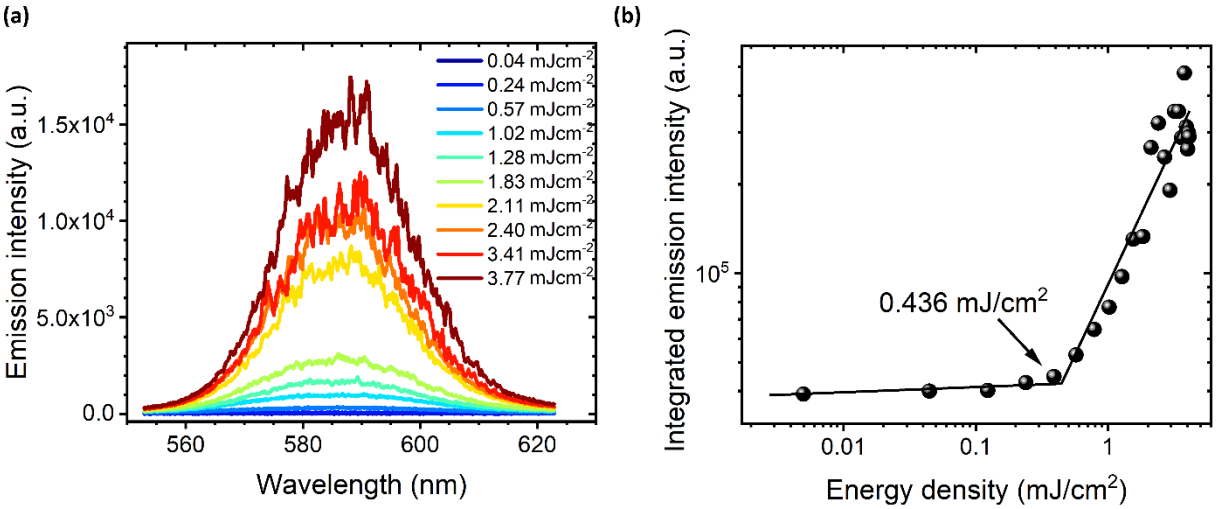

Figure 5.3.25. *(a) Random lasing spectra of 1%* ***HBT-4,6-TES****/PMMA, with corresponding (b) calculated lasing threshold (λ_{exc} = 355 nm).*

The last investigated ESIPT is the HBT bis-substituted with ethynyl-trimethylsilyl moieties and additionally a strong electron-accepting group (trifluoromethyl) – **HBT-CF3-4,6-TMS**. As already observed during measurements of spontaneous emission, the addition of electron-withdrawing species influences the proton transfer phenomena. In a manner similar to **HBO-ext-NEt2**, a dual emission in both toluene solutions and the PMMA film was recorded due to partial frustration of the ESIPT. However, pumping with a laser beam leads to the occurrence of stimulated emission at *ca.* 585 nm, with a relatively wide spectrum (FWHM = 15.9 nm, purely due to the radiative relaxation of the excited keto form. Even at low energies, very distinct and numerous lasing modes are present, as depicted in Figure 5.3.26. The threshold for this coherent random lasing was determined, with values comparable to other investigated dyes (0.34 ± 0.05 mJ·cm^{-2}). The net gain is slightly higher than for other HBTs

(2.09 ± 0.35 cm^{-1}), nevertheless, the obtained values are rather low in comparison to oxygen or nitrogen analogs. The **HBT-CF3-4,6-TMS** compound is in particular interesting when potential applications are considered, with the details enclosed in the next chapter (*6.2 Emission tuning and sensing*).

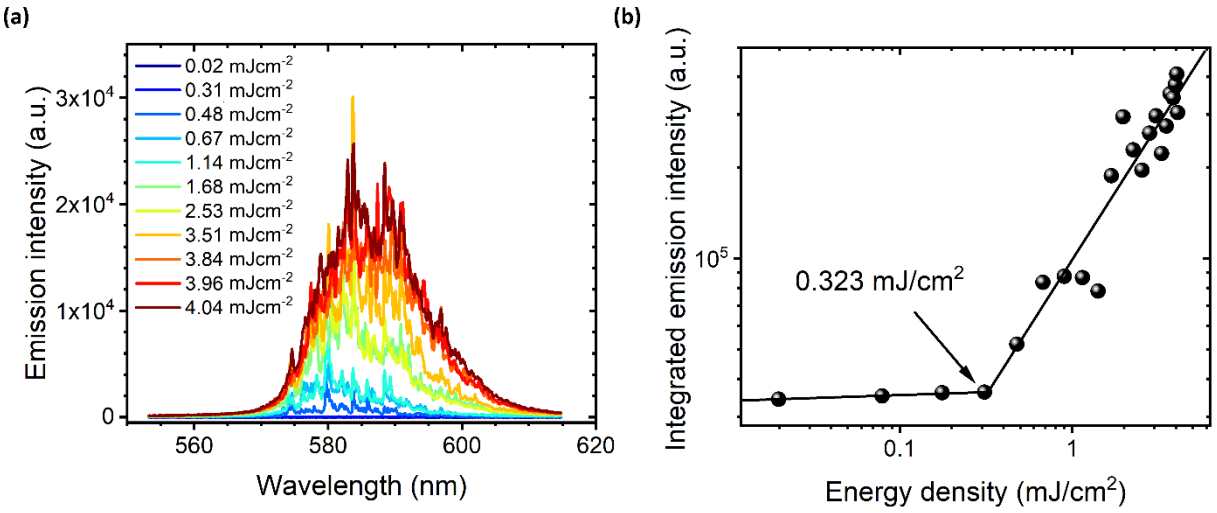

Figure 5.3.26. *(a) Random lasing spectra of 1% **HBT-CF3-4,6-TMS**/PMMA, with corresponding (b) calculated lasing threshold (λ_{exc} = 355 nm).*

For comparison purposes, exemplary spectra of investigated HBT/PMMA samples are depicted in Figure 5.3.27, with a photograph taken during the experiments conducted for **HBT-4,6-TIPS**. The summary of the stimulated emission parameters is delisted in Table 5.3.3.

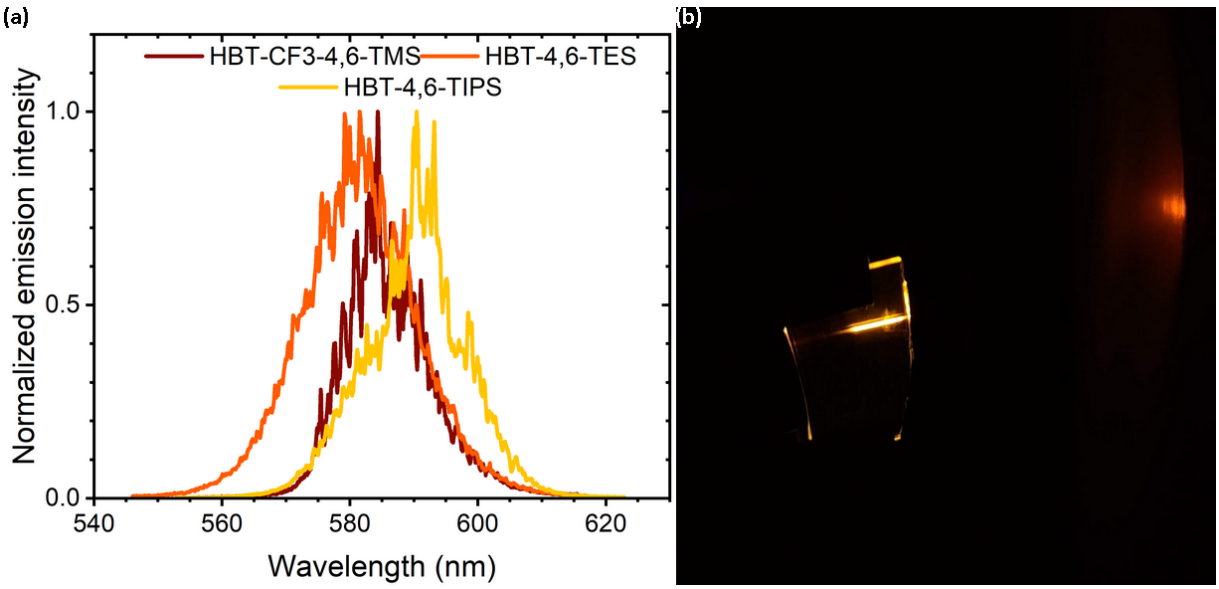

Figure 5.3.27*. (a) Random lasing spectra of investigated 1% **HBT**/PMMA samples (λ_{exc} = 355 nm). (b) Photograph taken during the measurement of **HBT-4,6-TIPS**.*

Table 5.3.3. *Random lasing parameters of HBT group in PMMA.*

Compound	λ_{em} [nm]	FWHM [nm]	CIEx	CIEy	ρ_{th} [mJcm^{-2}]	g [cm^{-1}]
HBT-CF3-4,6-TMS	585	15.9	0.550	0.450	0.34 ± 0.05	2.09 ± 0.35
HBT-4,6-TES	581	19.9	0.520	0.479	0.46 ± 0.13	1.44 ± 0.14
HBT-4,6-TIPS	591	17.1	0.572	0.428	0.41 ± 0.11	1.45 ± 0.44

λ_{em} – central emission wavelength, FWHM – full width at half maximum, CIEx/y – CIE 1931 coordinates, ρ_{th} – threshold energy density, g – net gain.

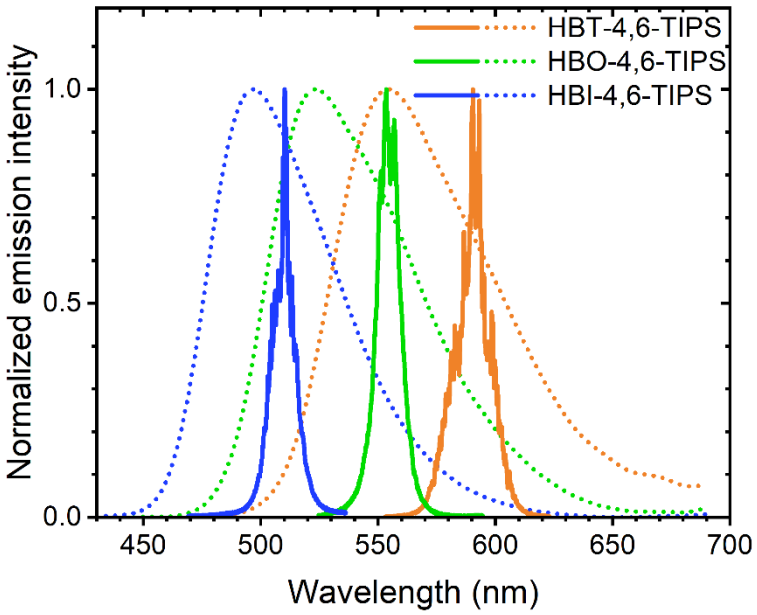

Figure 5.3.28. *Spontaneous (dotted) and stimulated (solid) emission of 1%* ***HBO/HBT/HBI****/PMMA samples (λ_{exc} = 355 nm).*

All hydroxyphenylbenzazole derivatives are capable of light amplification as dopants in the polymeric thin films. It is evident through the random lasing phenomenon, both coherent and incoherent, with the feedback provided by multiple scattering on aggregates and small crystals embedded in the films. It is further confirmed by the significant bathochromic shifts of the stimulated emission in comparison to fluorescence, which is at least 11 nm (**HBI-4-TIPS**) and at most 63 nm (**HBO-ext-NEt2**). The tuning of spontaneous emission through a relatively easy change of the heteroatom or substituent, or the place of its attachment to the hydroxyphenylbenzazole scaffold is also translated into stimulated emission. Hence, emitted photons have the lowest energy when hydroxyphenylbenzothiazoles are concerned (HBT), followed by oxygen analogs (HBO), with the nitrogen at the shortest wavelengths (HBI). This relationship, based on bis-substituted derivatives, is depicted in Figure 5.3.28. Photodegradation of studied samples was investigated, but as this lifetime parameter is dependent on various factors (atmosphere during sample fabrication/experiment, the layer thickness, dye loadings, *etc.*), the exact values are not repetitive and as such are not presented. However, rough estimations can be given. It was observed that the HBO derivatives have shown the best photostability out of investigated dyes (reaching even a few thousand pulses), followed by HBI, with the least stable HBTs in the end.

EMISSION TUNING BY POLYMERIC MATRIX - POLYSTYRENE

Besides poly(methyl methacrylate), other matrixes were taken into consideration, such as poly(vinyl carbazole), poly(vinyl alcohol), DNA, or even commercial liquid crystals. It was found that light amplification cannot be obtained in some of them, as the ESIPT process responsible for population inversion was frustrated. In others, random lasing was possible, for example in PVK, however, the stability of the compounds was much weaker, leading to quenching of the laser action after merely a few pumping pulses. Only one matrix, other than PMMA, was found to be applicable as a host for the ESIPT compounds – the polystyrene. No significant interaction between the chromophore molecules and the polymeric chains seems to take place, as the spontaneous emission spectra of doped PS films closely resemble the poly(methyl methacrylate) ones, as depicted in Figure 5.3.29. As polymer chains of used commercially available PMMA and PS are of different lengths, different geometries of ESIPT molecules can form in the thin films, evidenced by spectral shifts of the stimulated emission.

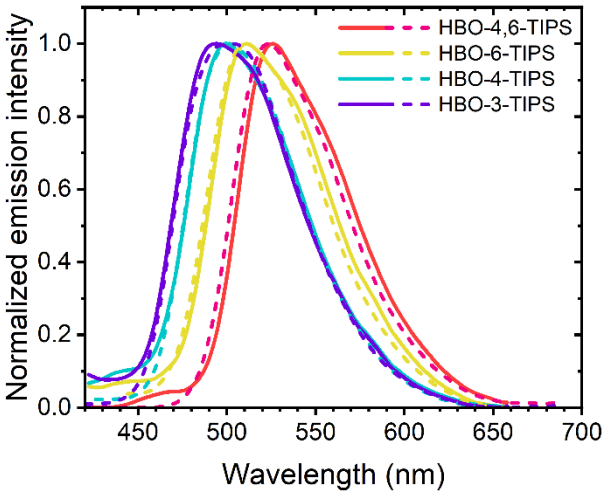

Figure 5.3.29. *Spontaneous emission spectra of 1% HBO-TIPS in PMMA (dashed) and PS (solid) thin films (λ_{exc}=355 nm).*

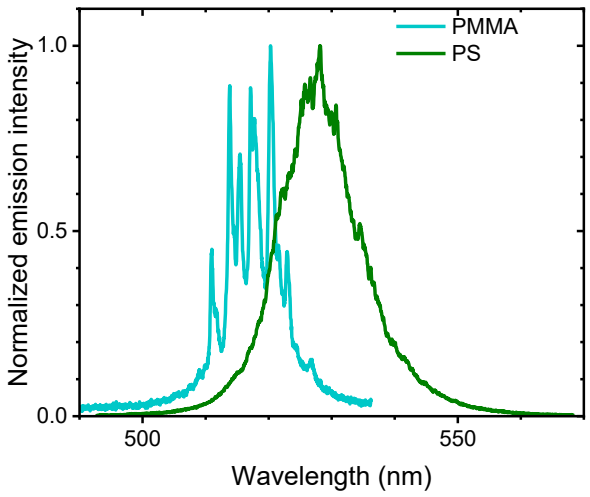

Figure 5.3.30. *Stimulated emission of 1% **HBO-3-TIPS** in PMMA and PS thin films.*

For example, **HBO-3-TIPS/PS** film is capable of random lasing action upon excitation with a 355 nm laser. The output emission is positioned at *ca.* 528 nm, which is red-shifted in comparison to the corresponding PMMA film of the same dye concentration (Figure 5.3.30). The spectra themselves are relatively broader, with an FWHM of 14.7 nm. The observed lasing action is rather incoherent, with weakly distinguishable peaks, as presented in Figure 5.3.31. The PMMA counterpart

enabled purely coherent lasing, with the modes well-defined and stable upon excitation. The lasing threshold is comparable, albeit relatively higher (0.51 ± 0.09 mJ·cm^{-2}). There is one parameter that is worth noticing – the net gain, which is more than twice as high (10.11 ± 0.52 cm^{-1}).

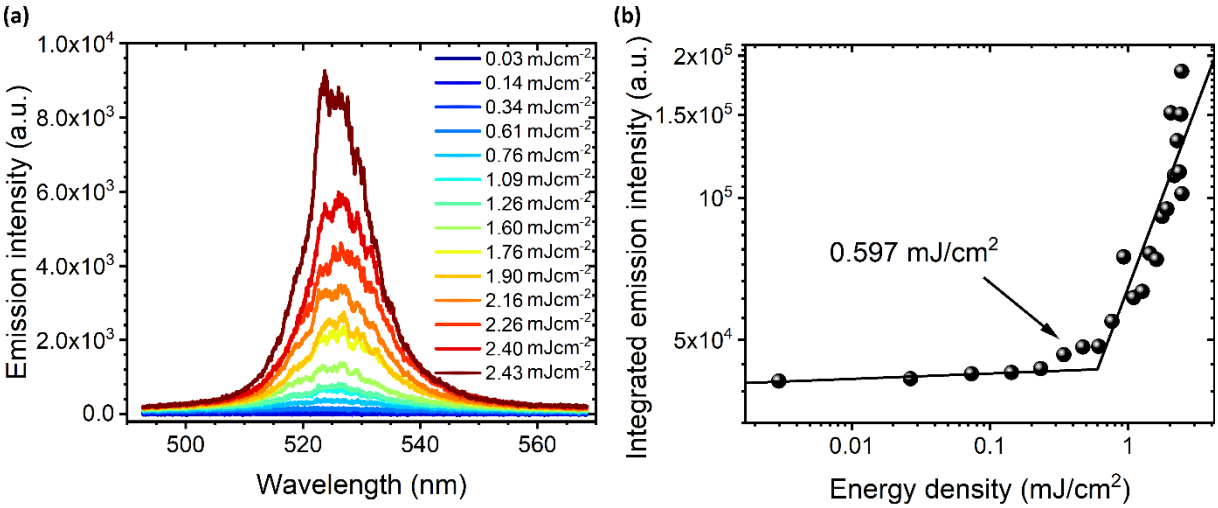

Figure 5.3.31. *(a) Random lasing spectra of 1%* ***HBO-3-TIPS****/PS, with corresponding (b) calculated lasing threshold (λ_{exc} = 355 nm).*

On the other hand, the differences in lasing parameters between PS and PMMA samples are less noticeable when the ethynyl-extended triisopropylsilyl group is substituted at the 4-position. The position of the stimulated emission is roughly the same for both polymeric matrices (Figure 5.3.32), as is the threshold value and the net gain, which for the polystyrene sample are 0.41 ± 0.11 mJ·cm^{-2} and 3.23 ± 0.94 cm^{-1}, respectively. The main difference lies in the full width at half maximum and the profile of the lasing spectra. Similarly to the previously described compound, **HBO-4-TIPS** is capable of coherent random lasing when in the PMMA matrix. The lasing modes are, however, not so easily distinguishable in polystyrene. The spectrum is much broader (14.0 nm in PS, 6.8 nm in PMMA), with singular spikes positioned more closely. The lasing action itself appears to be more chaotic (Figure 5.3.33a).

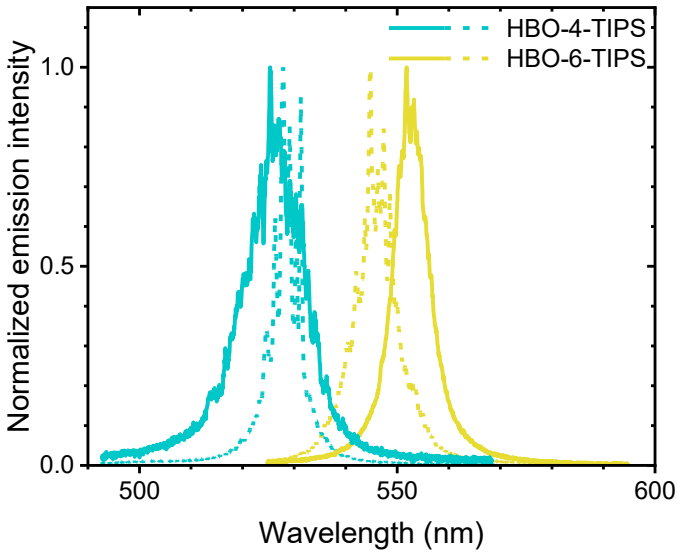

Figure 5.3.32. *Stimulated emission of 1%* ***HBO-4-TIPS*** *and* ***HBO-6-TIPS*** *in PMMA (dashed) and PS (solid) thin films.*

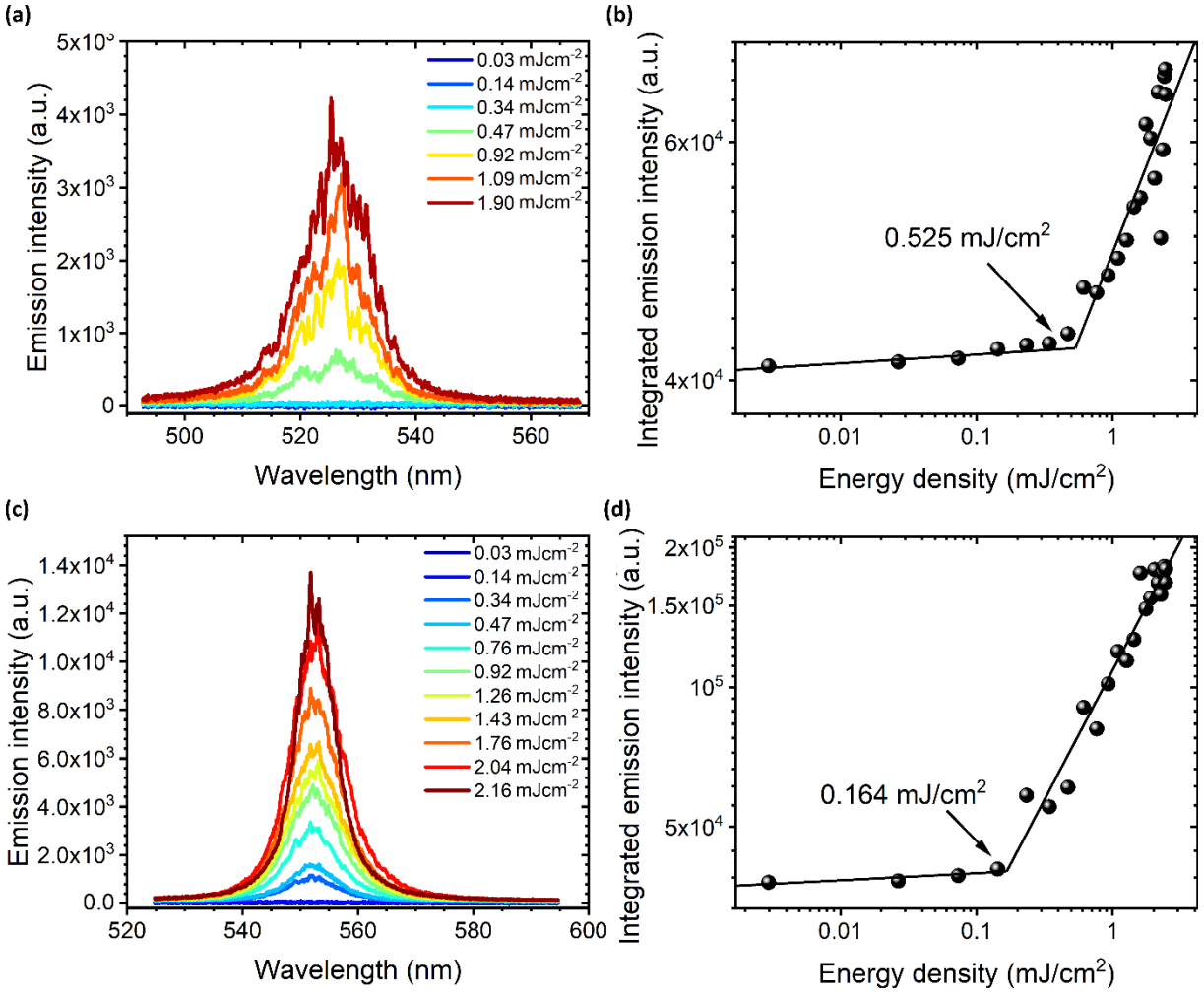

Figure 5.3.33. *Random lasing spectra with the corresponding calculated lasing threshold of 1% (a-b)* ***HBO-4-TIPS*** *and (c-d)* ***HBO-6-TIPS*** *in polystyrene (λ_{exc} = 355 nm).*

With the ethynyl-TIPS moiety at the 6-position, the bathochromic shift of the stimulated emission in polystyrene is more pronounced, with the central wavelength moved towards lower energies by 13 nm in comparison to the corresponding poly(methyl methacrylate) – Figure 5.3.32. Both lasing threshold and net gain values are two times lower in PS, than in the PMMA sample, with 0.19 ± 0.03 mJ·cm^{-2} and 4.04 ± 0.47 cm^{-1}, respectively. **HBO-6-TIPS**, like the rest of the mono-substituted derivatives, is prone to incoherent random lasing when doped in PS (Figure 5.3.33b). One of the explanations for such behavior lies in the structure of the polymer when deposited as a thin film. The polystyrene samples are much more brittle than PMMA, as it is less amorphous. The difference is visible even at the first glance, as the PS samples seem to have cracked during the solvent evaporation. Hence, they are less transparent and uniform. These irregularities, on one hand, provide additional scattering, but on the other, they prohibit the formation of well-defined cavities in the film. Therefore the lasing modes

cannot be easily extracted from the sample. As the PMMA is completely amorphous, the obtained films are more uniform.

Surprisingly, these additional effects are not as pronounced in bis-substituted **HBO-4,6-TIPS**. While the stimulated emission is indeed shifted towards longer wavelengths (λ_{las} = 564 nm), it is not significantly broader (Figure 5.3.34). The density of the lasing modes is smaller than in PMMA samples, however, the individual peaks are present even at the low energy densities (Figure 5.3.35). The determined values of threshold (0.34 ± 0.03 mJ·cm^{-2}) and net gain (1.49 ± 0.42 cm^{-1}) are also comparable.

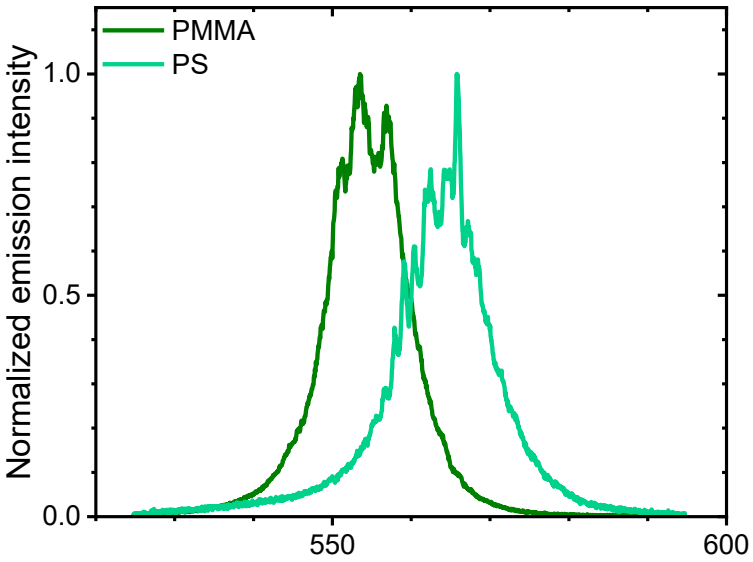

Figure 5.3.34. *Stimulated emission of 1%* ***HBO-4,6-TIPS*** *in PMMA and PS thin films.*

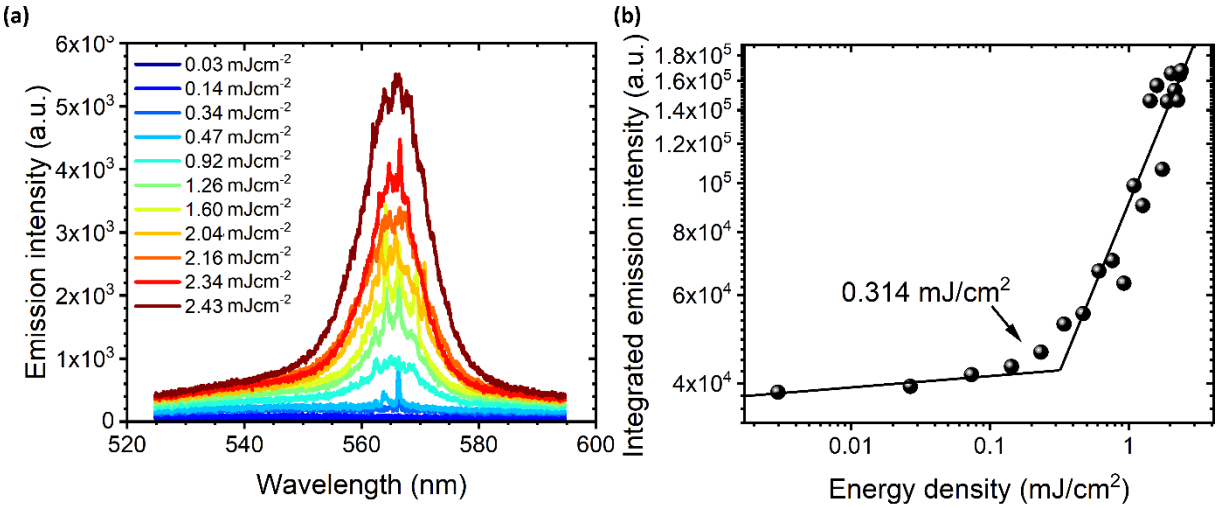

Figure 5.3.35. *(a) Random lasing spectra of 1%* ***HBO-4,6-TIPS****/PS, with the corresponding calculated (b) lasing threshold (λ_{exc} = 355 nm).*

The exemplary spectra of investigated hydroxyphenylbenzoxazoles, mono- or bis-substituted with ethynyl-TIPS moieties, applied as doping in polystyrene, are presented in Figure 5.3.36. The stimulated emission parameters are listed in Table 5.3.4.

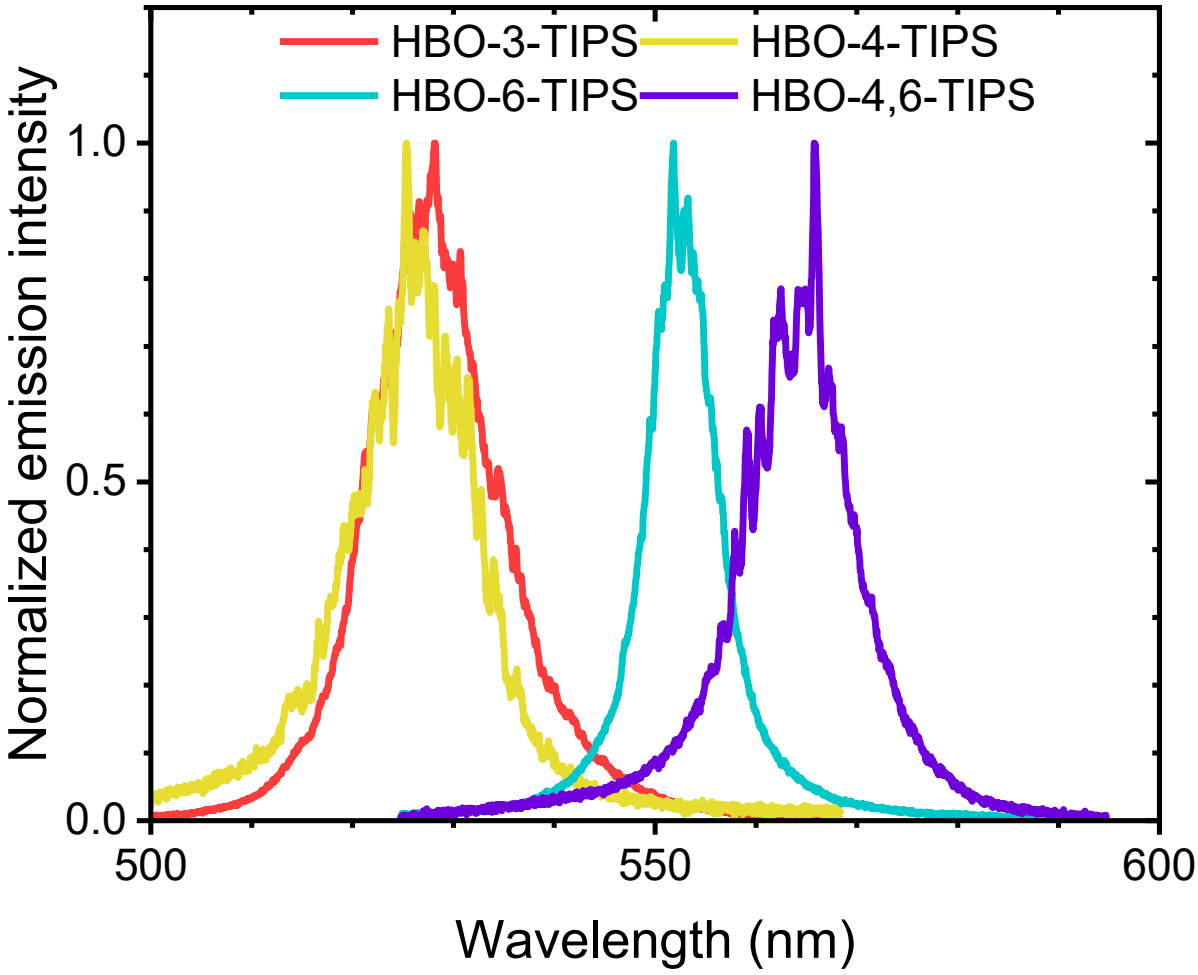

***Figure 5.3.36. S**timulated emission of 1% **HBO-TIPS**/PS thin films.*

***Table 5.3.4.** Random lasing parameters of selected **HBO-TIPS** dyes in polystyrene.*

Compound	λ_{em} [nm]	FWHM [nm]	CIEx	CIEy	ρ_{th} [mJcm^{-2}]	g [cm^{-1}]
HBO-6-TIPS	553	8.4	0.327	0.668	0.19 ± 0.03	4.04 ± 0.47
HBO-4-TIPS	526	14.0	0.138	0.794	0.41 ± 0.11	3.23 ± 0.94
HBO-3-TIPS	528	14.7	0.153	0.797	0.51 ± 0.09	10.11 ± 0.52
HBO-4,6-TIPS	564	12.7	0.401	0.596	0.34 ± 0.03	1.49 ± 0.42

λ_{em} – central emission wavelength, FWHM – full width at half maximum, CIEx/y – CIE 1931 coordinates, ρ_{th} – threshold energy density, g – net gain.

AMPLIFIED SPONTANEOUS EMISSION FROM AMORPHOUS POWDERS

Numerous reports in the literature concerning successful light amplification in crystals or other smaller structures, like nanowires, show promising properties of the ESIPTs in the solid state. As the hydroxyphenylbenzazoles presented in this dissertation are capable of random lasing from polymeric thin films, and their quantum yields of emission are high when dispersed in inert potassium bromide, their pure amorphous powders were investigated. Stimulated emission from such sample was previously obtained for **HBO-4,6-TES,**[1] with a maximum located at 560 nm. Simple sandwiching of the powder in between two glass slides made it possible to determine the threshold value, which in this case was less than 1 mJ·cm^{-2}. Hence, the possibility of light amplification from powders was investigated. Out of 18 ESIPT compounds, it was achieved only in four: two HBIs, and two HBOs.

The **HBI-3-TIPS** derivative, upon excitation by a 355 nm nanosecond laser of high enough energy density, is capable of Amplified Spontaneous Emission at $\lambda \approx 513$ nm. As is characteristic for ASE, the full width at half maximum was progressively decreasing along with an increase in pumping energy density (see Figure 5.3.37). At low excitation energies, the emission spectrum was initially very broad, with the FWHM = 68 nm. Along with the increase in pumping energy, FWHM decreased to 18 nm. The determined threshold is 2.3 mJ·cm^{-2}, which is a more than tenfold higher value than for the **HBI-3-TIPS**/PMMA sample. On the other hand, the ASE from powder is by 15 nm shifted towards longer wavelengths. However, if the profile of the spectrum is analyzed, then a second smaller band is visible (around 490 nm), which is significantly overlapping with the other band. These facts suggest that the chromophore forms crystals and aggregates of various geometries, which in turn influences the possibility of obtaining light amplification. The obtained ASE is surprising, as aggregation-caused quenching was observed

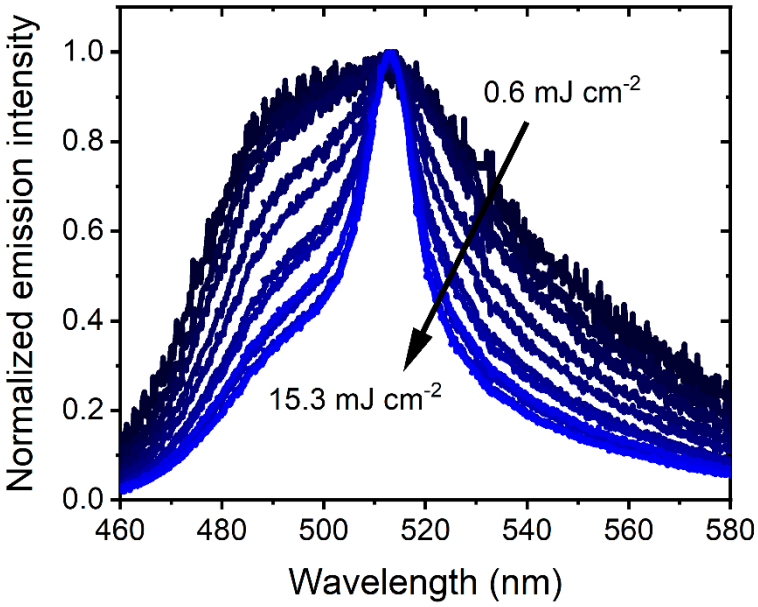

***Figure 5.3.37**. Amplified spontaneous emission of **HBI-3-TIPS** powder (λ_{exc} = 355 nm).*

when THF/water mixtures of **HBI-3-TIPS** were investigated. On the other hand, this derivative is characterized by the highest quantum yield of emission in potassium bromide powders (68%).

Similar to **HBI-3-TIPS**, the ASE was observed for **HBI-4-TIPS**, **HBO-3-TIPS**, and **HBO-6-TIPS**. The spectra in each case are not gaussian-like, as presented in Figure 5.3.38. Thus, the spontaneously formed crystals and aggregates were confirmed to provide gain for the light amplification to occur. The mechanism behind amplification in these derivatives is not clear at the time of the dissertation writing. Only two out of four exhibit AIEE properties (the HBOs), which eliminates this phenomenon as a possible mechanism. It should be noted, however, that ASE observed in these powders is dependent on the packing between individual particles, the thickness of the powder's layer, *etc*. Hence, for the exact determination of the stimulated emission parameters, single crystals should be grown and then investigated. The too-small amounts of the compounds made it impossible at that time. Therefore, the parameters estimated for randomly oriented particles of chosen HBX compounds are listed in the table below.

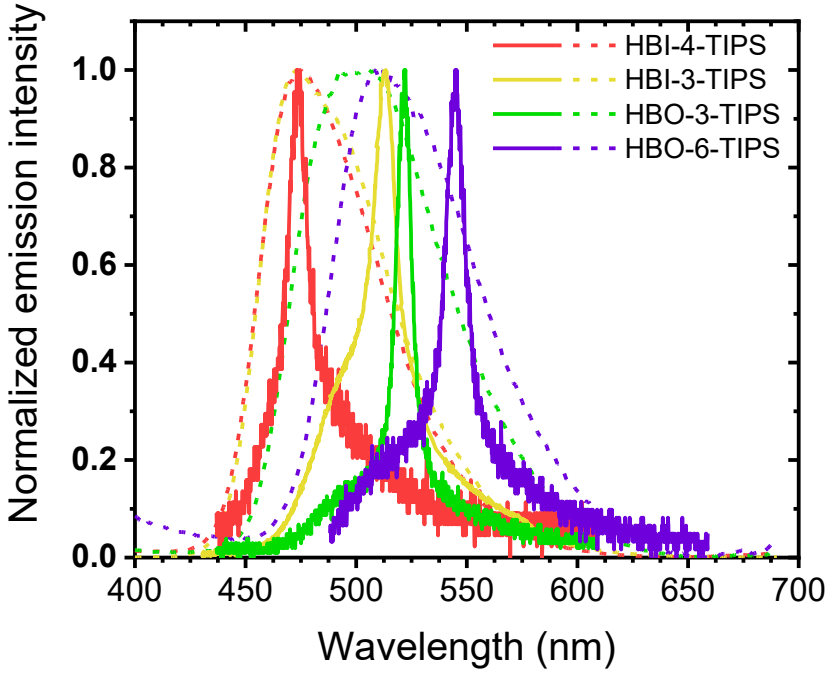

***Figure 5.3.38**. Amplified spontaneous emission recorded for pure **HBX** powders (solid) and fluorescence of corresponding potassium bromide pellets (λ_{exc} = 355 nm).*

***Table 5.3.5.** Stimulated emission parameters of selected **HBX** dyes as amorphous powders.*

Compound	λ_{em} [nm]	FWHM [nm]	CIEx	CIEy	ρ_{th} [mJcm^{-2}]
HBI-3-TIPS	511	18.0	0.156	0.588	2.3
HBI-4-TIPS	474	20.5	0.178	0.255	15.3
HBO-3-TIPS	522	11.1	0.193	0.633	14.8
HBO-6-TIPS	545	17.0	0.329	0.637	16.8

λ_{em} – central emission wavelength, FWHM – full width at half maximum, CIEx/y – CIE 1931 coordinates, ρ_{th} – threshold energy density.

STIMULATED EMISSION OF CONCENTRATED SOLUTIONS

The ESIPT phenomenon is responsible for population inversion, which is one of the crucial elements necessary for the lasing action to occur. This process takes place both in solutions and in solid-state. The application of hydroxyphenylbenzazoles for the latter was proven in previous paragraphs of this chapter, however, stimulated emission was observed also in dye solutions in non-polar toluene. The concentration of the mixtures had to be relatively high (1% w/w), as for lower quantities no amplification was obtained or it wasn't stable enough to validate the lasing parameters. Surprisingly, stimulated emission was recorded even in compounds prone to aggregation-caused quenching, like **HBI-3-TIPS**. In such cases, the determined thresholds are relatively higher.

Nonetheless, upon excitation with the laser beam, amplifies spontaneous emission was observed as a focused, and very bright spot. An increase in the pumping energy density promoted narrowing of the profile, resulting in an emission of at least three times smaller full width at half maximum than of the corresponding spontaneous one, as presented in Figure 5.3.39a on the example of **HBO-4,6-TIPS**. These radiative relaxation pathways correspond to intramolecular proton transfer in the excited state, evident by large Stokes shifts, which in turn prevent self-reabsorption. Such property of the HBX compounds is a searched-for characteristic in purely organic lasers. This feature is even more enhanced due to the shift of the ASE towards longer wavelengths in comparison to spontaneous emission. However, one

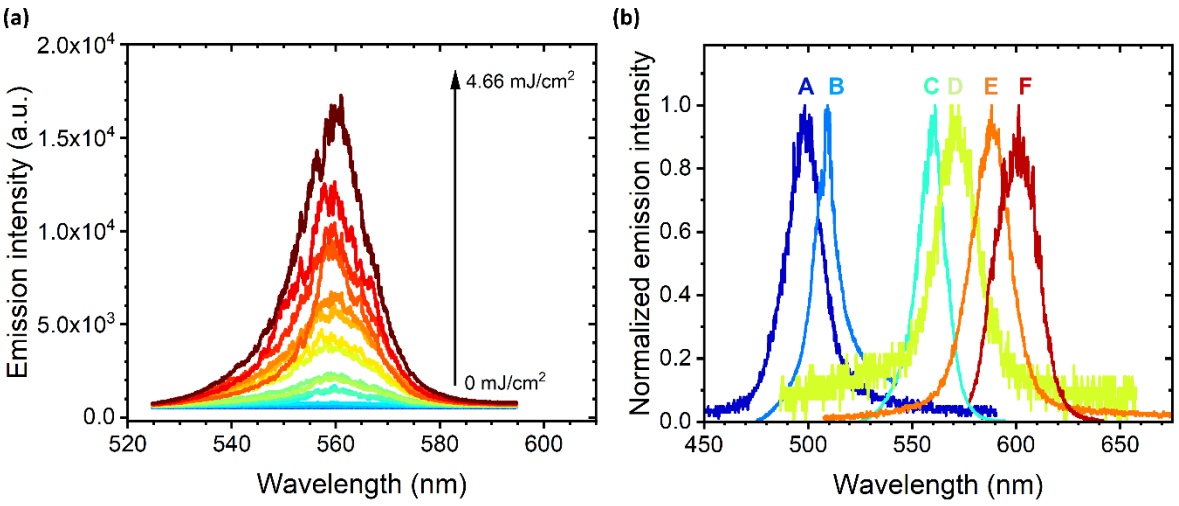

Figure 5.3.39. *(a) Lasing action of 1%* ***HBO-4,6-TIPS****/toluene, and (b) stimulated emission spectra of investigated 1% solutions: A –* ***HBI-3-TIPS****, B –* ***HBT-CF3-4,6-TMS****-deprotonated, C –* ***HBO-4,6-TIPS****, D –* ***HBO-ext-NMe2****, E –* ***HBT-4,6-TES****, F –* ***HBT-CF3-4,6-TMS*** *(λ_{exc} = 355 nm).*

significant drawback should be noted. The pumping with a focus laser beam from the UV range leads to local heating of the solution, and in turn, induces movements of the solvent and chromophore molecules. As a result, the local concentration at the focal point is changed with each pumping pulse. Hence, the emitted light is characterized by rather large fluctuations of its intensity. Moreover, as the molecules are not restricted, the photodegradation is much quicker. Nevertheless, ASE can ban be obtained from investigated HBX derivatives. As already observed for the PMMA thin films, the position of the substitution and the nature of the substituent determine the emitted wavelengths (see Figure 5.3.39b).

The fabrication of dye cells was not the subject of the research presented in this work, however, it is prudent to show that the investigated compounds are capable of light amplification even in solutions. While the stimulated emission was easily obtained for polymeric thin films due to beneficial rigidification and restriction of intramolecular motions, which limit the non-radiative deactivation pathways, the possibility of light amplification was not so obvious in solutions. Therefore, this short paragraph is given in this dissertation to emphasize the outstanding lasing properties of the ESIPTs, as ASE is present only in systems of very high optical gain. Additionally, due to the inherent sensitivity of these compounds due to the intramolecular hydrogen bond, their emission can be tuned. An example can be made of the **HBT-CF3-4,6-TMS** compound, which is capable of stimulated emission at two separate wavelengths (508 or 605 nm). This matter is described more in detail in *Chapter 6.2*.

The summary of chosen HBX dyes in toluene and the observed stimulated emission is listed in Table 5.3.6.

Table 5.3.6 *Stimulated emission parameters of selected HBX dyes in toluene (1% w/w).*

Compound	λ_{em} [nm]	FWHM [nm]	CIEx	CIEy	ρ_{th} [mJcm^{-2}]
HBI-3-TIPS	498	22.0	0.113	0.445	16.8
HBO-4,6-TIPS	559	16.4	0.370	0.625	1.0
HBO-ext-NMe2	571	25.0	0.442	0.541	9.5
HBT-CF3-4,6-TMS deprotonated	508	14.5	0.064	0.709	4.9
HBT-CF3-4,6-TMS	605	22.0	0.619	0.380	3.9
HBT-4,6-TES	588	23.2	0.545	0.453	2.5

λ_{em} – central emission wavelength, FWHM – full width at half maximum, CIEx/y – CIE 1931 coordinates, ρ_{th} – threshold energy density.

Literature

1. Massue, J. *et al.* An extended excited-state intramolecular proton transfer (ESIPT) emitter for random lasing applications. *Phys. Chem. Chem. Phys.* **20**, 19958–19963 (2018).
2. Das, K. *et al.* Excited-State Intramolecular Proton Transfer in 2-(2'-hydroxyphenyl)benzimidazole and 2-(2'-hydroxyphenyl)benzoxazole - Effect of Rotamerism and Hydrogen-Bonding. *J. Phys. Chem.* **98**, 9126–9132 (1994).
3. Mordzinski, A. & Grellmann, K. H. Excited-state proton-transfer reactions in 2-(2'-hydroxyphenyl)benzoxazole. Role of triplet states. *J. Phys. Chem.* **90**, 5503–5506 (1986).
4. Ding, K. *et al.* Excited-state intramolecular proton transfer and vibrational relaxation in 2-(2-hydroxyphenyl)benzothiazole. *J. Phys. Chem.* **87**, 1184–1188 (1983).
5. Manojai, N., Daengngern, R., Kerdpol, K., Ngaojampa, C. & Kungwan, N. Heteroatom effect on photophysical properties of 2-(2′-hydroxyphenyl)benzimidazole and its derivatives as fluorescent dyes: A TD-DFT study. *J. Lumin.* **188**, 275–282 (2017).
6. Massue, J. *et al.* Natural born laser dyes: Excited-state intramolecular proton transfer (ESIPT) emitters and their use in random lasing studies. *Nanomaterials* **9**, (2019).
7. Pariat, T. *et al.* Impact of Heteroatom Substitution on Dual-State Emissive Rigidified 2-(2'-hydroxyphenyl)benzazole Dyes: Towards Ultra-Bright ESIPT Fluorophores**. *Chem. – A Eur. J.* **27**, 3483–3495 (2021).
8. Carayon, C. & Fery-Forgues, S. 2-Phenylbenzoxazole derivatives: a family of robust emitters of solid-state fluorescence. *Photochem. Photobiol. Sci.* **16**, 1020–1035 (2017).
9. Zeng, X. *et al.* THF-induced emission enhancement and reversible stimulus response of a tetraphenylethylene luminogen dependent ESIPT mechanism. *Dye. Pigment.* **171**, 107699 (2019).
10. Bhattacharyya, A., Makhal, S. C. & Guchhait, N. Simple chloro substituted HBT derivative portraying coupling of AIE and ESIPT phenomenon: Ratiometric detection of S2- and CN- in 100% aqueous medium. *J. Photochem. Photobiol. A Chem.* **388**, 112177 (2020).
11. Zeng, G., Liang, Z., Jiang, X., Quan, T. & Chen, T. An ESIPT-Dependent AIE Fluorophore Based on HBT Derivative: Substituent Positional Impact on Aggregated Luminescence and its Application for Hydrogen Peroxide Detection. *Chem. – A Eur. J.* **28**, e202103241 (2022).

6. Applications

Previous parts of this thesis were dedicated to the characterization of investigated compounds. In this chapter, some of the possible practical applications of ESIPT dyes will be presented, showing a high degree of multifunctionality, from polychromatic lasers, through initiators for two-photon polymerization, to sensors and tunable light sources.

6.1. Distributed feedback lasers

Laser line adjustment can be quite easily performed nowadays, for example with the use of optical parametric oscillators or tuning of the gain medium operation on multiple resonator modes. The former is a complex system with a relatively high cost, while the latter can lead to mode hopping instead of continuous smooth tuning. There exists a simpler, compact and less expensive alternative, such as Distributed Feedback lasing. As described in the theoretical introduction, periodic modulation of the active material (through gain and/or refractive index) performed in a dynamic degenerated two-wave mixing setup enables real-time tuning of the emitted laser line. This enables rapid generation of one-dimensional impermanent patterns that can be readily modified by adjusting the intersection angle Θ of two pumping beams, in accordance with the Bragg equation. Moreover, the application of organic compounds as solid-state lasers enables easy and versatile emission engineering through molecular modifications introduced at the synthesis stage. As presented in *Chapter 5*, stimulated emission obtained from the investigated covers the whole visible spectrum. In order to fully utilize these properties and show potential in commercializing HBX derivatives as laser dyes, spectral narrowing through DFB can be executed.

The same 1% w/w dye in PMMA samples that were used for the RL measurements were investigated in the DTWM setup at the second order of the grating (m = 2). DFB lasing was successfully obtained for all films. In this subchapter, to show the possible application of ESIPTs as active material, a few of all investigated are presented: one HBI (**HBI-4,6-TIPS)**, an HBO (**HBO-4,6-TIPS**), and one HBT (**HBT-4,6-TIPS**) derivatives as doped PMMA thin films. Each compound was chosen as a representative of dyes emitting in the blue, green, and red regions of the visible spectra, correspondingly. The HBO was also investigated in concentrated toluene solution (at 1% w/w).

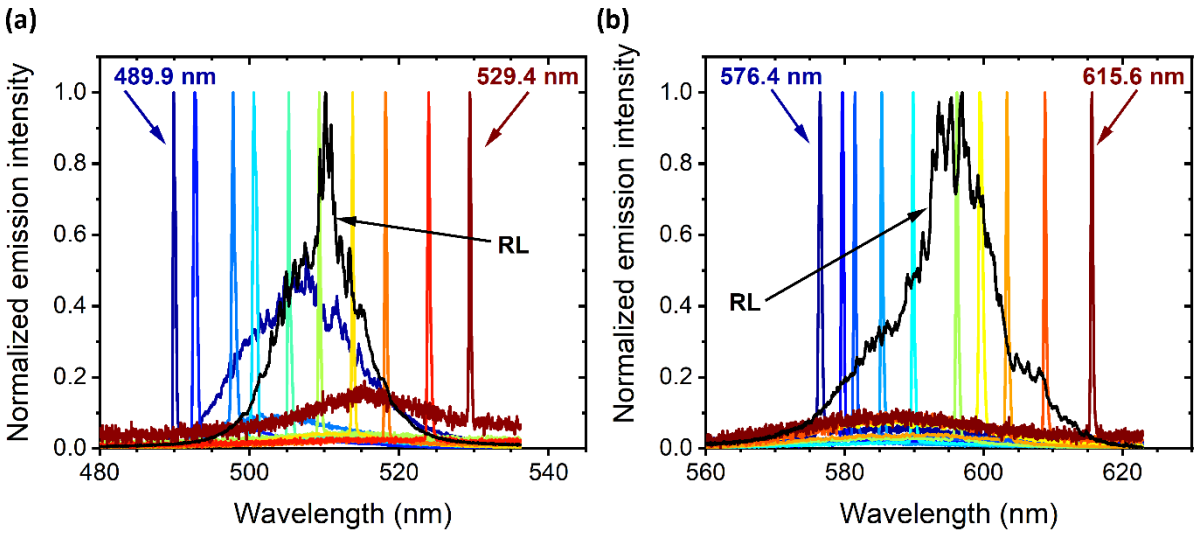

Figure 6.1.1. *Random lasing (RL) and Distributed Feedback lasing spectra recorded for 1% (a)* ***HBI-4,6-TIPS****/PMMA and (b)* ***HBT-4,6-TIPS****/PMMA.*

In all studied samples, no matter the chemical structure, lasing tunability exceeding random lasing spectra was achieved (see Table 6.1.1.). The difference of the spectra at extreme positions ($\Delta\lambda$) was equal to 39 nm for the **HBI-4,6-TIPS** and **HBT-4,6-TIPS**, as presented in Figure 6.1.1. Bigger tunability was achieved for the **HBO-4,6-TIPS** compound (53 nm). As described by Parafiniuk,[1,2] the presence of crystals and aggregates in the active material has a positive effect on the realization of tunable emission. Nevertheless, obtained DFB laser lines are very narrow (FWHM < 0.75 nm). On the other hand, residual random lasing can be observed at the extreme positions of the tuning range (Figure 6.1.1a.). One of the possible reasons is hidden in the feedback mechanism for the laser operation: in investigated samples, it is not dependent on the grating, even though the latter is beneficial for the outgoing stimulated emission. As such, random lasing provided by multiple light scattering on the film's irregularities does not have to be sufficiently blocked from propagating by the periodical grating introduced by the pumping beams. Additionally, constructive scattering leading to RL can occur in bright spots of the interference pattern.

Table 6.1.1. *DFB lasing parameters of chosen dyes.*

Compound	Δλ [nm]	λ_{DFB} [nm]	$\rho_{th,DFB}$ [mJcm^{-2}]	$FWHM_{DFB}$ [nm]	Λ [nm]	n_{eff}
HBI-4,6-TIPS	39	513.8	0.61	0.29	362	1.495
HBO-4,6-TIPS (PMMA)	53	566.0	1.08	0.71	380	1.490
HBO-4,6-TIPS (toluene)	40	566.7	1.96	0.74	375	1.489
HBT-4,6-TIPS	39	590.7	0.56	0.41	397	1.490

Δλ – DFB tunability, λ_{DFB} – DFB lasing at chosen wavelength and relevant parameters: ρ_{th} – lasing threshold, FWHM – full width at half-maximum, Λ – period of the diffraction grating, n_{eff} – calculated refractive index of the waveguide at the chosen wavelength.

The influence of light scattering can be minimized simply by changing the sample preparation method. As such, spin-coating is the most commonly used method to obtain thin films for the DFB experiments.[2–4] The morphology of samples prepared with this technique is smoother and more homogeneous than their drop-casted counterparts. Even though investigated films were prepared through the latter method, their morphology didn't prevent the formation of temporal periodic patterns due to two-beam interference, which further cements great light amplifying properties of HBX derivatives.

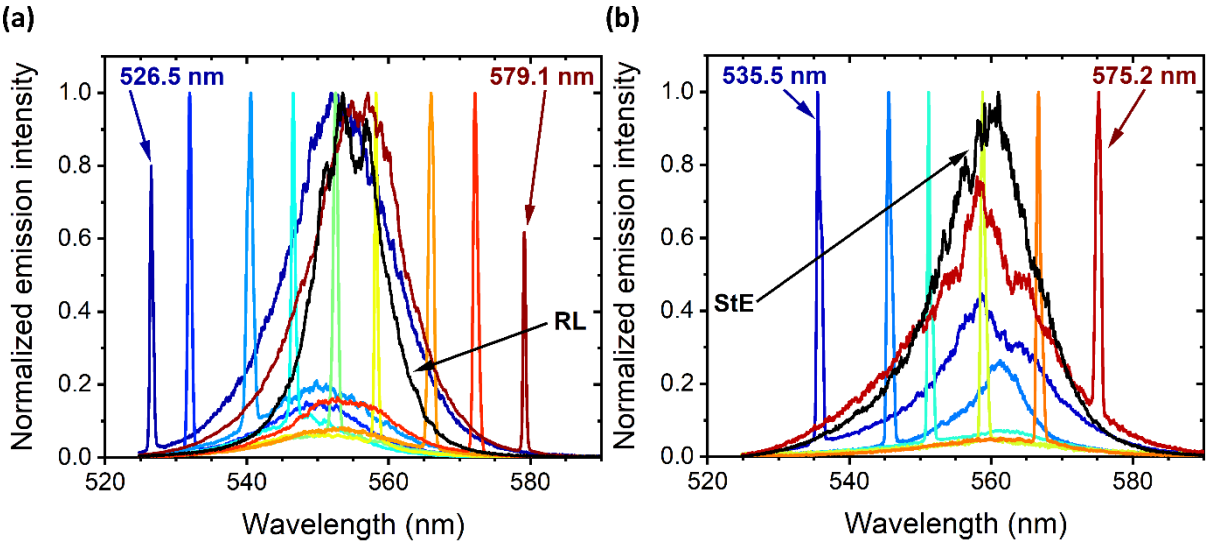

Figure 6.1.2. *Random lasing (RL), Stimulated Emission (StE), and Distributed Feedback lasing spectra recorded for 1%* ***HBO-4,6-TIPS*** *in (a) PMMA and (b) toluene.*

Even with surface irregularities and spontaneously formed crystals, efficient real-time tunable DFB lasing was realized. However, in such nonhomogenous film the thickness modulation, which was beneficial in random lasing, induces light scattering on the

irregularities, instead of in the volume of the film. This in turn increases losses, leading to a higher lasing threshold. Of course, the latter parameter is generally lower for the first order of grating than the second one.[3,5] Nevertheless, determined DFB thresholds vary depending on the lasing wavelength. For presented HBX compounds, these values are slightly higher than RL ρ_{th} but are of the same order of magnitude. As light amplification can also be obtained in concentrated solutions as presented in the previous chapter of this dissertation, the DTWM setup was used to investigate the DFB lasing in liquids. Hence, a 1% w/w solution of **HBO-4,6-TIPS** in toluene was prepared and successfully applied. The beneficial influence of restriction of molecules in the polymeric matrix is evident, as the tunability of laser line from concentrated solution is smaller than in corresponding thin film, while at the same time the determined lasing threshold is almost twice as high. Additionally, pumping with the laser beam leads to local heating, followed by thermally-induced movements of molecules of both the dye and the solvent. Hence, the interference pattern is continuously disturbed, resulting in a presence of residual stimulated emission throughout the whole tuning range (see Figure 6.1.2b).

Presented results show that DFB lasers can be fabricated in investigated ESIPT compounds. Continuous and precise laser line tuning can be performed in real-time throughout the whole visible spectra. Low determined values of lasing energy threshold and very narrow emission profiles (FWHM <0.5 nm) prove the great potential of these molecules as purely organic, tunable solid-state lasers.

6.2. Emission tuning and sensing

This section contains fragments of the following publication:

M. Durko-Maciąg, D. Jacquemin, G. Ulrich, J. Massue, J. Myśliwiec, **Color-tunable Multifunctional Excited-State Intramolecular Proton Transfer Emitter: Stimulated Emission of a Single Molecule**, Chemistry – A European Journal, *under review*

As described in *Chapter 3*, ESIPT dyes have inherent sensitivity toward the local conditions, such as polarity, resulting in an environment-depended emission profile. Several reports on deprotonation of the HBX molecules in the protic solvents were already published,[6–8] prompting the Author to investigate available compounds. As one of the examples, **HBT-**

CF3-4,6-TMS is presented in this subchapter (Figure 6.2.1.). The mentioned deprotonation is evident by a formation of highly fluorescent species (anions), blue-shifted in comparison to the keto form. Since partial frustration of the ESIPT phenomena is also possible in polar solvents, triple-band emission can be achieved in a single-dye system. This opportunity was exploited by the Author.

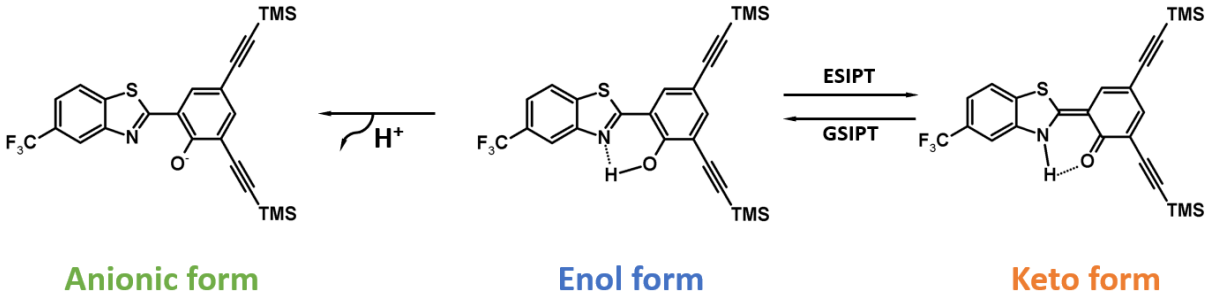

Figure 6.2.1. *Possible conformations of* ***HBT-CF3-4,6-TMS.***

Photophysical properties in toluene of **HBT-CF3-4,6-TMS** are presented in previous subchapters, however additional measurements in other solvents were also performed. Depending on the medium polarity, one or two absorption bands were observed, which can be ascribed to enol (*ca*. 370 nm) and anionic (428-466 nm) forms. The former was present in all nonpolar solvents (and acetonitrile), while the latter forms in polar and protic solutions. Corresponding emission was obtained, with multiple bands: first, E^* localized in the blue region of the visible spectra (376-407 nm), followed by a red-shifted band at 493-496 nm (A^*), with excited K^* at 566-568 nm. Quantum yields of fluorescence varied depending on the solvent (4-45%), which is on par with examples from the literature.[6,9]

Emissive properties in solid-state were also investigated. Unlike in solutions, only single bands were recorded for dye-doped 1% w/w PMMA film, or KBr pellet, corresponding to the keto emission in the orange-red region of the spectrum (560/573 nm). Such simple modification of the system, as is the change of the medium, allows easy engineering of the emission from blue, through green, to red (as evidenced by CIE 1931, Figure 6.2.2.), to suit one's needs.

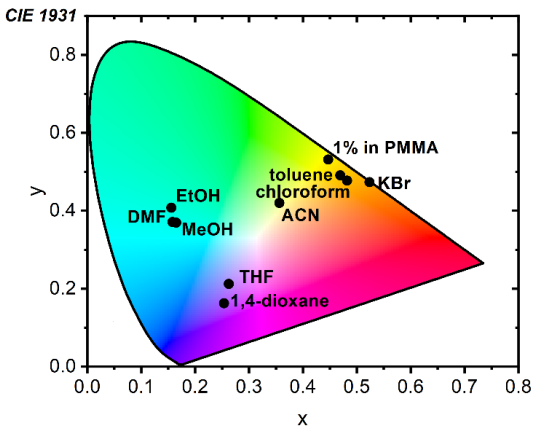

Figure 6.2.2. *CIE 1931 coordinates of* ***HBT-CF3-4,6-TMS*** *in various matrices.*

***Table 6.2.1**. Photophysical properties of **HBT-CF3-4,6-TMS** dye in various matrices; E – enol, A – anion, and K – keto form.*

Solvent	λ_{abs} [nm][a]	ε ($M^{-1} \cdot cm^{-1}$)[b]	λ_{em} [nm][c]	$\Delta\nu$ [cm^{-1}][d]	Φ_F[e]
1,4-dioxane	369	18000	407 (E^*); 566 (K^*)	9432	0.07
toluene	376	16200	376 (E^*); 567 (K^*)	8959	0.13
chloroform	378	11600	383 (E^*); 566 (K^*)	8725	0.24
THF	368	24000	395 (E^*); 568 (K^*)	9475	0.08
EtOH	429	8400	383 (E^*); 493 (A^*)	3026	0.09
MeOH	427	24500	386 (E^*); 496 (A^*)	3176	0.45
DMF	466	24200	382 (E^*); 496 (A^*)	1216	0.25
ACN	371,459	12200; 10900	390 (E^*); 493 (A^*); 558 (K^*)	9033	0.04
PMMA	379	-	560 (K^*)	8528	0.02
KBr	370	-	573 (K^*)	9575	0.34

[a] Maximum absorption wavelength; [b] Molar attenuation coefficient; [c] Maximum emission wavelength (λ_{exc} = 355 nm); [d] Maximum Stokes' shift; [e] Absolute fluorescence quantum yield values determined by integrating sphere.

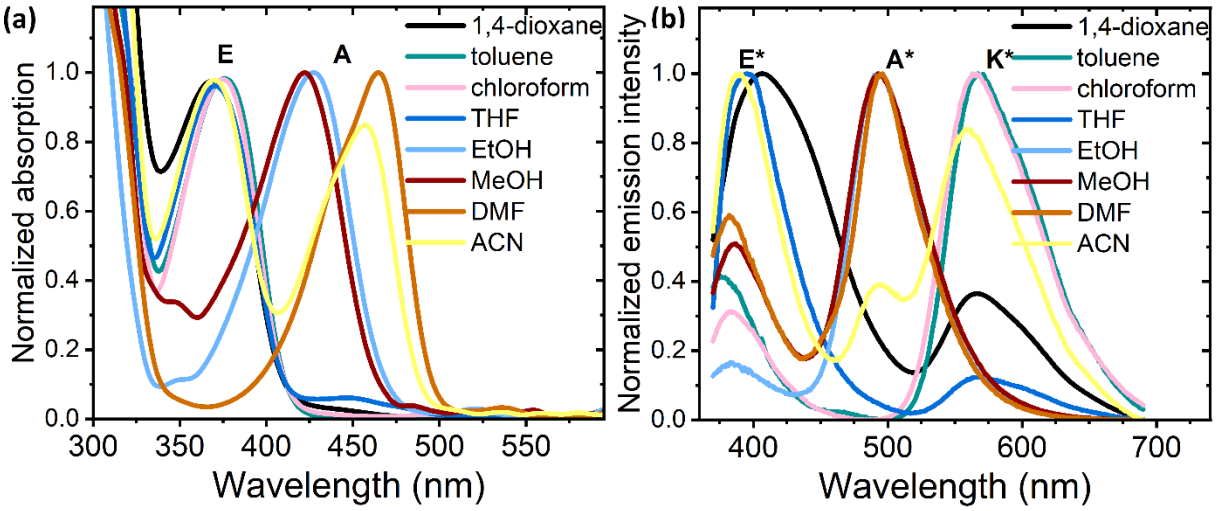

***Figure 6.2.3**. Normalized (a) absorption and (b) emission spectra of diluted **HBT-CF3-4,6-TMS** solutions (10^{-6} M) in: 1,4-dioxane (black), toluene (dark green), chloroform (pink), tetrahydrofuran (dark blue), ethanol (light blue), methanol (dark red), dimethylformamide (light brown) and acetonitrile (yellow); λ_{exc} = 355 nm.*

To confirm that the deprotonation was indeed occurring, simple titration of aprotic solutions with the base was performed. The appearance of an intense band localized in between E^* and K^* was recorded upon the addition of the sodium hydroxide aqueous solution to **HBT-CF3-4,6-TMS**/1,4-dioxane (Figure 6.2.4.). The position of the observed band (497 nm) was the same as for the protic polar solvents, like DMF.

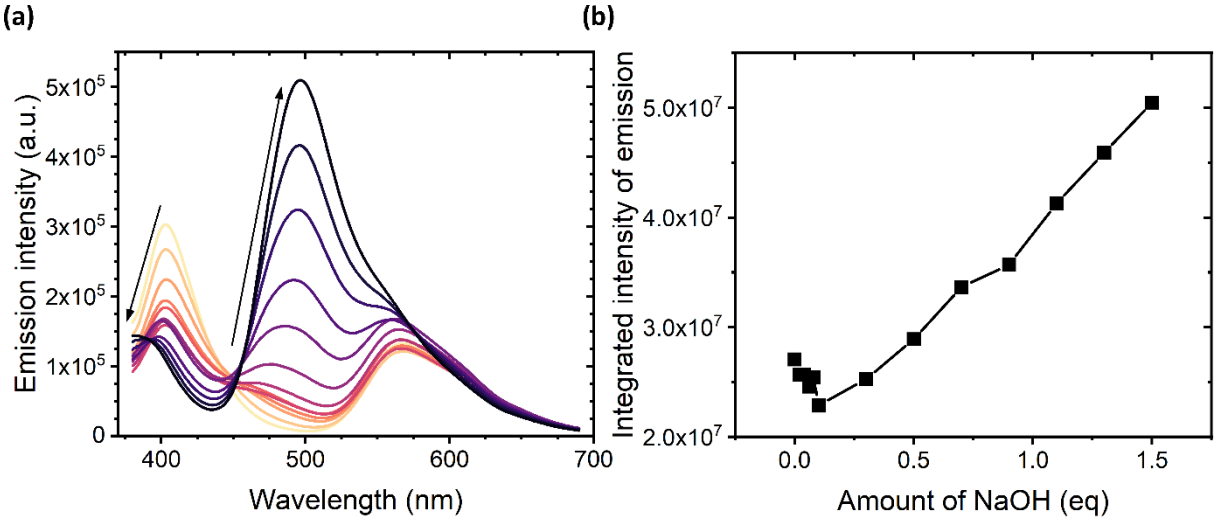

Figure 6.2.4. *(a) Emission spectra of* ***HBT-CF3-4,6-TMS****/1,4-dioxane 10 μM solution during titration with base, with (b) corresponding recorded changes of emission intensity,* λ_{exc} *= 355 nm.*

Deprotonation is a controllable process, making it possible to fabricate systems with specific absorption/emission profiles. As with **HBT-CF3-4,6-TMS**/1,4-dioxane solution: titration with the base results in a blue shift of the emission from orange to green by simple changes in the intensity ratio of enol, anion, and keto species in the excited state. This fine-tuning made it possible to achieve white emission when the amount of base was equal to

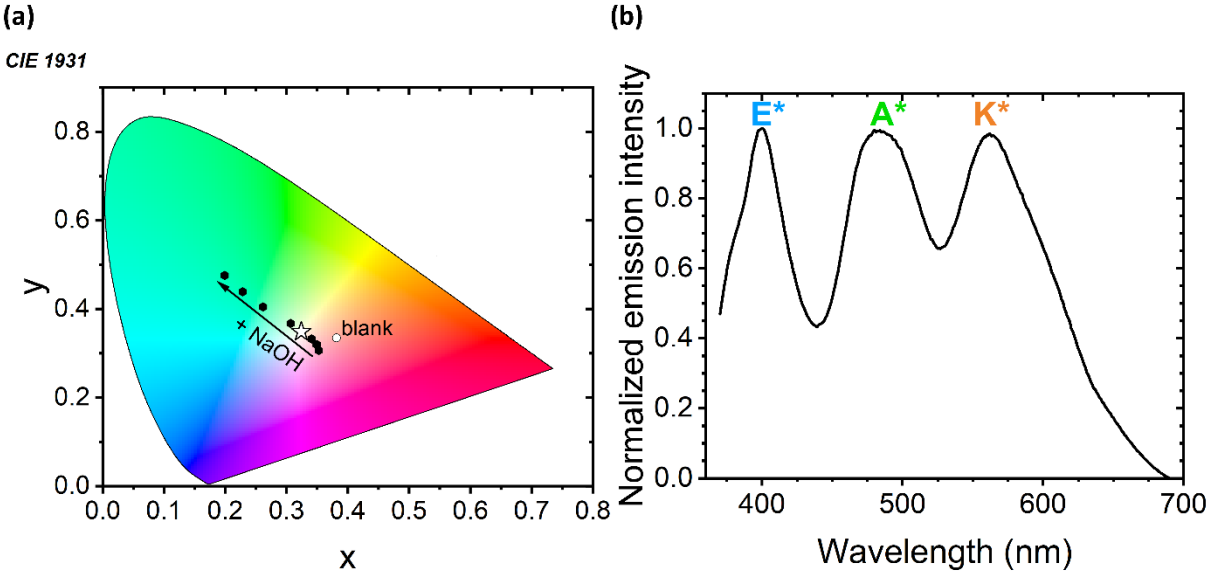

Figure 6.2.5. *(a) Calculated CIE 1931 coordinates of emission spectra obtained during titration of 10 μM solution of* ***HBT-CF3-4,6-TMS*** *in 1,4-dioxane: "blank" refers to pure dye solution, with a star point marking white emission: x=0.34, y=0.33. (b) Normalized emission spectra of the solution titrated with one molar equivalent of NaOH.*

0.6 molar equivalents (Figure 6.2.5a, CIE 1931: x=0.34, y=0.33). Upon further titration, an equilibrium of all forms was reached, as shown in Figure 6.2.5b. To further investigate deprotonation, additional titration of the nonpolar solution (in aprotic toluene) with a polar solvent (ethanol) was performed. In accordance with NaOH-titrations, an additional green band appeared in the spectra, with simultaneous blue-shift and decrease of the band related to excited keto emission (Figure 6.2.6).

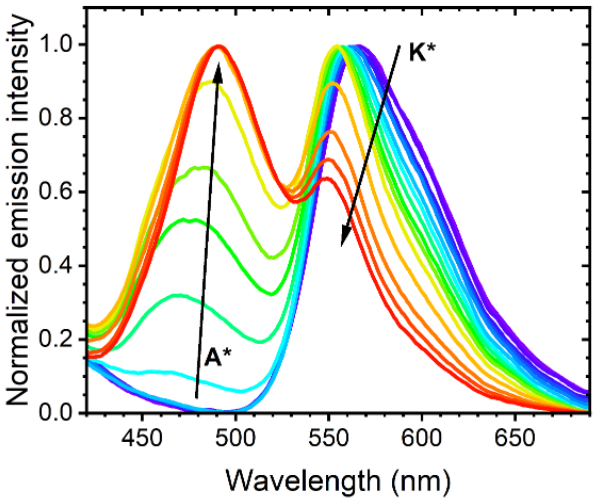

***Figure 6.2.6**. Normalized absorption spectra of **HBT-CF3-4,6-TMS**/toluene solution during addition of ethanol.*

As evidenced in previous chapters of this dissertation, Aggregation-Induced Emission Enhancement properties play a big role in possible applications of the compounds as light sources. Such property was also investigated for the chosen HBT dye in two sets of mixtures: 1,4-dioxane/water (nonpolar-aprotic/polar-protic) and ethanol/water (polar-protic/polar-protic). The different molecular response was recorded for each set. For the former, at up to 60% of the water fraction, an increase in emission intensity was observed along with dye aggregation, evidenced by the formation of the anionic form due to dye-water interaction. When the water/1,4-dioxane ratio is increased even further a deprotonated band (490 nm) disappears, with K^* band remaining (Figure 6.2.7). The quenching of the anionic species is a result of the π-π stacking, to which this form is visibly prone.[10,11] Additional close-up studies at low water fractions (up to 10%) have shown a linear relationship between emission intensity anion/keto emission ratio and the water fractions (with very good fitting coefficients: $R^2 = 0.994$), enabling the application of the chosen HBT derivative as a ratiometric sensor of polar species. Further aggregation of the **HBT-CF3-4,6-TMS** results in a decrease in the emission intensity, however, overall emission enhancement is visible in comparison to the pure, non-aggregated solution (two-fold).

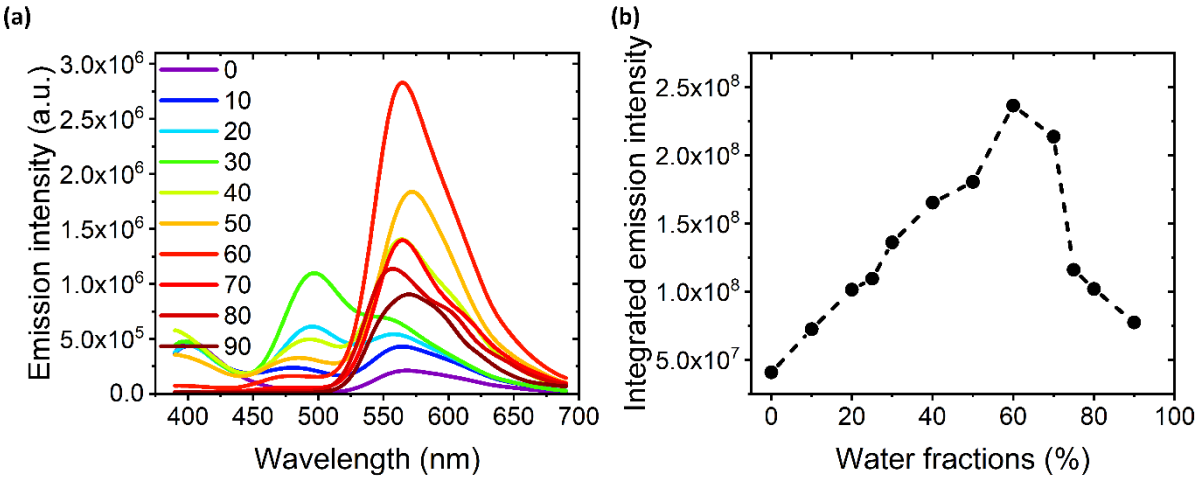

***Figure 6.2.7**. (a) Emission spectra of **HBT-CF3-4,6-TMS** in 1,4-dioxane/water suspensions, along with (b) corresponding changes in emission intensity. Numbers in the legend of (a), mark water fraction in recorded suspension.*

AIEE measurements conducted for ethanol/water mixtures confirm the theory that deprotonated form is more emissive in the solutions in comparison to K^*, while at the same time is subjected to ACQ. As both solvents used for the experiments are protic, in a non-aggregated state two emission bands are visible (from enol and anionic forms, Figure 6.2.8). An increase in water fraction results in a blue shift of the deprotonated form, along with a decrease in the intensity, as is common for H-aggregated formation. Along with the quenching of the anionic form, a third band is recorded (*ca*. 567 nm), corresponding to the keto form

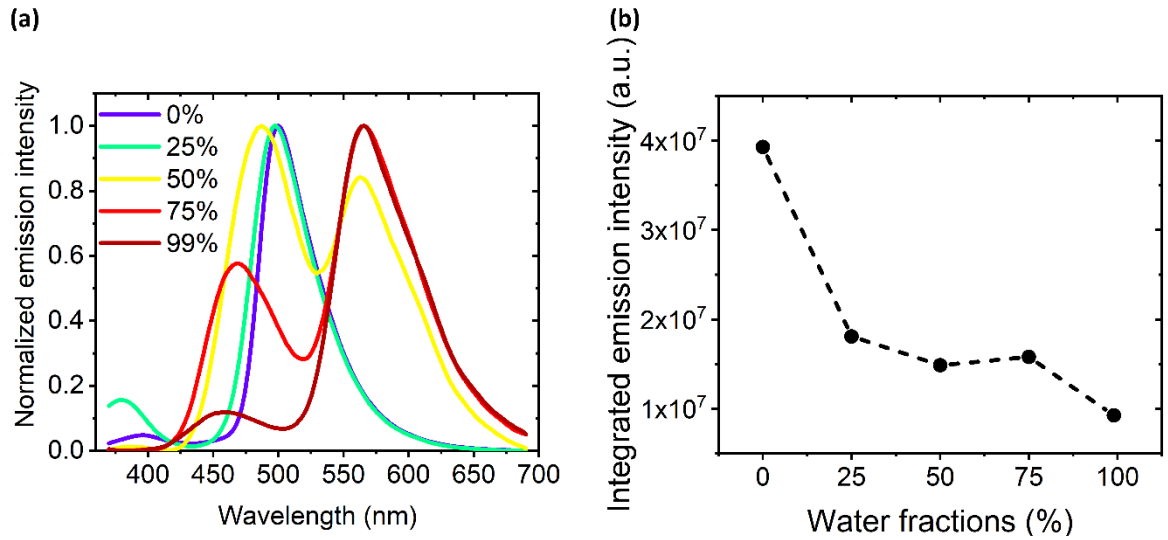

***Figure 6.2.8**. (a) Normalized emission spectra of **HBT-CF3-4,6-TMS** in ethanol/water suspensions, along with (b) observed emission intensity. Numbers in the legend of (a), mark water fraction in recorded suspension.*

emission, that remains emissive due to beneficial Restriction of the Intramolecular Motion. Observed behavior proves that the deprotonation is reversible by simple aggregation.

Previously presented results show that spontaneous emission tuning throughout the whole visible spectra is easily achievable for **HBT-CF3-4,6-TMS**. These good properties prompted the Author to investigate the matter in terms of light amplification. Such application was already studied by other groups, but it was limited to solid-state systems, with little-to-none real-time tunability.[12,13] Additionally, lasing properties of ESIPTs in solutions have been studied, but to the best of the Author's knowledge, only K^* band was found useful in light amplification. As such, concentrated solutions (1.5 mM) of HBT derivatives in various solvents, including THF and ethanol. The latter was unstable: for the complete dissolution of the dye ultrasounds had to be applied, however quite quickly precipitation of the compound started to take place, preventing the stimulated emission measurement. Nevertheless, observed spontaneous emission consisted of an anionic band. In nonpolar solvents solubility of the dye is higher, enabling observation of the stimulated emission at *ca*. 605 nm upon 355 nm excitation. The recorded emission was intense and much more narrow ($FWHM_{THF}$ = 48 nm) than the corresponding spontaneous one. Additionally, a four-level lasing system was confirmed on the basis of the THF solution (Figure 6.2.9). In this case, two emission bands are observed with low energy excitation sources (such as xenon lamps in spectrofluorometers), whereas upon pumping population inversion can only be obtained with the keto band, proving the applicability of the ESIPT photocycle as a four-level laser. While no stimulated emission experiments could be performed in polar solvents, the solubility issue was overcome through titration with the base, resulting in deprotonation.

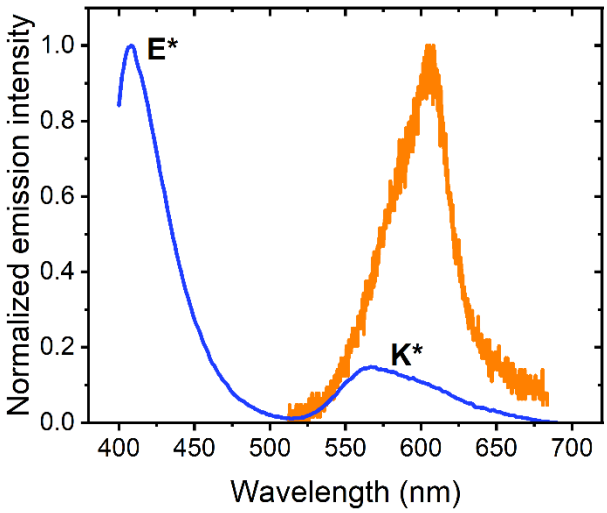

***Figure 6.2.9**. Normalized spontaneous (blue) and stimulated (orange) emission of **HBT-CF3-4,6-TMS**/THF solution.*

In order to ensure complete mixability and to prevent the formation of a two-phase mixture, a sodium hydroxide/ethanol solution was prepared and further used for the titration of the toluene solution, which exhibited stimulated emission in the orange-red region (605 nm, $FWHM_{toluene}$ = 22 nm). The addition of the NaOH leads to instant deprotonation of the **HBT-**

CF3-4,6-TMS, much quicker than in previous titration measurements, due to the high concentration of the dye. Formed anionic species turned out to be capable of population inversion: upon pumping with 355 nm laser a much narrower and blue-shifted stimulated emission was observed ($FWHM_{toluene+NaOH}$ = 13 nm, λ_{em} = 509 nm), as presented in Figure 6.2.10. The inset photo shows ongoing diffusion in the investigated sample. Stimulated emission was obtained from both parts of the solution. The lasing thresholds were determined for both cases, with 3.9 ± 0.15 mJ·cm^{-2} for the toluene, and 4.9 ± 0.15 mJ·cm^{-2} for the deprotonated one. These results show unprecedented real-time stimulated emission shifting of almost 100 nm.

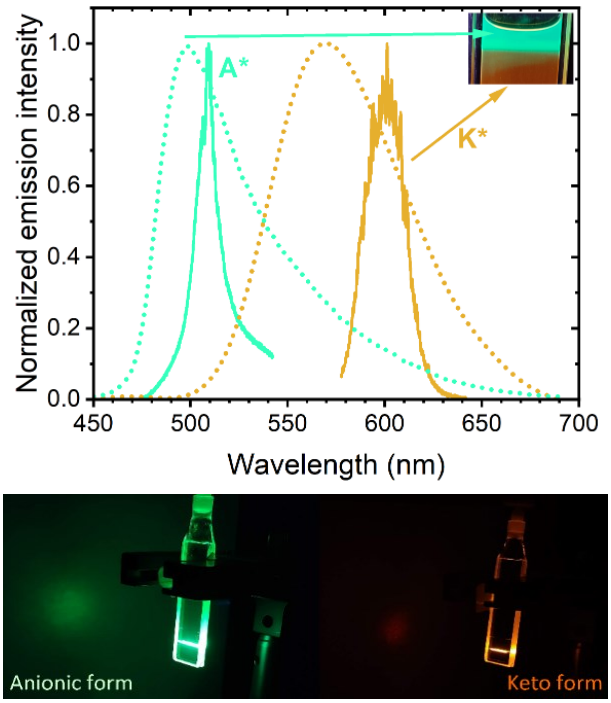

***Figure 6.2.10**. Stimulated emission spectra of anionic and keto forms in 1.5 mM **HBT-CF3-4,6-TMS**/toluene solutions, along with photographs taken during experiment.*

Light amplification properties of anionic form were also investigated in solid-state through doping of the dye/PMMA mixture at the preparation stage. While enlargement of the spontaneous emission spectra was achieved through the introduction of the second emissive band, Random lasing could only be obtained from the keto species (Figure 6.2.11.). The determined lasing threshold for doped- and non-doped 2% w/w PMMA films were 0.90 ± 0.10 mJ·cm^{-2} and 0.54 ± 0.10 mJ·cm^{-2}, accordingly. The higher value of the latter is a result of the depletion of the enol population, resulting in a subsequent decrease of the species involved in the lasing process.

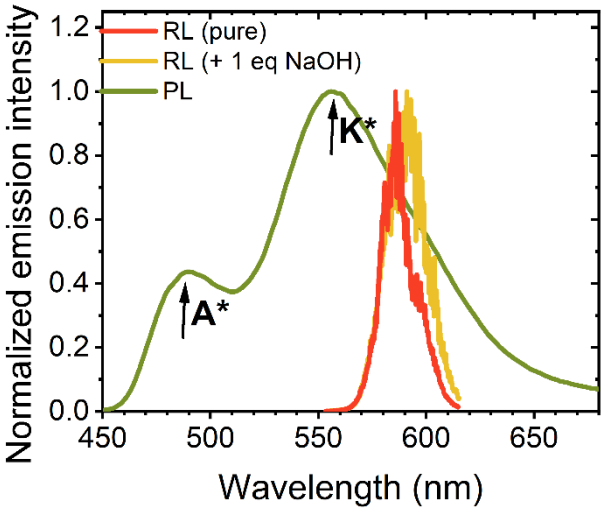

***Figure 6.2.11.** (a) Normalized fluorescence (PL) and random lasing (RL) emission spectra of 2% **HBT-CF3-4,6-TMS**/PMMA film: non-(pure) and doped with 1.0 eq. NaOH.*

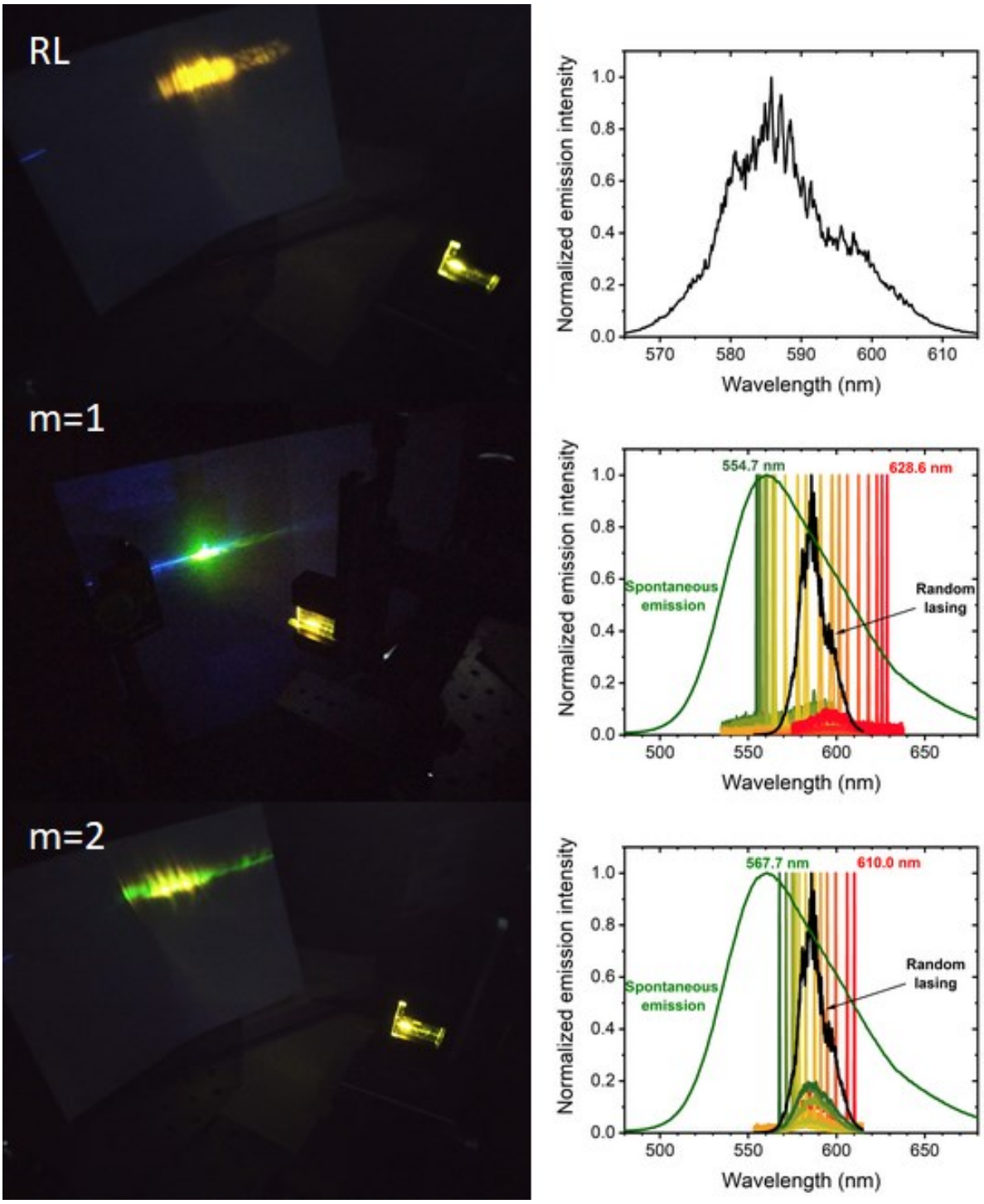

Figure 6.2.12. *Photographs taken during the experiment (left) and corresponding spectra (right) of 2% w/w* ***HBT-CF3-4,6-TMS****/PMMA.*

As described in the previous section, ESIPTs doped polymeric films are good candidates for the holographic DFB. These experiments were conducted for two orders of diffraction, m = 1 and m = 2, with successful execution. As with previously shown films, tunability of the lasing line exceeds random lasing spectra for both diffraction orders. Due to the gain profile position, full emission tunability is possible from the green to red region of the visible spectra, as presented in Figure 6.2.12. For second-order, real-time tuning of 42 nm was achieved (567.7 – 610.0 nm), with spectra heavily influenced by the crystals and aggregates of the dye that formed during the film preparation (visible in Figure 6.2.13). Those structures are responsible for the light scattering, which in turn is responsible for the RL phenomena. If one looks at the light emitted from the sample during the measurements, it can be easily said that dual-emission is observed for m = 2. The green-orange emission is a result of both DFB (green) and RL lasing (orange) emitted from the sample. The blue spot visible on the paper comes from the transmitted pumping beam. However, at m = 1 the periodical modulation in the film is efficient enough to almost completely block the RL. Additionally, the tunability of the DFB lasing is wider in this case and equals 74 nm (554.7 – 628.6 nm). The different response of the sample at m = 1 and m = 2 is most probably due to different feedback mechanisms.[3,14] Nevertheless, the DFB lasing thresholds were lower than the RL values, with energy density as low as 100 μJ·cm^{-2} for m = 1.

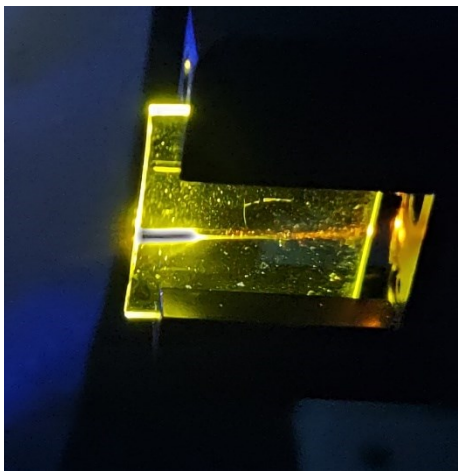

Figure 6.2.13. *Light propagation in the excited 2%* ***HBT-CF3-4,6-TMS****/PMMA film.*

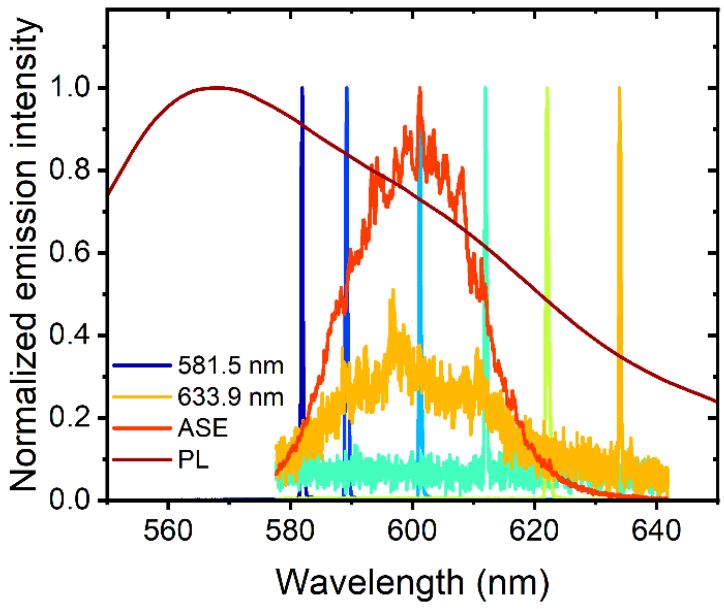

Figure 6.2.14*. Normalized emission spectra of 1.5 mM* ***HBT-CF3-4,6-TMS****/toluene solution.*

DFB lasing was also successfully achieved in the concentrated solutions, for example in toluene. Due to

technical problems only the second order of diffraction was studied, nevertheless, real-time emission tuning of 52.4 nm was realized: from yellow-green (581.5 nm) to pure red 633.9 nm (Figure 6.2.14).

Presented results show broad multifunctionality of the investigated HBT derivative. Due to inherent hydrogen bond sensing of the polar species can be performed ratiometrically through deprotonation, which is a great advantage, since it excludes the need to perform calibration beforehand. This sensitivity can also be exploited in designing the system in regards to the emission in the desired range of the visible spectra, simply by changing the solvent. Real-time tuning of the stimulated emission can also be realized, either in solution or in a solid-state. These parameters prove that **HBT-CF3-4,6-TMS** is a great candidate for a commercial laser dye.

6.3. RGB Polychromatic lasers

While monochromaticity is an inherent characteristic parameter of lasers, due to new applications, the ability to obtain multicolored emission is sought after. It enables the development of lighting technologies,[15] projection displays,[16,17] or the emerging Li-Fi technology.[18] Proposed solutions usually involve a specific preparation of the active material, like dispersion of hydrophobic liquid crystal droplets of the dye in hydrophilic medium,[19,20] or by blending of blue-emissive molecules which leads to exciplex emission.[21] Difficult preparation is a direct result of the inherent risk of reabsorption or color variation in the system.

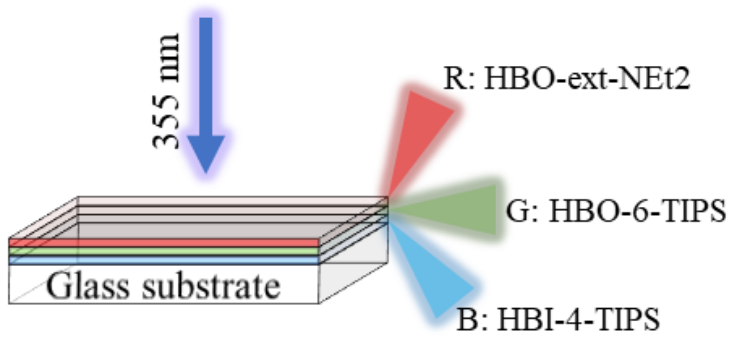

Figure 6.3.1. *Schematical representation of RGB hybrid PMMA film. The arrow (355 nm) shows direction of the pumping beam.*

HBX derivatives presented in this dissertation were used for light amplification studies mostly as dye-doped polymeric thin films and further excited with the same source, namely 355 nm laser. Due to the large Stokes' shift there is no risk of reabsorption of the emitted light by other molecules since the absorption band does not exceed

400 nm. These properties enable easy integration of multiple compounds in one device. In addition, the lasing thresholds are in the same order of magnitude, which simplifies possible commercial applications even further.

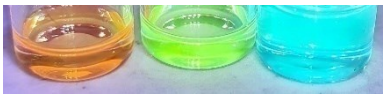

Figure 6.3.2. *Photograph of R, G and B polymer blends taken under the UV lamp.*

In this subchapter two hybrid devices based on ESIPT compounds are presented. Just as described in *Chapter 4*, three different 1% w/w dye/PMMA blends were prepared: **R (HBO-ext-NEt2), G (HBO-6-TIPS)** and **B (HBI-4-TIPS).** The compounds were chosen through analysis of their CIE 1931 coordinates. To ensure that each dye could be excited by the pumping beam a three-step deposition took place, as presented in Figure 6.3.1. First, **B**-layer was formed on a glass substrate using the drop-casting method. **G**-film was applied on top of the blue-emissive one after the complete solvent evaporation, followed by **R**. As the solvent used to prepare blends was the same in each case, slight dissolution of the bottom layer took place each time a new layer was added, which ensured smooth blending of the layers with one another. The proposed RGB sequence is due to the determined laser thresholds of the individual compounds: during the experiment, the compound with the highest threshold is first excited (R), then the green-emissive layer, with efficient B at the end. It prevents the need to apply higher energy density to obtain stimulated emission from each layer, thus prolonging the device lifetime. In addition, an **RB** blend was prepared in the same way. Analysis of CIE 1931 coordinates of RL has shown, that it is possible to obtain emission with the impression of white color from only two components.

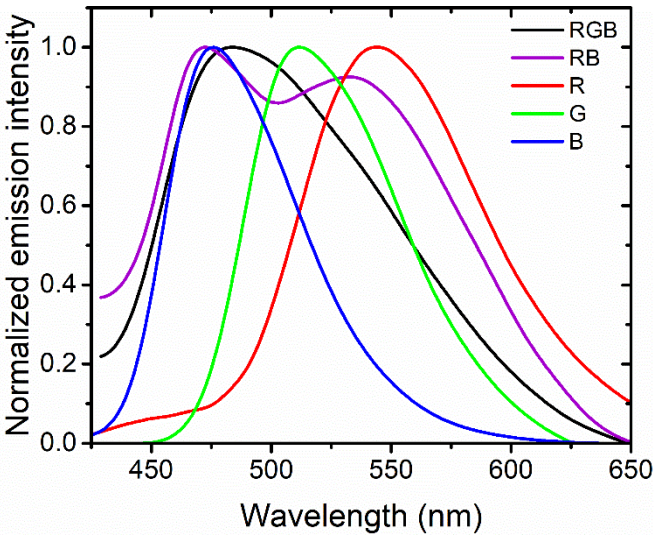

Figure 6.3.3. *The normalized spontaneous emission intensity of investigated doped PMMA thin films: R – HBO-ext-NEt2, G – HBO-6-TIPS, B – HBI-4-TIPS.*

Analysis of spontaneous emission of both RGB and RB devices (Figure 6.3.3.) shows that the green component limits the intensity of the red band, even though it was the first excited

layer. In the latter device the R-band can be easily distinguished, albeit a bit blue-shifted in comparison to a single **HBO-ext-NEt2** film. On the other hand, in both hybrid structures the blue emissive band is the most pronounced. The observed relations show that in terms of properties engineering one should take into account stimulated emission instead of the spontaneous one, as RGB/RB fluorescence is far from white. Polychromatic random lasing was indeed obtained from both devices under the pumping with 355 nm. Due to the deposition of each compound as separate layers, the obtained lasing diverged spatially from one another, as presented in Figure 6.3.4. on which a photograph taken during the measurement of **RB** is shown. Two colors, blue and red, corresponding to each layer, are clearly visible on the paper. Thanks to the slight blending of R and B during the sample preparation also a mix of those two stimulated bands was achieved, seen as a white spot between the red and blue emission. In this region with an almost 2:1 intensity ratio of blue to red, a polychromatic lasing with x = 0.32, y= 0.29 CIE 1931 coordinates is achieved (see Figure 6.3.5). Measurement of the whole stimulated emission spectra was not possible with the available Andor Shamrock fiber spectrometer. The presented "W" emission is a collection of obtained spectra, with an intensity ratio given to show how should the RB profile look like to work as a white laser.

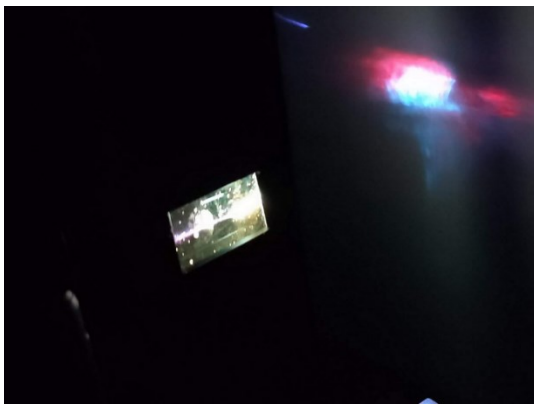

Figure 6.3.4. *Polychromatic lasing of* ***RB****/PMMA.*

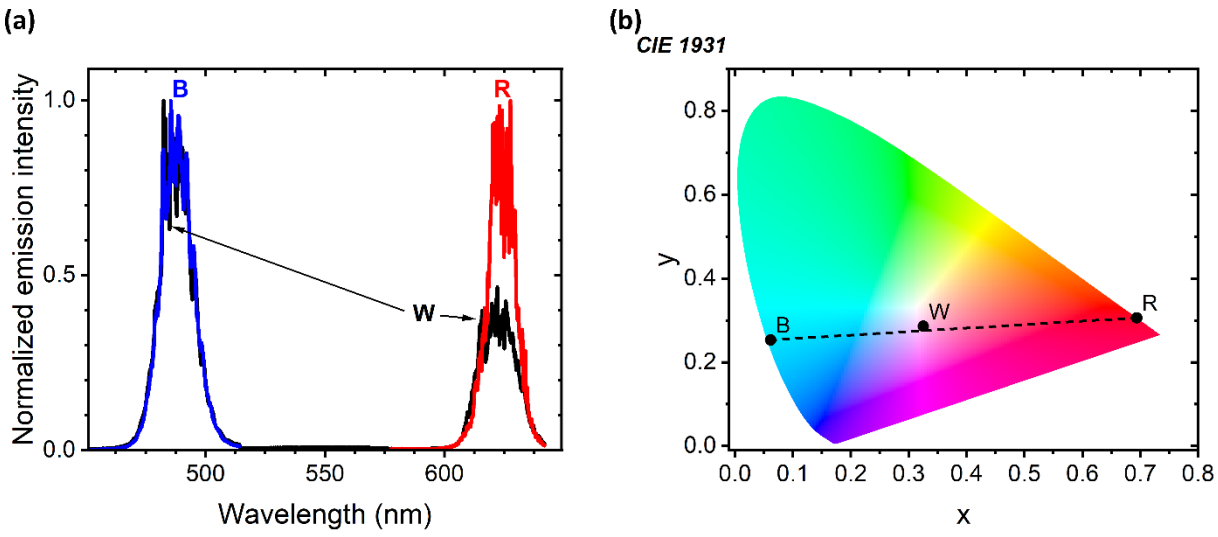

Figure 6.3.5. *(a) Normalized random lasing spectra of* ***RB****. (b) CIE 1931 coordinates of emission of B (****HBI-4-TIPS****) and R (****HBO-ext-NEt2****).* ***W*** *marks white emission of* ***RB****.*

The lasing thresholds of each compound were determined separately. Surprisingly, lower values were calculated for the red-emissive layer: 0.47 ± 0.10 mJ · cm^{-2} (instead of 1.38 mJ · cm^{-2} that was recorded for the pure **HBO-ext-NEt2**/PMMA sample). It can be explained by the simple fact, that the substrate changed: glass + doped polymeric thin films were used instead of clean glass, which in turn influences the refractive index of the substrate and the outgoing emission. On the other hand, for the **B** layer the difference in determined threshold in RB device and for HBI-4-TIPS film is negligible and within the measurement error. A summary of these parameters is given in Table 6.3.1., while random lasing action and corresponding threshold calculation are depicted in Figure 6.3.6.

Table 6.3.1. *Stimulated emission parameters of each component of the RB/PMMA device.*

Compound	λ_{em} [nm]	FWHM [nm]	CIEx	CIEy	ρ_{th} [mJ·cm^{-2}]
HBO-ext-NEt2	624	13.6	0.693	0.306	0.47 ± 0.10
HBI-4-TIPS	488	15.9	0.062	0.253	0.31 ± 0.10

λ_{em} – central emission wavelength, FWHM – full width at half maximum, CIEx/y – CIE 1931 coordinates, ρ_{th} – threshold energy density.

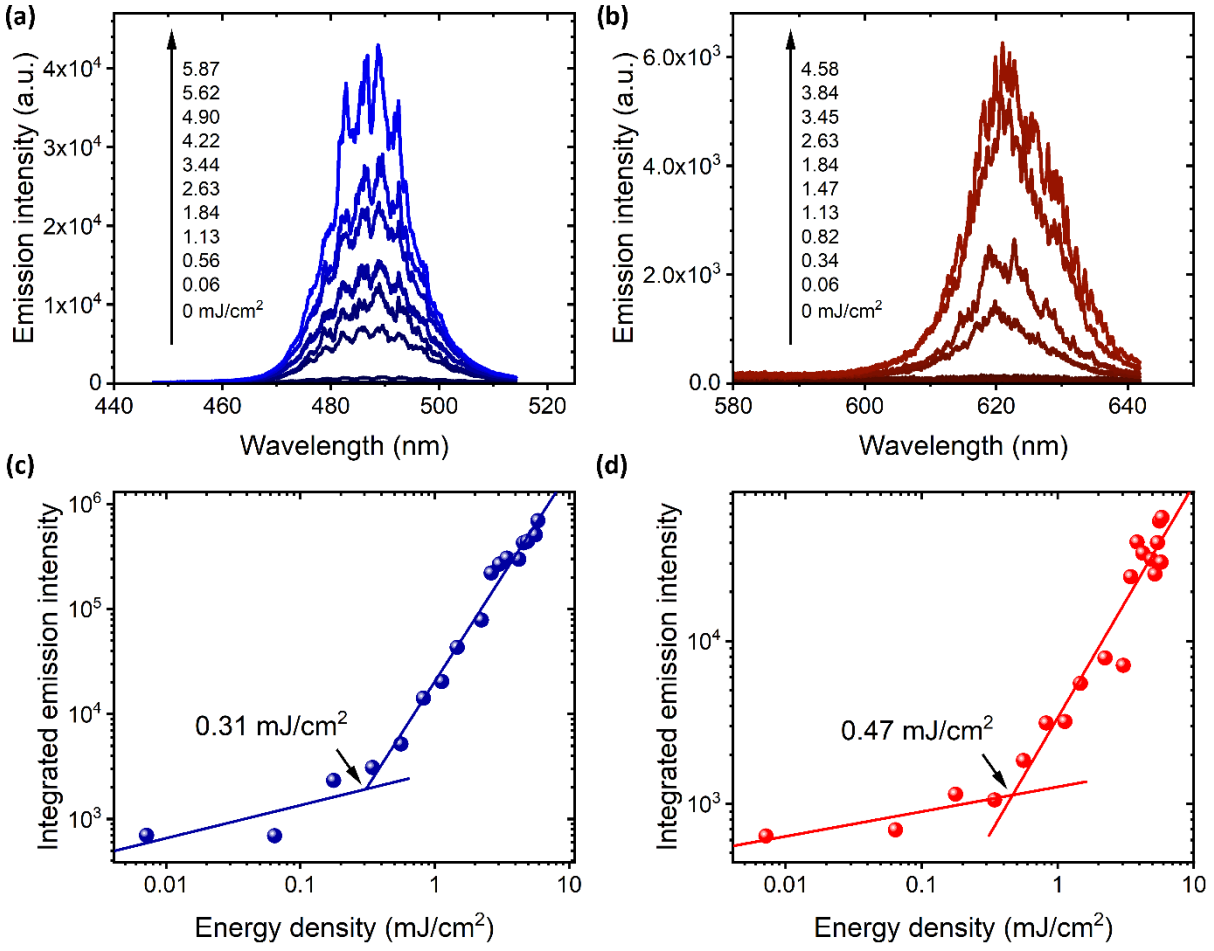

Figure 6.3.6. *Random lasing action of (a)* ***B (HBI-4-TIPS)*** *and (b)* ***R (HBO-ext-NEt2),*** *with corresponding lasing thresholds (c), (d).*

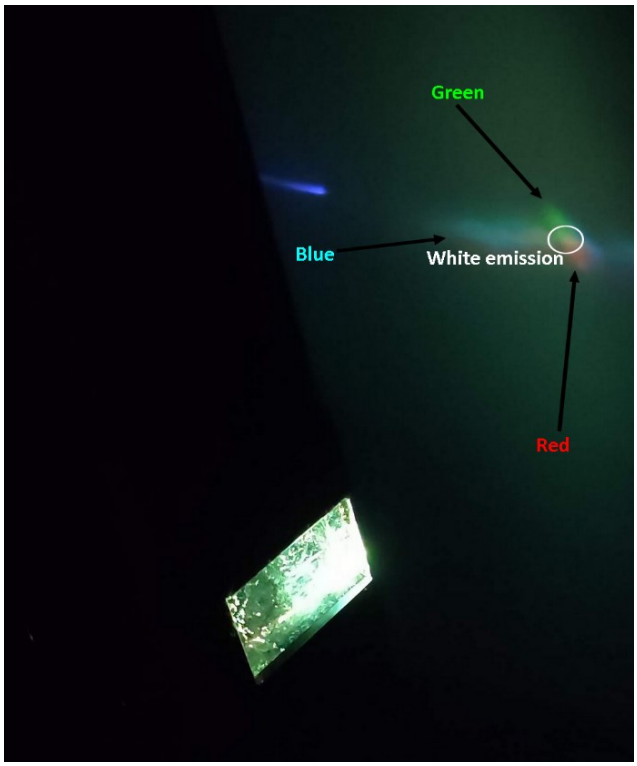

Figure 6.3.7. *Polychromatic lasing of RGB/PMMA.*

Similarly to RB, polychromatic lasing was also obtained for the three-component system. The introduction of the green-emissive dye made it possible to observe RGB lasing. Each of the colors can be easily distinguished, as seen in the photograph in Figure 6.3.7. In addition, emitted light from each layer overlapped with one another, giving emission that seems white to the human eye. Based on CIE 1931 coordinates the ideal ratio of each component to one another in order to obtain white lasing (x = 0.33, y = 0.33) equals 4:1:2, for the red, green and blue layers correspondingly. The recorded stimulated emission of each component is presented in Figure 6.3.8. The use of three compounds instead of one has a major advantage in comparison to the RB device: it allows emission engineering throughout the whole visible spectrum by simple modifications in the ratio of emission intensity of blue, green, and red emissive species, as marked by the triangle at the CIE 1931 graph (Figure 6.3.8b).

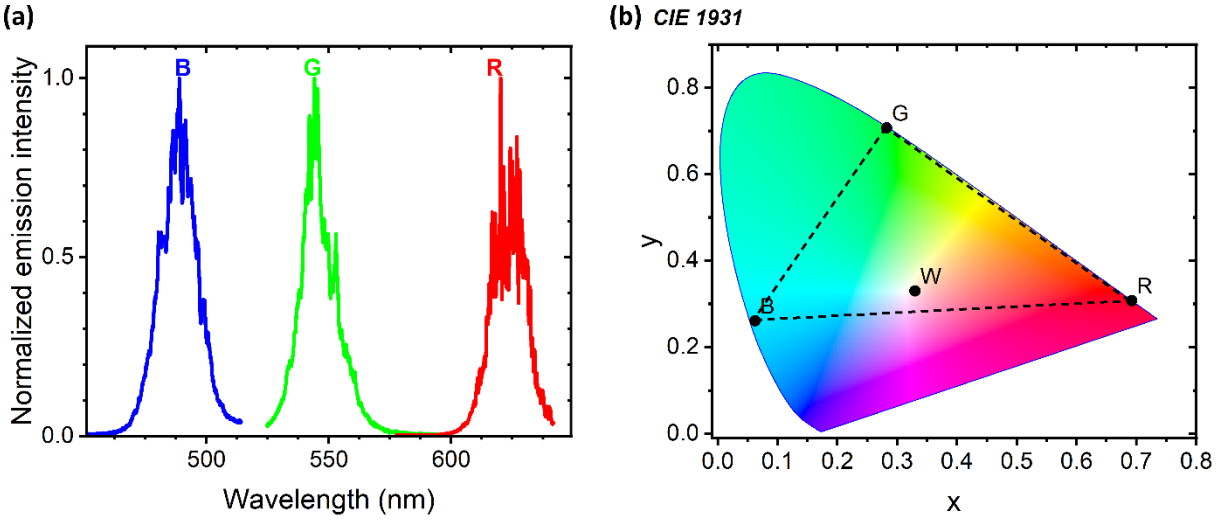

Figure 6.3.8. *(a) Normalized random lasing spectra of* ***RGB****. (b) CIE 1931 coordinates of emission of B (****HBI-4-TIPS****), G (****HBO-6-TIPS****) and R (****HBO-ext-NEt2****).* ***W*** *marks white emission (x = 0.33, y= 0.33).*

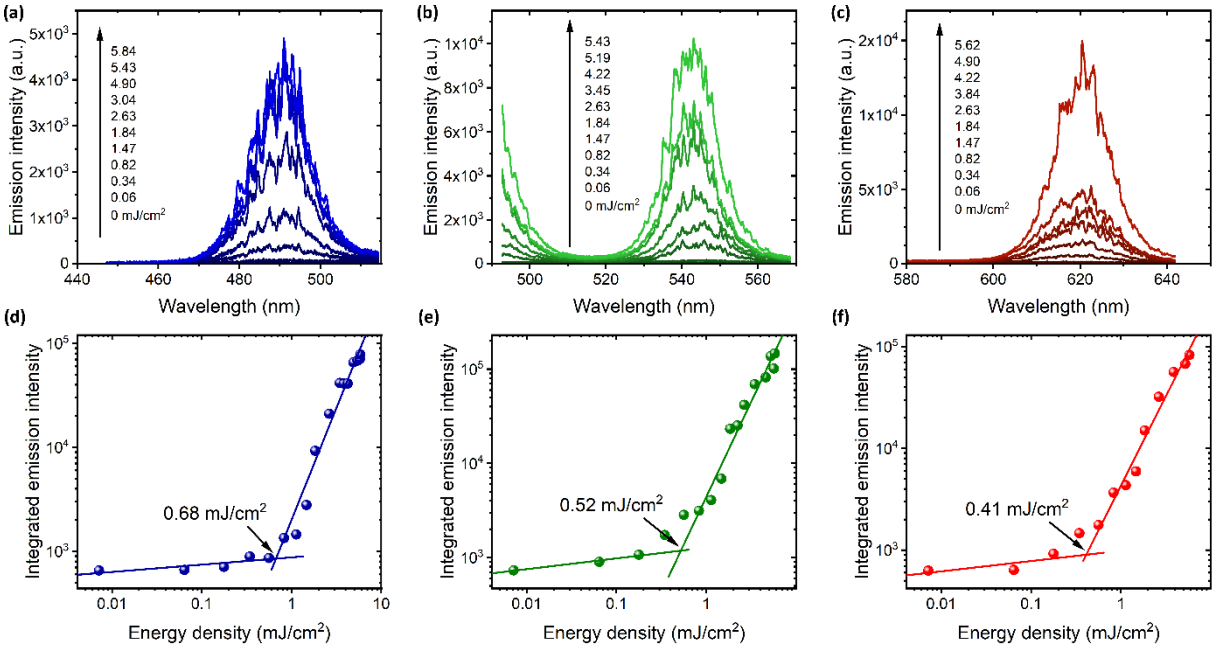

Figure 6.4.9. *Random lasing action of (a)* ***B (HBI-4-TIPS)****, (b)* ***G (HBO-6-TIPS)*** *and (c)* ***R (HBO-ext-NEt2),*** *with corresponding lasing thresholds (d) – (f).*

Lasing thresholds parameters were determined for each of the stimulated bands (Figure 6.4.9.). The values for the red-emissive layer are almost the same, as in the RB system. On the other hand, ρ_{th} for the **HBI-4-TIPS** is of two times higher value. It can be explained by the introduction of the third part (green) in between R and B. Hence, the pumping beam has to travel through two dye-doped layers, significantly increasing losses due to scattering on each of them. The summary of these parameters is listed in Table 6.3.2.

Table 6.3.2. *Stimulated emission parameters of each component of the RGB/PMMA device.*

Compound	λ_{em} [nm]	FWHM [nm]	CIEx	CIEy	ρ_{th} [mJ·cm^{-2}]		
HBO-ext-NEt2	624	17.4	0.693	0.306	0.41	±	0.10
HBO-6-TIPS	545	16.0	0.282	0.707	0.52	±	0.10
HBI-4-TIPS	489	18.0	0.062	0.261	0.68	±	0.10

λ_{em} – central emission wavelength, FWHM – full width at half maximum, CIEx/y – CIE 1931 coordinates, ρ_{th} – threshold energy density.

Results presented in this subchapter prove great light amplifying capabilities of ESIPTs. Even in such a simple system as multilayer dye-doped film realization of polychromatic lasing was possible. White-emissive lasing device was fabricated through selection based on the emission color of each component.

6.4. Microfabrication

Microfabrication through two-photon polymerization (TPP) is one of the very precise and innovative techniques to manufacture one-, two- or three-dimensional structures on nano- and microscale. This method utilizes a laser beam by focusing it on a chosen material, in which, if two-photon absorption occurs, a three-step photochemical reaction is induced (Figure 6.4.1.).[22] As a result, radical polymerization of the material occurs, but only in the focus,[22–24] creating the so-called voxel. This specific reaction can only be achieved when the laser intensity is strong enough to induce efficient two-photon absorption, which is a nonlinear process. As such, the polymerization takes place only at the focal point of the laser. Structurization in all three dimensions can be realized by a simple XYZ scan of the sample. With this setup, there is no risk of unwanted one-photon polymerization, since the matrix and used photoinitiators are chosen in such a way, that no linear absorption of the laser wavelength should occur.

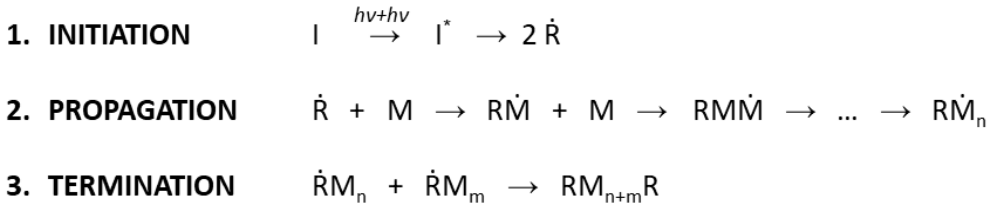

Figure 6.4.1. *Photochemical reactions for two-photon polymerization: I – initiator, R – radical, M - monomer.*

Up to now ESIPT compounds were not investigated as possible photoinitiators for the two-photon polymerization. While their optical nonlinear properties were investigated, applications were limited to two-photon absorption/emission sensing or bioimaging.[25–27] Promising characteristics were reported, such as great photostability in the solid-state and a significant two-photon absorption cross-section.[28–30] As such, available ESIPT compounds were investigated by the Author toward possible application as photoinitiators.

The experiments were performed in a self-build setup based on a Nikon IX71 inverted microscope (Figure 6.4.2). As a light source, a picosecond 532 nm laser (Teem Photonics, τ=650 ps, 100 kHz repetition rate, maximum power: 800 mW) was chosen. The beam was directed through the half-wave plate and Glan-Thompson double polarizer into the microscope and then focused with an x60 microscope objective (NA = 0.85). The piezoelectric stage was used for sample positioning, which enabled XYZ scan at 300 μm maximum in all directions. With custom software, two-photon polymerization threshold determination was possible by

fabrication of 100 μm long separated test lines (write speed: 100 μm/s) with increasing beam energy. The threshold was determined as the first line polymerized across its entire length.

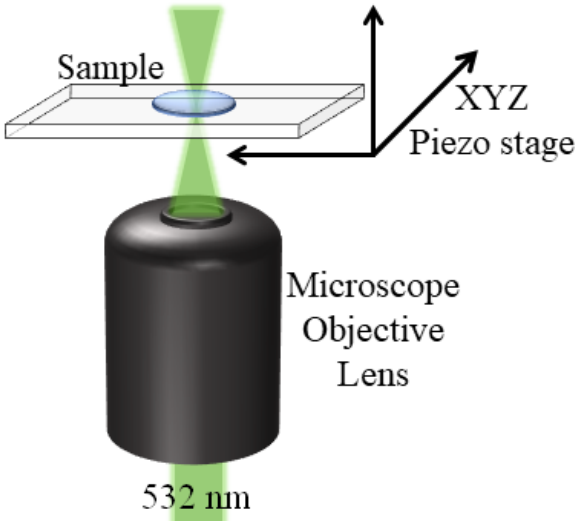

***Figure 6.4.2**. Schematical close-up of the sample in the microfabrication experimental setup.*

Seven ESIPT compounds were investigated: four HBO derivatives (**HBO-4-TES**, **HBO-6-TES, HBO-4,6-TES, HBO-4,6-TMS**), two extended anils (**A-CN**, **A-F**) and commercially available salicylic acid (**SA**, Warchem, Poland). Chosen molecules do not absorb light with a wavelength exceeding 500 nm (Figure 6.4.3.), enabling their use for 532 nm two-photon absorption. Commercially available poly(ethylene glycol) diacrylate (**PEG-DA**) was used as a monomer and pentaerythritol triacrylate (**PETA**) as a crosslinking agent (Figure 6.4.4.).

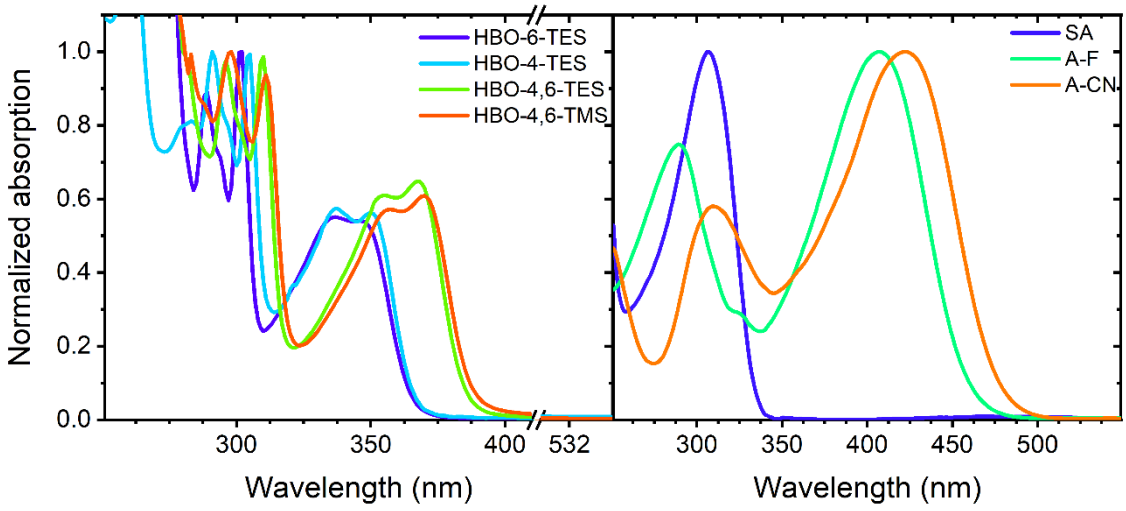

***Figure 6.4.3.** Normalized absorption spectra of investigated compounds in dichloromethane.*

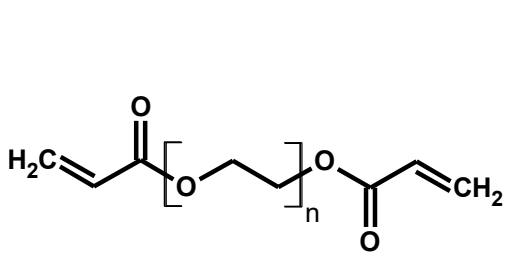

PEG-DA:

Poly(ethylene glycol diacrylate

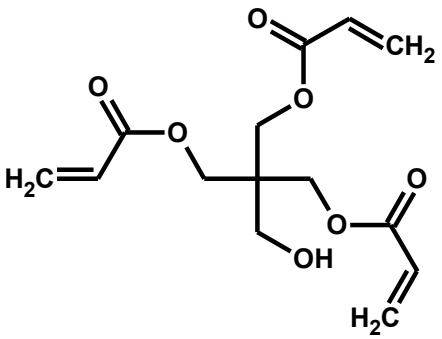

PETA:

Pentaerythritol triacrylate

Figure 6.4.4. *Chemical structure of monomer (**PEG-DA**) and crosslinking agent (**PETA**).*

For the experiments ESIPT/PEG-DA:PETA mixtures were prepared, as follows: first monomer and crosslinking agent were mixed, with varying mass ratios (from 100:0 to 0:100). In separate flasks dichloromethane solutions of ESIPTs were prepared, then injected into PEG-DA:PETA mixtures to obtain blends with different compound/medium weight ratios (0.5 – 10%), followed by room temperature evaporation of the solvent. The dichloromethane had to be completely removed from the mixture before microfabrication to avoid solvent influence on the polymer solidification. Any liquid residues may locally disrupt the focusing of the laser beam and change the concentration of the photoinitiator. For the experiments, 10 µl of the studied mixture was deposited on a clean glass coverslip. Additionally, non-doped PEG-DA:PETA blends were examined as a reference.

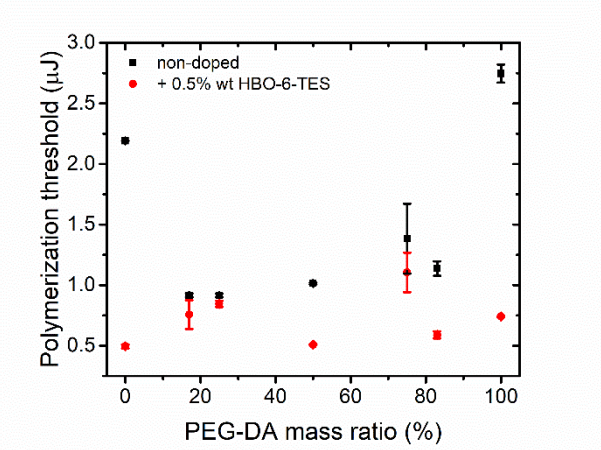

Figure 6.4.5. *The polymerization threshold versus PEG-DA:PETA mass ratio for 0.5% wt HBO-6-TES/PEG-DA:PETA and non-doped PEG-DA:PETA mixtures.*

There was no discernible effect of mass ratio on the polymerization thresholds of non-doped PEG-DA:PETA mixtures (Figure 6.4.5., Table 6.4.1.). The inclusion of the crosslinker PETA, however, allows for more exact form control of polymerized structures. It solidifies immediately, preventing the mixture from flowing uncontrollably. The examined ratio also has a negligible influence on the polymerization line width, which is restricted by the utilized microscopic objective.

Table 6.4.1. *The polymerization threshold (E_{th}) determined during microfabrication by TPP for non-doped PEG-DA:PETA mixtures.*

	Non-doped			**0.5% wt HBO-6-TES**		
PEG-DA:PETA mass ratio	**E_{th} (µJ)**			**E_{th} (µJ)**		
100:0	2.75	±	0.07	0.74	±	0.01
83:17	1.14	±	0.06	0.59	±	0.03
75:25	1.38	±	0.29	1.11	±	0.16
50:50	1.01	±	0.01	0.51	±	0.02
25:75	0.92	±	0.02	0.85	±	0.03
17:83	0.92	±	0.02	0.76	±	0.12
0:100	2.19	±	0.02	0.49	±	0.01

Photoinitiators are required for PEG-DA:PETA mixes as they decrease the TPP threshold, evidenced by an investigation with HBO-6-TES as doping. At the same time, excessive local heating is reduced, preventing the polymerized structure from disruption. This is a significant benefit for microfabrication techniques because it allows for more accurate monomer solidification, allowing for 3D structuration. If the sample is overheated, bubbles develop at the focal point, which then rupture, causing microfabrication to be disrupted. Figure 6.4.6. depicts it.

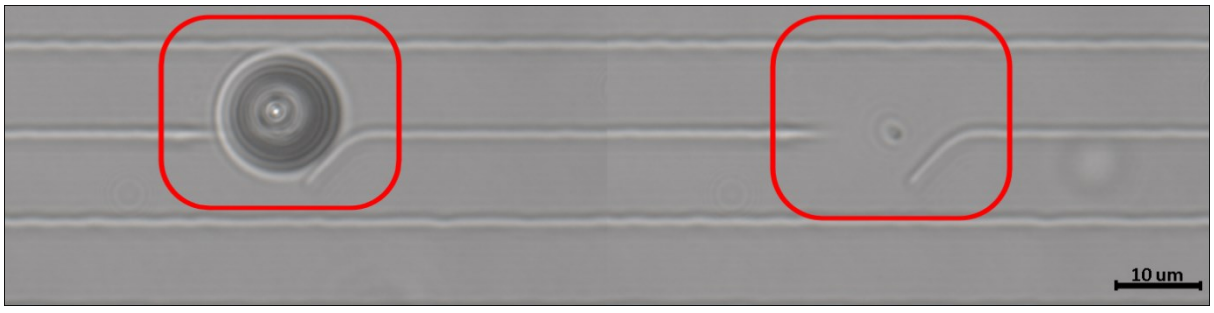

Figure 6.4.6. *Thermal effects disrupting microfabrication process for 50:50 PEG-DA:PETA medium: (left) before and (right) after bursting.*

The polymerization threshold was lowered in all investigated PEG-DA:PETA mixes, independent of their mass ratio, due to doping with the **HBO-6-TES** (Table 6.4.1.). Although there is no apparent association between % of doping and E_{th}, polymerization performed on

doped media is more reproducible. Only one PEG-DA:PETA combination was used for doping with different dyes in subsequent experiments: 50:50.

For most compounds, a general trend towards decreasing of the E_{th} while increasing the dye concentration was observed (see Figure 6.4.7a.). All samples when illuminated with the picosecond laser were emissive. Hence, two-photon absorption of 532 nm was confirmed. Furthermore, when doping levels rise, aggregates and crystals form, at various doping % for each ESIPT. This effect was pronounced enough at some concentrations that it rendered microfabrication impossible — doped PEG-DA:PETA mixtures were so thick and solid-like that their deposition on a coverslip was impossible. Salicylic acid is worth noting: even at 10% doping, no significant crystals develop — in terms of polymerization threshold the sample behaved exactly like the one with 1% doping. On the other hand, 10% SA/PEG-DA:PETA has a higher thermal resistance: during the threshold determination the characteristic bubbles appeared at much higher energies, allowing for more controlled and precise solidification.

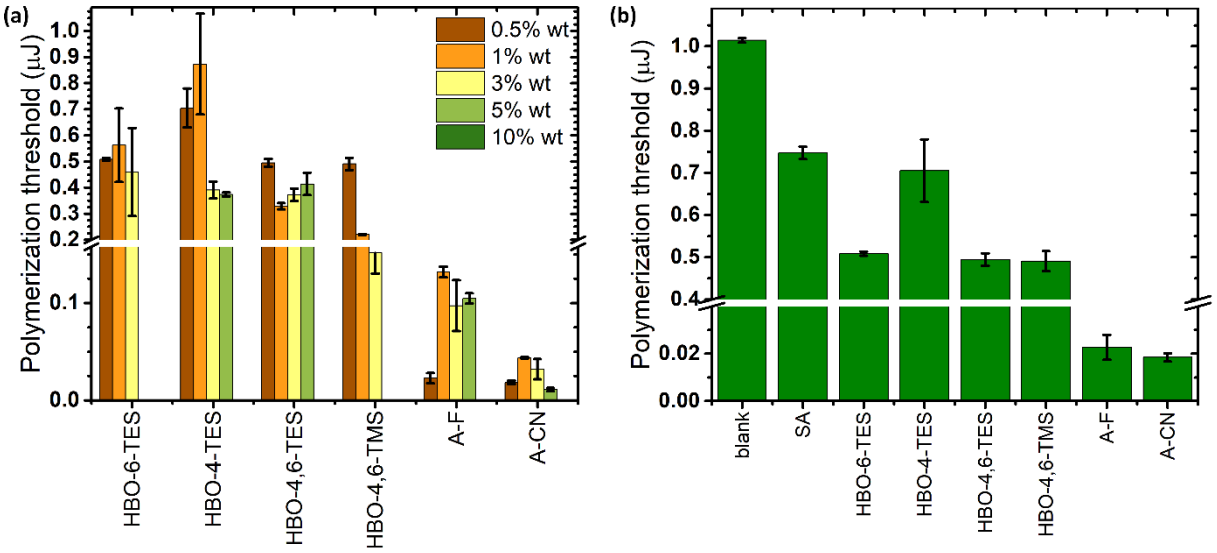

Figure 6.4.7. *Obtained polymerization thresholds for doped PEG-DA:PETA 50:50 mixtures: (a) for all concentrations and (b) at 0.5% wt of doping.*

The impact of doping on the composition was significantly more obvious for the other photoinitiators. Crystals and aggregates formed spontaneously, reducing the quantity of dye dispersed in PEG-DA:PETA. The development of these aggregates and crystals did not, however, hinder polymerization, as seen in Fig. 6.4.8. Furthermore, because microfabrication begins at the glass-mixture interface, the desired form of solidified objects was preserved. Furthermore, thermal effects in these samples were minimal.

Characteristics at 0.5% doping can be examined to rule out the impact of crystals on the polymerization threshold (Figure 6.4.7b). Salicylic acid was found to have the greatest value (1.01 μJ), but still lower than the undoped medium (0.75 μJ). Furthermore, anils with ESIPT features (**A-CN** & **A-F**) appear to have the best performance, since the E_{th} is at the lowest value: approximately 20 nJ for both dyes, which is 50 times lower than for the blank sample. Their behavior, with respect to one another, does not appear to alter significantly with crystallization. With such a low energy value, the potential of overheating in the medium is considerably reduced, allowing for the precise and controlled fabrication of three-dimensional structures.

HBO derivatives, on the other hand, can be successfully used in light amplification. At 0.5 percent doping their determined polymerization thresholds (0.49 – 0.71 μJ) are not significantly higher than those of other investigated compounds. Their characteristics differ substantially from one another, as per their chemical structure. Further examination (Table 6.4.2.) indicates that bis-substitution ensures better dispersion of the dye in the matrix (crystals form at higher mass concentration) and lowers the polymerization threshold in comparison to mono-substituted HBOs. Moreover, a shorter alkyl moiety (Me) seems to beneficently influence the photoinitiating characteristics of the dye.

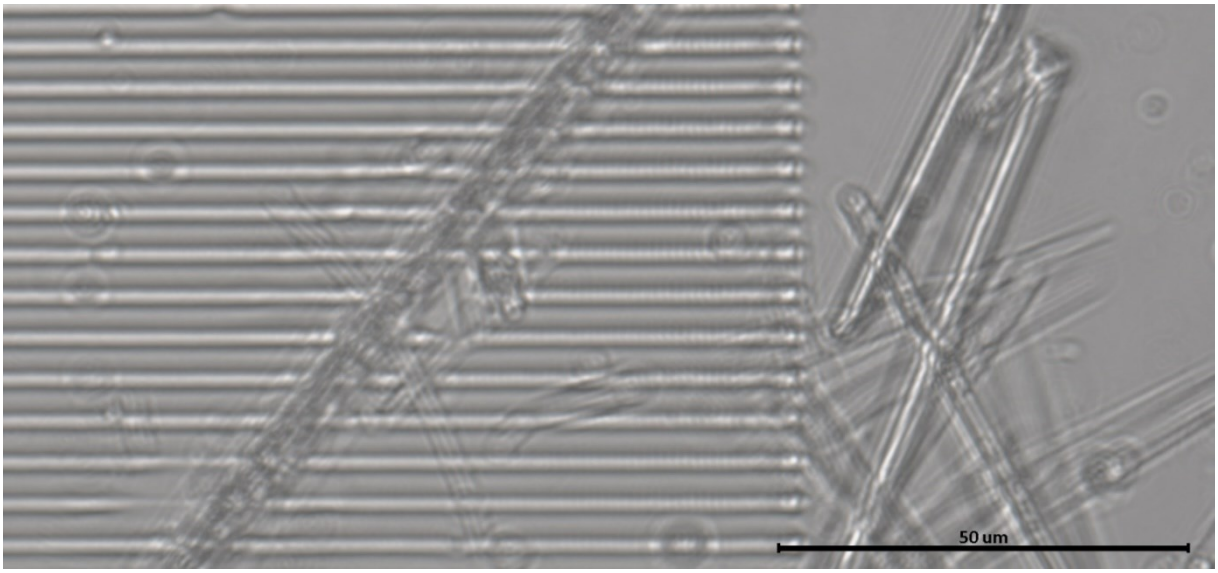

Figure 6.4.8*. Microfabricated lines in 3%* ***HBO-4,6-TMS****/PEG-DA:PETA medium at 300 nJ.*

HBOs light amplifying properties were proven as part of the research presented in this dissertation. Hence their use for microfabrication is of great interest. Further integration would enable the polymerization of desirable 3D structures, which would eventually function as laser resonators. As presented in the previous subchapter, micro- or nanoscale polychromatic laser

could be designed, with excitation at a different wavelength (preferably 355 nm) since separate absorption bands are responsible for photoinitiating or the lasing activity.

Table 6.4.2. *Polymerization thresholds obtained during microfabrication experiments for doped PEG-DA:PETA 50:50 mixtures. Cryst – polymerization was not possible due to excessive crystallization.*

	PEG-DA/PETA 50:50 mass ratio + dye (% w/w)	**Polymerization threshold – E_{th} (µJ)**
SA	0.5	0.75 ± 0.01
	1.0	0.67 ± 0.01
	3.0	1.00 ± 0.01
	5.0	0.80 ± 0.06
	10.0	0.68 ± 0.01
HBO-6-TES	0.5	0.51 ± 0.01
	1.0	0.56 ± 0.14
	3.0	0.46 ± 0.17
	5.0	*cryst*
	10.0	*cryst*
HBO-4-TES	0.5	0.71 ± 0.07
	1.0	0.87 ± 0.19
	3.0	0.39 ± 0.03
	5.0	0.37 ± 0.01
	10.0	*cryst*
HBO-4,6-TES	0.5	0.49 ± 0.01
	1.0	0.33 ± 0.01
	3.0	0.37 ± 0.02
	5.0	0.41 ± 0.04
	10.0	*cryst*
HBO-4,6-TMS	0.5	0.49 ± 0.02
	1.0	0.22 ± 0.01
	3.0	0.15 ± 0.21
	5.0	*cryst*
	10.0	*cryst*
A-F	0.5	0.023 ± 0.005
	1.0	0.132 ± 0.006
	3.0	0.097 ± 0.026
	5.0	0.105 ± 0.005
	10.0	*cryst*
A-CN	0.5	0.018 ± 0.002
	1.0	0.044 ± 0.001
	3.0	0.032 ± 0.010
	5.0	0.011 ± 0.002
	10.0	*cryst*

In summary, all investigated compounds were successfully applied as photoinitiators. Doping with ESIPTs leads to a significant decrease in the pumping energy required for polymerization, proving that two-photon absorption occurs in studied samples. The threshold for non-doped mixtures with picosecond pulses is at least 0.92 μJ, depending on the PEG-DA:PETA mass ratio. With doping, this value was reduced to 11 nJ (**A-CN**, 5% w/w), which is an outstanding 92 times smaller than the corresponding non-doped 50:50 PEG-DA:PETA blank sample (1.01 μJ).

Literature

1 Parafiniuk, K., Sznitko, L. & Mysliwiec, J. Distributed feedback and random lasing in DCNP aggregates dispersed in a polymeric layer. *Opt. Lett.* **40**, 1552 (2015).

2. Parafiniuk, K., Sznitko, L., Zelechowska, M. & Mysliwiec, J. Near-infrared distributed feedback laser emission based on cascade Förster resonance energy transfer to Nile Blue aggregates. *Org. Electron.* **33**, 121–127 (2016).

3. Karnutsch, C. *et al.* Low threshold blue conjugated polymer lasers with first- and second-order distributed feedback. *Appl. Phys. Lett.* **89**, 1–4 (2006).

4. Kranzelbinder, G. *et al.* Optically written solid-state lasers with broadly tunable mode emission based on improved poly (2,5-dialkoxy-phenylene-vinylene). *Appl. Phys. Lett.* **80**, 716–718 (2002).

5. Forget, S. & Chenais, S. *Organic Solid- State Lasers*. (Springer, 2013).

6. Pariat, T. *et al.* Impact of Heteroatom Substitution on Dual-State Emissive Rigidified 2-(2'-hydroxyphenyl)benzazole Dyes: Towards Ultra-Bright ESIPT Fluorophores**. *Chem. - A Eur. J.* **27**, 3483–3495 (2021).

7. Massue, J., Jacquemin, D. & Ulrich, G. Molecular Engineering of Excited-state Intramolecular Proton Transfer (ESIPT) Dual and Triple Emitters. *Chem. Lett.* **47**, 1083–1089 (2018).

8. Kwon, J. E. & Park, S. Y. Advanced Organic Optoelectronic Materials: Harnessing Excited-State Intramolecular Proton Transfer (ESIPT) Process. *Adv. Mater.* **23**, 3615–3642 (2011).

9. Massue, J. *et al.* Solution and solid-state Excited-State Intramolecular Proton Transfer (ESIPT) emitters incorporating Bis-triethyl-or triphenylsilylethynyl units. *Dye. Pigment.* **160**, 915–922 (2019).

10. Yang, M. *et al.* Aggregation-Induced Fluorescence Behavior of Triphenylamine-Based Schiff Bases: The Combined Effect of Multiple Forces. *J. Org. Chem.* **78**, 10344–10359 (2013).

11. Hong, Y., Lam, J. W. Y. & Tang, B. Z. Aggregation-induced emission. *Chem. Soc. Rev.* **40**, 5361–5388 (2011).

12. Cheng, X. *et al.* Multicolor Amplified Spontaneous Emissions Based on Organic Polymorphs That Undergo Excited-State Intramolecular Proton Transfer. *Chem. - A Eur. J.* **22**, 4899–4903 (2016).

13. Zhang, W., Yan, Y., Gu, J., Yao, J. & Zhao, Y. S. Low-threshold wavelength-switchable organic nanowire lasers based on excited-state intramolecular proton transfer. *Angew.*

Chemie - Int. Ed. **54**, 7125–7129 (2015).
14. Jory, M. J., Barnes, W. L., Samuel, I. D. W., Turnbull, G. A. & Andrew, P. Relationship between photonic band structure and emission characteristics of a polymer distributed feedback laser. *Phys. Rev. B - Condens. Matter Mater. Phys.* **64**, 1–6 (2001).
15. Neumann, A. *et al.* Four-color laser white illuminant demonstrating high color-rendering quality. *Opt. Express* **19**, A982–A990 (2011).
16. Nebel, A. & Wallenstein, R. E. Concepts and performance of solid state RGB laser sources for large-frame laser projection displays. in *Proc.SPIE* vol. 3954 (2000).
17. Hollemann, G. *et al.* RGB lasers for laser projection displays. in *Proc.SPIE* vol. 3954 (2000).
18. Dimitrov, S. & Haas, H. *Principles of LED Light Communications: Towards Networked Li-Fi*. *Principles of LED Light Communications: Towards Networked Li-Fi (2015).* doi:10.1017/CBO9781107278929 WE - Book Citation Index – Science (BKCI-S).
19. Adamow, A. *et al.* Electrically controlled white laser emission through liquid crystal/polymer multiphases. *Light Sci. Appl.* **9**, (2020).
20. Adamow, A., Szukalski, A., Justyniarski, A., Sznitko, L. & Mysliwiec, J. Light amplification in tunable multicolor liquid crystalline system. *J. Lumin.* **220**, 116903 (2020).
21. Mazzeo, M. *et al.* Organic single-layer white light-emitting diodes by exciplex emission from spin-coated blends of blue-emitting molecules. *Appl. Phys. Lett.* **82**, 334–336 (2003).
22. Maruo, S., Nakamura, O. & Kawata, S. Three-dimensional microfabrication with two-photon-absorbed photopolymerization. *Opt. Lett.* **22**, 132–134 (1997).
23. Iosin, M., Stephan, O., Astilean, S., Dupperay, A. & Baldeck, P. L. Microstructuration of protein matrices by laser-induced photochemistry. *J. Optoelectron. Adv. Mater.* **9**, 716–720 (2007).
24. Zhou, X., Hou, Y. & Lin, J. A review on the processing accuracy of two-photon polymerization. *AIP Adv.* **5**, (2015).
25. Chen, L., Park, S. J., Wu, D., Kim, H. M. & Yoon, J. A two-photon ESIPT based fluorescence probe for specific detection of hypochlorite. *Dye. Pigment.* **158**, 526–532 (2018).
26. Shang, X. *et al.* Optical nonlinearities and transient dynamics of 2-(2′-hydroxyphenyl)benzoxazole studied by single-beam and time-resolved two-color Z-scan techniques. *J. Opt. Soc. Am. B* **15**, 854–862 (1998).
27. Zhou, L. *et al.* Localizable and Photoactivatable Fluorophore for Spatiotemporal Two-Photon Bioimaging. *Anal. Chem.* **87**, 5626–5631 (2015).
28. Skonieczny, K. *et al.* Bright, emission tunable fluorescent dyes based on imidazole and π-expanded imidazole. *J. Mater. Chem.* **22**, 20649–20664 (2012).
29. Kim, H. M. & Cho, B. R. Two-Photon Fluorescent Probes for Metal Ions. *Chem. – An Asian J.* **6**, 58–69 (2011).
30. Zheng, J., Guo, Y., Li, X., Zhang, G. & Chen, W. Two-photon-induced excited state intramolecular proton transfer process and nonlinear optical properties of HBT in cyclohexane solution. *J. Opt. A Pure Appl. Opt.* **8**, 835–839 (2006).

7. Conclusions

In the research work presented in this dissertation, various aspects concerning the development of purely organic light amplifying systems have been addressed, starting with fundamental spectroscopic measurements of 18 non-commercial compounds showing the Excited-State Intramolecular Proton-Transfer ability: sixteen 2-(2'-hydroxyphenyl)benzazole derivatives and two Schiff bases. A thorough analysis of relationships between the chemical structure and emission properties of these materials was conducted in dilute solutions and as solid-state systems: dispersed in potassium bromide and poly(methyl methacrylate). Aggregation-induced emission (or its enhancement) experiments were performed. The obtained photophysical properties made it possible to fabricate purely organic lasing systems, both in solutions and in solid-state.

While the application of the ESIPTs as an active medium in laser systems has been performed since the 1970s, such extensive research on the correlation between the chemical structure of the chromophore and its lasing ability was conducted for the first time. Below findings related to each experimental subchapter are addressed:

Photophysical properties:

All investigated compounds absorb ultraviolet light and are fluorescent in non-polar toluene. The observed emission varies depending on the structure, however, some major relationships can be distinguished. In the case of 2-(2'-hydroxyphenyl)benzazoles, at first, spontaneous emission can be tuned by substitution with a different heteroatom. Hence, the fluorescence of the highest energies (and shortest wavelengths) was recorded for nitrogen analogs (HBI: 475-502 nm), followed by oxygen (HBO: 496-567 nm), with sulfur at the end (HBT: 561-568 nm). Dual substitution of HBX compounds promotes a bathochromic shift of emission in comparison to mono-substituted analogs. The Schiff bases, on the other hand, can be excited with both UV and visible light, leading to orange-red emission. The observed fluorescence bands are a direct result of radiative deactivation of the excited keto form, which is formed due to excitation of the molecule and following intramolecular proton transfer in the excited state. The introduction of electron-donating or -withdrawing groups results in additional electronic distribution. Hence, intramolecular charge transfer is responsible for partial frustration of the ESIPT process, observed as dual emission (**HBT-CF3-4,6-TMS** and **HBO-ext-NEt2**). All presented ESIPTs are characterized by large Stokes shifts (at least 7900 cm^{-1} - **HBI-6-TIPS**, with the highest exceeding 11000 cm^{-1} - **HBO-ext-NMe2**), and absolute quantum

yields of emission spanning from relatively low to very high (4-98%). For the majority of the compounds, the beneficial restriction of intramolecular motion in solid-state led to improved quantum yield values (30-82%) of doped potassium bromide pellets, with the exception of Schiff bases (**A-CN**, **A-F**), for which emission quenching was observed. Nevertheless, the ESIPT phenomenon was confirmed in the polymeric thin films doped with investigated chromophores.

Aggregation-Induced Emission:

Both Schiff bases and 2-(2'-hydroxyphenyl)benzazoles are fluorescent in solutions. Hence, induced aggregation can lead to either emission quenching or its enhancement. A few of the 18 studied compounds exhibit such AIEE properties: **HBO-3-TIPS, HBO-4-TIPS, HBO-4,6-TMS, HBI-6-TIPS, HBI-4,6-TIPS, HBT-CF3-4,6-TMS**. In others, additional effects take place, such as hydrogen bonding interactions with polar solvent molecules, or π-π stacking. Hence, ACQ is a prevailing phenomenon. Nonetheless, complete quenching of emission was observed only for the Schiff bases (**A-CN**, **A-F**).

Light amplification:

The two last-mentioned compounds, the anil derivatives, are the only ones that are not capable of stimulated emission. All sixteen 2-(2'-hydroxyphenyl)benzazoles were successfully implemented in polymeric thin films, which upon excitation are capable of both coherent and incoherent random lasing. Population inversion necessary for the lasing action was achieved through a four-level system based on the ESIPT photocycle, with the optical feedback provided by multiple scattering. Crystals and aggregates forming spontaneously during the fabrication of thin films, along with molecular excimers, are responsible for the observed bathochromic shifts of the stimulated emission in comparison to fluorescence. The lasing thresholds (0.15 - 1.38 $mJ \cdot cm^{-2}$) and net gain values (1.44 - 20.38 cm^{-1}) were determined. The relationship between the nature and position of substitution of the HBX and the final stimulated emission is in tune with findings reported for toluene solutions. Therefore, blue-green lasing was obtained for HBI derivatives, green for HBOs, and orange-red for HBTs, which covers almost the whole visible spectrum. The only compound that does not follow this behavior is the **HBO-ext-NEt2**, in which the most red-shifted emission was observed (ca. 620 nm) due to the competing ICT phenomenon. Additionally, it was found that a change of the polymer matrix can be used to tune the final stimulated emission, as different polymer chains promote different packing of the chromophore. A graph with exemplary stimulated emission spectra of all investigated thin films

is given in Figure 7.1, along with CIE 1931 coordinates. Four of the investigated HBX derivatives are capable of Amplified Spontaneous Emission as amorphous powders: **HBI-3-TIPS, HBI-4-TIPS, HBO-3-TIPS, HBO-6-TIPS**. As the properties of such samples depend on the packing of individual particles, single crystals need to be grown and then investigated. The ASE was also obtained in concentrated solutions of the ESIPTs, which proves the outstanding properties of these compounds as laser dyes.

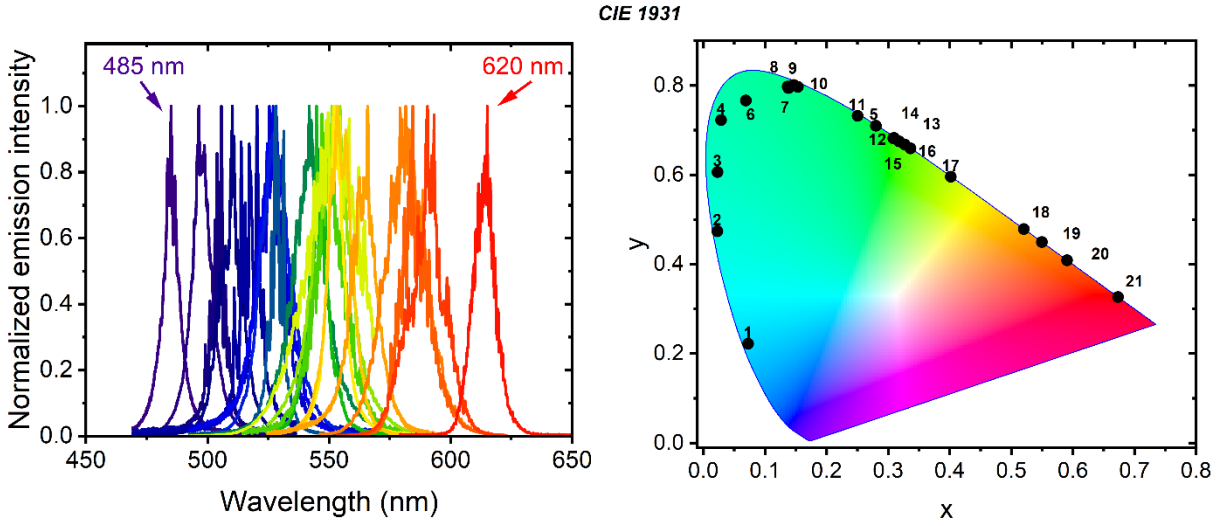

Figure 7.1. *(a) Normalized random lasing spectra of investigated ESIPT compounds in PMMA or PS matrix, with the corresponding CIE 1931 coordinates (b).*

Applications:

The same thin films, which were fabricated for the random lasing studies, can be used in degenerated two-wave mixing experiments. Hence, real-time tunable distributed feedback lasers are achieved, with the temporal resonators formed due to periodical modulation of gain and/or refractive index of the active material. The obtained DFB lasers are characterized by tunability that exceeds the profile of random lasing action (>39 nm). The DFB lasers were also achieved in concentrated solutions.

When the inherent sensitivity of the ESIPTs is taken into consideration, in the future the DFB sensors can be constructed. The first steps have been taken in this direction, but quite possibly fabrication of permanent DFB gratings will need to be involved. However, a tunable laser source based on a single dye was fabricated (**HBT-CF3-4,6-TMS**). Due to ICT and ESIPT processes, an emission spanning from blue to red was achieved in solvents of different polarities. Additionally, an instant shifting of the ASE in solution from 605 (red) to 508 nm (green) was realized by deprotonation of the chromophore. To the best of the Author's

knowledge, it is the first time that stimulated emission was observed in the anionic form of the ESIPT.

The complete prevention of the self-reabsorption of the HBX derivatives makes it possible to easily fabricate panchromatic hybrid devices. Dual (red-blue) and triple (red-green-blue) stimulated emission was observed as random lasing action was achieved in the sandwich-type structures consisting of two or three chromophores. White emission was obtained in both cases, with the possibility of switching between the emitted colors by the change in the energy density, as the used dyes have different threshold values when pumped with the same source.

The last presented application opens a new path for the ESIPTs. The possibility to use these compounds as photoinitiators in the two-photon polymerization process enables the fabrication of precise structures on a microscopic scale. So far only 1D geometries were achieved. Additional research is performed to enable the preparation of 3D compositions, in which the ESIPTs would act at the same time as the photoinitiator and an active medium for laser action. Furthermore, as panchromatic lasing was already achieved in a simple sandwich structure, microfabrication will make it possible to make tunable microlasers, which could find their applications for example in small-scale modern integrated photonics.

Perspectives:

Research conducted on the presented ESIPT-type compounds shows great multifunctionality of these materials, not only in terms of light amplification. Additional research can be performed to fully exploit these properties. The ESIPTs, due to their innate sensory abilities, can be implemented in sensing applications. Since these compounds are great candidates as an active medium for lasers, the possibility to obtain laser-based sensors is high. Such application would be highly desired, as such devices would be characterized by high resolution and sensitivity. Additionally, since the ESIPTs applicability in two-photon polymerization was proven, the possibility to fabricate intricate structures on a microscopic scale is very high. Hence, microfluidic devices could be obtained. On the other hand, panchromatic lasers are another possibility. As proven in the presented research, desired stimulated emission spectra can be quite easily engineered, making it possible to fit the properties of the final device to the desired application. White emission and the corresponding Li-Fi implementation can be highlighted in this regard.

APPENDIX A: SYNTHETIC DETAILS

Synthesis and characterization of investigated compounds supplied by dr Julien Massue can be found in the following publications:

1) Thibault Pariat, Maxime Munch, Martyna Durko-Maciag, Jaroslaw Mysliwiec, Pascal Retailleau, Pauline M. Verite, Denis Jacquemin, Julien Massue, and Gilles Ulrich, **Impact of Heteroatom Substitution on Dual-State Emissive Rigidified 2-(2'-hydroxyphenyl)benzazole Dyes: Towards Ultra- Bright ESIPT Fluorophores**, *Chemistry - A European Journal*, 2021, 27, 3483 - 3495

HBI-3-TIPS, HBI-4-TIPS, HBI-6-TIPS, HBI-4,6-TIPS, HBO-3-TIPS, HBO-4-TIPS, HBO-6-TIPS, HBO-4,6-TIPS, HBT-4,6-TIPS

2) Julien Massue, Thibault Pariat, Pauline M. Verite, Denis Jacquemin, Martyna Durko, Tarek Chtouki, Lech Sznitko, Jaroslaw Mysliwiec, and Gilles Ulrich, **Natural Born Laser Dyes: Excited-State Intramolecular Proton Transfer (ESIPT) Emitters and Their Use in Random Lasing Studies**, *Nanomaterials*, 2019, 9, 3483 - 1093

HBO-4,6-TES, HBO-4-TES, HBO-6-TES, HBO-4,6-TMS, HBO-4,6-TIPS

3) Julien Massue, Abdellah Felouat, Pauline M. Verite, Denis Jacquemin, Konrad Cyprych, Martyna Durko, Lech Sznitko, Jaroslaw Mysliwiec, and Gilles Ulrich, **An extended excited-state intramolecular proton transfer (ESIPT) emitter for random lasing applications**, *Physical Chemistry Chemical Physics*, 2018, 20, 19958-19963

HBO-4,6-TES

4) Thibault Pariat, Timothee Stoerkler, Clement Diguet, Adele D. Laurent, Denis Jacquemin, Gilles Ulrich, and Julien Massue, **Dual Solution-/Solid-State Emissive Excited-State Intramolecular Proton Transfer (ESIPT) Dyes: A Combined Experimental and Theoretical Approach**, *The Journal of Organic Chemistry*, 2021, 86, 24, 17606-17619

HBO-ext-NEt2, HBO-ext-NMe2

5) Julien Massue, Abdellah Felouat, Mathieu Curtil, Pauline M. Verite, Denis Jacquemin, and Gilles Ulrich, **Solution and solid-state Excited-State Intramolecular Proton Transfer (ESIPT) emitters incorporating Bis-triethyl-or triphenylsilylethynyl units**, *Dyes and Pigments*, 2019, 160, 915-922

HBO-4,6-TES, HBT-4,6-TES

2-hydroxy-3,5-bis((triisopropylsilyl)ethynyl)benzaldehyde was synthesized as described in the literature,[1] then used as a precursor for synthesis of **HBI-4,6-TIPS**, **HBO-4,6-TIPS,** and **HBT-4,6-TIPS**, as shown in Scheme 1.

Synthesis of compound **HBT-CF3-4,6-TMS** at the time of dissertation writing is not published yet but can be found below. Synthetic details and compound characterization were supplied by dr. Massue.

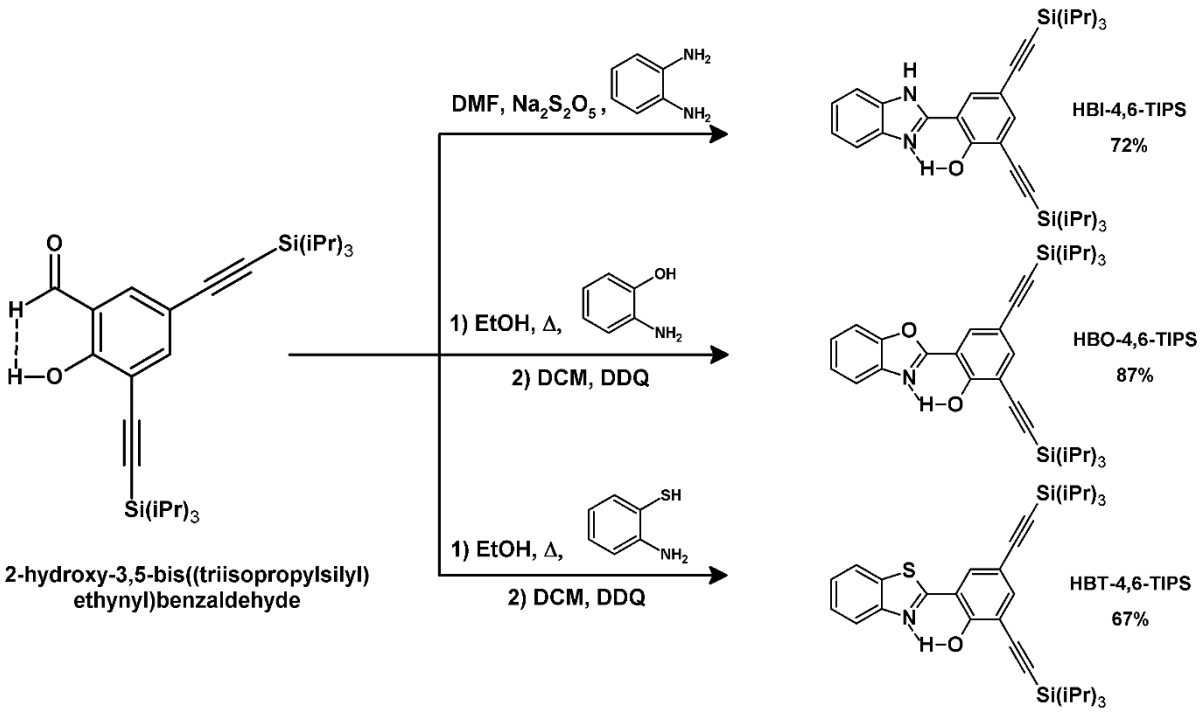

Scheme 1. Synthesis of HBX-4,6-TIPS compounds.

2-(1H-benzo[d]imidazol-2-yl)-4,6-bis((triisopropylsilyl)ethynyl)phenol **(HBI-4,6-TIPS)**

1,2-benzenediamine (49.8 mg, 0.46 mmol) and sodium metabisulfite (87.5 mg, 0.46 mmol) were added to a solution of 2-hydroxy-3,5-bis((triisopropylsilyl)ethynyl)benzaldehyde (200 mg, 0.46 mmol) in DMF and degassed with air for 30 minutes, followed by heating at 120°C for 16h. After cooling down, the reaction mixture was taken up in ethyl acetate and washed with brine, then water (four times), followed by drying over magnesium sulfate and concentrated *in vacuo*. The crude residue was purified by chromatography on silica gel, with petroleum ether/dichloromethane (50:50) as eluent. HBI-4,6-TIPS was obtained as a bright, yellow powder (173mg, 72%). ^{1}H NMR, ^{13}C NMR, and HRMS data can be found in the literature.[1]

2-(benzo[d]oxazol-2-yl)-4,6-bis((triisopropylsilyl)ethynyl)phenol **(HBO-4,6-TIPS)**

A solution of 2-hydroxy-3,5-bis((triisopropylsilyl)ethynyl)benzaldehyde (200 mg, 0.46 mmol) and 2-aminophenol (50.2 mg, 0.46 mmol) was prepared in ethanol and refluxed for 3h. After cooling down, the solvent was evaporated. The obtained red oil was dissolved in DCM (200 ml), followed by the dropwise addition of a solution of DDQ (125 mg, 1.2eq, in 200 ml of

DCM). The solution was stirred at room temperature overnight, followed by concentration *in* vacuo. The crude residue was purified by chromatography on silica gel, with petroleum ether/dichloromethane (90:10) as eluent. HBO-4,6-TIPS was obtained as a bright powder (210mg, 87%). ^{1}H NMR, ^{13}C NMR, and HRMS data can be found in the literature.[1]

2-(benzo[d]thiazol-2-yl)-4,6-bis((triisopropylsilyl)ethynyl)phenol **(HBT-4,6-TIPS)**

A solution of 2-hydroxy-3,5-bis((triisopropylsilyl)ethynyl)benzaldehyde (200 mg, 0.46 mmol) and 2-aminobenzenethiol (57.6 mg, 0.46 mmol) was prepared in ethanol and refluxed for 3h. After cooling down, the solvent was evaporated. The obtained orange powder was dissolved in DCM (200 ml), followed by dropwise addition of a solution of DDQ (125 mg, 1.2eq, in 250 ml of DCM). The solution was stirred at room temperature overnight, followed by concentration *in* vacuo. The crude residue was purified by chromatography on silica gel, with petroleum ether/dichloromethane (80:20) as eluent. HBT-4,6-TIPS was obtained as a yellow powder (180mg, 67%). ^{1}H NMR, ^{13}C NMR, and HRMS data can be found in the literature.[1]

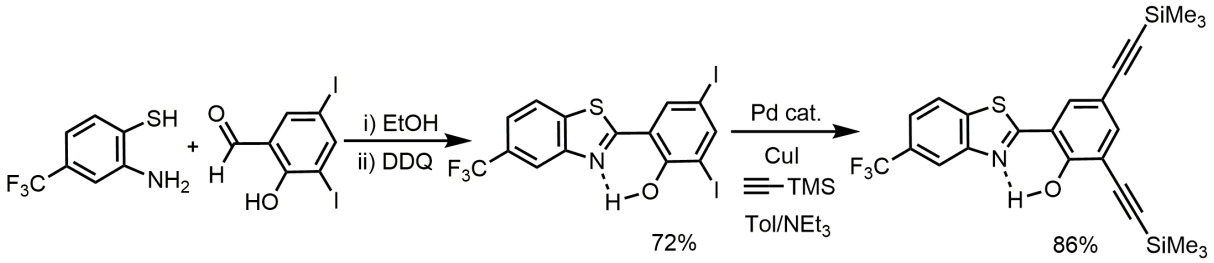

Scheme 2. Synthesis of HBT-CF3-4,6-TMS

2,4-diiodo-6-(5-(trifluoromethyl)benzo[d]thiazol-2-yl)phenol

To a solution of 4-trifluoromethyl-2-aminophenol (1 mmol.) in 50 mL of absolute ethanol was added 3,5-diiodo-2-hydroxybenzaldehyde (1 mmol.) and the resulting suspension was refluxed for one hour before an orange precipitate formed. After cooling down, the precipitate was filtered and washed with ethanol. It was then redissolved in dry dichloromethane and 2,3-dichloro-5,6-dicyano-1,4-benzoquinone (DDQ) (1.2 mmol.) was added as a concentrated dichloromethane solution. The resulting dark mixture was stirred at room temperature overnight. After solvent evaporation, the crude residue was purified by silica gel

chromatography eluting with CH_2Cl_2/Pet. Ether 1 :1 leading to 2,4-diiodo-6-(5-(trifluoromethyl)benzo[d]thiazol-2-yl)phenol (0.72 mmol., 72%) as a white powder, after recrystallisation in pentane.

^{1}H NMR (500MHz, $CDCl_3$) δ (ppm): 13.24 (s, 1H), 8.24 (dt, ^{4}J = 1.5 Hz, ^{4}J =0.8 Hz, 1H), 8.14 (d, ^{4}J = 2.0 Hz, 1H), 8.05 (dt, ^{3}J = 8.5 Hz, ^{4}J = 0.7 Hz, 1H), 7.93 (d, ^{4}J = 2.0 Hz, 1H), 7.70 (d, ^{3}J = 8.5 Hz, 1H). ^{13}C NMR (125MHz, $CDCl_3$) δ (ppm) : 168.8, 156.8, 150.9, 149.7, 136.7, 136.2, 122.7, 122.7, 122.5, 119.6, 119.6, 117.9, 87.9, 80.9. HRMS (ESI-TOF) m/z: [M+H] Calcd for $C_{14}H_7F_3I_2NOS$ 547.8284; Found 547.8278.

2-(5-(trifluoromethyl)benzo[d]thiazol-2-yl)-4,6-bis((trimethylsilyl)ethynyl)phenol **(HBT-CF3-4,6-TMS)**

To a degassed solution of 2,4-diiodo-6-(5-(trifluoromethyl)benzo[d]thiazol-2-yl)phenol (1 mmol.) and $Pd(PPh_3)_2Cl_2$ (5 % mol.) in toluene and triethylamine (3/1, v/v), was added (trimethylsilyl)acetylene (6 mmol.) and CuI (10 % mol.). The resulting mixture was stirred overnight at 90°C. After cooling down, it was extracted with CH_2Cl_2, and washed with water three times. The organic layers were dried over $MgSO_4$ and evaporated *in vacuo*. The product was purified by column chromatography on SiO_2 (CH_2Cl_2/ Pet. Ether. 1:9) to afford a clean white powder (0.86 mmol., 86%).

^{1}H NMR (500MHz, $CDCl_3$) δ (ppm): 13.06 (s, 1H), 8.23 (dt, ^{4}J = 1.5 Hz, ^{4}J = 0.8 Hz, 1H), 8.05 (dt, ^{4}J = 8.4 Hz, ^{4}J =0.8 Hz, 1H), 7.76 (d, ^{4}J = 2.0 Hz, 1H), 7.69 (dd, ^{3}J =8.1 Hz, ^{4}J =1.9 Hz, 2H), 0.30 (s, 9H), 0.27 (s, 9H). ^{13}C NMR (125MHz, $CDCl_3$) δ (ppm) : 170.1, 159.1, 151.2, 140.6, 136.2, 131.9, 122.5, 122.5, 122.4, 119.5, 119.5, 116.4, 114.7, 113.8, 103.0, 100.8, 99.0, 94.1. HRMS (ESI-TOF) m/z: [M+H] Calcd for $C_{14}H_{25}F_3NOSSi_2$ 488.1142; Found 488.1131.

Literature

1 T. Pariat, M. Munch, M. Durko-Maciag, J. Mysliwiec, P. Retailleau, P. M. Verite, D. Jacquemin, J. Massue and G. Ulrich, *Chem. – A Eur. J.*, 2021, **27**, 3483-3495.

APPENDIX B: AUTHOR'S RESEARCH ACHIEVEMENTS

This section contains information on the research achievements and activities conducted by the Author.

Articles in scientific journals:

1. M. Blaszczyk, **M. Durko,** Z. Iwanicka, P. Lochynski, A. Sikora, *Investigations of Reconstruction of Passivation Layer on Stainless Steel Surface Using AFM-Based Techniques*. Mater. Sci. 2018, 36 (3), 381–386. doi.org/10.2478/msp-2018-0066.

2. J. Massue, A. Felouat, P. M. Verite, D. Jacquemin, K. Cyprych, **M. Durko**, L. Sznitko, J. Mysliwiec, *An extended excited-state intramolecular proton transfer (ESIPT) emitter for random lasing applications*. PCCP 2018, 20 (30), 19958-19963. doi.org/10.1039/c8cp03814g.

3. J. Massue, T. Pariat, P. M. Vérité, D. Jacquemin, **M. Durko**, T. Chtouki, L. Sznitko, J. Mysliwiec, G. Ulrich, *Natural Born Laser Dyes: Excited-State Intramolecular Proton Transfer (ESIPT) Emitters and Their Use in Random Lasing Studies*. Nanomaterials 2019, 9 (8). doi.org/10.3390/nano9081093.

4. T. Pariat, M. Munch, **M. Durko-Maciag,** J. Mysliwiec, P. Retailleau, P.M. Vérité, D. Jacquemin, J. Massue, G. Ulrich, *Impact of Heteroatom Substitution on Dual-State Emissive Rigidified 2-(2'-Hydroxyphenyl)Benzazole Dyes: Towards Ultra-Bright ESIPT Fluorophores*. Chem. - A Eur. J. 2021, 27 (10), 3483–3495. doi.org/10.1002/chem.202004767.

5. **M. Durko-Maciag**, A. Popczyk, M. Remond, Z. Zheng, Y. Bretonniere, Ch. Andraud, J. Mysliwiec, *Widely Real-Time Tunable Solid-State Emitters Fitting in the First Biological Window: 9,9-diethyl-2-diphenylaminofluorene Fluorophores for DFB and Random Lasing Applications,* ChemPhotoChem, 2022, accepted article. doi.org/10.1002/cptc.202200008.

6. **M. Durko-Maciag**, D. Jacquemin, G. Ulrich, J. Massue, J. Mysliwiec, *Color-Tunable Multifunctional Excited-State Intramolecular Proton Transfer Emitter: Stimulated Emission of a Single Molecule*, Chem. – A Eur. J., 2022, under review

Oral presentations at conferences:

1. **M. Durko**, K. Cyprych, L. Sznitko, J. Mysliwiec, J. Massue, P. M. Vérité, D. Jacquemin, G. Ulrich - Excited State Intramolecular Proton Transfer (ESIPT) for random lasing studies. The 11th International Conference on Nanophotonics (ICNP 2018), Wroclaw, Poland, 2-6.07.2018

2. **M. Durko**, L. Sznitko, J. Mysliwiec, J. Massue, T. Pariat, P. M. Vérité, D. Jacquemin, G. Ulrich - Natural Born Laser Dyes: Random Lasing Studies based on Excited-State Intramolecular Proton Transfer (ESIPT) Emitters. The 8th International Symposium on Optical Materials, Wroclaw, Poland, 9-14.06.2019

Participation in research projects:

1. 2018 – duration: 3 months - *Fabrication and study of microfabricated photonic structures for light amplification using compounds of biological origin*, 2016/23/D/ST5/00278, SONATA 12, funded by Polish National Science Center - the task: "Investigation of the properties of natural luminescent compounds, in particular the possibility of light amplification, two-photon absorption and energy transfer".

2. 2020 – duration: 3 months - *Optical nanomanipulation: stochastic motion of a nanoparticle trapped by structured light*, 2016/23/P/ST3/02156, POLONEZ 3, funded by Polish National Science Center – the task: "Development of a method of producing polymer microparticles doped with up-converting nanocrystals of β-NaYF4: Yb3 +, Er3 + and organic dyes and characterization of the produced microparticles".

3. 2020 – duration: 6 months - Participation in a project - *Disordered photonics: nano and microresonators as laser light sources*, 2016/21/B/ST8/00468, OPUS 11, funded by Polish National Science Center

4. 2021 – duration: 3 months - *Fabrication and study of microfabricated photonic structures for light amplification using compounds of biological origin*, 2016/23/D/ST5/00278, SONATA 12, funded by Polish National Science Center - the task: "Organic dyes of the ESIPT and BORANIL type as photoinitiators in two-photon polymerization".

5. 2022 – duration: 7 months – Participation in a project - *Liquid crystal systems as sources of electrically tuned white laser light*, 2018/31/B/ST8/02832, OPUS 16, funded by Polish National Science Center

International traineeships:

1. July – September 2017 – at the Department of Advanced Materials, Jozef Stefan Institute, Ljubljana, Slovenia
2. March - May 2019 – at The Institute of Chemistry and Processes for Energy, the Environment and Health (ICPEES), Strasbourg, France
3. July 2021 – at The Institute of Chemistry and Processes for Energy, the Environment and Health (ICPEES), Strasbourg, France